Aus der Klinik und Poliklinik für Augenheilkunde der Universitätsmedizin Rostock

Direktor: Prof. Dr. med. Dr. rer. nat. Thomas Fuchsluger

Wundheilungsmodulation im vorderen Augenabschnitt – experimentelle und klinische Betrachtungen

Habilitationsschrift
zur
Erlangung des akademischen Grades
doctor rerum naturalium habilitatus (Dr. rer. nat. habil.)
der Universitätsmedizin Rostock

Vorgelegt von:
Thomas Stahnke
geboren am 4. März 1969 in Wilhelmshaven
Wohnhaft in Rostock

Rostock, den 02.07.2019

https://doi.org/10.18453/rosdok_id00002930

Gutachter:

Prof. Dr. Berthold Seitz, Universitätsklinikum des Saarlandes, Klinik für Augenheilkunde

Prof. Dr. Gerhard K. Lang, Universitätsklinikum Ulm, Klinik für Augenheilkunde

Prof. Dr. Dr. Thomas Fuchsluger, Universitätsmedizin Rostock, Klinik und Poliklinik für Augenheilkunde

Jahr der Einreichung: 2019
Jahr der Verteidigung: 2020

Inhaltsverzeichnis

Einleitung

1. Wundheilungsmechanismen nach fistulierender Glaukomchirurgie

Das Auge kann im Laufe des Lebens durch unterschiedliche Faktoren und Pathologien in Mitleidenschaft gezogen werden, woraus häufig ein zunehmender Verlust der optischen Qualität resultiert. Ohne die Anwendung adäquater Therapiekonzepte kann ein fortschreitender Krankheitsverlauf schließlich zum vollständigen Verlust der Sehfähigkeit führen.

Eine der häufigsten irreversiblen Erblindungsursachen in den Industrienationen ist der Grüne Star (Glaukom). Unter dem Begriff Glaukom werden verschiedene Augenerkrankungen zusammengefasst, bei denen durch einen progredienten Krankheitsverlauf der Sehnerv geschädigt wird, was zunächst zu Gesichtsfeldausfällen und in späten Stadien zur irreversiblen Erblindung führen kann. Über Prävalenzraten des Glaukoms liegen in Deutschland bislang nur wenige Studien vor, epidemiologische Erhebungen in anderen Ländern (Friedman et al., 2004) erlauben, projiziert auf die deutsche Bevölkerung, eine Abschätzung von ca. 1 Mio. Betroffenen (DOG Weißbuch, 2012), mit einer steigenden Tendenz durch die demographische Entwicklung der Gesellschaft.

Der Hauptrisikofaktor für die Entstehung eines Glaukoms ist der Anstieg des intraokularen Augendrucks (IOD). Die Reduktion des IOD stellt derzeit das einzige Therapieverfahren dar, welches den Krankheitsverlauf nachweislich verlangsamen kann. In einem Großteil von Glaukom-Patienten kann über eine tägliche Applikation von hypotensiven Augentropfen der IOD auf physiologische Werte eingestellt werden. Die Wirkstoffe und die Wirkmechanismen variieren und werden nach der Ursache der Glaukomerkrankungen, dem Patientenalter und der Höhe des IOD ausgewählt. Therapeutisch werden primär zwei unterschiedliche Konzepte verfolgt:

(1) Medikamentöse Reduktion der Kammerwasserproduktion durch Betablocker, Karboanhydrasehemmer und α-Agonisten.

(2) Steigerung der Kammerwasserabflussfazilität (-leichtigkeit) durch Prostaglandine, Cholinergika und α-Agonisten.

Nebenwirkungen, wie ein durch Konservierungsstoffe verursachtes trockenes Auge (Sarkar et al., 2012), allergische Reaktionen (Baudouin, 2008; Droy-Lefaix et al., 2013) oder eine zu geringe Therapieeffizienz machen alternative, dauerhafte Therapieformen

zur Behandlung des Glaukoms notwendig. Mangelnde Adhärenz der Glaukom-Patienten hebt die Notwendigkeit dauerhafter Lösungsansätze noch hervor (Frech et al., 2018). Zu den derzeit klinisch häufig angewendeten dauerhaften Therapieformen gehören Koagulationsverfahren zur Reduktion der Kammerwasserproduktion (Fong et al., 2011; Raivio et al., 2008) oder Lasertrabekuloplastik-Verfahren, welche die Abflussleichtigkeit des Kammerwassers erhöhen und somit den IOD senken (Koller et al., 1996; Kuerzinger und Eckert 2010; Wacker und Eckert, 2009). Auch chirurgische Interventionen werden häufig als dauerhafte Therapieformen angewendet, wobei fistulierende Eingriffe wie die Trabekulektomie (Cairns, 1968) und die tiefe Sklerektomie (Fedorov et al., 1982; Lim et al., 1998) über chirurgisch angelegte Drainagewege Kammerwasser überwiegend in den subkonjunktivalen Raum ableiten (Guthoff et al., 2009). Neben den chirurgischen Verfahren stellt auch die minimalinvasive Implantation von drainierenden Mikroimplantaten einen weiteren dauerhaften Lösungsansatz dar, um den IOD zu senken (Schmidt et al., 2010; Hengerer et al., 2019).

Dennoch sind sowohl die konventionellen chirurgischen Glaukomtherapien mittels Trabekulektomie und tiefer Sklerektomie, als auch die Implantation alloplastischer Glaukom Drainage Implantate (GDI) bei Betrachtung der Langzeiteffizienz mit Problemen behaftet. Die Langzeit-Erfolgsraten von Trabekulektomien liegen oft nur bei 40-50 % (Ehrnrooth et al., 2002; Gedde et al., 2012). Oft werden durch einen erneuten Anstieg des IOD zusätzliche Interventionen zur Drucksenkung notwendig. Im Falle der implantatbasierten Therapien sind inadäquate IOD-Senkungen, Hypotonie, eine Ablatio der Choroidea oder Retina sowie Implantatdislokationen oder -erosionen als schwerwiegende Komplikationen zu nennen. Die Komplikationsrate liegt bei diesen Therapiekonzepten bei ca. 50 % (Valimaki et al., 1998; Valimaki, 2012; Rolim de Moura et al., 2005; Christakis et al., 2013).

Die Hauptursache für das Versagen der chirurgischen Verfahren ist jedoch eine oftmals nicht steuerbare, überschießende Narbenbildung im Heilungsverlauf, was zu einer Zunahme des Abflusswiderstandes oder einem vollständigen Verschluss der neu geschaffenen Abflusswege im anterioren Segment führen kann. Ein erneuter Anstieg des IOD und das Scheitern der Therapie ist dann zu erwarten (Yamanaka et al., 2015; Lockwood et al., 2013; Smith et al., 2019). Die einsetzenden Wundheilungsmechanismen nach chirurgischen Interventionen sind dabei mit mehrphasigen Reaktionen des Körpers bzw.

Implantationsgewebes assoziiert. In der inflammatorischen Phase werden durch Blutgerinnungsprozesse direkt nach dem Eingriff pro-inflammatorische Zellen chemotaktisch rekrutiert, welche wiederum Wachstumsfaktoren sezernieren, die überwiegend Bindegewebszellen (Fibroblasten) aktivieren, die daraufhin zu Myofibroblasten differenzieren. In der Proliferationsphase kommt es zu einer verstärkten Zellteilung der Myofibroblasten. Zudem führen sie durch ihre Kontraktilität und eine gesteigerte Proteinsynthese von Komponenten der extrazellulären Matrix (EZM) zum Verschluss der Wunde (Narbenbildung). In der Remodulationsphase wird die EZM wieder umgestaltet und an die Gewebeeigenschaften angepasst (Eming et al., 2014; Krzyszczyk et al., 2018).

Eine andauernde Narbenbildung im Verlauf einer postoperativen Gewebereparatur oder als Reaktion gegen ein Implantat wird als Fibrose bezeichnet. Um die Fibrosierung in der fistulierenden Glaukomtherapie zu verhindern werden derzeit Zytostatika verwendet, welche die Proliferation von für die Fibrose verantwortlichen Fibroblasten und deren Transformation in Myofibroblasten hemmen, wodurch die Narbenbildung verlangsamt bzw. unterbunden wird und so die Funktionalität der geschaffenen Abflusswege längerfristig aufrechterhalten wird. Es kommen hauptsächlich die Pharmaka Mitomycin C (MMC) sowie 5-Fluoruracil (5-FU) zur Anwendung, beide inhibieren die Zellteilung der Fibroblasten (Mostafaei, 2011). Durch die Unspezifität der zytostatischen Wirkung ist die Anwendung dieser Pharmaka jedoch mit Nebenwirkungen assoziiert (Dunn et al., 1991; Hovakimyan et al., 2015; Mearza et al., 2007; Sauder et al., 2006), welche oftmals einen erneuten operativen Eingriff erfordern (Abb. 1).

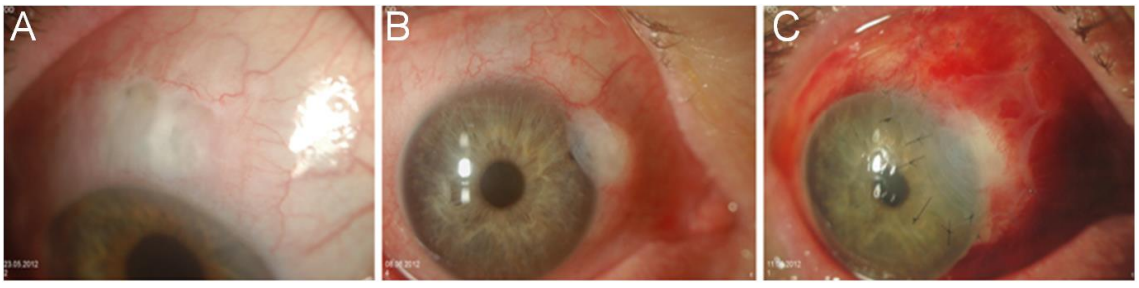

Abb. 1: Postoperative Komplikationen von MMC behandelten Sickerkissen nach Trabekulektomie.
A: *Noch intaktes Sickerkissen mit MMC bedingtem Gewebsverlust der Sklera und bereits durchschimmernder Choroidea. Die deckelnde Konjunktiva weist bereits einen Gefäßverlust auf.* ***B:*** *Nach einer Trabekulektomie mit intraoperativer MMC-Applikation rupturiertes Sickerkissen.* ***C:*** *Rupturiertes Sickerkissen von b nach erfolgtem Amnion-Verschluss. (Quelle: Postoperative Befunde der Universitätsaugenklinik Rostock)*

Die häufig auftretenden postoperativen Komplikationen durch die derzeit verwendeten Zytostatika machen alternative chirurgische Therapieansätze erforderlich. Dabei stehen Konzepte im Fokus, die spezifisch die Transformation von Fibroblasten in Myofibroblasten oder die Sekretion von Komponenten der EZM inhibieren und somit dem überschießenden postoperativen Vernarbungsprozessen entgegenwirken. Neuere Strategien zur spezifischen Hemmung von fibrotischen Prozessen fokussieren auf die Inhibition der durch Zytokine vermittelten Zellkommunikation, wodurch eine Zellaktivierung verhindert werden kann. Eines der Schlüsselzytokine in Wundheilungsprozessen ist der *transforming growth factor beta* (TGF-β), welcher die Transformation von Fibroblasten zu Myofibroblasten induziert und zu einer gesteigerten Proliferationsrate sowie zur erhöhten Sekretion von EZM-Komponenten durch Zellen führt (Park et al., 2013; Stahnke et al., 2012).

Neu entwickelte Substanzen, welche die durch TGF-β vermittelte Signalweiterleitung unterdrücken, könnten auch in der fistulierenden Glaukomchirurgie Nebenwirkungen minimieren und zu einem langandauernden funktionellen Erhalt der angelegten Drainagewege führen. Der Ansatz der spezifischen Inhibition fibrotischer Prozesse ist auch bei der Entwicklung neuer alloplastischer GDI von besonders hoher Relevanz, da deren Bedeutung gegenüber der Trabekulektomie, dem bisherigen Goldstandard der konventionellen chirurgischen Glaukomtherapie, stetig zunimmt (Gedde et al., 2012). Dabei geht der Trend zu immer kleineren, minimalinvasiv zu implantierenden Mikroimplantaten, die (Lavia et al., 2017; Pillunat et al., 2017; Hengerer et al., 2019). Die minimalinvasive chirurgische Implantation verschiedener Mikroimplantate wird unter dem Begriff Mikroinvasive Glaukomchirurgie (MIGS) zusammengefasst. Die gegenwärtig am Markt befindlichen Implantate nutzen dabei unterschiedliche Drainageräume, um das Kammerwasser aus der Vorderkammer abzuleiten. Während die Mikroimplantate häufig unter die Bindehaut in den subkonlunktivalen Raum drainieren (z.B. EX-PRESS®, XEN® Gel Stent, XEN45®, InnFocus®), wird auch der Schlemm-Kanal (iStent®, iStent Inject®, Hydrus™) sowie der suprachoroidale Raum (z.B. SOLX® Gold Shunt, iStent Supra®, CyPass®) aufgrund seines im Vergleich zur Vorderkammer geringeren Drucks als Drainageraum einiger Implantate verwendet (Lenzhofer et al., 2018; Kammer und Mundy, 2015).

Das häufige Auftreten von Komplikationen mit kornealer Dekompensation hat inzwischen dazu geführt, dass das CyPass®-Implantat wieder vom Markt genommen wurde.
Allen zurzeit auf dem Markt befindlichen Mikroimplantaten ist gemein, dass ihnen eine pharmakologische Funktionalisierung fehlt. Ein Einsatz entsprechender Pharmaka als Bestandteil der Implantate kann dazu dienen fibrotische Prozesse zu unterdrücken und dadurch die Implantatfunktionalität langfristig zu erhalten. In eigenen Studien konnte gezeigt werden, dass sich die Fibroblasten-Subpopulationen unterschiedlicher Gewebe entsprechend der Drainageräume zwar hinsichtlich ihres Expressionsmusters von Proteinen der EZM unterscheiden, sie aber dennoch alle das Potenzial für fibrotische Prozesse aufweisen (Stahnke et al., 2012; Stahnke et al., 2017).
Das Prinzip, Mikroimplantate direkt als antifibrotische Drug-Delivery-Systeme (DDS) zu nutzen, wurde bereits in Studien untersucht. Dabei wurde hauptsächlich auf die bereits bekannten und mit Nebenwirkungen assoziierten Zytostatika MMC und 5-FU fokussiert (Hovakimyan et al., 2015; Ponnusamy et al., 2013; Yuan et al., 2019). Mikroimplantate mit einer antifibrotischen Funktionalisierung, welche spezifisch in die Zellkommunikation eingreift ohne ungewollte Nebenwirkungen zu verursachen, befinden sich bereits in eigenen Forschungsvorhaben in der Entwicklung (Siewert et al., 2017; Stahnke et al., 2018). In diesem Zusammenhang wurden die anatomischen Mikrostrukturen des Implantationsortes mittels verschiedener Bildgebungsmodalitäten näher untersucht und charakterisiert (Stahnke et al., 2016). Ziel dieser Konzepte war es, durch lokale Freisetzung antifibrotischer Pharmaka nach der GDI-Implantation, die Wundheilungsprozesse gezielt über eine Inhibition der Fibroblasten zu modulieren und in der Folge eine langfristige Verbesserung der Prognose zu gewährleisten.
Um die Langzeitfunktionalität implantierter GDI-DDS analysieren zu können, werden tierexperimentelle Glaukommodelle benötigt. In diversen Kaninchenstudien unserer Arbeitsgruppe konnten alle die in der Literatur beschriebenen Glaukommodelle nicht reproduziert werden (Allemann et al., 2013). Daher wurde, parallel zur eigenen GDI-Entwicklung, die Okulopressionstonometrie (OPT) nach Ulrich an ein Kaninchenmodell *in vivo* adaptiert (Stahnke et al., 2015). Dieses nicht invasive Verfahren wurde zur Ermittlung des okulären Perfusionsdrucks und der Durchblutungsregulation entwickelt (Ulrich und Ulrich, 1985; Ulrich et al., 2015). Die Methode führt durch ein am Bulbus angelegtes Vakuum zu einer spezifischen Bulbusdeformation, woraus ein definierter

Anstieg des IOD über einen festgelegten Zeitraum resultiert. Durch die erfolgreiche Adaptation steht nun ein reproduzierbares Verfahren zur Verfügung, mit dem der IOD definiert, temporär erhöht werden kann. Während das Vakuum anliegt werden zeitgleich IOD Messungen durchgeführt, wodurch die Abflussleichtigkeit des Kammerwassers ermittelt werden kann. Dies erlaubt eine postoperative Beurteilung der Langzeitfunktionalität von GDI (Stahnke et al., 2015).
Weiterhin wird neben der inhibitorischen Modulation der TGF-β Signalkaskade bei der Weiterentwicklung des GDI-DDS auch die Identifikation anderer Zytokine und durch sie vermittelte Signalwege, die einen Einfluss auf die Transformation, Proliferation und EZM-Syntheseleistung von Fibroblasten zeigen, verfolgt (Gajda-Derylo und Stahnke et al., 2019). Eine umfassendere Modulation der komplexen Signalprozesse in Wundheilungs- bzw. Vernarbungsreaktionen kann die Effektivität der Fibroseinhibition nach fistulierender oder minimalinvasiver Glaukomchirurgie noch deutlich steigern. Eine Projektion auf andere Gewebe bzw. Fibrose-assoziierte Pathologien des vorderen Augenabschnitts ist ebenfalls möglich.

2. Fibrotische Wundheilungsmechanismen der Kornea

Die Hornhaut (Kornea) des Auges ist die transparente, anteriore Bulbuswand und maßgeblich an der Brechung und Fokussierung einfallenden Lichts auf die Retina beteiligt. Durch Traumata, chirurgische Interventionen oder Infektionen induzierte Wundheilungsprozesse können auch hier zu fibrotischen Reaktionen führen (Torricelli et al., 2016). Innerhalb der Kornea stattfindende Fibrose kann bei ausbleibenden Therapiemaßnahmen zu einem Verlust der kornealen Tranzparenz führen, welche bis zur vollständigen stromalen Eintrübung und somit zur Erblindung fortschreiten kann (Wilson et al., 2012). Mit weltweit über 10 Millionen Betroffenen, von denen 90 % eine permanente Fibrose und Neovaskularisation der Kornea aufweisen, stellt diese Pathologie die zweithäufigste Erblindungsursache dar (Wilson et al., 2012). Derzeit stehen nur die Transplantation einer Spenderkornea oder die Implantation alloplastischer Systeme oder autoplastischer Implantate als Therapieoptionen zur Verfügung.
Einen entscheidenden Faktor für fibrotische Prozesse in der Kornea scheinen Störungen in der kornealen Integrität, speziell der Verlust der Barrierefunktionen der anterioren Basalmembran (Bowman Membran) sowie der posterioren Basalmembran (Descemet

Membran), darzustellen (Wilson et al., 2017). Verletzungen innerhalb beider Membransysteme führen zu einem Zusammenbruch der Homöostase. Dadurch können die zuvor strikt voneinander getrennten und vollkommen unterschiedlichen Zelltypen in Kontakt treten und auch mit Zytokinen in Verbindung kommen, die eine Aktivierung fibrotischer Prozesse in den Zellen auslösen können (Medeiros et al., 2018).

Im Falle der stromalen Keratozyten, eine spezielle Fibroblasten-Subpopulation, welche für die Aufrechterhaltung der strikt organisierten EZM und der damit assoziierten Transparenz der Kornea verantwortlich ist, kann eine Aktivierung und Transformation in Myofibroblasten mit gesteigerter Proteinsynthese eine korneale Eintrübung verursachen (Simirskii, 2014). Auch korneale Epithel- und Endothelzellen können durch Zytokine und Botenstoffe vermittelte Kommunikationsprozesse über die Epithelial-mesenchymale Transition (EMT) in Myofibroblasten redifferenzieren (Hinz et al., 2007). Abbildung 2 veranschaulicht die Transition der Epithel- bzw. Endothelzellen sowie die Transformationen von Zellen anderer Gewebe in Myofibroblasten, welche beide durch die für die Migrationsfähigkeit der Zellen notwendige Expression von *alpha-smooth muscle actin* (α-SMA) gekennzeichnet sind. Als Voraussetzung für die Migrationsfähigkeit der entstehenden Myofibroblasten verlieren sowohl die Epithel- als auch die Endothelzellen während der EMT ihre Polarisierung. Die EMT stellt einen grundlegenden Heilungsmechanismus der Kornea dar, welcher für die Restitution der Barrierefunktionen und für die Normalisierung der stromalen Hydratation essenziell ist (Rieck et al., 2003). Weiterhin ist sie für die Regeneration der kornealen stromalen Nerven sowie des subbasalen Nervenplexus der Kornea von entscheidender Bedeutung, deren sezernierte Zytokine wiederum die epitheliale Wundheilung begünstigen (Kowtharapu und Stahnke et al., 2014). Dennoch kann eine andauernde Stimulation der Epithel-/Endothelzellen, verursacht durch eine unvollständige Rekonstruktion der Basalmembranen und damit zusammenhängender fehlender Barrierefunktion, eine korneale Fibrose begünstigen.

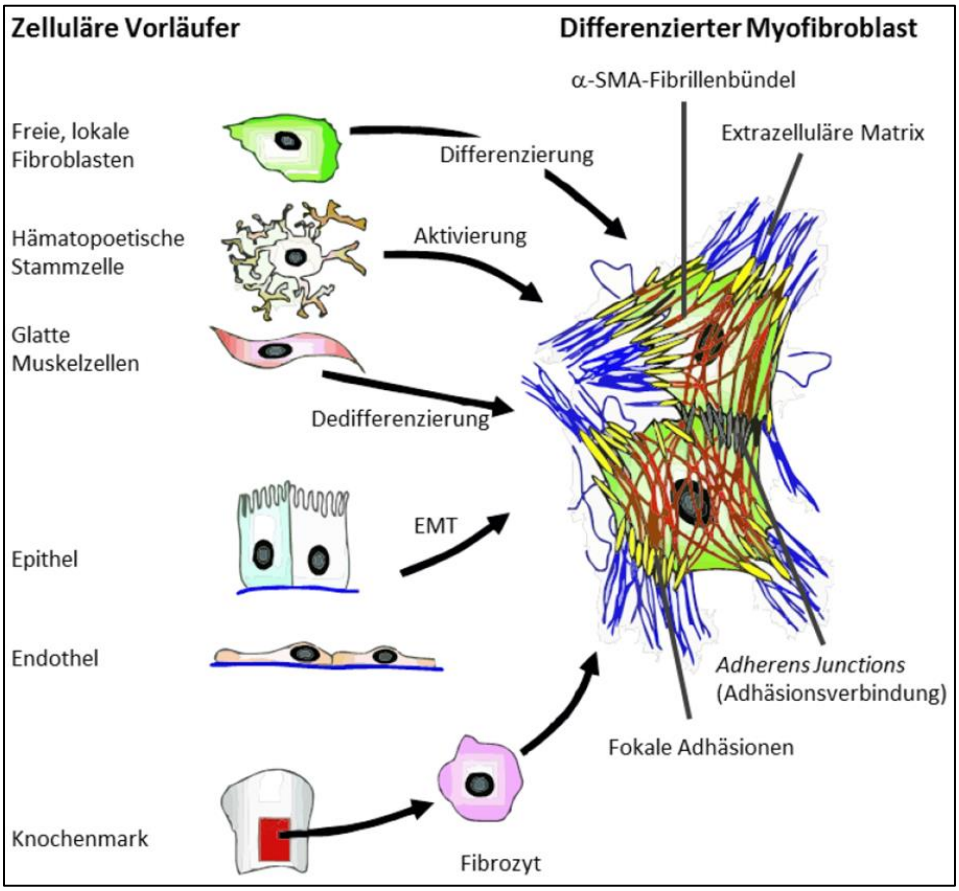

Abb. 2: Schematische Darstellung zellulärer Transformationsmechanismen zu Myofibroblasten.
Fibrotische Prozesse während der Wundheilung sind die Hauptursache für den Funktionsverlust eines heilenden Gewebes oder eines Implantates. Die Fibrose ist eine pathologische Vermehrung von Myofibroblasten und deren Überproduktion von Proteinen der extrazellulären Matrix. Myofibroblasten können aus diversen Zelltypen (freie lokale Fibroblasten, hämatopoetische Stammzellen, glatte Muskelzellen, Epithelzellen, Endothelzellen, Knochenmarkszellen) in unterschiedlichen Geweben bzw. Organsystemen entstehen. Somit können auch nahezu alle Gewebe bei Wundheilungsprozessen durch Fibrose beeinträchtigt werden. (modifiziert nach Hinz et al., 2007).

3. Kataraktchirurgie als Initiator der Epithelial-mesenchymalen Transition

Neben fibrotischen Prozessen in der Kornea spielt die EMT auch bei dem Grauen Star (Katarakt) eine entscheidende Rolle. Die Katarakt ist global betrachtet die häufigste Erblindungsursache, führt aber in den Industrienationen dank erfolgreicher Operationsmöglichkeiten selten zur Erblindung. In Deutschland stellt die Katarakt lediglich 2 % aller Erblindungsursachen dar (DOG-Weißbuch, 2012), obwohl die geschätzte Prävalenz bei ca. 1 Million Erkrankten liegt (Congdon et al., 2004). Im Verlauf der Katarakt entwickelt sich eine zunehmende Eintrübung der Augenlinse, wodurch die Transparenz progredient abnimmt, was bei ausbleibender Linsenersatztherapie zur Blindheit führt. Die Ursachen für den Verlust der Transparenz der Linse sind vielfältig und umfassen

neben verschiedenen Risikofaktoren wie Stoffwechselerkrankungen und Diabetes mellitus auch Drogen- und Tabakkonsum, Traumata, Mangelernährung, genetische Dispositionen, UV-Expositionen, oxidativen Stress, den normalen Alterungsprozess, sowie Augenentzündungen und andere Augenerkrankungen wie bspw. das Glaukom (Agarwal et al., 2013; Cheng, 1989; Khokhar et al., 2017; Pollreisz et al., 2010; Roberts et al., 2001). Aufgrund der unterschiedlichen Genese wird die Katarakt in (i) altersbedingte, (ii) kindliche, (iii) sekundäre und (iiii) traumatische Katarakt unterteilt.

Die derzeit einzige Therapie zur Behandlung der Katarakt ist die operative Resektion der trüben Linse mit anschließender Implantation einer alloplastischen Intraokularlinse (IOL), meist in den erhaltenen, natürlichen Kapselsack. Dieses Therapieverfahren ist die weltweit häufigste Operation, allein in Deutschland liegt die Zahl durchgeführter Eingriffe bei 650.000 jährlich (DOG-Weißbuch, 2012; Kohnen, 2008). Neben dem Verlust der Akkommodationsfähigkeit sind postoperativ auftretende fibrotische Prozesse, sogenannter Nachstar, die häufigste Komplikation dieses Therapieverfahrens. Die Inzidenz des Nachstars liegt bei 10-30 % (Lee et al., 2016). Zur Entfernung des fibrotischen Gewebes und der posterioren Linsenkapsel wird in der Regel eine Nd-YAG-Laserkapsulotomie als sichere und effektive Methode eingesetzt, um die optische Achse wieder zu bereinigen (Lee et al., 2016).

Der Nachstar wird durch bei der Linsenresektion im Kapselsack verbliebene Linsenepithelzellen hervorgerufen. Das einschichtige Linsenepithel ist lediglich im anterioren Linsensegment lokalisiert (Stahnke et al., 2016) und für die Bildung des Kapselsacks (Basalmembran der Linsenepithelzellen) während der Embryogenese verantwortlich. Bei der Phakoemulsifikation am Kapselsack verbliebene Linsenepithelzellen durchlaufen durch den Verlust der Barrierefunktion, ähnlich wie in der Kornea stimuliert durch Zytokine und Botenstoffe, den Prozess der EMT (Boswell et al., 2017). Die damit zusammenhängende gesteigerte Proliferationsrate und erhöhte Synthese von EZM-Komponenten wie Fibronektin und verschiedenen Kollagenen führt zur vollständigen und meist mehrschichtigen Besiedelung des gesamten verbliebenen posterioren Kapselsacks, woraus eine posteriore kapsuläre Eintrübung (PCO) resultiert. Das dabei entstehende fibrotische Gewebe ist nicht mehr transparent und verursacht beim Erreichen der optischen Achse einen entsprechenden Visusabfall, der bei ausbleibender Laserkapsulotomie bis zur erneuten Erblindung fortschreiten kann.

Das derzeit einzige bekannte Zytokin, was in einem Großteil der beschriebenen experimentellen PCO-Modellsystemen (primäre Linsenepithelzellen der Ratte, Linsenepithelzelllinien, primäre humane Linsenepithelzellen) eine EMT und die Entstehung von α-SMA positiven Myofibroblasten induziert, ist TGF-β (Wormstone et al., 2006; Wormstone und Eldred, 2016). Spezifisch in die Zellkommunikation eingreifende Pharmaka bzw. Therapiekonzepte könnten also neben der fistulierenden sowie minimalinvasiven Glaukomchirurgie sowohl in der Nachstarprophylaxe als auch bei fibrotischen Prozessen der Kornea die Wundheilungsmechanismen positiv beeinflussen, Nebenwirkungen reduzieren und überschießende Vernarbungsreaktionen verhindern. Eine intraoperative Applikation oder Freisetzung entsprechender Pharmaka aus Implantaten mit lokaler Drug Delivery (LDD)-Funktion zur Wundheilungsmodulation eröffnet also in allen drei Anwendungsfeldern Möglichkeiten, die Langzeitfunktionalität der Implantate zu garantieren, Sekundäreingriffe zu vermeiden und den Visus zu erhalten.

Fragestellung

Chirurgische Interventionen im anterioren Segment des Auges stellen oftmals die einzige Therapieoption zur Behandlung häufig auftretender Augenerkrankungen oder Traumata dar. Je nach Art des chirurgischen Eingriffs sind postoperative Wundheilungsprozesse meistens gewünscht; es existieren jedoch Operationstechniken, bei denen eine postoperative Wundheilung minimiert werden muss, um den Langzeiterfolg des chirurgischen Eingriffs zu garantieren. In Bezug auf die postoperativen Wundheilungsmechanismen des anterioren Segments des Auges ergeben sich daraus im Wesentlichen drei praxisrelevante Anwendungsfelder, auf die sich die vorliegenden Arbeiten konzentrieren.

1. Spezifische Inhibition fibrotischer Prozesse nach fistulierender Glaukomchirurgie

Überschießende postoperative Wundheilungsprozesse sowie Vernarbungsreaktionen führen in der fistulierenden Glaukomchirurgie häufig zum Versagen der jeweiligen Therapiekonzepte und erfordern erneute chirurgische Interventionen im Rahmen der klinischen Nachsorge. Die derzeit in der Anwendung befindlichen Zytostatika zur Vermeidung postoperativer Fibrose sind aufgrund ihrer unspezifischen Wirkungsmechanismen häufig mit Nebenwirkungen assoziiert. Es stellte sich daher die Frage, ob es Möglichkeiten einer spezifischen Wundheilungsmodulation gibt, mit denen neben dem langfristigen Erhalt der neu geschaffenen Abflusswege zusätzlich die Nebenwirkungen reduziert werden können. Insbesondere ist die Frage zu stellen, ob es sogar möglich ist, ausschließlich die für die Fibrose verantwortlichen Fibroblasten und deren Transformation in Myofibroblasten zu inhibieren. Somit wurde ein Fokus auf interzelluläre Signalkaskaden gelegt, die es zunächst in *in vitro* Experimenten zu identifizieren galt. Anhand identifizierter Signalmoleküle und deren Inhibition wurden die Auswirkungen auf die Proliferation, die Viabilität sowie die Synthese von EZM-Proteinen durch okulare Fibroblasten bewertet und final im Tierexperiment evaluiert.

2. Fibroseprävention in der Kornea

In der Kornea können Wundheilungsprozesse zu einer fibrotischen Reaktion führen, welche oftmals mit einer kornealen Eintrübung einhergeht und bei ausbleibender The-

rapie bis zur Erblindung fortschreitet. Diese sehr häufige Erblindungsursache beruht größtenteils auf dem Verlust der Barrierefunktionen der anterioren und posterioren Basalmembranen (Bowman- und Descemet Membran) der Kornea, wodurch es zu unphysiologischen Kontakten zwischen eigentlich voneinander getrennten Zelltypen sowie differenziellen Zytokinen und Botenstoffen kommen kann. Neben den aktivierten Keratozyten können sowohl die Epithel- als auch die Endothelzellen über die EMT in Myofibroblasten redifferenzieren und zur Fibrose beitragen. Die dabei neu synthetisierte EZM unterliegt nicht der zuvor strikt organisierten EZM-Struktur des Stromas und führt zum Transparenzverlust der Kornea. Es stellte sich also die Frage, welche Faktoren die zelluläre Kommunikation zwischen trigeminalen Neuronen und kornealen Epithelzellen vermitteln und welchen Einfluss die Zytokine und Botenstoffe auf das Regenerationsverhalten der unterschiedlichen Zelltypen in der kornealen Wundheilung ausüben. Die Identifizierung spezieller Faktoren könnte Möglichkeiten einer spezifischen kornealen Wundheilungsmodulation bieten, um in kornealen Wundheilungsprozessen die Barrierefunktionen und somit die Integrität des kornealen Gewebes schnellstmöglich zu regenerieren.

3. Nachstarprophylaxe

Die durch unterschiedliche Ursachen induzierte Eintrübung der humanen Linse, die Katarakt, ist global die häufigste Erblindungsursache und kann derzeit nur durch eine chirurgische Intervention, die Resektion der trüben Linse mit anschließender Implantation einer alloplastischen IOL, therapiert werden. Im postoperativen Verlauf kann es zur Ausprägung eines Nachstars kommen, der durch die unkontrollierte Proliferation verbliebener Linsenepithelzellen hervorgerufen wird. Diese können über die EMT in Myofibroblasten redifferenzieren, welche sich durch Migrationfähigkeit, eine gesteigerte Proliferationsrate sowie eine erhöhte Syntheseleistung von Proteinen der EZM auszeichnen. Dieser fibrotische Prozess und das dabei entstehende fibrotische Gewebe können zum erneuten Transparenzverlust und einem daraus resultierenden Visusabfall führen. Das Ziel der vorliegenden Arbeit war es daher, zunächst den gesamten Akkommodationsapparat sowie die Linse des humanen Auges mit Hilfe dedizierter Bildgebungsmodalitäten hinsichtlich relevanter anatomischer Strukturen zu visualisieren sowie charakterisieren und mit der klassischen Histologie zu vergleichen. Aufgrund geringer

Eindringtiefen der Ultraschallbiomikroskopie und der Lichtundurchlässigkeit des Irisepithels, was Licht-/Laser-basierte Untersuchungsverfahren in der Darstellung der gesamten Linse limitiert, wurde die Ultrahochfeld-Magnetresonanzmikroskopie (UHF-MRM) als Bildgebungsverfahren gewählt. In einem nächsten Schritt sollen die Erkenntnisse in den Entwicklungsprozess eines akkommodationsfähigen Linsenersatzimplantates mit implementiertem antifibrotischen Pharmakon, als Nachstarprophylaxe, einfließen.

Originalarbeiten

1. Unterschiedliche Fibroblasten-Subpopulationen des Auges: Therapeutisches Ziel zur Vermeidung postoperativer Fibrose in der Glaukomchirurgie.

Stahnke T, Löbler M, Kastner C, Stachs O, Wree A, Sternberg K, Schmitz KP, Guthoff R. Different fibroblast subpopulations of the eye: a therapeutic target to prevent post-operative fibrosis in glaucoma therapy. Experimental Eye Research. 2012, 100:88-97. DOI: 10.1016/j.exer.2012.04.015.

Fragestellung: Mögliche Behandlungsmethoden des Glaukoms sind fistulierende chirurgische Eingriffe wie die Trabekulektomie oder die Implantation von Mikrostents, welche den IOD regulieren und das Kammerwasser in unterschiedliche Drainageräume ableiten. Fibrotische Prozesse können zu einem Versagen beider Therapiekonzepte führen und sind durch die Proliferation sowie die verstärkte Synthese von Komponenten der EZM von Fibroblasten gekennzeichnet. Die TGF-β Signalkaskade spielt eine entscheidende Rolle bei der Regulation von Proliferationsprozessen sowie der Expression von EZM-Proteinen. Innerhalb dieser Studie sollten verschiedene primäre humane okulare Fibroblasten-Subpopulationen hinsichtlich ihres Expressionsmusters charakterisiert und möglicher Inhibitionsmechanismen evaluiert werden.

Material und Methoden: Um die Fibrose näher zu charakterisieren, wurden verschiedene primäre humane okulare Fibroblasten-Subpopulationen (Sklera (hSF), Choroidea (hCF), Tenonkapsel (hTF), intrakonaler Fettkörper (hOF)) der möglichen Drainageräume isoliert und kultiviert. Die Zellen wurden mittels 1-D SDS-PAGE mit anschließendem Western Blot analysiert, um quantitative Unterschiede innerhalb der einzelnen Fibroblasten-Subpopulationen auf Proteinebene aufzuzeigen. Durch die Methode der indirekten Immunfluoreszenz konnten Aussagen über die Lokalisation und Organisation der Proteine gemacht werden. Zusätzlich wurden die Wirkungskurven der Zytostatika MMC und Paclitaxel (PTX) durch Viabilitäts- (CellQuanti-Blue) und Proliferations-Assays (BrdU) ermittelt.

Ergebnisse: Es wurde gezeigt, dass alle analysierten okularen Fibroblasten-Subpopulationen die für fibrotische Prozesse relevanten EZM-Proteine Fibronektin, verschiedene Mitglieder der Kollagenfamilie (Kollagen I, III, VI) sowie TGF-β1 exprimieren. Dabei konnten Unterschiede in den synthetisierten Proteinmengen zwischen

den einzelnen Fibroblasten-Subpopulationen beobachtet werden. Neben der quantitativen Bestimmung der synthetisierten Proteine im Western Blot (Abb. 3) wurde die extrazelluläre Sekretion und Organisation der EZM-Proteine evaluiert (Abb. 4). Die Auswertung der Zytotoxizitätsassays ermöglichte zudem eine Bestimmung der therapeutischen Fenster der Zytostatika MMC und PTX.

Schlussfolgerungen: Alle Fibroblasten-Subpopulationen der möglichen Drainageräume besitzen das Potenzial durch eine gesteigerte EZM-Synthese zu einem Versagen der neu geschaffenen Abflusswege in der fistulierenden Glaukomtherapie zu führen. Diese fibrotischen Prozesse können durch die unspezifisch wirkenden Zytostatika MMC und PTX zwar inhibiert werden, die Unspezifität der Inhibitoren lässt jedoch durch die ungewollte Hemmung anderer Zellpopulationen Nebenwirkungen erwarten. Die dargestellte Expression des Zytokins TGF-β1 aller Fibroblasten-Subpopulationen eröffnet jedoch die Möglichkeit, spezifisch in die Wundheilungsmechanismen einzugreifen und postoperative fibrotische Prozesse ohne Nebenwirkungen zu inhibieren.

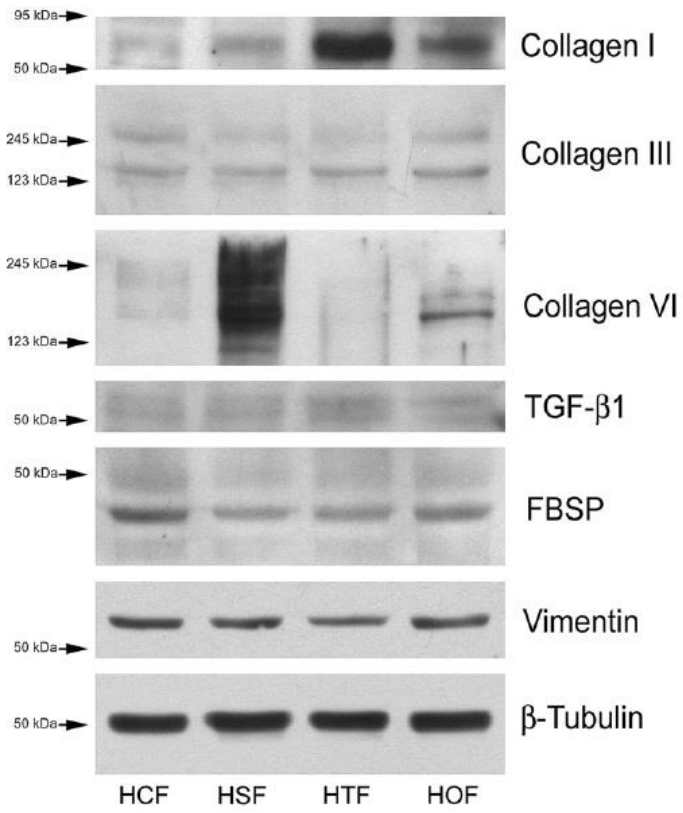

Abb. 3: Western Blot Analyse der primären okularen Fibroblasten-Subpopulationen.
Die Proteine der EZM (Kollagen I, III, VI; Fibronektin) werden von allen Fibroblasten-Subpopulationen exprimiert, unterscheiden sich aber in der synthetisierten Menge. Weiterhin wird das Zytokin TGF-β1 sowie das Fibroblasten-Spezifische-Oberflächenprotein (FBSP) synthetisiert. Das Zytoskelettprotein Vimentin verdeutlicht den mesenchymalen Ursprung der Zellen, β-Tubulin dient als Ladekontrolle.

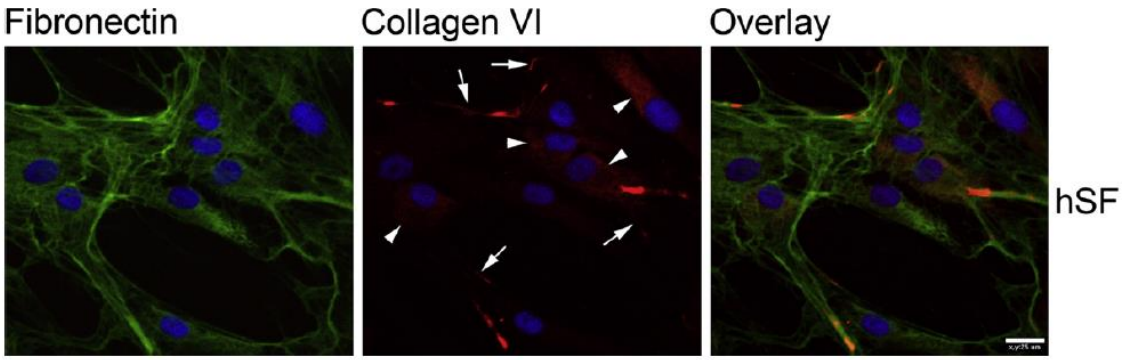

Abb. 4: Exemplarische Darstellung der intra- und extrazellulären Lokalisation synthetisierter EZM-Komponenten in hSF mittels indirekter Immunfluoreszenz.
Das synthetisierte Kollagen VI kommt sowohl intrazellulär (Pfeilspitzen) als auch sezerniert extrazellulär (Pfeile) vor. Sezerniertes Kollagen VI ist mit den Fibronektinfibrillen kolokalisiert. Messbalken: 25 µm.

2. Die Suppression der TGF-β Signalkaskade durch Pirfenidon vermindert die EZM-Sekretion in okularen Fibroblasten in vitro.

Stahnke T, Kowtharapu BS, Stachs O, Schmitz KP, Wurm J, Wree A, Guthoff RF, Hovakimyan M. Suppression of TGF-β pathway by pirfenidone decreases extracellular matrix deposition in ocular fibroblasts in vitro. PLoS One. 2017, 23;12(2):e0172592. DOI: 10.1371/journal.pone.0172592.

Fragestellung: Fibrotische Prozesse sind die Hauptursache für das postoperative Versagen der fistulierenden Glaukomchirurgie. Daher stellen neue Strategien bzw. Therapiekonzepte der Fibroseprävention eines der wichtigsten klinischen Ziele dar. In dieser Studie sollte evaluiert werden, ob der Wirkstoff Pirfenidon (PFD) in humanen primären okularen Fibroblasten-Subpopulationen antifibrotische Eigenschaften aufweist. Es ist bekannt, das PFD die Expression des Zytokins TGF-β senkt und somit die TGF-β-Signalkaskade, welche einen direkten Einfluss auf die Synthese fibroserelevanter EZM-Proteine aufweist, modulieren kann. Das Ziel dieser Studie war es daher, den Einfluss des Wirkstoffs PFD auf die EZM-Synthese verschiedener okularer Fibroblasten-Subpopulationen zu analysieren.

Material und Methoden: Zur Charakterisierung möglicher antifibrotischer Eigenschaften des Wirkstoffs PFD wurden verschiedene primäre humane okulare Fibroblasten-Subpopulationen (Tenonkapsel (hTF), intrakonaler Fettkörper (hOF)) isoliert und

kultiviert. Nach Inkubation der Zellen mit PFD wurde die EZM-Synthese mittels 1-D SDS-PAGE mit anschließendem Western Blot sowie der Methode der indirekten Immunfluoreszenz analysiert. Die Evaluierung relevanter Gene erfolgte durch rtPCR und zur Untersuchung des Einflusses des Wirkstoffs auf die Proliferationsrate wurden Proliferations-Assays (BrdU) verwendet.

Ergebnisse: Die alleinige Inkubation der Zellen mit dem Zytokin TGF-β1 führte in beiden Fibroblasten-Subpopulation zu einer gesteigerten Proliferationsrate. Weiterhin konnte eine Erhöhung der Genexpression fibroserelevanter Gene sowie der entsprechenden Proteine gezeigt werden. Die alleinige Inkubation mit dem Wirkstoff PFD wies hingegen nur einen geringen Einfluss auf die Proliferationsrate sowie die Synthese fibroserelevanter Proteine in beiden Fibroblasten-Subpopulationen auf. Nach kombinierter Applikaton des Zytokins und des Wirkstoffs (TGF-β1 und PFD) konnten hingegen inhibitorische Effekte in Bezug auf die Expression der Fibrose-Markerproteine Fibronektin und Kollagen I der EZM, sowie des Markerproteins α-SMA nachgewiesen werden (Abb. 5 und 6).

Schlussfolgerungen: Durch die Inkubation mit dem Zytokin TGF-β1 konnte ein fibrotisches Zellkulturmodell in humanen primären okularen Fibroblasten-Subpopulationen *in vitro* etabliert werden, welches viele relevante Eigenschaften fibrotischer Prozesse *in vivo* aufweist. Dieses fibrotische Zellkulturmodell eröffnet die Möglichkeit, antifibrotische Pharmaka hinsichtlich ihres antifibrotischen Potenzials *in vitro* zu evaluieren. Der Wirkstoff PFD konnte in diesem Zellkulturmodell seinen inhibitorischen Einfluss auf fibrotische Prozesse demonstrieren und scheint ein vielversprechendes Pharmakon für die spezifische Modulation von Wundheilungsmechanismen nach fistulierender Glaukomchirurgie darzustellen.

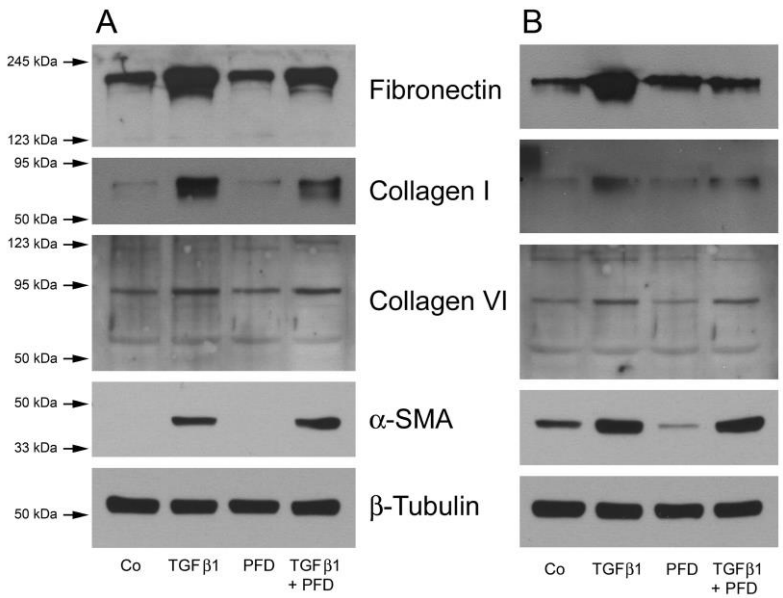

Abb. 5: Expressionsmuster fibroserelevanter Proteine primärer okularer Fibroblasten-Subpopulationen nach Stimulation und Inhibition.

*Die Stimulation der Zellen mit TGF-β1 führt zu einer gesteigerten Syntheserate der EZM-Proteine Kollagen I und VI sowie Fibronektin in **A** (hTF) und **B** (hOF). Auch das Fibrose-Markerprotein α-SMA wird verstärkt in beiden Subpopulationen exprimiert. PFD kann im Kombinationsansatz die gesteigerte Syntheseleistung reduzieren, aber nicht vollständig aufheben.*

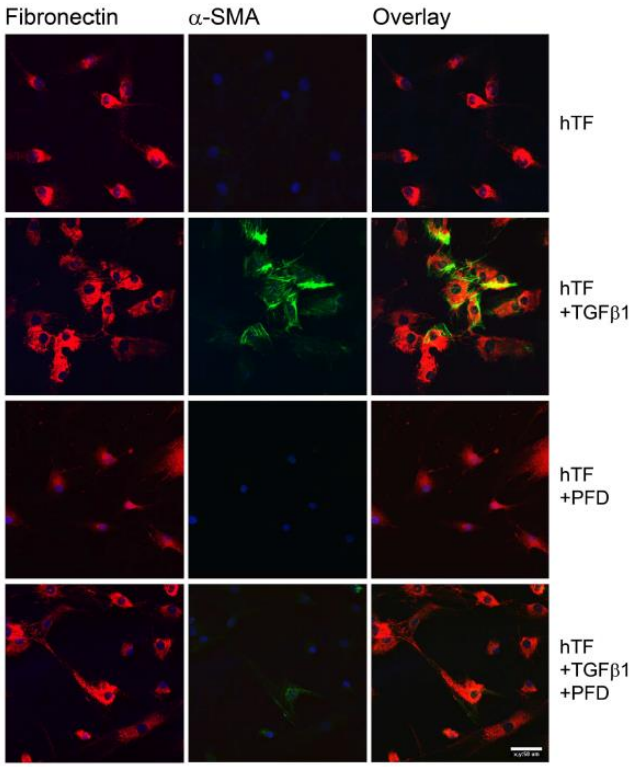

Abb. 6: Darstellung der Expression fibroserelevanter Proteine primärer okularer Fibroblasten-Subpopulationen nach Stimulation und Inhibition mittels indirekter Immunfluoreszenz.

Das Zytokin TGF-β1 bewirkt eine verstärkte Expression des EZM-Proteins Fibronektin sowie des Fibrose-Markerproteins α-SMA. Die Expression beider Proteine wird im Kombinationsansatz deutlich vermindert. Messbalken: 50 µm.

3. Entwicklung eines biodegradierbaren lokalen Drug Delivery Systems für Mikroglaukomstents.

Stahnke T, Siewert S, Reske T, Schmidt W, Schmitz KP, Grabow N, Guthoff RF, Wree A. Development of a biodegradable antifibrotic local drug delivery system for glaucoma microstents. Biosci Rep. 2018, 31;38(4). pii: BSR20180628. DOI: 10.1042/BSR20180628.

Fragestellung: Fibrotische Prozesse sind die häufigste Ursache für das Versagen implantierter GDI. In dieser Studie wurden GDI-Prototypen gefertigt und mit potenziellen antifibrotischen Wirkstoffen beschichtet. Neben einer Bestimmung der Wirkstofffreisetzungskinetik *in vitro* wurde ebenfalls die Wirkstofffreisetzung in einer tierexperimentellen Langzeitstudie *in vivo* evaluiert. Das Langzeit-Tierexperiment sollte zudem klären, welchen antifibrotischen Effekt die unterschiedlichen Pharmaka *in vivo* aufweisen.

Material und Methoden: GDI-Prototypen von 10 mm Länge wurden aus einem Bipolymer, bestehend aus poly(4-hydroxybutyrate) und ataktischem poly(3-hydroxybutyrate) im Verhältnis 1:1, gefertigt. Die Prüfkörper wurden mit einer LDD-Beschichtung versehen, die jeweils aus den Wirkstoffen PTX, Kaffeesäure-Phenethylester (CAPE) sowie PFD bestand. Unbeschichtete und beschichtete Prüfkörper wurden durch einen minimalinvasiven chirurgischen Eingriff in die subkutanen weißen Fettdepots der rechten Hinterläufe von Ratten (Wistar, Crl:WI BR, Charles River Wiga GmbH, Sulzfeld, Germany) implantiert und nach einem festgelegten Zeitschema bis zu sechs Monaten wieder explantiert. Die Gewebeexplantate, inklusive der unterschiedlichen Prüfkörper, wurden histologisch mit den Standardfärbungen AZAN und H&E sowie immunhistochemisch mit Antikörpern gegen fibrotische Markerproteine evaluiert. Die Bestimmung der Wirkstofffreisetzungskinetik *in vitro* und *in vivo* erfolgte mittels Hochdruckflüssigkeitschromatographie (HPLC).

Ergebnisse: Die *in vitro* Wirkstofffreisetzungsanalysen zeigten für alle LDD-Prüfkörper einen initialen „*burst release*“. Hingegen wurde der Wirkstoff PTX *in vivo* über einen langen Zeitraum freigesetzt, die Freisetzung der Wirkstoffe CAPE und PFD erfolgte innerhalb einer Woche nach der Implantation. Eine Woche postoperativ konnte mittels der histologischen Analysen eine massive Zellinfiltration bei allen GDI-Prototypen ohne und mit LDD-Beschichtung detektiert werden. Im Falle der PTX LDD

Systeme konnten zudem Gewebsveränderungen und Gewebsläsionen 1 und 2 Wochen nach der Implantation gezeigt werden (Abb. 7). Über den gesamten Zeitraum von sechs Monaten wurde um alle GDI-Prototypen eine fibrotische Kapsel gebildet. Die Auswertung der Kapseldicken zeigten, dass die unbeschichteten Implantate die stärkste fibrotische Reaktion verursachten, gefolgt von den mit PTX und CAPE beschichteten LDD Systemen. Die dünnste Kapseldicke, also die geringste fibrotische Reaktion wurde bei den LDD Systemen mit PFD Beschichtung gemessen (Abb. 8). Die immunhistochemische Auswertung konnte zudem demonstrieren, dass das fibrotische Gewebe in der Peripherie der Implantate erhöhte Mengen der fibrotischen Markerproteine Kollagen I, VI sowie Fibronektin aufweist.

Schlussfolgerung: Das Langzeit-Tierexperiment erlaubte die Evaluation fibrotischer Prozesse nach GDI-Implantation sowie des inhibitorischen Einflusses unterschiedlicher Pharmaka auf die Wundheilungsmechanismen. Während der Wirkstoff PTX mit gravierenden Nebenwirkungen assoziiert ist, kann mit den Wirkstoffen CAPE und PFD eine moderate Wundheilungsmodulation erzielt werden. Der Wirkstoff PFD zeigt in dieser Studie die effektivsten antifibrotischen Eigenschaften.

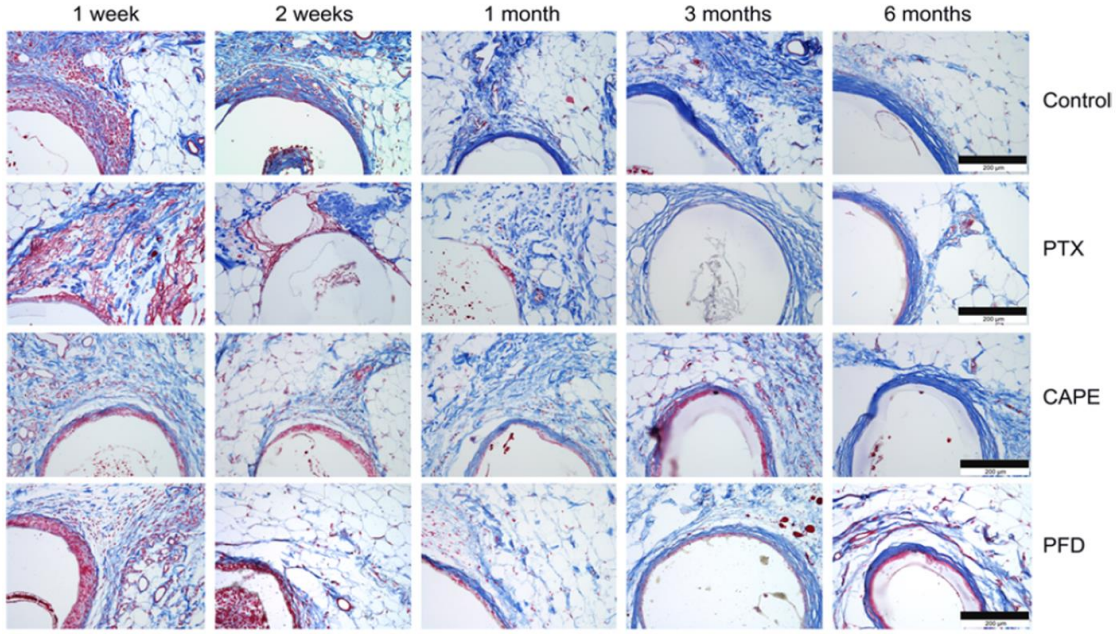

Abb. 7: Histologische Darstellung der subkutanen weißen Fettdepots der Ratte mit implantierten GDI-Prototypen. *Die Gewebe wurden zu den angegebenen Zeitpunkten entnommen, aufbereitet und mit AZAN gefärbt. Über den Zeitraum von sechs Monaten ist die Bildung von bindegewebsreichen fibrotischen Kapseln in der Peripherie der Implantate zu erkennen. Das PTX LDD führt in den ersten 2 Wochen nach Implantation zudem zu Gewebeschäden und Läsionen. Messbalken: 200 µm.*

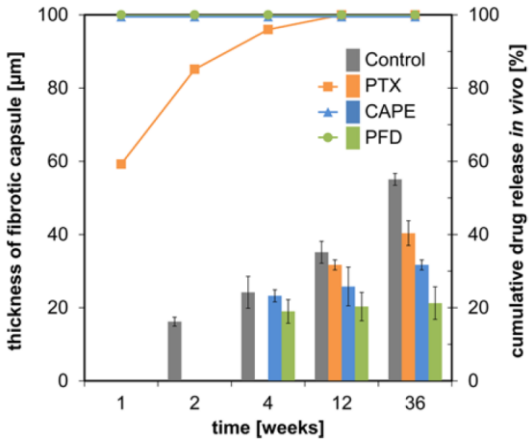

Abb. 8: Evaluierung der fibrotischen Gewebereaktion im Vergleich zur Wirkstofffreisetzung in vivo.
Die Auswertung der Dicke der fibrotischen Kapseln in µm erfolgte durch Vermessen histologischer Schnitte und ist auf der linken y-Achse aufgetragen. Die Wirkstofffreisetzung in vivo ist mit der gleichen Farbcodierung auf der rechten y-Achse aufgetragen. Die Wirkstoffe CAPE und PFD konnten bereits nach einer Woche nicht mehr nachgewiesen werden, die vollständige Freisetzung von PTX erfolgt hingegen zwischen der 4. und der 12. Woche postoperativ. Die fibrotischen Kapseln der PFD LDD Systeme sind nach 6 Monaten geringer ausgeprägt und weniger als halb so dick (21 µm) im Vergleich zu unbeschichteten GDI-Prototypen.

4. Anpassung und Etablierung der Okulopressionstonometrie als temporäres in vivo Kaninchen Glaukommodell.

Stahnke T, Siewert S, Walther E, Schmidt W, Stachs O, Schmitz KP, Guthoff RF. Adopting oculopressure tonometry as a transient in vivo rabbit glaucoma model. Current Directions in Biomedical Engineering. 2015, 1:127–130. DOI: 10.1515/cdbme-2015-0033.

Fragestellung: Kaninchen stellen in der ophthalmologischen Forschung aufgrund des Größenverhältnisses Körper zu Auge das bevorzugte Tiermodell dar. Es konnte jedoch in eigenen Studien gezeigt werden, dass alle in der Literatur beschriebenen Kaninchen Glaukommodelle nicht reproduzierbar oder ethisch nicht vertretbar waren (Allemann et al., 2013). Das Ziel dieser Studie war es daher, ein transientes Modellsystem zu etablieren, mit dem der IOD minimalinvasiv definiert erhöht werden kann. Dieses temporäre Glaukommodell soll dann in kommenden tierexperimentellen Studien zur Überprüfung der Langzeitfunktionalität implantierter GDI eine Anwendung finden.

Material und Methoden: Um die aus der Humanmedizin stammende nicht invasive Methode der Okulopressionstonometrie (OPT) nach Ulrich an die anatomischen Gegebenheiten des Kaninchenauges anzupassen, wurden zunächst Saugnapftrichter im kleineren Maßstab aus Polyoxymethylene (POM, SUSTARIN C, ThyssenKrupp Plastics

GmbH, Essen, Germany) gefertigt. Die gefertigten Trichter wurden dann in narkotisierten Kaninchen (New Zealand White Rabbit, Charles River Wiga GmbH, Sulzfeld, Germany) mittels der Saugnapftonometrie und parallel durchgeführter minütlicher IOD-Messung mit einem Icare® TAO1 Tonometer hinsichtlich der optimalen Größe evaluiert. In einem nächsten Schritt wurden nach dem gleichen Schema vielfache Messungen mit dem favorisierten Trichter durchgeführt, um eine standardisierte Methode eines transienten Glaukommodells zu etablieren.

Ergebnisse: Die Methode der OPT konnte erfolgreich auf das Auge des Kaninchens transferiert werden. Es konnte gezeigt werden, dass der Trichter mit einem Durchmesser von 11 mm für die Messung am Kaninchenauge am besten geeignet war (Abb. 9). Dieser Trichter wies auch ein ähnliches Trichter- zu Augendurchmesser-Verhältnis wie der Trichter mit einem Durchmesser von 13 mm aus der Humanmedizin auf. In der anschließenden Evaluierung des Messverfahrens konnte ein IOD von 45.8±14.2 mmHg für das rechte und 50.0±12.3 mmHg (n = 9) für das linke Auge nach einer Minute erreicht werden. Der IOD fiel dann kontinuierlich über die gesamte Messdauer von 9 Minuten auf IOD Werte von 29.9±13.3 mmHg im rechten- und 31.0±11.5 mmHg (n = 9) im linken Auge ab.

Schlussfolgerungen: Die Anpassung der OPT bzw. Saugnapftonometrie an das Kaninchenauge ermöglicht es den IOD definiert auf ein höheres Niveau zu heben. Es konnte somit ein transientes Glaukommodell im Kaninchen etabliert werden, welches in derzeit laufenden tierexperimentellen Studien zur Überprüfung der Langzeitfunktionalität implantierter GDI eine Anwendung findet.

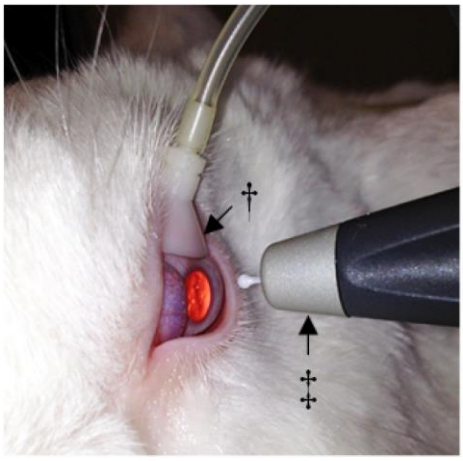

Abb. 9: IOD Messung mit dem Icare® rebound Tonometer TAO1 während der OPT.
Der limbusnah auf das Kaninchenauge aufgesetzte Saugnapftrichter (†) und das Tonometer (‡) sind dargestellt.

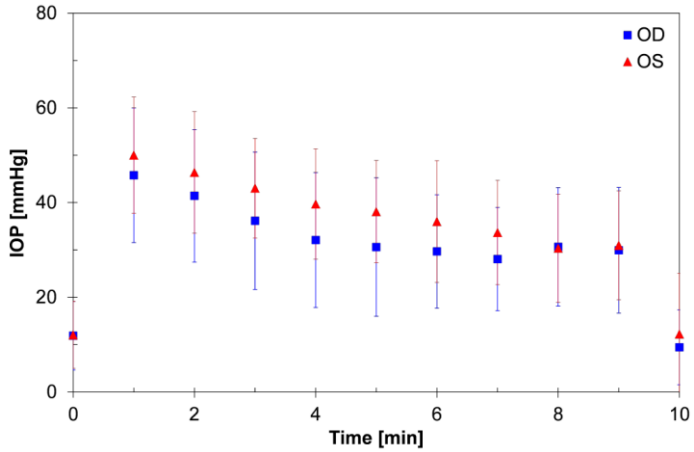

Abb. 10: IOD-Verlauf während der OPT unter Verwendung des Saugnapftrichters mit einem Durchmesser von 11 mm.
Während der 9 minütigen OPT wurde der IOD jede Minute mit dem Icare® am rechten Auge (OD) und am linken Auge (OS) gemessen. Über die Messdauer von 9 Minuten konnte eine Reduktion des IOD um 40 % in beiden Augen ermittelt werden.

5. Vergleichende Analyse der Zytokin/Chemokin-Level im Kammerwasser von Patienten mit primärem Offenwinkelglaukom nach Trabekulektomie mit positivem oder negativem Ergebnis.

Gajda-Deryło B, Stahnke T*, Struckmann S, Warsow G, Birke K, Birke MT, Hohberger B, Rejdak R, Fuellen G, Jünemann AG. Comparison of cytokine/chemokine levels in aqueous humor of primary open-angle glaucoma patients with positive or negative outcome following trabeculectomy. Biosci Rep. 2019, 2;39(5). pii: BSR20181894. DOI: 10.1042/BSR20181894. (* Autoren haben zu gleichen Teilen beigetragen).*

Fragestellung: Fibrotische Prozesse führen nach fistulierender Glaukomchirurgie wie der Trabekulektomie häufig zum Verschluss der neu angelegten Drainagewege und zum Versagen der Therapie. Das Ziel dieser Pilotstudie war es daher, den Zytokin/Chemokin-Level des Kammerwassers von Patienten mit primärem Offenwinkelglaukom (POAG) nach erfolgter Trabekulektomie zu evaluieren und zu vergleichen, wobei erfolgreiche und durch Fibrose fehlgeschlagene Eingriffe gegenübergestellt wurden.

Material und Methoden: Während der Trabekulektomie entnommene Kammerwasserproben, wobei darauf geachtet wurde eine Kontamination mit Blut zu vermeiden, bildeten die Grundlage dieser Studie. Alle Proben wurden mittels eines Zytokin-Antikörper-Arrays, welcher 274 differenzielle Proteine detektiert, analysiert (RayBio

Cytokine Antibody Array C Series 4000; RayBiotech, Inc, Norcross GA 30092, U.S.A.). Die Ergebnisse des Zytokin-Assays wurden basierend auf bekannten Eigenschaften der Proteine in profibrotische, inflammatorische, Adhäsion-vermittelnde und apoptotische Eigenschaften gruppiert. Die Unterschiede der Expressionsmuster beider Gruppen wurden im Anschluss mit der *ExprEssence* Software prozessiert, um neue Protein-Protein-Interaktionen zu identifizieren und diese zu visualisieren.

Ergebnisse: Die Analysen des Zytokin-Antikörper-Arrays zeigten, dass von den insgesamt 274 Proteinen in der Patientengruppe mit negativem Ergebnis (fibrotische Narbenbildung) 104 Proteine im Vergleich zur Patientengruppe mit positivem Ergebnis (keine postoperative Fibrose) signifikant hochreguliert und 27 Proteine signifikant runterreguliert wurden. Unter den hochregulierten Proteinen wurden Proteine mit profibrotischen Eigenschaften, wie z.B. die Wachstumsfaktoren *vascular endothelial growth factor* (VEGF), TGF-β und Knochen morphogenetische Proteine (BMP) detektiert.
Weiterhin wurden 49 für inflammatorische Prozesse verantwortliche Zytokine hochreguliert. Hier sind vor allem verschiedene Mitglieder der Familie der Interleukine (IL), das B-Zell reifende Antigen (BCMA) und der Granulozyten Kolonie-stimulierender Faktor (GCSF) zu nennen. Zusätzlich wurden aber auch adhäsionsvermittelnde Proteine wie bspw. Mitglieder der Gruppe der Interzellulären Adhäsions-Moleküle (ICAM) sowie Matrix Metalloproteinasen (MMP) hochreguliert.
Die Prozessierung der Assay-Daten mit der *ExprEssence* Software konnte zudem die Interaktionen verschiedener Proteine untereinander identifizieren und visualisieren. Dabei konnte gezeigt werden, dass verschiedene Mitglieder der TGF-β Familie, VEGF sowie IL8 eine zentrale Rolle in fibrotischen Prozessen einnehmen (Abb. 11).

Schlussfolgerungen: Diese Studie konnte zeigen, dass es im Kammerwasser von Patienten mit negativem Ergebnis nach einer durchgeführten Trabekuletomie zu Veränderungen im Zytokin-/Chemokin-Gehalt im Vergleich zu Patienten mit positivem Ergebnis kommt. Viele der identifizierten Proteine weisen profibrotische Eigenschaften auf und es konnte dargestellt werden, dass TGF-β, VEGF und IL8 zentrale Rollen bei fibrotischen Prozessen einnehmen. Die aufgezeigten Protein-Protein-Interaktionen bieten somit die Möglichkeit mittels entsprechender Inhibitoren spezifisch in die Zytokin-vermittelte Zellkommunikation einzugreifen.

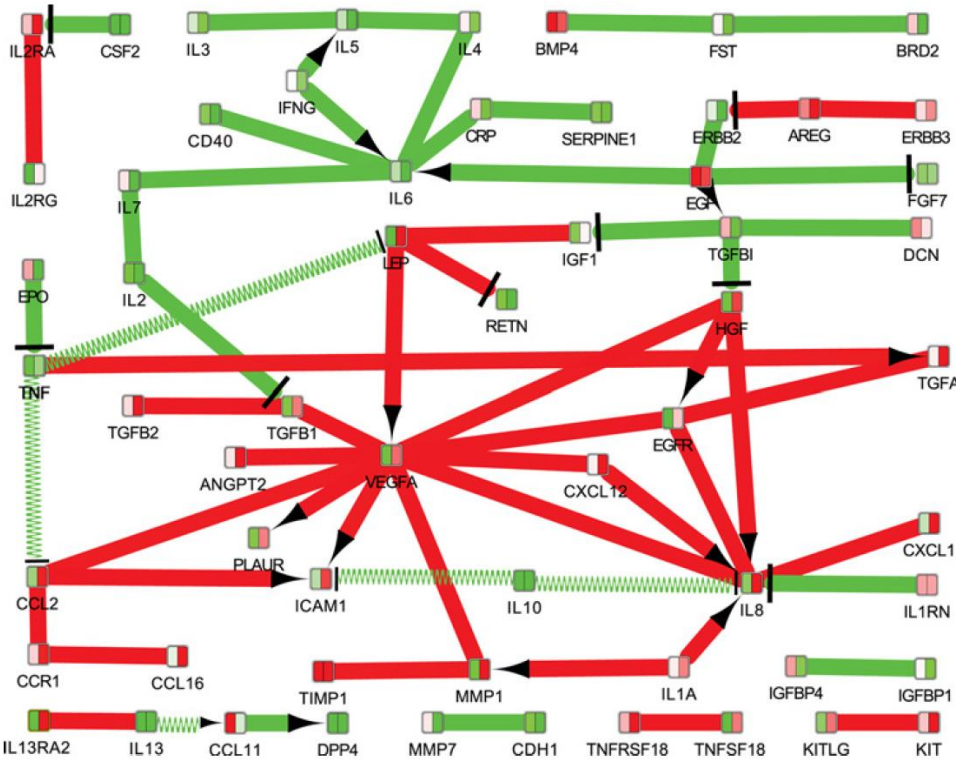

Abb. 11: Darstellung fibrotischer Prozesse und der Protein- (Zytokin-) Interaktionen nach Trabekulektomie, basierend auf Expressionsdaten und deren Kartierung durch das STRING-Netzwerk.
Im generierten Netzwerk sind lediglich jeweils 10 % der Zytokine, die mit der stärksten Hoch- und Runterregulation zwischen den Patientengruppen mit positivem sowie negativem Trabekuletomie-Ergebnis, dargestellt. Die rote Farbe kodiert hochregulierte, die grüne Farbe runterregulierte Zytokine. Stimulierende Protein-Protein-Interaktionen werden durch Pfeilspitzen, inhibitorische durch Striche dargestellt. Unbekannte Protein-Protein-Interaktionen zeigen weder einen Pfeil noch einen Strich. Die Knotenpunkte repräsentieren das jeweilige Expressionsmuster der beiden Patienten-Kollektive (links = positives, rechts = negatives (Fibrose) Ergebnis nach Trabekulektomie) bei gleicher Farbkodierung.

6. Neuronale Interaktionen mit dem kornealen Epithel: Die Rolle bei Wundheilungsprozessen.

Kowtharapu BS, Stahnke T*, Wree A, Guthoff RF, Stachs O. Corneal epithelial and neuronal interactions: role in wound healing. Exp Eye Res. 2014, 125:53-61. DOI: 10.1016/j.exer.2014.05.006. (* Autoren haben zu gleichen Teilen beigetragen).*

Fragestellung: Die Beeinträchtigung der kornealen Sensitivität und Innervation ist eine der Hauptursachen für die Entstehung einer kornealen neurotrophen Keratopathie, welche wiederum mit einer gestörten Wundheilung des kornealen Epithels einhergeht. Daraus kann sich die Symptomatik eines trockenen Auges entwickeln, wodurch die Wundheilung des Epithels weiterhin erschwert wird. Als Folge kann es zur Entwicklung von Geschwüren, fibrotischen Prozessen im Stroma, aseptischer Nekrose und Perforati-

onen der Hornhaut kommen. Daher war es das Ziel dieser Studie, Einblicke in die zelluläre Kommunikation zwischen trigeminalen Neuronen und kornealen Epithelzellen zu erhalten, um Möglichkeiten einer spezifischen kornealen Wundheilungsmodulation zu identifizieren.

Material und Methoden: Zur Analyse der zellulären Kommunikation wurden primäre Neurone trigeminalen Ursprungs sowie primäre korneale Epithelzellen der Maus *in vitro* kultiviert. Um den Effekt der Neurone auf die Epithelzellen und *vice versa* in kornealen Wundheilungsprozessen zu untersuchen, wurden die Kulturen mit konditioniertem Medium des jeweils anderen Zelltyps versetzt und mit einer Cokultur beider Zelltypen verglichen. Mittels eines Neuriten-Wachstums-Kits (Molecular Probes) wurde die Wachstumsrate der Neuriten bestimmt. Zusätzlich wurden rtPCR, Western Blots, und Immunfluoreszenzanalysen zur Evaluation des Einflusses konditionierten Mediums auf das Neuritenwachstum durchgeführt. Für die Untersuchungen der epithelialen Wundheilungsmechanismen wurde ein Scratch-Assay etabliert und mit rtPCR, Western Blot sowie Immunfluoreszenzmikroskopie analysiert.

Ergebnisse: In den Versuchsansätzen konnte gezeigt werden, dass konditioniertes Medium der Epithelzellen sowie Cokulturbedingungen zu einem verstärkten Auswachsen der Neuriten in Neuronen trigeminalen Ursprungs führten. Unter diesen Kulturbedingungen konnte weiterhin eine Zuhnahme der Expression von Substanz P (SP) mRNA sowie eine Expressionsabnahme der mRNA des Mikrotubuli-assoziierten Proteins 1b (Mab1b) gezeigt werden. Im Scratch-Assay konnte in kornealen Epithelzellen eine über EMT stattgefundene Transformation, gekennzeichnet durch die einsetzende Expression von Vimentin, aufgezeigt werden (Abb. 12). Weiterhin konnten die rtPCR und Western Blot Analysen belegen, dass die EMT, ausgelöst durch einen Scratch, mit einer gesteigerten Expression der Zytokine BMP7 und dem paired box protein 6 (Pax6) assoziiert sind. Sowohl die Expression von BMP7 als auch die von Pax6 werden unter der Kulturbedingung mit konditioniertem neuronalen Medium runterreguliert (Abb. 13).

Schlussfolgerungen: Innerhalb dieser Studie konnte gezeigt werden, dass es bei Wundheilungsprozessen der Kornea zu einer über Zytokine vermittelten Zellkommunikation zwischen Neuronen und den kornealen Epithelzellen kommt. Die Beteiligungen des aus der TGF-β Familie stammenden BMP7, des Master-Kontrollgens Pax6 und SP zeigen die Bedeutung für die Regenerationsfähigkeit der kornealen Nerven sowie für

die EMT des kornealen Epithels auf und eröffnen neue Möglichkeiten der spezifischen Wundheilungsmodulation der Kornea.

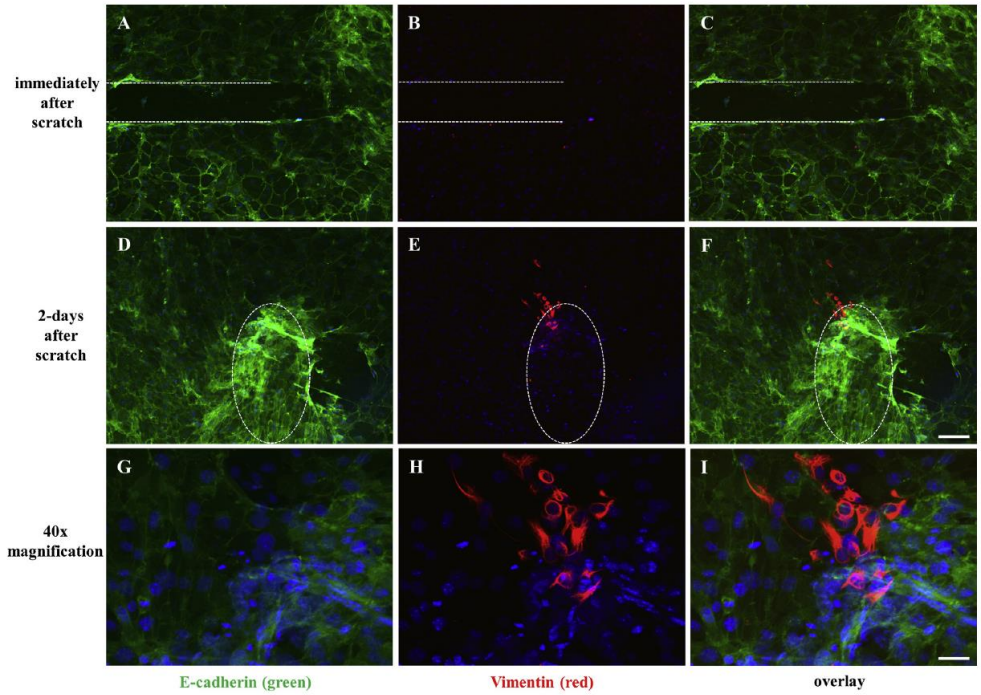

Abb. 12: Darstellung der einsetzenden EMT in Wundheilungsprozessen in kornealen Epithelzellen in vitro.
A-C: *In einem konfluenten Zellrasen von Epithelzellen, charakterisiert durch die Expression von E-Cadherin (grün), wurde durch einen definierten Scratch eine Verletzung simuliert. Unter diesen Kulturbedingungen exprimieren die Epithelzellen kein Vimentin (rot).* ***D-F:*** *Innerhalb der Verletzung im Zellrasen kommt es nach zwei Tagen zur vermehrten Zellteilung. Einige der Epithelzellen exprimieren das Intermediär-Zytoskelettprotein Vimentin, was die EMT dieser Zellen belegt. Messbalken: 25 µm.* ***G-I:*** *40 fache Vergrößerungen der gepunkteten Bereiche aus D-F. Es ist deutlich die Expression des Proteins Vimentin im Bereich der Verletzung zu erkennen. Messbalken: 10 µm.*

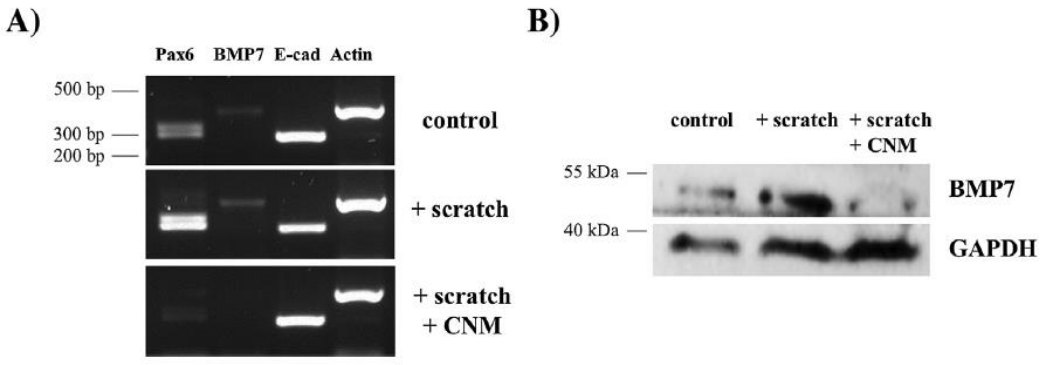

Abb. 13: Einfluss trigeminaler Neurone auf die Wundheilungsprozesse in kornealen Epithelzellen.
A: *rtPCR Analyse der Gene Pax6, BMP7 und E-Cadherin in unbehandelten Kontrollzellen während der Wundheilung (+ Scratch) sowie während der Wundheilung mit konditioniertem neuronalen Medium (+ Sratch + CNM). Innerhalb der alleinigen Wundheilung kommt es zu einer verstärkten Expression der Gene Pax6 und BMP7, was durch die kombinierte Kulturbedingung mit konditioniertem Neuronenmedium (CNM) verhindert wird. Die Expressionen der Gene E-Catherin und Aktin bleibt hingegen unverändert.* ***B:*** *Western Blot der BMP7 Expression unter den gleichen Kulturbedingungen wie in A. Die alleinige Wundheilung führt zu einer verstärkten Synthese von BMP7, was durch die Kultivierung mit konditioniertem Neuronenmedium verhindert wird. Das Protein GAPDH dient als Ladekontrolle.*

7. Magnetresonanzmikroskopie des Akkommodationsapparats.

Stahnke T, Hadlich S, Wree A, Guthoff RF, Stachs O, Langner S. Magnetic Resonance Microscopy of the Accommodative Apparatus. Klin Monbl Augenheilkd. 2016, 233(12):1320-1323. DOI: 10.1055/s-0042-118599.

Fragestellung: Die humane Linse unterliegt einem lebenslangen Wachstumsprozess. Ab einem Alter von 50 Jahren ist die Linse aufgrund der Änderungen ihrer viskoelastischen Eigenschaften nicht mehr in der Lage zu akkommodieren und es wird eine Lesebrille für die Nahsicht notwendig. Weiterhin kann eine auftretende Katarakt die chirurgische Implantation einer IOL erfordern, wodurch ebenfalls die Akkommodationsfähigkeit verloren geht. Eine häufige Folge des Operationsverfahrens ist die Entwicklung eines Nachstars, welcher durch eine EMT verbliebener Linsenepithelzellen im Kapselsack und der daraus resultierenden unkontrollierten Proliferation verursacht wird. Daher war es das Ziel dieser Studie, die Linse und den gesamten Akkommodationsapparat des humanen Auges mit Hilfe der Ultrahochfeld-Magnetresonanzmikroskopie (MRM) hinsichtlich der anatomischen Strukturen zu charakterisieren und die Befunde mit der klassischen Histologie zu vergleichen.

Material und Methoden: Bei hohen Feldstärken über 7 Tesla (T) wird die Magnetresonanztomografie (MRT) auch als MRM bezeichnet. In dieser Studie wurde ein 9,4 T Ultrahochfeld-MRT (BioSpec 94/30 USR, Bruker BioScan GmbH, Ettlingen, Deutschland) unter Verwendung einer 4-Kanal-Empfangsspule (MRI CryoProbe, Bruker BioScan GmbH, Ettlingen, Deutschland) und einem Untersuchungsfeld (FOV) von 20 mm zur Akquisition von MR-Bildern mit einer Auflösung im Submillimeterbereich eingesetzt. Aufgrund der besseren Abgrenzbarkeit der Strukturen des Auges wurden für die MRM T2-gewichtete 3-D-Sequenzen verwendet. Die Untersuchung erfolgten an einem enukleierten humanen Spenderauge (65 Jahre) ohne okulare Vorerkrankungen 24-36 Stunden nach Enukleation. Für die histologischen Untersuchungen wurde ein enukleiertes humanes Spenderauge (67 Jahre) für 48 Stunden in Formalin fixiert und in Paraffin eingebettet. Mittels eines Mikrotoms wurden 5 µm dicke Schnitte erstellt und mit H&E gefärbt und mikroskopiert.

Ergebnisse: Es wurde gezeigt, dass die MRM ein bildgebendes Verfahren darstellt, mit dem eine detaillierte Charakterisierung des Akkommodationsapparats erfolgen kann. So wurden beispielsweise die Linsenkapsel, das einschichtige Linsenepithel und

der Linsenkern aufgrund der unterschiedlichen Intensitäten, basierend auf dem Wassergehalt der verschiedenen Strukturen, voneinander differenziert (Abb. 14). Weiterhin konnten mittels der MRM Substrukturen der Iris (Epithel, Stroma, *M. sphincter pupillae*) und des Ziliarkörpers (Epithel, Stroma, Ziliarmuskel) identifiziert und charakterisiert werden. Zudem ermöglicht die MRM eine artefaktfreie und hochaufgelöste Darstellung möglicher Implantat- und Drainageräume und kann auch *in vivo* eine Anwendung finden. Die klassische histologische Aufarbeitung ist hingegen durch die Konservierungs- und Schnitttechniken mit Schrumpfungsartefakten assoziiert. Dennoch werden durch die Histologie die einzelnen Strukturen noch wesentlich detailreicher und bis auf zelluläre Ebene dargestellt. So können beispielsweise sogar die Zellkerne der einzelnen Linsenepithelzellen visualisiert sowie eine Unterscheidung des Ziliarmuskels in seine submuskulären Anteile des Müller- und des Brücke-Muskels vorgenommen werden. Neben den methodenbedingt entstehenden Artefakten der Histologie ist ein weiterer Nachteil, dass die Methode ausschließlich *ex vivo* eine Anwendung findet.

Schlussfolgerungen: Die MRM im Ultrahochfeld kann als komplementäre Methode zur konventionellen Histologie betrachtet werden, welche offensichtliche Nachteile der Histologie des Auges kompensieren kann. Sie eröffnet Möglichkeiten zu völlig neuen anatomischen Studien des anterioren Segments des Auges, auch wenn das Verfahren derzeit nur bedingt in der Lage ist, Strukturen bis auf zelluläre Ebene aufzulösen. Eine Anwendung dieser Methode *in vivo* kann dennoch die postoperative Beurteilung ophthalmologischer Implantate sowie eine Charakterisierung einsetzender Vernarbungsprozesse ermöglichen.

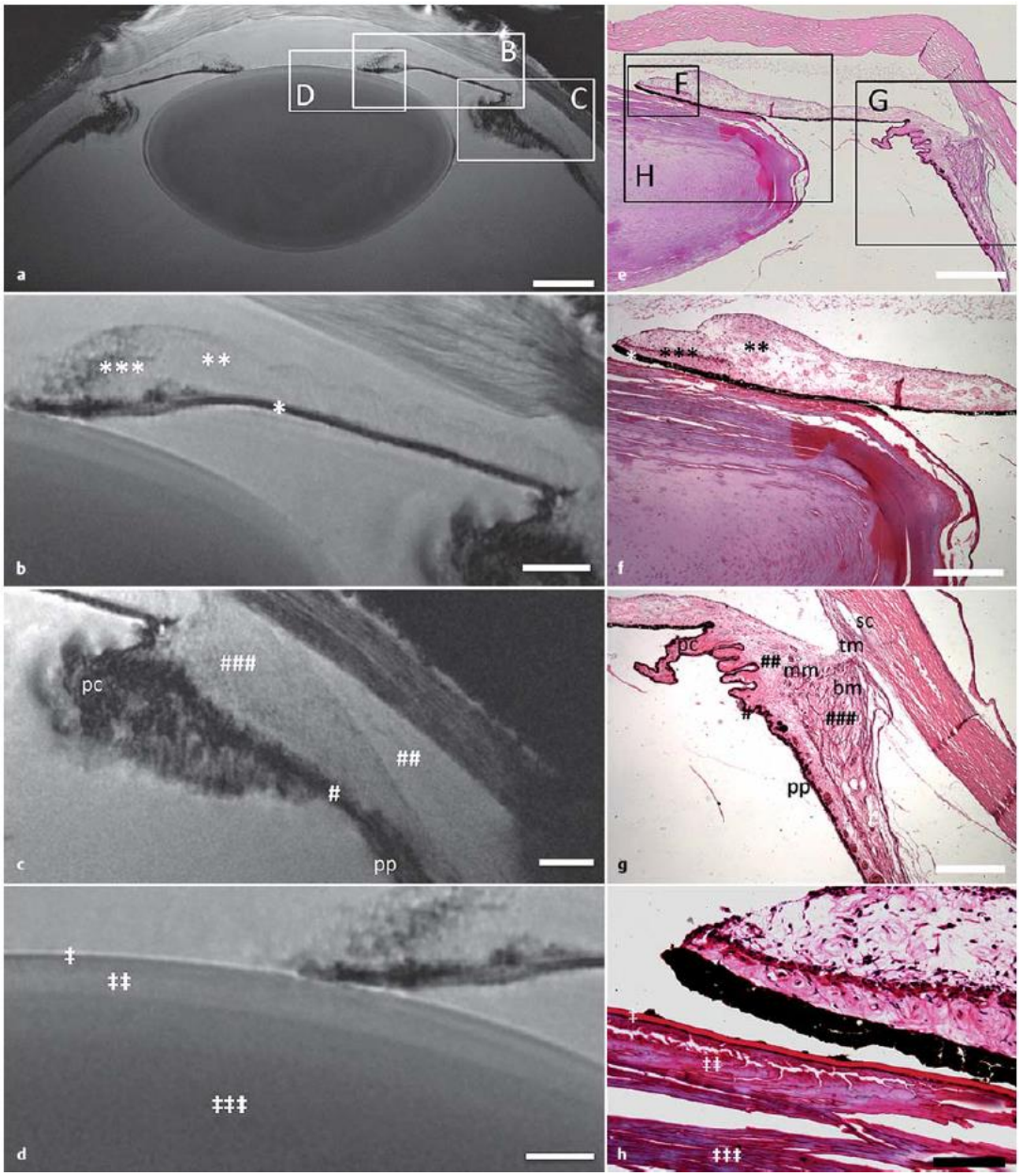

Abb. 14: T2-gewichtete MR-Mikroskopie des anterioren Abschnitts eines humanen Auges im Vergleich mit konventioneller Histologie (H&E-Färbung).

Axiale T2-gewichtete 3-D-Aufnahmen mit einer örtlichen Auflösung von 13 × 13 µm (a–d). ***a:*** *Übersichtsdarstellung des humanen anterioren Augenabschnitts und des Akkommodationsapparats. Die weißen Markierungen (B–D) geben die jeweiligen Ausschnitte der Detaildarstellungen wieder. Messbalken: 1500 µm.* ***b:*** *Detaildarstellung der Iris. * = Irispigmentepithel; ** = Stroma der Iris; *** = M. sphincter pupillae. Messbalken: 500 µm.* ***c:*** *Detaildarstellung des Ziliarkörpers. # = Pigmentepithel des Ziliarkörpers; ## = Stroma des Ziliarkörpers; ### = M. ciliaris; pc = Plicae circulares; pp = Pars plana. Messbalken: 500 µm.* ***d:*** *Detaildarstellung der Linse. ‡ = Linsenkapsel; ‡‡ = Linsenepithel und Linsenkortex; ‡‡‡ = adulter Nukleus der Linse. Messbalken: 150 µm.* ***e:*** *Übersichtsdarstellung des humanen anterioren Augenabschnitts und des Akkommodationsapparats in der H&E-Färbung. Die schwarzen Markierungen (F–H) geben die jeweiligen Ausschnitte der Detaildarstellungen wieder. Messbalken: 1000 µm. f: Detaildarstellung der Iris. * = Irispigmentepithel; ** = Stroma der Iris; *** = M. sphincter pupillae. Messbalken: 500 µm.* ***g:*** *Detaildarstellung des Ziliarkörpers. # = Pigmentepithel des Ziliarkörpers; ## = Stroma des Ziliarkörpers; ### = M. ciliaris; pc = Plicae circulares; pp = Pars plana; mm = Müller-Muskel; bm = Brücke-Muskel; sc = Schlemm-Kanal; tm = Trabekelmaschenwerk. Messbalken: 500 µm.* ***h:*** *Detaildarstellung der Linse. ‡ = Linsenkapsel; ‡‡ = Linsenepithel und Linsenkortex; ‡‡‡ = adulter Nukleus der Linse. Messbalken: 100 µm.*

Diskussion

1. Spezifische Inhibition fibrotischer Prozesse nach fistulierender Glaukomchirurgie

Postoperativ einsetzende, unkontrollierbare Vernarbungsprozesse stellen eine der großen Herausforderungen in der fistulierenden Glaukomchirurgie dar, da sie zum Versagen der Therapiemaßnahmen führen können. Der Markt für die antifibrotische Behandlung nach Glaukomoperationen wird derzeit durch Zellgifte aus der Krebstherapie, insbesondere MMC und 5-FU, dominiert. Diese Wirkstoffe sind aufgrund ihrer Unspezifität mit Nebenwirkungen assoziiert und führen zu ernsten Gewebeschäden (Hovakimyan et al., 2015; Mearza et al., 2007). Daher ist es von wesentlicher Bedeutung, Substanzen zu identifizieren, welche spezifisch die Proliferation von für die Fibrose verantwortlichen Fibroblasten oder die Sekretion von Komponenten der EZM inhibieren und somit den postoperativen Vernarbungsprozessen entgegenwirken. Um Kenntnisse über die zellulären Wundheilungsmechanismen zu erhalten, wurden in den vorliegenden Arbeiten Fibroblasten aus allen Geweben des Auges isoliert, die bei chirurgischen Interventionen innerhalb der fistulierenden Glaukomtherapie involviert sind. Die biochemische Charakterisierung der Fibroblasten-Subpopulationen zeigte, dass die TGF-β-Signalkaskade unter den Kulturbedingungen *in vitro* einen Einfluss auf das Proliferationsverhalten und die Synthese von Proteinen der EZM ausübt (Stahnke et al., 2012; Stahnke et al., 2017). Eine Beteiligung des Zytokins TGF-β sowie eine Aktivierung der TGF-β-Signalkaskade an fibrotischen Prozessen ist auch in der Literatur beschrieben (Chung et al., 2012; Saika et al., 2009; Schlunck et al., 2016). Weiterhin ist publiziert, dass TGF-β eine Schlüsselrolle in postoperativen Wundheilungsprozessen einnimmt (Park et al., 2013; Stahnke et al., 2019). Eine Wundheilungsmodulation über die TGF-β vermittelte interzelluläre Kommunikation stellt daher einen vielversprechenden Ansatz der spezifischen Inhibition fibrotischer Prozesse dar.

Inzwischen sind Substanzen entwickelt worden, die zu einer verminderten Expression von TGF-β führen. Hier sind besonders die N-substituierten 2(1H)-Pyridone (PFD) und N-substituierte 3(1H)-Pyridone zu nennen. Das als aktive antifibrotische Substanz bereits zur Behandlung der idiopathischen Lungenfibrose zugelassene PFD (Esbriet®, Roche) konnte auch in Tenonfibroblasten des Auges *in vitro* zu einer Reduktion der Zytokinexpression von TGF-β 1-3 führen (Lin et al., 2009). In eigenen Studien wurde durch

die Applikation von TGF-β in das Kulturmedium von Fibroblasten-Subpopulationen ein fibrotisches Zellkulturmodell etabliert und biochemisch charakterisiert, welches sich durch eine gesteigerte Proliferationsrate sowie Synthese der fibrotischen Markerproteine Kollagen I, Fibronektin und α-SMA auszeichnet (Stahnke et al., 2017). Innerhalb dieses fibrotischen Zellkulturmodells führte PFD zu einer Reduktion der durch TGF-β vermittelten fibrotischen Prozesse und zur Abnahme der Expression fibrotischer Markerproteine (Stahnke et al., 2017).

Aufgrund der vielversprechenden Resultate der *in vitro*-Experimente wurde PFD als Wirkstoff für eine antifibrotische Beschichtung von GDI-Prototypen selektiert und in einem Langzeit-Tierexperiment *in vivo* evaluiert (Stahnke et al., 2018). Auch in dieser Studie konnte PFD die fibrotische Gewebereaktion verringern und zeigte das beste Ergebnis im Vergleich zu den zusätzlich untersuchten Wirkstoffen CAPE und PTX. Eine antifibrotische Wirkung von PFD nach Trabekulektomie wurde ebenfalls in einem Kaninchen-Tiermodell nachgewiesen (Zhong et al., 2011). Auch in einer weiteren tierexperimentellen Studie in Kaninchen konnte die postoperative Injektion von PFD in das Sickerkissen, zusammen mit einer topischen Applikation nach erfolgter GDI-Implantation (Model FP8 Ahmed glaucoma valve), die fibrotische Gewebereaktion verringern (Jung und Park, 2016).

Derzeit befinden sich in eigenen Forschungsarbeiten entwickelte funktionalisierte GDI mit LDD Funktion (PFD) in einer weiteren tierexperimentellen Langzeitstudie. Hierfür wurden GDI mit Ventilfunktion subkonjunktival drainierend in jeweils ein Auge von New Zealand White Kaninchen implantiert. Im Vergleich zu unbeschichteten GDI wird das Tierexperiment zeigen, ob die zuvor *in vitro* beschriebenen antifibrotischen Eigenschaften von PFD auch *in vivo* am Implantationsort Auge den Wundheilungsprozess modulieren und fibrotische Vernarbungsreaktionen verlangsamen, bzw. verhindern können.

Während der tierexperimentellen Studie sind zeitlich gestaffelt Funktionalitätsprüfungen der GDI mit OPT nach Ulrich vorgesehen, mit der sehr einfach und gut reproduzierbar das regulative Augeninnendruckverhalten untersucht und eine gestörte Hydrodynamik erkannt werden kann (Ulrich et al., 1987; Ulrich et al., 2015). Innerhalb der vorliegenden Arbeit wurde die Methode bereits durch geringfügige Modifikationen an das Kaninchenauge adaptiert und steht nun für die postoperative Evaluation implantier-

ter GDI in Kaninchenmodellen zur Verfügung (Stahnke et al., 2015). Das Funktionsprinzip, durch einen Provokationstest kurzzeitig den IOD zu erhöhen und somit ein temporäres Glaukommodell zu generieren, hat inzwischen zu einer Weiterentwicklung geführt (Kopp et al., 2018), welche derzeit in einer Humanstudie zur Funktionalitätsprüfung von GDI eine Anwendung findet und auch in zukünftigen tierexperimentellen Studien zum Einsatz kommen wird.

Neben der TGF-β vermittelten Signalkaskade spielen auch weitere Zytokine und zelluläre Kommunikationswege wichtige Rollen bei überschießenden Vernarbungsreaktionen und fibrotischen Prozessen (Gillies und Su, 1991; Friedlander, 2007; Cvenkel et al., 2010; Yu-Wai-Man C und Khaw PT, 2016). Besonders die durch den Blutplättchen abgeleiteten Wachstumsfaktor (PDGF) und den Bindegewebswachstumsfaktor (CTGF) vermittelten Signalwege weisen profibrotische Eigenschaften auf und stellen weitere Schlüsselmediatoren dar (Klinkhammer et al., 2018; Lipson et al., 2012). Auch diese Signalkaskaden werden durch PFD inhibitorisch beeinflusst. Eine durch PFD vermittelte Reduktion der Expression verschiedener PDGF-Isoformen und ein daraus resultierender antifibrotischer Effekt konnte in einem Bleomycin-Modell der Lungenfibrose in Hamstern *in vivo* nachgewiesen werden (Gurujeyalakshmi et al., 1999). Weiterhin konnte gezeigt werden, dass PFD zu einer verminderten Expression des Zytokins CTGF führt, wodurch die Migration, Proliferation und Differenzierung in humanen retinalen Pigmentepithelzellen *in vitro* inhibiert wurde (Wang et al., 2013). Fibrotische Prozesse sind zudem eng mit Zytokinen der Immunantwort verknüpft (Cvenkel et al., 2010). Diese Zytokine führen zum einen zur Rekrutierung von Entzündungszellen, welche wiederum differenzielle Zytokine sezernieren, können aber auch direkt einen Einfluss auf die Fibroblasten und somit auf die Wundheilungsmechanismen ausüben (Scheibe et al., 2019). Zu den inflammatorischen Zytokinen mit profibrotischen Eigenschaften zählen vor allem Mitglieder der Familie der Interleukine (IL) (Zahir-Jouzdani et al., 2017) sowie auch der Tumornekrosefaktor-α (TNF-α) (Nikita et al., 2017). Sowohl die differenzielle Modulation der IL-Expression IL (Lopez-de la Mora et al., 2015) als auch eine reduzierte Expressionsrate von TNF-α (Oku et al., 2002) durch PFD sind in der Literatur beschrieben, wodurch eine zusätzliche antifibrotische Wundheilungsmodulation hervorgerufen wird. Durch das breit gefächerte inhibitorische Wirkspektrum von PFD auf verschiedene Zytokin vermittelte zelluläre Signalkaskaden wird die Identifikation

eines hauptverantwortlichen Signalweges zur Entstehung einer postoperativen Fibrose schwierig, die antifibrotischen Eigenschaften von PFD basieren vermutlich gerade auf der mannigfaltigen Modulation der komplexen interzellulären Kommunikation (Lopez-de la Mora et al., 2015).

Innerhalb der vorliegenden Arbeit wurde in einer eigenen Studie das Zytokin/Chemokin-Muster des Kammerwassers von Patienten mit POAG nach erfolgter Trabekulektomie miteinander verglichen, wobei erfolgreiche und durch Fibrose fehlgeschlagene Eingriffe gegenübergestellt wurden (Gajda-Deryło und Stahnke et al., 2019). Diese Studie bestätigte die Komplexität der Zytokin-vermittelten Zellkommunikation durch die Identifikation von 104 signifikant hochregulierten und 27 signifikant runterregulierten Zytokinen im Kammerwasser von Patienten, die postoperativ eine Fibrose entwickelten im Vergleich zu Patienten ohne Fibroseentwicklung. Neben den profibrotischen Zytokinen TGF-β, BMP und VEGF wurden auch 49 für inflammatorische Prozesse verantwortliche Zytokine hochreguliert, darunter auch verschieden Mitglieder der IL-Familie sowie TNF-α. Neben TNF-α werden besonders den Zytokinen IL1, IL-6 und IL-8 profibrotische Eigenschaften bei postoperativen okularen Vernarbungsprozessen zugesprochen (Yamanaka et al., 2015). Ein Anstieg der Expression von IL-6, IL-8 und TNF-α konnte ebenfalls nach erfolgter, fistulierender Glaukomchirurgie in Patienten mit durch Fibrose verursachtem negativem Ergebnis im Vergleich zu Patienten mit positivem Ergebnis nachgewiesen werden (Cvenkel et al., 2010). In einer weiteren Studie, in welcher der Gehalt inflammatorischer Zytokine von POAG Patienten ohne Glaukomchirurgie in im Rahmen von Katarakt-Operation entnommenen Kammerwasserproben mit einer Kontrollgruppe verglichen wurde, konnte hingegen eine signifikant niedrigere IL-6 Konzentration in der POAG Gruppe gezeigt werden (Borkenstein et al., 2013). Zudem sind auch in der akuten idiopathischen Lungenfibrose (IPF) die Konzentrationen der Zytokine IL-6 und 8 gegenüber Patienten mit einer stagnierenden IPF signifikant erhöht (Papiris et al., 2018).

Dennoch kann anhand der Ergebnisse der eigenen Studie demonstriert werden, dass noch eine Vielzahl weiterer Zytokine und Proteine und durch diese vermittelte Signalwege, für die nur sehr wenige durch PFD verursachte Modulationen in der Literatur beschrieben sind, in der Gruppe der POAG-Patienten mit negativem Operationsergebnis identifiziert werden konnten und zudem differenziell exprimiert wurden. Dabei handelt

es sich z.B. um interzelluläre Adhäsionsmoleküle (ICAM 1-3) und Proteine mit proapoptotischen Eigenschaften, wie bspw. das Apoptose-Antigen 1 (APO-1 oder Fas-Rezeptor) oder den Tumornekrosefaktor-verwandten Apoptose-induzierenden Liganden (TRAIL) (Gajda-Deryło und Stahnke et al., 2019). Ein vereinfachter wahrscheinlicher Pathomechanismus postoperativer fibrotischer Prozesse ist auf Grundlage der in dieser Arbeit identifizierten und über Zytokine vermittelten komplexen interzellulären Kommunikation schematisch dargestellt (Abb. 15).

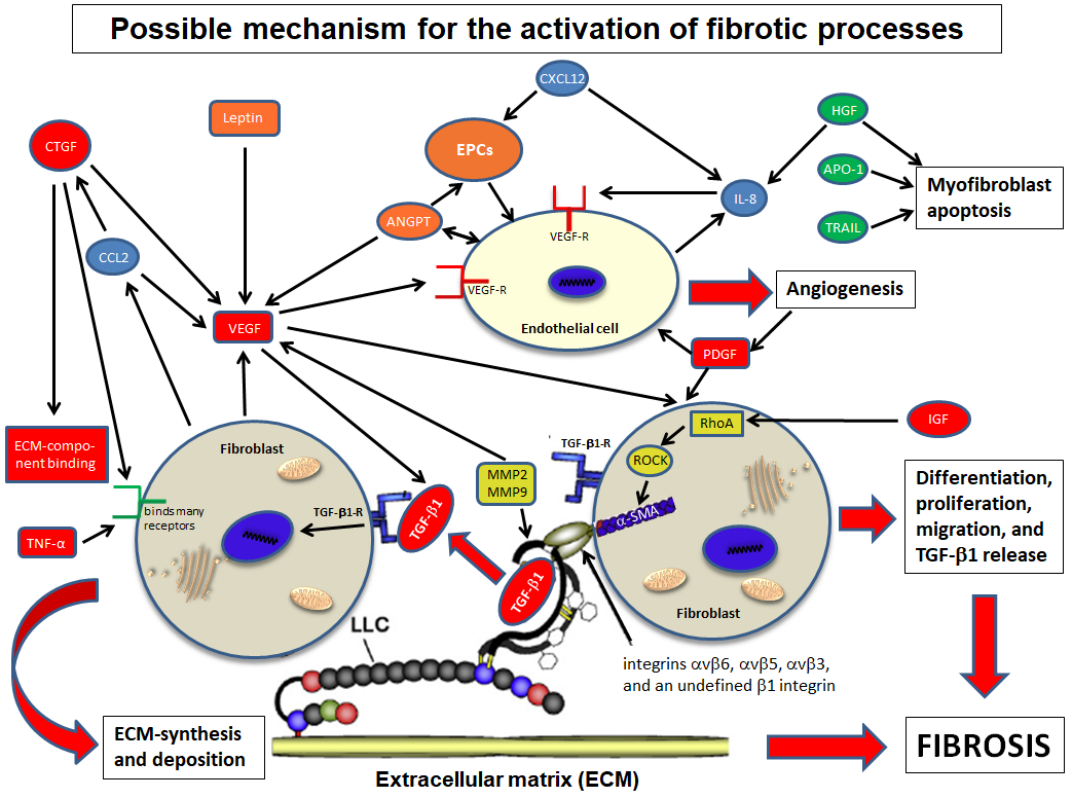

Abb. 15: Schematische Darstellung der interzellulären Kommunikation bei postoperativen fibrotischen Wundheilungsprozessen.
Die bei fibrotischen Prozessen identifizierten und in die Wundheilung involvierten Zytokine führen zu einer Aktivierung und Myodifferenzierung von Fibroblasten. Dabei nehmen die Zytokine TGF-β1, VEGF, CTGF, PDGF und IL8 Schlüsselfunktionen ein, die zur Aktivierung weiterer Fibroblasten sowie zu gesteigerten Syntheseraten von Proteinen der EZM führen. Farbcodierung dargestellter Zytokine / Proteine: Profibrotische Zytokine (rot), antifibrotische Zytokine (grün), chemotoktische oder inflammatorische Zytokine (hellblau), intra- und extrazelluläre Enzyme (gelb).

Die Komplexität der zellulären Interaktionen bei postoperativen Wundheilungsmechanismen *in vivo* nach fistulierender Glaukomchirurgie verdeutlicht, dass die Etablierung adäquater experimenteller Zellkulturmodellsysteme zur Analyse der Zytokin-vermittelten Zellkommunikation eine Herausforderung ist. Allerdings konnte eine gene-

rische Computeranalyse einer vergleichenden Genexpressionsstudie des eigenen fibrotischen Zellkulturmodells mit unbehandelten Fibroblasten einen Wirkstoff identifizieren, welcher der differenziellen Genexpression optimal entgegenwirkt. Die Evaluierung der antifibrotischen Eigenschaften dieses für die humane Anwendung zugelassenen Antibiotikums konnte inzwischen im fibrotischen Zellkulturmodell auch auf Proteinebene durch die Inhibition fibrotischer Markerproteine nachgewiesen werden. Diese Ergebnisse liefern die Basis einer eigenen nebenwirkungsarmen Therapieoption zur Vermeidung postoperativer Fibrose nach fistulierenden Glaukomoperationen und sind in einer Erfindungsmeldung zusammengefasst bereits eingereicht (Struckmann et al., 2019).

Es bleibt jedoch bei allen erfolgsversprechenden Resultaten und dem stattgefundenen Transfer der Erkenntnisse in die Entwicklung eines eigenen GDI-Therapiekonzeptes mit LDD Funktion zu bedenken, dass ein Zellkultursystem *in vitro* immer nur partiell die *in vivo* Situation repräsentieren kann und als Modellsystem betrachtet werden muss. Daher geht der Trend in der experimentellen Analyse der zellulären Zytokin-vermittelten Kommunikation bei Wundheilungsprozessen über die Verwendung primärer humaner Zellen eines Typs hinaus und hin zu Cokulturen, in denen 2 bis 4 unterschiedliche Zelltypen eines Gewebes gemeinsam kultiviert werden (Kirkpatrick, 2014). Die unterschiedlichen Zellen innerhalb solch komplexer Zellkultursysteme beeinflussen sich über die differenzielle Sekretion von Zytokinen gegenseitig, wodurch neue Erkenntnisse der interzellulären Kommunikation und der damit zusammenhängenden postoperativen Regeneration von Geweben zu erwarten sind (Herath et al., 2018). Die Verwendung von polymerbasierten Scaffolds in Cokultursystem kann zusätzlich eine Besiedelung durch die verschiedenen Zellen ermöglichen und zur Ausbildung völlig neuer zellulärer Interaktionen innerhalb einer räumlichen 3-D Struktur *in vitro* führen, wodurch weitere Einflüsse auf zelluläre Expressionsmuster ausübt werden (Kasper et al., 2017, Kirkpatrick, 2014). Die komplexen Cokulturmodellsysteme adressieren die Problematiken adäquater postoperativer Wundheilungsprozesse sowie Geweberekonstruktionen und eröffnen neue Modulationsmöglichkeiten, inhibitorisch in Wundheilungsprozesse einzugreifen, um postoperativ einsetzende fibrotische Prozesse zu unterbinden und die Langzeitfunktionalität fistulierender Interventionen im Rahmen der Glaukomchirurgie zu gewährleisten.

2. Fibroseprävention in der Kornea

Die global betrachtet sehr häufig auftretenden fibrotischen Prozesse in der Kornea können zu Eintrübungen und Erblindung führen und durch verschiedene Ursachen induziert werden (Torricelli et al., 2016). Einen besonders in Drittweltländern prominenten Auslöser stellt die Infektion der Konjunktiva mit *Chlamydia trachomatis* dar, die sich unbehandelt zu einer chronischen Konjunktivitis, dem Trachom, manifestieren kann (Derrick et al., 2016). Im Krankheitsverlauf kommt es sekundär durch permanente Verletzungen des kornealen Epithels durch die Wimpern zu einer bindegewebsartigen fibrotischen Gewebsneubildung mit Vaskularisation der Kornea (Abdelfattah et al., 2015), die als Pannus bezeichnet wird (Mohammadpour et al., 2016). Neben dem Trachom können auch weitere Infektionen, Traumata (auch chirurgische Interventionen) und Verätzungen zu einer gestörten kornealen Wundheilung führen und fibrotische Prozesse auslösen (Karamichos et al., 2010; Simirskii, 2014). Je nach Verletzungsursache sind verschiedene korneale Zellpopulationen in die Wundheilungsmechanismen zur Wiederherstellung der kornealen Integrität involviert (Medeiros et al., 2018).

In der vorliegenden Arbeit wurden korneale Wundheilungsmechanismen anhand eines zellulären Cokultursystems aus primären murinen kornealen Epithelzellen und Neuronen des trigeminalen Ganglions, deren Axone *in vivo* in direktem Kontakt zu den Epithelzellen stehen, evaluiert (Kowtharapu und Stahnke et al., 2014). Als entscheidendes Ergebnis konnte gezeigt werden, dass die Cokulturbedingungen ein schnelleres neuronales Wachstum induzierten. Eine unter diesen Bedingungen nachgewiesene Verminderung der Expressionsrate von Mab1b kann für diesen Effekt direkt verantwortlich sein, da eine verminderte Stabilisierung der axonalen Mikrotubuli ein höheres Maß an Flexibilität sowie Polymerisation der einzelnen Tubulin-Untereinheiten erlaubt. In eigenen Arbeiten konnten die stabilisierenden Effekte der Maps auf das Mikrotubuli-Netzwerk im Laufe der Entwicklung von Oligodendrozyten bereits gezeigt werden (Gorath et al., 2001).

Zusätzlich zu Mab1b konnte eine differenzielle Expression der Zytokine SP, BMP7 und Pax6 sowie eine EMT in den Epithelzellen nachgewiesen werden. Ein stimulierender Einfluss von SP auf das epitheliale Zellwachstum der Kornea *in vitro* konnte bereits 1993 demonstriert werden (Reid et al., 1993). Auch in einer weiteren Studie führte die topische Applikation eines SP-Derivats in Kaninchenaugen mit persistierenden Oberflä-

chendefekten der Kornea zu einem schnellen Ausheilen der kornealen Defekte und zur Wiederherstellung der kornealen Integrität *in vivo* (Yamada et al., 2008). In neueren Arbeiten konnte hingegen *in vitro* demonstriert werden, dass eine alleinige Stimulation kornealer Epithelzellen mit SP keiner Beschleunigung der Proliferation oder Aktivierung der EMT herbeiführt, sondern erst die Kombination mit weiteren sezernierten Zytokinen von Keratozyten diese Effekte auslösen und zu einer schnelleren kornealen Wundheilung beitragen (Kowtharapu et al., 2018a).

In diesem Zusammenhang spielt das Zytokin BMP7 eine entscheidende Rolle. Chung et al. konnten demonstrieren, dass BMP7 einen inhibitorischen Effekt auf die EMT kornealer Epithelzellen und auf die Myodifferenzierung von Keratozyten *in vitro* sowie nach topischer Applikation in Kaninchenaugen *in vivo* ausübt (Chung et al., 2017). In einer eigenen Arbeit zur Evaluation kornealer Wundheilungsmechanismen wurde hingegen gezeigt, dass das Zytokin BMP7 in kornealen Epithelzellen eine EMT induzieren und so Wundheilungsmechanismen modulieren kann (Kowtharapu et al., 2018b). Weiterhin wurden auch stromale Keratozyten durch Stimulation mit BMP7 aktiviert und differenzierten in Myofibroblasten, wodurch belegt werden konnte, dass BMP7 in kornealen Wundheilungsprozessen eine ähnliche Funktion wie das Zytokin TGF-β aufweist (Kowtharapu et al., 2018b). Eine dadurch vermittelte schnellere Wundheilung mit Beteiligung beider Zellpopulationen kann somit zu einer Beschleunigung der Wiederherstellung der kornealen Integrität führen, bei anhaltender Stimulation allerdings auch fibrotische Prozesse in der Kornea generieren. Eine Beteiligung epithelialer EMT an fibrotischen Prozessen in der Kornea ist in der Literatur beschrieben (Bukowiecki et al., 2017; Kawashima et al., 2010).

Eine limbale Stammzellinsuffizienz kann zusätzlich eine regelrechte korneale Wundheilung beeinflussen oder gänzlich verhindern, da die Stammzellen für den physiologischen Erhalt sowie innerhalb von Wundheilungsprozessen des kornealen Epithels, aber auch der stromalen Keratozyten, essenziell sind (Bukowiecki et al., 2017; Kawashima et al., 2010; Navas et al., 2018; Nicula et al., 2017).

Auch dem identifizierten Zytokin Pax6 kommt bei kornealen Entwicklungs- und Wundheilungsprozessen eine Schlüsselfunktion zu (Bukowiecki et al., 2017; Davis und Piatigorsky, 2011). Es konnte in einem Pax6 Maus-knockout-Modell gezeigt werden, dass das korneale Epithel dünner und aus weniger Zellschichten aufgebaut ist (Swamy-

nathan, 2013). Zusätzlich ist die interzelluläre Adhäsion der Epithelzellen durch niedrigere Expressionsraten der Proteine Desmoglein, β-Catenin, γ-Catenin, and Keratin-12 vermindert, woraus eine verstärkte Erosion resultiert (Davis et al., 2003).
Die in der vorliegenden Arbeit identifizierten Zytokine bieten somit Möglichkeiten regulatorisch und spezifisch in die Wundheilungsprozesse der Kornea einzugreifen. Dabei kann die Modulation durch eine Applikation der Zytokine, also eine Stimulation erfolgen, weiterhin ist aber auch eine Verwendung von in der Literatur beschriebenen Inhibitoren für SP (Johnson et al., 2017) oder BMP7 (Ma et al., 2017) als regulatorische Maßnahme und Therapieoption mit dem Ziel denkbar, die korneale Integrität schnellst möglich wieder herzustellen oder das Einwachsverhalten alloplastischer Keratoprothesen zu fördern.

3. Nachstarprophylaxe

Im Rahmen der weltweit sehr häufig durchgeführten Linsenresektion als einziges Therapiekonzept zur Behandlung der Katarakt kann es zur postoperativen Ausprägung einer PCO mit Inzidenzraten von 10-30 % kommen (Lee et al., 2016). Der dadurch verursachte erneute Visusabfall beruht auf einer unkontrollierten Vermehrung von Linsenepithelzellen, die ausschließlich subkapsulär im anterioren Linsensegment der natürlichen Linse lokalisiert sind (Stahnke et al., 2016). Während einer Kataraktoperation erfolgt zu Beginn eine Kapsulorhexis im anterioren Linsensegment, welche einen Zugang zum Cortex und Nucleus der Linse erlaubt und durch den mittels der Phakoemulsifikation die Linsenresektion sowie die Implantation der Kunstlinse erfolgt. Bei dieser Operationstechnik können einige Linsenepithelzellen im Kapselsack verbleiben, welche durch den Verlust der Barrierefunktion des Kapselsacks, der Basalmembran der Linsenepithelzellen, den Prozess der EMT durchlaufen (Boswell et al., 2017). Eine damit zusammenhängende Zellvermehrung sowie gesteigerte Expressionsrate von Proteinen der EZM führt zur Bildung von fibrotischem Gewebe, welches die Visusminderung verursacht und erneute Interventionen erfordert (Lee et al., 2016).
In der Literatur sind viele Ansätze beschrieben, die eine Vermeidung einsetzender PCO nach erfolgter Linsenimplantation adressieren (Raj et al., 2007; Nibourg et al., 2015). Dazu zählen neben neuen IOL-Designs auch adhäsionsmindernde IOL-Materialeigenschaften (Nibourg et al., 2015; Nishi et al., 2007; Xu et al, 2016). Weiter-

hin werden IOL-LLD-Konzepte beschrieben, die durch die Verwendung unterschiedlicher Wirkstoffe die PCO-Problematik beheben sollen (Wertheimer et al., 2017). Der Fokus untersuchter Pharmaka liegt auf der Inhibition inflammatorischer Prozesse durch Diclofenac und Cyclosporin A (Cortina et al., 1997), sowie unspezifischen Inhibitoren wie 5-FU, PTX, Retinolsäure und MMC (Koopmans et al., 2014, Inan et al., 2001), als auch der Inhibition von Adhärenz- und Migrationseigenschaften (Raj et al., 2007) und Zelltod-induzierenden Wirkstoffen (Nishi et al., 2001; Malecaze et al., 2006; Nanavaty et al., 2006). Dennoch existieren derzeit am Markt noch keine Verfahren oder IOL-LLD-Konzepte, die eine postoperative PCO verhindern können. Neue Arbeiten demonstrieren jedoch eine Inhibition von Linsenepithelzellen in einem humanen Kapselsackmodell über ein IOL-LLD (Methotrexat) (Kassumeh et al., 2018). Auch in Arbeiten der eigenen Kooperationspartner konnten inzwischen in einem *in vivo* Lens-Refilling-Kaninchen-Modell Actinomycin D und Methotrexat eine postoperative Ausprägung der PCO über einen Zeitraum von 4 Jahren verhindern, PTX und Tween 20 zeigten hingegen keine präventiven Effekte (van Kooten et al., 2019). In der gleichen Arbeit wurde aber auch beschrieben, dass es im Verlauf der tierexperimentellen Studie in einigen Tieren zum Verlust der kornealen Integrität über eine Schädigung des kornealen Endothels gekommen ist (van Kooten et al., 2019). Die Minimierung der Nebenwirkungen von experimentellen IOL-LDD sowie Lens-Refilling-Konzepten genießt also nach wie vor höchste Priorität. In diesem Zusammenhang ist interessant, dass auch die Zytokine TGF-β und BMP7 eine entscheidende Rolle bei der EMT und dadurch verursachten PCO spielen (Shu et al., 2017). In eigenen Arbeiten konnte die Beteiligung von BMP7 an der EMT epithelialer Zellen der Kornea bereits demonstriert werden (Kowtharapu und Stahnke et al., 2014; Kowtharapu et al., 2018b). Ein Transfer dieser Erkenntnisse in den Bereich der Nachstarprävention scheint daher einen vielversprechenden Ansatz darzustellen. Eine spezifische Wundheilungsmodulation der über die Zytokine TGF-β und BMP7 vermittelten Zellkommunikation könnte somit überschießende Vernarbungsreaktionen bzw. eine EMT induzierte PCO nebenwirkungsarm unterbinden und zur Entwicklung neuer IOL-DDS-Therapiekonzepte beitragen.

Zusammenfassung

Die vorliegende Arbeit betrachtet Aspekte der Wundheilungsmodulation im vorderen Augenabschnitt. Dabei werden drei ophthalmologische Anwendungsfelder mit hoher klinischer Relevanz betrachtet, welche alle mit fibrotischen Prozessen assoziiert sind.

Der erste Themenkomplex beschreibt induzierte Wundheilungsmechanismen nach fistulierender Glaukomchirurgie, die in experimentellen Arbeiten anhand dedizierter Modellsysteme evaluiert wurden. Für die Analysen konnten Fibroblasten-Subpopulationen aller durch die chirurgischen Interventionen involvierten Gewebe des anterioren Segments isoliert, kultiviert und biochemisch charakterisiert werden. Die Fibroblasten-Subpopulationen zeichneten sich durch die Synthese und Sekretion der für Wundheilungsprozesse relevanten und zu Vernarbungsreaktionen beitragenden Proteine der EZM,wie Fibronektin und unterschiedliche Kollagene, aus. Eine Aktivierung der TGF-β-Signalkaskade führte zu gesteigerten Expressionsraten der EZM Proteine sowie zur Myodifferenzierung. In diesem etablierten fibrotischen Zellkulturmodell konnte für das Pharmakon PFD eine antifibrotische Wirkung *in vitro* nachgewiesen werden, die durch verminderte Proliferations- und Expressionsraten gekennzeichnet war. Die antifibrotischen Eigenschaften konnten innerhalb einer tierexperimentellen Studie *in vivo*, in der beschichtete GDI-DDS-Prototypen in das subkutane weiße Fettgewebe von Ratten implantiert wurden, bestätigt werden. Gegenüber den zusätzlich untersuchten Wirkstoffen CAPE und PTX stellte sich PFD als effektivstes Antifibrotikum heraus und wurde für weitere, derzeit laufende Tierstudien selektiert. Zur postoperativen Beurteilung implantierter GDI-DDS wurde ein temporäres Glaukommodell entwickelt und etabliert. Die Methode der OPT wurde hierfür an die anatomischen Gegebenheiten des Kaninchenauges *in vivo* adaptiert, was über die Bestimmung der Kammerwasserabflussfazilität eine Beurteilung der Langzeitfunktionalität implantierter GDI erlaubt.

In einer weiteren Studie über postoperative Wundheilungsmechanismen wurden die Zytokin/Chemokin-Level des Kammerwassers von Patienten mit POAG nach erfolgter Trabekulektomie evaluiert. Es konnte gezeigt werden, dass bei Patienten mit durch Fibrose verursachtem negativen Ergebnis 104 Proteine im Vergleich zur Patientengruppe mit positivem Operationsergebnis (ohne Fibrose) signifikant hochreguliert und 27 Proteine signifikant runterreguliert wurden. Es ist bekannt, dass viele der identifizierten Zy-

tokine profibrotische Eigenschaften aufweisen. Weiterhin wurden 49 für inflammatorische Prozesse verantwortliche Zytokine hochreguliert. Eine generische Computer-Datenprozessierung konnte den Zytokinen TGF-β1, VEGF, CTGF, PDGF und IL8 Schlüsselfunktionen in der Fibrose zuordnen. Die identifizierten Zytokine bieten Möglichkeiten, mittels entsprechender Inhibitoren in die Zellkommunikation einzugreifen und die Wundheilung spezifisch zu modulieren.

In einem zweiten Themenkomplex wurden in experimentellen Studien *in vitro* die Wundheilungsmechanismen der Kornea untersucht. Unter der Verwendung von murinen Cokultursystemen aus kornealen Epithelzellen und Neuronen trigeminalen Ursprungs konnte eine gegenseitige Stimulation der Zellen demonstriert werden. Es wurde gezeigt, dass die Zytokine SP, BMP7 und Pax6 im Mittelpunkt kornealer Wundheilungsprozesse stehen. Weiterhin konnte eine EMT der Epithelzellen nach Verletzungen nachgewiesen werden, die mit gesteigerten Expressionsraten von BMP7 und Pax6 einhergingen. Die Zytokin-vermittelte Zelltyp-übergreifende interzelluläre Kommunikation bietet demnach Möglichkeiten der spezifischen Wundheilungsmodulation der Kornea, die fibrotische Prozesse unterbinden oder zu einer beschleunigten Genese beitragen kann.

In einem letzten Themenkomplex wurden postoperative Wundheilungsprozesse nach durchgeführter Kataraktchirurgie näher betrachtet. Hierzu wurden zunächst mittels der MRM die anatomischen Mikrostrukturen der humanen Linse artefaktfrei visualisiert und mit der klassischen Histologie verglichen. Da sich die PCO aus intraoperativ im Kapselsack verbliebenen Linsenepithelzellen entwickelt, welche den Prozess der EMT durchlaufen, wurde ein Transfer der Erkenntnisse aus der kornealen Wundheilungsstudien detailliert erörtert und diskutiert sowie Lösungsansätze zur Vermeidung einer PCO durch Wundheilungsmodulation aufgezeigt. Neben der Linse wurde zusätzlich der Ziliarkörper mit den Bildgebungsmodalitäten untersucht und ermöglichte eine hochaufgelöste Darstellung und Charakterisierung möglicher Implantat- und Drainageräume für die fistulierende Glaukomchirurgie. Eine Anwendung der MRM *in vivo* erlaubt somit die postoperative Charakterisierung einsetzender Vernarbungsprozesse in beiden Anwendungsfeldern.

Die in dieser Arbeit dargelegten Ergebnisse zeigen Möglichkeiten für alle drei ophthalmologischen Anwendungsfelder auf, um gezielt in Wundheilungsprozesse einzu-

greifen. Die spezifische Modulation der fibrotischen Vernarbungsreaktionen könnte zukünftig dazu beitragen, eine Langzeitfunktionalität chirurgischer Interventionen bzw. von Implantaten nebenwirkungsarm zu garantieren, den Visus zu erhalten und Sekundäreingriffe zu vermeiden.

Literaturverzeichnis

Abdelfattah NS, Amgad M, Zayed AA, Salem H, Elkhanany AE, Hussein H, Abd El-Baky N. Clinical correlates of common corneal neovascular diseases: a literature review. Int J Ophthalmol. 2015, 18;8(1):182-93. DOI: 10.3980/j.issn.2222-3959.2015.01.32.

Agarwal R, Iezhitsa IN, Agarwal P, Spasov AA. Mechanisms of cataractogenesis in the presence of magnesium deficiency. Magnes Res. 2013, 26(1):2-8. DOI: 10.1684/mrh.2013.0336.

Allemann R, Stachs O, Falke K, Schmidt W, Siewert S, Sternberg K, Chichkov B, Wree A, Schmitz KP, Guthoff RF. Neue Konzepte für druckgesteuerte Glaukomimplantate. Ophthalmologe. 2013, 110(8):733-9. DOI: 10.1007/s00347-013-2839-5.

Baudouin C. Detrimental effect of preservatives in eyedrops: implications for the treatment of glaucoma. Acta Ophthalmol. 2008, 86(7):716-26. DOI: 10.1111/j.1755-3768.2008.01250.x.

Borkenstein, A., Faschinger, C., Maier, R., Weger, M., Theisl, A., Demel, U, Graninger W, Holzer I, Mossböck G. Measurement of tumor necrosis factor-alpha, interleukin-6, Fas ligand, interleukin-1alpha, and interleukin-1beta in the aqueous humor of patients with open angle glaucoma using multiplex bead analysis. Mol. Vis. 2013, 19, 2306–2311. PMCID: PMC3834596.

Boswell BA, Korol A, West-Mays JA, Musil LS. Dual function of TGFβ in lens epithelial cell fate: implications for secondary cataract. Mol Biol Cell. 2017, 1;28(7):907-921. DOI: 10.1091/mbc.E16-12-0865.

Bukowiecki A, Hos D, Cursiefen C, Eming SA. Wound-Healing Studies in Cornea and Skin: Parallels, Differences and Opportunities. Int J Mol Sci. 2017, 18(6):1257. DOI: 10.3390/ijms18061257.

Cairns JE. Trabeculectomy. Preliminary report of a new method. Am J Ophthalmol. 1968, 66(4):673-679. DOI: 10.1016/0002-9394(68)91288-9.
Cheng H. Causes of cataract. BMJ. 1989, 3;298(6686):1470–1471. DOI: 10.1136/bmj.298.6686.1470.

Christakis PG, Tsai JC, Kalenak JW, Zurakowski D, Cantor LB, Kammer JA, Ahmed IIK. The Ahmed versus Baerveldt study: three-year treatment outcomes. Ophthalmology. 2013, 120(11)2232–2240. DOI: 10.1016/j.ophtha.2013.04.018.

Chung EJ, Lee HK, Jung SA, Lee SJ, Chee HY, Sohn YH, Lee JH. Transduction of PTEN Proteins Using the Tat Domain Modulates TGF-β1–Mediated Signaling Pathways and Transdifferentiation in Subconjunctival Fibroblasts. Invest Ophthalmol Vis Sci. 2012, 53:379-386. DOI: 10.1167/iovs.11-8491.

Congdon N, Vingerling JR, Klein BE, West S, Friedman DS, Kempen J, O'Colmain B, Wu SY, Taylor HR; Eye Diseases Prevalence Research Group. Prevalence of cataract and pseudophakia/aphakia among adults in the United States. Arch Ophthalmol. 2004, 122(4):487-94. DOI: 10.1001/archopht.122.4.487.

Cortina P, Gomez-Lechon MJ, Navea A, Menezo JL, et al. Diclofenac sodium and cyclosporin A inhibit human lens epithelial cell proliferation in culture. Graefes. Arch. Clin. Exp. Ophthalmol. 1997, 235:180. PMID: 9085114.

Cvenkel B, Kopitar AN, Ihan A. Inflammatory Molecules in Aqueous Humour and on Ocular Surface and Glaucoma Surgery Outcome Mediators Inflamm. 2010, 2010:939602. DOI: 10.1155/2010/939602.

Davis J, Duncan MK, Robison Jr. WGG, Piatigorsky J. Requirement for Pax6 in corneal morphogenesis: a role in adhesion. J. Cell Sci. 2003, 116(11):2157–2167. DOI: 10.1242/jcs.00441.

Davis J, Piatigorsky J. Overexpression of Pax6 in Mouse Cornea Directly Alters Corneal Epithelial Cells: Changes in Immune Function, Vascularization, and Differentiation. Invest Ophthalmol Vis Sci. 2011, 52(7):4158–4168. DOI: 10.1167/iovs.10-6726.

Derrick T, Holland MJ, Cassama E, Markham-David R, Nabicassa M, Marks M, Bailey RL, Last AR. Can corneal pannus with trachomatous inflammation – follicular be used in combination as an improved specific clinical sign for current ocular Chlamydia trachomatis infection? Parasit Vectors. 2016, 9:30. DOI: 10.1186/s13071-016-1308-9.

Deutsche Ophthalmologische Gesellschaft (DOG), Weißbuch zur Situation der ophthalmologischen Forschung in Deutschland. 2012, 8-9.

Droy-Lefaix MT, Bueno L, Caron P, Belot E, Roche O. Ocular inflammation and corneal permeability alteration by benzalkonium chloride in rats: a protective effect of a myosin light chain kinase inhibitor. Invest Ophthalmol Vis Sci. 2013, 17;54(4):2705-10. DOI: 10.1167/iovs.12-10193.

Dunn JP, Seamone CD, Ostler HB, Nickel BL, Beallo A. Development of scleral ulceration and calcification after pterygium excision and mitomycin therapy. Am J Ophthalmol. 1991, 112:343-344. DOI: 10.1016/S0002-9394(14)76738-8.

Ehrnrooth, P, Lehto, I, Puska, P, Laatikainen, L. Long-term outcome of trabeculectomy in terms of intraocular pressure. Acta ophthalmologica Scandinavica, 2002, 80(3):267-271. DOI: 10.1034/j.1600-0420.2002.800307.x.

Eming, S. A., Martin, P., & Tomic-Canic, M. Wound repair and regeneration: Mechanisms, signaling, and translation. Science Translational Medicine, 2014, 6(265):265sr6–265sr6. DOI: 10.1126/scitranslmed.3009337.

Fedorov SN, Ioffe, DI, Ronkina TI. Glaucoma surgery – deep sclerectomy. Vestn Ophthal. 1982, 4:6-10. PMID: 7135737

Fong AW, Lee GA, O'Rourke P, Thomas R. Management of neovascular glaucoma with transscleral cyclophotocoagulation with diode laser alone versus combination transscleral cyclophotocoagulation with diode laser and intravitreal bevacizumab. Clin and Exp Ophthalmol. 2011, 39:318-323. DOI: 10.1111/j.1442-9071.2010.02449.x.

Frech S, Kreft D, Guthoff RF, Doblhammer G. Pharmacoepidemiological assessment of adherence and influencing co-factors among primary open-angle glaucoma patients-An observational cohort study. PLoS One. 2018, 12;13(1):e0191185. DOI: 10.1371/journal.pone.0191185

Friedlander M. Fibrosis and diseases of the eye. J Clin Invest. 2007, 117(3):576-86. DOI: 10.1172/JCI31030.

Friedman DS, Wolfs RC, O'Colmain BJ, Klein BE, Taylor HR, West S, Leske MC, Mitchell P, Congdon N, Kempen J; Eye Diseases Prevalence Research Group. Prevalence of open-angle glaucoma among adults in the United States. Arch Ophthalmol. 2004, 122(4):532-8. DOI: 10.1001/archopht.122.4.532

Gajda-Deryło B, Stahnke T, Struckmann S, Warsow G, Birke K, Birke MT, Hohberger B, Rejdak R, Fuellen G, Jünemann AG. Comparison of cytokine/chemokine levels in aqueous humor of primary open-angle glaucoma patients with positive or negative outcome following trabeculectomy. Biosci Rep. 2019, 2;39(5). pii: BSR20181894. DOI: 10.1042/BSR20181894.

Gedde SJ, Schiffman JC, Feuer WJ, Herndon LW, Brandt JD, Budenz DL. Treatment outcomes in the Tube Versus Trabeculectomy (TVT) study after five years of follow-up. Am J Ophthalmol. 2012, 153(5)789-803.e2. DOI: 10.1016/j.ajo.2011.10.026.

Gillies MC, Su, T. Cytokines, fibrosis and the failure of glaucoma filtration surgery. Aust N Z J Ophthalmol. 1991, 19(4):299-304. DOI: 10.1111/j.1442-9071.1991.tb00676.x.

Gorath M, Stahnke T, Mronga T, Goldbaum O, Richter-Landsberg C. Developmental changes of tau protein and mRNA in cultured rat brain oligodendrocytes. Glia 2001;36:89-101. DOI: 10.1002/glia.1098.

Gurujeyalakshmi G, Hollinger MA, Giri SN. Pirfenidone inhibits PDGF isoforms in bleomycin hamster model of lung fibrosis at the translational level. Am. J. Physiol. 1999, 276:L311–L318. DOI: 10.1152/ajplung.1999.276.2.L311.

Guthoff RF, Schmidt W, Buß D, Schultze C, Ruppin U, Stachs O, Sternberg K, Klee D, Chichkov B, Schmitz K-P. Entwicklung eines Glaukommikrostents mit Drainage in den suprachoroidalen Raum. Fluidmechanische Modellbetrachtungen. Ophthalmologe 2009, 106:805-812. DOI: 10.1007/s00347-009-1929-x.

Hengerer FH, Auffarth GU, Riffel C, Conrad-Hengerer I. Second-Generation Trabecular Micro-Bypass Stents as Standalone Treatment for Glaucoma: A 36-Month Prospective Study. Adv Ther. 2019, 22. DOI: 10.1007/s12325-019-00984-9.

Herath TDK, Larbi A, Teoh SH, Kirkpatrick CJ, Goh BT. Neutrophil-mediated enhancement of angiogenesis and osteogenesis in a novel triple cell co-culture model with endothelial cells and osteoblasts. J Tissue Eng Regen Med. 2018, 12(2):e1221-e1236. DOI: 10.1002/term.2521.

Hinz B, Phan SH, Thannickal VJ, Galli A, Bochaton-Piallat ML, Gabbiani G. The myofibroblast: one function, multiple origins. Am J Pathol. 2007, 170(6):1807-16. DOI: 10.2353/ajpath.2007.070112.

Hovakimyan M, Siewert S, Schmidt W, Sternberg K, Reske T, Stachs O, Guthoff R, Wree A, Witt M, Schmitz KP, Allemann R. Development of an Experimental Drug Eluting Suprachoroidal Microstent as Glaucoma Drainage Device. Transl Vis Sci Technol. 2015, 30;4(3):14. DOI: 10.1167/tvst.4.3.14.

Inan UU, Ozturk F, Kaynak S, Ilker SS, et al. Prevention of posterior capsule opacification by retinoic acid and mitomycin. Graefes. Arch. Clin. Exp. Ophthalmol. 2001, 239: 693. PMID: 11688670.

Johnson MB, Young AD, Marriott I. The Therapeutic Potential of Targeting Substance P/NK-1R Interactions in Inflammatory CNS Disorders. Front Cell Neurosci. 2017, 4;10:296. DOI: 10.3389/fncel.2016.00296.

Jung KI, Park CK. Pirfenidone inhibits fibrosis in foreign body reaction after glaucoma drainage device implantation. Drug Des Devel Ther. 2016, 10:1477–1488. DOI: 10.2147/DDDT.S99957.

Kammer JA, Mundy KM. Suprachoroidal Devices in Glaucoma Surgery. Middle East Afr J Ophthalmol. 2015, 22(1):45–52. DOI: 10.4103/0974-9233.148348.

Karamichos D, Guo XQ, Hutcheon AEK, Zieske JD. Human Corneal Fibrosis: An In Vitro Model. Invest Ophthalmol Vis Sci. 2010, 51(3):1382–1388. DOI: 10.1167/iovs.09-3860.

Kasper JY, Hermanns MI, Unger RE, Kirkpatrick CJ. A responsive human triple-culture model of the air-blood barrier: incorporation of different macrophage phenotypes. J Tissue Eng Regen Med. 2017, 11(4):1285-1297. DOI: 10.1002/term.2032.

Kassumeh SA, Wertheimer CM, von Studnitz A, Hillenmayer A, Priglinger C, Wolf A, Mayer WJ, Teupser D, Holdt LM, Priglinger SG, Eibl-Lindner KH. Poly(lactic-co-glycolic) Acid as a Slow-Release Drug-Carrying Matrix for Methotrexate Coated onto Intraocular Lenses to Conquer Posterior Capsule Opacification. Curr Eye Res. 2018, 43(6):702-708. DOI: 10.1080/02713683.2018.1437455.

Kawashima M, Kawakita T, Higa K, Satake Y, Omoto M, Tsubota K, Shimmura S, Shimazaki J. Subepithelial corneal fibrosis partially due to epithelial-mesenchymal transition of ocular surface epithelium. Mol Vis. 2010, 15;16:2727-32. PMCID: PMC3002964.

Khokhar SK, Pillay G, Dhull C, Agarwal E, Mahabir M, Aggarwal P. Pediatric cataract. Indian J Ophthalmol. 2017, 65(12): 1340–1349. DOI: 10.4103/ijo.IJO_1023_17.

Kirkpatrick CJ. Developing cellular systems in vitro to simulate regeneration. Tissue Eng Part A. 2014, 20(9-10):1355-7. DOI: 10.1089/ten.tea.2014.0002.

Klinkhammer BM, Floege J, Boor P. PDGF in organ fibrosis. Mol Aspects Med. 2018, 62:44-62. DOI: 10.1016/j.mam.2017.11.008.

Kohnen, T., Katarkt- und Refraktive Chirurgie. 2008, Köln: Biermann-Verlag.

Koller T, Stürmer J, Remé C, Gloor B. Risikofaktoren für die Entstehung einer zum Versagen der Argonlasertrabekuloplastik führenden Membran im Kammerwinkel. Ophthalmologe 1996, 93(5):552-557. DOI: 10.1007/s003470050037.

Koopmans SA, Terwee T, Hanssen A, Martin H, Langner S, Stachs O, van Kooten TG. Prevention of capsule opacification after accommodating lens refilling: pilot study of strategies evaluated in a monkey model. J Cataract Refract Surg. 2014, 40(9):1521-35. DOI: 10.1016/j.jcrs.2014.02.034.

Kopp F, Koschmieder A, Stahnke T, Pfensig S, Specht O, Grabow N, Schmitz K-P, Guthoff R, Siewert S. Development of an oculopressor to evaluate efficiency of glaucoma drainage devices. Klin Monatsbl Augenheilkd. 2018, 235(12):1360-1365. DOI: 10.1055/a-0792-1247.

Kowtharapu BS, Murín R, Jünemann AGM, Stachs O. Role of Corneal Stromal Cells on Epithelial Cell Function during Wound Healing. Int J Mol Sci. 2018a, 4;19(2). pii: E464. DOI: 10.3390/ijms19020464.

Kowtharapu BS, Prakasam RK, Murín R, Koczan D, Stahnke T, Wree A, Jünemann AGM, Stachs O. Role of Bone Morphogenetic Protein 7 (BMP7) in the Modulation of Corneal Stromal and Epithelial Cell Functions. Int J Mol Sci. 2018b, 9;19(5). pii: E1415. DOI: 10.3390/ijms19051415.

Kowtharapu BS, Stahnke T, Wree A, Guthoff RF, Stachs O. Corneal epithelial and neuronal interactions: role in wound healing. Exp Eye Res. 2014, 125:53-61. DOI: 10.1016/j.exer.2014.05.006.

Krzyszczyk P, Schloss R, Palmer A, Berthiaume F. The Role of Macrophages in Acute and Chronic Wound Healing and Interventions to Promote Pro-wound Healing Phenotypes. Front. Physiol., 2018, 9:419. DOI: 10.3389/fphys.2018.00419.

Kuerzinger GRK und Eckert S. Verfügbare Lasersysteme und Wirkprinzip der Lasertrabekuloplastik. Available laser systems and mechanism of action in laser trabeculoplasty. Ophthalmologe 2010, 107:8-12. DOI: 10.1007/s00347-009-2051-9.

Lavia C, Dallorto L, Maule M, Ceccarelli M, Fea AM. Minimally-invasive glaucoma surgeries (MIGS) for open angle glaucoma: A systematic review and meta-analysis. PLoS One. 2017, 29;12(8):e0183142. DOI: 10.1371/journal.pone.0183142.

Lee JS, Chung CC, Lin KK, Yu KH, Kuo CF, See LC. Time trends in cataract surgery and after-cataract laser capsulotomy in Taiwan: A population-based retrospective cohort study. Int J Surg. 2016, 36(Pt A):265-273. DOI: 10.1016/j.ijsu.2016.11.011.

Lenzhofer M, Hohensinn M, Strohmaier C, Reitsamer HA. Subconjunctival minimally invasive glaucoma surgery: Methods and clinical results. Ophthalmologe. 2018, 115(5):381-387. DOI: 10.1007/s00347-018-0669-1.

Lim KS, Allan BD, Lloyd AW, Muir A, Khaw PT. Glaucoma drainage devices; past present, and future. Br J Ophthalmol. 1998, 82:1083-1089. DOI: 10.1136/bjo.82.9.1083.

Lipson KE, Wong C, Teng Y, Spong S. CTGF is a central mediator of tissue remodeling and fibrosis and its inhibition can reverse the process of fibrosis. Fibrogenesis & Tissue Repair 2012, 5(1):S24. https://doi.org/10.1186/1755-1536-5-S1-S24.

Lockwood, A.; Brocchini, S.; Khaw, P.T. (2013): New developments in the pharmacological modulation of wound healing after glaucoma filtration surgery. Current Opinion in Pharmacology, 2013, 13:65-71. DOI: 10.1016/j.coph.2012.10.008.

Lopez-de la Mora DA, Sanchez-Roque C, Montoya-Buelna M, Sanchez-Enriquez S, Lucano-Landeros S, Macias-Barragan J, Armendariz-Borunda J. Role and New Insights of Pirfenidone in Fibrotic Diseases. Int J Med Sci. 2015, 12(11): 840–847. DOI: 10.7150/ijms.11579.

Ma T, Huang C, Xu Q, Yang Y, Liu Y, Meng X, Li J, Ye M, Liang H. Suppression of BMP-7 by histone deacetylase 2 promoted apoptosis of renal tubular epithelial cells in acute kidney injury. Cell Death Dis. 2017, 26;8(10):e3139. DOI: 10.1038/cddis.2017.552.

Malecaze F, Decha A, Serre B, Penary M, Duboue M, Berg D, Levade T, Lubsen NH, Kremer EJ, Couderc B. Prevention of posterior capsule opacification by the induction of therapeutic apoptosis of residual lens cells. Gene Ther. 2006, 13:440. DOI: 10.1038/sj.gt.3302667.

Mearza AA, Aslanides JM. Uses and complications of mitomycin C in ophthalmology. Expert Opinion on Drug Safety. 2007, 6:27-32. DOI: 10.1517/14740338.6.1.27.

Medeiros CS, Marino GK, Santhiago MR, Wilson SE. The Corneal Basement Membranes and Stromal Fibrosis. Invest Ophthalmol Vis Sci. 2018, 1;59(10):4044-4053. DOI: 10.1167/iovs.18-24428.

Mohammadpour M, Abrishami M, Masoumi A, Hashemib H. Trachoma: Past, present and future. J Curr Ophthalmol. 2016, 28(4):165–169. DOI: 10.1016/j.joco.2016.08.011.

Mostafaei A. Augmenting trabeculectomy in glaucoma with subconjunctival mitomycin C versus subconjunctival 5-fluorouracil: a randomized clinical trial. Clin Ophthalmol. 2011, 5:491-494. DOI: 10.2147/OPTH.S17328.

Nanavaty MA, Johar K, Sivasankaran MA, Vasavada AR, et al. Effect of trypan blue staining on the density and viability of lens epithelial cells in white cataract. J. Cataract Refract Surg. 2006, 32:1483. DOI: 10.1016/j.jcrs.2006.04.017.

Navas A, Magaña-Guerrero FS, Domínguez-López A, Chávez-García C, Partido G, Graue-Hernández EO, Sánchez-García FJ, Garfias Y. Anti-Inflammatory and Anti-Fibrotic Effects of Human Amniotic Membrane Mesenchymal Stem Cells and Their Potential in Corneal Repair. Stem Cells Transl Med. 2018, 7(12):906-917. DOI: 10.1002/sctm.18-0042.

Nibourg LM, Gelens E, Kuijer R, Hooymans JM, van Kooten TG, Koopmans SA. Prevention of posterior capsular opacification. Exp Eye Res. 2015, 136:100-15. DOI: 10.1016/j.exer.2015.03.011. Epub 2015 Mar 14.

Nicula C, Szabo I, Ivan O. Stem cells treatment in the ocular surface regeneration. Rom J Ophthalmol. 2017, 61(4):239-243. PMCID: PMC5827138.

Nikita E, Moulin A, Vergados I, Brouzas D, Theodossiadis PG. A Pilot Study on Ocular Safety and Efficacy of Infliximab as an Antifibrotic Agent After Experimental Glaucoma Filtration Surgery. Ophthalmol Ther. 2017, 6(2):323-334. DOI: 10.1007/s40123-017-0096-4.

Nishi O, Nishi K, Wada K, Ohmoto Y, Akura J. Inhibition of lens epithelial cells by Fas-specific antibody activating Fas-Fas ligand system. Curr. Eye Res. 2001, 23:192. PMID: 11803481.

Nishi O, Yamamoto N, Nishi K, Nishi Y. Contact inhibition of migrating lens epithelial cells at the capsular bend created by a sharp-edged intraocular lens after cataract surgery. J Cataract Refract Surg. 2007, 33(6):1065-70. DOI: 10.1016/j.jcrs.2007.02.022.

Oku H, Nakazato H, Horikawa T, Tsuruta Y, Suzuki R. Pirfenidone suppresses tumor necrosis factor-alpha, enhances interleukin-10 and protects mice from endotoxic shock. Eur J Pharmacol. 2002, 20;446(1-3):167-76. DOI: 10.1016/S0014-2999(02)01757-0.

Papiris SA, Tomos IP, Karakatsani A, Spathis A, Korbila I, Analitis A, Kolilekas L, Kagouridis K, Loukides S, Karakitsos P, Manali ED. High levels of IL-6 and IL-8 characterize early-on idiopathic pulmonary fibrosis acute exacerbations. Cytokine. 2018, 102:168-172. DOI: 10.1016/j.cyto.2017.08.019.

Park HY, Kim JH, Park CK. VEGF induces TGF-β1 expression and myofibroblast transformation after glaucoma surgery. Am J Pathol. 2013, 182(6):2147-54. DOI: 10.1016/j.ajpath.2013.02.009.

Pillunat LE, Erb C, Jünemann AG, Kimmich F. Micro-invasive glaucoma surgery (MIGS): a review of surgical procedures using stents. Clin Ophthalmol. 2017, 29;11:1583-1600. DOI: 10.2147/OPTH.S135316.

Pollreisz A, Schmidt-Erfurth U. Diabetic cataract-pathogenesis, epidemiology and treatment. Ophthalmol. 2010, 2010:608751. DOI: 10.1155/2010/608751.

Ponnusamy T, Yu H, John VT, Ayyala RS, Blake DA. A Novel Antiproliferative Drug Coating for Glaucoma Drainage Devices. J Glaucoma. 2013, 23(8)526–534. DOI: 10.1097/IJG.0b013e318294869b

Raivio VE, Puska PM, Immonen IJR. Cyclophotocoagulation with the transscleral contact red 670-nm diode laser in the treatment of glaucoma. Acta Ophthalmol. 2008, 86:558-564. DOI: 10.1111/j.1600-0420.2007.01090.x.

Raj SM, Vasavada AR, Johar SR, Vasavada VA, Vasavada VA. Post-operative capsular opacification: a review. Int J Biomed Sci. 2007, 3(4):237-50. PMCID: PMC3614664.

Reid TW, Murphy CJ, Iwahashi CK, Foster BA, Mannis MJ. Stimulation of epithelial cell growth by the neuropeptide substance P. J. Cell. Biochem.1993, 52:476–485. DOI: 10.1002/jcb.240520411.

Rieck PW, Sherif ZAR, Hartmann C, Pleyer U. Wundheilung der Hornhaut. Teil I: Biologische Grundlagen und ihre klinische Relevanz. Ophthalmologe. 2003, 100:749–770. DOI 10.1007/s00347-003-0892-1.

Roberts JE, Finley EL, Patat SA, Schey KL. Photooxidation of lens proteins with xanthurenic acid: a putative chromophore for cataractogenesis. Photochem Photobiol. 2001, 74(5):740-4. DOI: 10.1562/0031-8655(2001)0740740POLPWX2.0.CO2.

Rolim de Moura C, Fraser-Bell S, Stout A, Labree L, Nilfors M, Varma R. Experience with the baerveldt glaucoma implant in the management of pediatric glaucoma. Am J Ophthalmol. 2005, 139(5)847–854. DOI: 10.1016/j.ajo.2004.12.028.

Saika S, Yamanaka O, Okada Y, Tanaka S, Miyamoto T, Sumioka T, Kitano A, Shirai K, Ikeda K. TGF beta in fibroproliferative diseases in the eye. Front Biosci (Schol Ed). 2009, 1;1:376-90. PMID: 19482708.

Sarkar J, Chaudhary S, Namavari A, Ozturk O, Chang J-H, Yco L, Sonawane S, Khanolkar V, Hallak J, Jain S. Corneal Neurotoxicity Due to Topical Benzalkonium Chloride. Invest Ophthalmol Vis Sci. 2012, 53(4):1792-1802. DOI: 10.1167/iovs.11-8775

Sauder G, Jonas JB. Limbal stem cell deficiency after subconjunctival mitomycin C injection for trabeculectomy. Am J Ophthalmol. 2006, 141(6):1129-30. DOI: 10.1016/j.ajo.2006.01.018

Scheibe K, Kersten C, Schmied A, Vieth M, Primbs T, Carlé B, Knieling F, Claussen J, Klimowicz AC, Zheng J, Baum P, Meyer S, Schürmann S, Friedrich O, Waldner MJ, Rath T, Wirtz S, Kollias G, Ekici AB, Atreya R, Raymond EL, Mbow ML, Neurath MF, Neufert C. Inhibiting Interleukin 36 Receptor Signaling Reduces Fibrosis in Mice With Chronic Intestinal Inflammation. Gastroenterology. 2019, 156(4):1082-1097.e11. DOI: 10.1053/j.gastro.2018.11.029.

Schlunck G, Meyer-ter-Vehn T, Klink T, Grehn F. Conjunctival fibrosis following filtering glaucoma surgery. Exp Eye Res. 2016, 142:76-82. DOI: 10.1016/j.exer.2015.03.021.

Schmidt W, Schultze C, Stachs O, Allemann R, Löbler M, Sternberg K, Hinze U, Chichkov B, Guthoff RF, Schmitz K-P. Konzept eines druckgesteuerten Mikrostents für die Glaukomtherapie. Concept of a Pressure-Controlled Microstent for Glaucoma Therapy. Klin Monatsbl Augenheilkd. 2010, 227:946-952. DOI: 10.1055/s-0029-1245928.

Shu DY, Wojciechowski MC, Lovicu FJ. Bone Morphogenetic Protein-7 Suppresses TGFβ2-Induced Epithelial-Mesenchymal Transition in the Lens: Implications for Cataract Prevention. Invest Ophthalmol Vis Sci. 2017, 58(2):781–796. DOI: 10.1167/iovs.16-20611.

Siewert S, Schmidt W, Kaule S, Kohse S, Stiehm M, Kopp F, Stahnke T, Guthoff R, Grabow N, Schmitz K-P. Development of a microstent system for minimally invasive glaucoma surgery. Current Directions in Biomedical Engineering2017; 3(2):779–781. DOI: 10.1515/cdbme-2017-0164.

Simirskii VN. Regeneration and Fibrosis of Corneal Tissues. Russian Journal of Developmental Biology, 2014, 45(5):257–266. DOI: 10.1134/S1062360414050099.

Smith M, Charles R, Abdel-Hay A, Shah B, Byles D, Lim LA, Rossiter J, Kuo CH, Chapman P, Robertson S. 1-year outcomes of the Xen45 glaucoma implant. Eye, 2019, 33:761–766. DOI: 10.1038/s41433-018-0310-1.

Stahnke T, Hadlich S, Wree A, Guthoff RF, Stachs O, Langner S. Magnetic Resonance Microscopy of the Accommodative Apparatus. Klin Monbl Augenheilkd. 2016, 233(12):1320-1323. DOI: 10.1055/s-0042-118599.

Stahnke T, Kowtharapu BS, Stachs O, Schmitz KP, Wurm J, Wree A, Guthoff RF, Hovakimyan M. Suppression of TGF-β pathway by pirfenidone decreases extracellular matrix deposition in ocular fibroblasts in vitro. PLoS One. 2017, 23;12(2):e0172592. DOI: 10.1371/journal.pone.0172592.

Stahnke T, Löbler M, Kastner C, Stachs O, Wree A, Sternberg K, Schmitz KP, Guthoff R. Different fibroblast subpopulations of the eye: a therapeutic target to prevent postoperative fibrosis in glaucoma therapy. Exp Eye Res. 2012, 100:88-97. DOI: 10.1016/j.exer.2012.04.015.

Stahnke T, Siewert S, Reske T, Schmidt W, Schmitz KP, Grabow N, Guthoff RF, Wree A. Development of a biodegradable antifibrotic local drug delivery system for glaucoma microstents. Biosci Rep. 2018, 31;38(4). pii: BSR20180628. DOI: 10.1042/BSR20180628.

Stahnke T, Siewert S, Walther E, Schmidt W, Stachs O, Schmitz KP, Guthoff RF. Adopting oculopressure tonometry as a transient in vivo rabbit glaucoma model. Current Directions in Biomedical Engineering. 2015, 1:127–130. DOI: 10.1515/cdbme-2015-0033.

Swamynathan SK. Ocular Surface Development and Gene Expression. Journal of Ophthalmology. 2013, 2013:103947. DOI: 10.1155/2013/103947.

Torricelli AA, Santhanam A, Wu J, Singh V, Wilson SE. The corneal fibrosis response to epithelial-stromal injury. Exp Eye Res. 2016, 142:110-8. DOI: 10.1016/j.exer.2014.09.012.

Ulrich WD, Moeller A, Ulrich C, Siebert G, Wernecke KD, Erb C. Ocular Blood Flow Regulation in Glaucoma – Examination with the Ocular Pressure Flow Analyzer (OPFA). Klin Monatsbl Augenheilkd. 2015; 232:152–161. DOI: 10.1055/s-0034-1396210.

Ulrich WD, Ulrich C, Neunhöffer E, Fuhrmann P. Oculopression Tonometry (OPT): A New Tonographic Procedure in Glaucoma Diagnosis. Klin Monatsbl Augenheilkd. 1987, 190(2):109-113. DOI: 10.1055/s-2008-1050339.

Ulrich WD, Ulrich C. Oculo-oscillo-dynamography: a diagnostic procedure for recording ocular pulses and measuring retinal and ciliary arterial blood pressures. Ophthalmic Res. 1985, 17(5):308-17. DOI: 10.1159/000265391

Valimaki J, Tuulonen A, Airaksinen PJ. Outcome of Molteno implantation surgery in refractory glaucoma and the effect of total and partial tube ligation on the success rate. Acta Ophthalmol Scand. 1998, 76(2)213–219. DOI: 10.1034/j.1600-0420.1998.760218.x.

Valimaki J. Surgical management of glaucoma with Molteno3 implant. J Glaucoma. 2012, ;21(1)7–11. DOI: 10.1097/IJG.0b013e3181fc8039.

van Kooten TG, Koopmans SA, Terwee T, Langner S, Stachs O, Guthoff RF. Long-term prevention of capsular opacification after lens-refilling surgery in a rabbit model. Acta Ophthalmol. 2019, 22. DOI: 10.1111/aos.14096.

Wacker T und Eckert S. Behandlungsmethoden und Komplikationen der Lasertrabekuloplastik. Laser trabeculoplasty: therapeutic options and adverse effects. Ophthalmologe 2009, 107(1):13-17. DOI: 10.1007/s00347-009-2052-8.

Wang J, Yang Y, Xu J, Lin X, Wu K, Yu M. Pirfenidone inhibits migration, differentiation, and proliferation of human retinal pigment epithelial cells in vitro. Mol Vis. 2013, 19: 2626–2635. PMCID: PMC3883732.

Wertheimer C, Kassumeh S, Piravej NP, Nilmayer O, Braun C, Priglinger C, Luft N, Wolf A, Mayer WJ, Priglinger SG, Eibl-Lindner KH. The Intraocular Lens as a Drug Delivery Device: In Vitro Screening of Pharmacologic Substances for the Prophylaxis of Posterior Capsule Opacification. Invest Ophthalmol Vis Sci. 2017, 1;58(14):6408-6418. DOI: 10.1167/iovs.17-22555.

Wilson SE, Marino GK, Torricelli AAM, Medeiros CS. Injury and defective regeneration of the epithelial basement membrane in corneal fibrosis: A paradigm for fibrosis in other organs? Matrix Biol. 2017, 64:17-26. DOI: 10.1016/j.matbio.2017.06.003.

Wilson SL, El Haj AJ, Yang Y. Control of Scar Tissue Formation in the Cornea: Strategies in Clinical and Corneal Tissue Engineering. J Funct Biomater. 2012, 3(3):642–687. DOI: 10.3390/jfb3030642.

Wormstone IM, Anderson IK, Eldred JA, Dawes LJ, Duncan G. Shortterm exposure to transforming growth factor beta induces long-term fibrotic responses. Exp Eye Res. 2006, 83:1238–1245. DOI: 10.1016/j.exer.2006.06.013.

Wormstone IM, Eldred JA. Experimental models for posterior capsule opacification research. Exp Eye Res. 2016, 142:2–12. DOI: 10.1016/j.exer.2015.04.021.

Xu X, Tang JM, Han YM, Wang W, Chen H, Lin QK. Surface PEGylation of intraocular lens for PCO prevention: An in vivo evaluation. J Biomater Appl. 2016, 31(1):68-76. DOI: 10.1177/0885328216638547.

Yamada N, Matsuda R, Morishige N, Yanai R, Chikama TI, Nishida T, Ishimitsu T, Kamiya A. Open clinical study of eye-drops containing tetrapeptides derived from substance P and insulin-like growth factor-1 for treatment of persistent corneal epithelial defects associated with neurotrophic keratopathy. Br J Ophthalmol. 2008 Jul;92(7):896-900. DOI: 10.1136/bjo.2007.130013.

Yamanaka O, Kitano-Izutani A, Tomoyose K, Reinach PS. Pathobiology of wound healing after glaucoma filtration surgery. BMC Ophthalmol.. 2015, 17;15 Suppl 1:157. DOI: 10.1186/s12886-015-0134-8.

Yuan H, Aimeng D, Liang H, Shao Z, Fan P, Zhou X. Glaucoma Drainage Device Coated with Mitomycin C Loaded Opal Shale Microparticles to Inhibit Bleb Fibrosis. ARVO Abstract 2019, #3750 — B0297.

Yu-Wai-Man C und Khaw PT. Personalized Medicine in Ocular Fibrosis: Myth or Future Biomarkers. Advances in Wound Care. 2016, 5(9):390-402. DOI: 10.1089/wound.2015.0677.

Zahir-Jouzdani F, Atyabi F, Mojtabavi N. Interleukin-6 participation in pathology of ocular diseases. Pathophysiology. 2017, 24(3):123-131. DOI: 10.1016/j.pathophys.2017.05.005.

Zhong H, Sun G, Lin X, Wu K, Yu M. Evaluation of Pirfenidone as a New Postoperative Antiscarring Agent in Experimental Glaucoma Surgery. Invest Ophthalmol Vis Sci. 2011, 52(6):3136-3142. DOI: 10.1167/iovs.10-6240.

Abkürzungsverzeichnis

5-FU	5-Fluoruracil
ANGPT	Angiopoetin
APO-1	Apoptose-Antigen-1 (oder Fas-Rezeptor)
AZAN	Azokarmin G und Anilinblau-Goldorange Färbung
BCMA	B-Zell reifendes Antigen / B-cell maturation antigen
BMP	Knochenmorphogenetische Proteine / Bone morphogenetic proteins
BrdU	Bromdesoxyuridin
CAPE	Kaffeesäure-Phenethylester / Caffeic acid phenethyl ester
CCL2	CC-Chemokinligand 2 / CC-chemokine ligand 2
CTGF	Bindegewebswachstumsfaktor / Connective tissue growth factor
CXCL12	C-X-C Motif Chemokine 12 / C-X-C motif chemokine 12
DDS	Drug-Delivery-System
DOG	Deutsche Ophthalmologische Gesellschaft
EMT	Epithelial-mesenchymale Transition
EPCs	Endotheliale Vorläuferzellen / Endothelial precursor cells
EZM	Extrazelluläre Matrix
FBSP	Fibroblasten-Spezifisches-Oberflächenprotein / Fibroblast specific surface protein
FOV	Untersuchungsfeld / Field of view
GAPDH	Glycerinaldehyd-3-phosphat-Dehydrogenase
GCSF	Granoluzyten Kolonie-stimulierender Faktor / Granulocyte colony-stimulating factor
GDI	Glaukom Drainage Implantat
H&E	Hämatoxylin-Eosin-Färbung
HGF	Hepatozyten-Wachstumsfaktor / Hepatocyte growth factor
hCF	Humane Choroidea-Fibroblasten
hOF	Humane orbitale Fibroblasten
hSF	Humane Sklera-Fibroblasten
hTF	Humane Tenon-Fibroblasten
HPLC	Hochdruckflüssigkeitschromatographie / High pressure liquid chromatography
ICAM	Interzelluläre Adhäsions-Moleküle
IGF	Insulinähnlicher Wachstumsfaktor / Insulin-like growth factor
IL	Interleukine
IOD/IOP	intraokularer Druck / Intraocular pressure
IOL	Intraokularlinse
IPF	Idiopathische Lungenfibrose / Idiopathic pulmonary fibrosis
LDD	Local drug-delivery
LLC	Großer latenter Proteinkomplex / Large latent protein complex
Mab1b	Mikrotubuli-assoziiertes Protein 1b
MIGS	Mikroinvasive Glaukomchirurgie / Minimally-invasive glaucoma surgery
MMC	Mitomycin C
mmHg	Millimeter Quecksilbersäule
MMP	Matrix Metalloproteinasen
MMP2/9	Matrix-Metalloprotease 2 und 9
MRM	Ultrahochfeld-Magnetresonanzmikroskopie
MRT	Magnetresonanztomographie
Nd:YAG	Neodym-dotierter Yttrium-Aluminium-Granat-Laser
OD	Oculus dexter / rechtes Auge
OPT	Okulopressionstonometrie

OS	Oculus sinister / linkes Auge
Pax6	Gepaartes Box-Protein 6 / Paired box protein 6
PCO	Posterior capsule opacification
PDGF	Blutplättchen abgeleiteter Wachstumsfaktor / Plateled derived growth factor
PFD	Pirfenidon
POAG	Primäres Offenwinkelglaukom / Primary open angle glaucoma
PTX	Paclitaxel
RhoA	Rho-GTPase / Ras homologe gene family member A (GTPase)
ROCK	Rho assozierte Proteinkinase / Rho-associated protein kinase
rtPCR	Reverse-Transkriptase-Polymerase- Kettenreaktion / Reverse transcription polymerase chain reaction
α-SMA	α-smooth muscle actin
SDS-PAGE	Natriumdodecylsulfat-Polyacrylamidgelelektrophorese / sodium dodecyl sulfate polyacrylamide gel electrophoresis
SP	Substanz P
STRING	Search Tool for the Retrieval of Interacting Genes/Proteins
TGF-β	Transformierender Wachstumsfaktor beta / transforming growth factor beta
TNF-α	Tumornekrosefaktor alpha
TRAIL	Tumornekrosefaktor-verwandter Apoptose-induzierender Ligand / Tumor Necrosis Factor Related Apoptosis Inducing Ligand
VEGF	Vascular Endothelial Growth Factor

Selbstständigkeitserklärung

Hiermit erkläre ich, diese Arbeit selbstständig angefertigt, alle verwendeten Ergebnisse und Daten anderer vollständig angegeben und korrekt zitiert sowie jedwede weitere Mitwirkung Dritter offengelegt zu haben.
Weiterhin erkläre ich, dass mir die Bestimmungen der Habilitationsordnung bekannt sind und von mir anerkannt werden. Ich habe bisher weder an einer anderen Fakultät noch an einer anderen Hochschule ein Habilitationsverfahren eingeleitet.

Rostock, 02.07.2019 Dr. rer. nat. Thomas Stahnke

Danksagung

Diese Schrift ist das Ergebnis eines Teils der wissenschaftlichen Aktivitäten der experimentellen Ophthalmologie der Universitätsaugenklinik Rostock in den Jahren 2012 bis 2019 und wäre ohne die Unterstützung durch die ärztlichen und naturwissenschaftlichen Kollegen nicht möglich gewesen.

Mein herzlicher Dank geht an Herrn Prof. Dr. med. Rudolf Guthoff für die vertrauensvolle Zusammenarbeit, die fachliche und freundschaftliche Unterstützung sowie dafür, mir alle Freiheiten gelassen zu haben.

Weiterhin bedanke ich mich besonders bei Herrn Prof. Dr. rer. nat. Oliver Stachs für die gute interdisziplinäre Zusammenarbeit, die zahlreichen Diskussionen sowie für seine exzellenten Anmerkungen und konstruktiven Kritiken.

Mein Dank gilt ebenso Prof. Dr. med. Andreas Wree, der mir jederzeit bei anatomischen Fragestellungen zur Seite stand und mir die Nutzung der Labore ermöglichte.

Prof. Dr.-Ing. Klaus-Peter Schmitz danke ich für seine stete Unterstützung, ohne die diese Arbeit nicht entstanden wäre. Ich danke auch den Teams des IBMT und IIB e.V. für die gute kooperative Zusammenarbeit.

Bedanken möchte ich mich ebenfalls bei Prof. Dr. med. Anselm Jünemann und Prof. Dr. rer. nat. Georg Füllen für die hilfreichen fachlichen Diskussionen und die gemeinsamen interessanten Projekte.

Mein Dank gilt auch Herrn Prof. Dr. med. Dr. rer. nat. Thomas Fuchsluger für seine Unterstützung und für die Anregungen zu neuen Projekten im Bereich der kornealen Wundheilung.

Ich danke von Herzen allen derzeitigen und natürlich auch ehemaligen Kollegen und Kooperationspartnern für das hervorragende Arbeitsklima sowie die Hilfsbereitschaft. Mein besonderer Dank gilt Dr. rer. nat. habil. Marina Hovakimyan, Dr. rer. nat. Bhavani Kowtharapu, Dr. rer. nat. Franziska Kopp und Dipl. Biol. Marko Schulze, die mir jederzeit freundschaftlich mit ihrem Fachwissen zur Seite standen.

Nicht zuletzt möchte ich vor allem meinen Eltern und meiner Familie, insbesondere meiner Frau Miriam sowie meinem Sohn Thore, für ihre unendliche Geduld, Motivation, Unterstützung und Liebe, ohne die diese Arbeit nicht möglich gewesen wäre, danken.

Lebenslauf

Name:	Dr. rer. nat. Thomas Stahnke
Geb.:	04.03.1969 in Wilhelmshaven
Familienstand:	verheiratet, 1 Kind
Adresse:	Sebastian-Bach-Straße 3, 18069 Rostock

Schulabschluss:	1989 Abitur, Humboldt-Gymnasium, Wilhelmshaven
Berufsausbildung:	1992 - 1994, Berufsfachschule „Die Schule“, Abschluss: Biologisch-technischer Assistent (BTA).
Wehrdienst:	1990 - 1992, Dienst als Zeitsoldat (Navigation) in der Bundesmarine auf der Fregatte Bremen.

Universitätsausbildung:

1994 - 2001:	Studium der Biologie, Carl von Ossietzky Universität Oldenburg
27.02.2001:	Diplom der Biologie. Thema der Diplomarbeit: „Entwicklungsabhängige Veränderung des Tau-Proteins und chemischer Stress in Oligodendrozyten“ (Note: sehr gut)
2001 - 2004:	Promotion in der AG Molekulare Neurobiologie und Neurochemie, Carl von Ossietzky Universität Oldenburg. Thema der Dissertation: „Oxidativer Stress in Oligodendrozyten und die Bedeutung bei demyelinisierenden Erkrankungen“ (Note: *magna cum laude*)
02/2005 – 07/.2007	Wissenschaftlicher Mitarbeiter in der AG Molekulare Neurobiologie und Neurochemie, Carl von Ossietzky Universität Oldenburg. Projekt: „Inbibition of the Notch-Pathway: A potential strategy to promote oligodendrocyte differentiation?”
08/2007 – 05/2008	Mitarbeiter im familieneigenen Betrieb Minicar Dirks Ltd. In Wilhelmshaven (Management und Geschäftsaufbau).
06/2008 – 12/2010	Wissenschaftlicher Mitarbeiter in der AG Neuroembryologie unter Leitung von Herrn Prof. Dr. med. Norbert Ulfig, Institut für Anatomie, Universitätsmedizin Rostock.

01/2011 – 09/2014	Wissenschaftlicher Mitarbeiter unter Leitung von Herrn Prof. Dr. med. Rudolf Guthoff in der Universitätsaugenklinik, Universitätsmedizin Rostock
10/2014 – 03/2016	Wissenschaftlicher Mitarbeiter unter Leitung von Herrn Prof. Dr. med. Rudolf Guthoff im Institut für Biomedizinische Technik, Universitätsmedizin Rostock.
Seit 01.04.2016	Wissenschaftlicher Mitarbeiter unter Leitung von Herrn Prof. Dr. med. Rudolf Guthoff in der Universitätsaugenklinik in der AG RESPONSE, Universitätsmedizin Rostock.

Gutachtertätigkeiten:

- Current Eye Research
- Ophthalmic Research
- PLOS ONE
- Experimental Eye Research

Auszeichnungen und Preise:

- 111. Kongress der Deutschen Ophthalmologischen Gesellschaft (19.09. - 22.09.2013, Berlin, Deutschland). Posterpreis der DOG
- 112. Kongress der Deutschen Ophthalmologischen Gesellschaft (25.09. - 28.09.2014, Leipzig, Deutschland). Posterpreis der DOG

Rostock, 02.07.2019 Dr. rer. nat. Thomas Stahnke

Publikationsliste

Die in der kumulativen Habilitationsschrift integrierten Originalarbeiten sind mit einem ♦ markiert.

Originalarbeiten mit Impact-Factor:

1) ♦Gajda-Deryło B*, **Stahnke T***, Struckmann S, Warsow G , Birke K, Birke MT, Hohberger B, Rejdak R, Juenemann A. Comparison of Cytokine/Chemokine levels in aqueous humor of primary open-angle glaucoma patients with positive or negative outcome following trabeculectomy. Biosci Rep. 2019 May 2;39(5). pii: BSR20181894. doi: 10.1042/BSR20181894. (* Authors contributed equally). (5-year Impact Factor: 2,903)

2) Kopp F, Koschmieder A, **Stahnke T**, Pfensig S, Specht O, Grabow N, Schmitz K-P, Guthoff R, Siewert S. Development of an oculopressor to evaluate efficiency of glaucoma drainage devices. Klinische Monatsblätter für Augenheilkunde. 2018 Dec;235(12):1360-1365. DOI: 10.1055/a-0792-1247. (Impact Factor: 0,882)

3) ♦**Stahnke T**, Siewert S, Reske T, Schmidt W, Schmitz KP, Grabow N, Guthoff RF, Wree A. Development of a biodegradable antifibrotic Local Drug Delivery System for Glaucoma Microstents. Biosci Rep. 2018 Aug 31;38(4). pii: BSR20180628. DOI: 10.1042/BSR20180628. (5-year Impact Factor: 2,903)

4) Streckenbach F, Klose R, Langner S, Langner I, Frank M, Wree A, Neumann AM, Glass Ä, **Stahnke T**, Guthoff RF, Stachs O, Lindner T. Ultrahigh-Field Quantitative MR Microscopy of the Chicken Eye In Vivo Throughout the In Ovo Period. Mol Imaging Biol. 2018 May 23. doi: 10.1007/s11307-018-1208-9. (Impact Factor: 3,608)

5) Kowtharapu BS, Prakasam RK, Murin R, Koczan D, **Stahnke T**, Wree A, Jünemann AGM, Stachs O. Role of bone morphogenetic protein 7 (BMP7) in corneal wound healing. Int J Mol Sci. 2018 May 9;19(5). pii: E1415. doi: 10.3390/ijms19051415. (5-Year Impact Factor: 3,878)

6) Klose R, Streckenbach F, **Stahnke T**, Hadlich S, Kühn JP, Guthoff RF, Wree A, Neumann AM, Frank M, Glass Ä, Langner S, Stachs O, Lindner T. Ultrahochfeld-MRT am Hühnerembryo in ovo – ein Modell für die experimentelle Ophthalmologie / Ultrahigh-field MRI in chicken embryo in ovo – a model for experimental ophthalmology. Klinische Monatsblätter für Augenheilkunde. 2017 Dec;234(12):1458-1462. doi: 10.1055/s-0043-120675. Epub 2017 Nov 16. (Impact Factor: 0,882)

7) Lindner T, Klose R, Streckenbach F, **Stahnke T**, Hadlich S, Kühn JP, Guthoff RF, Wree A, Neumann AM, Frank M, Glass Ä, Langner S, Stachs O. Morphologic and biometric evaluation of chick embryo eyes in ovo using 7 Tesla MRI. Sci Rep. 2017 Jun 1;7(1):2647. doi: 10.1038/s41598-017-02755-. (5-year Impact Factor: 4,609)

8) Kowtharapu BS, Winter K, Marfurt C, Allgeier S, Köhler B, Hovakimyan M, **Stahnke T**, Wree A, Stachs O, Guthoff RF. Comparative quantitative assessment of the human corneal sub-basal nerve plexus by in vivo confocal microscopy and histological staining. Eye (Lond). 2017;31(3):481-490. (Impact Factor: 2,478)

9) ♦**Stahnke T**, Kowtharapu BS, Stachs O, Schmitz KP, Wurm J, Wree A, Guthoff RF, Hovakimyan M. Suppression of TGF-β pathway by pirfenidone decreases extracellular matrix deposition in ocular fibroblasts in vitro. PLoS One. 2017;23;12(2):e0172592. (Impact Factor: 2,806)

10) Lindner T, Klose R, Streckenbach F, **Stahnke T**, Hadlich S, Kühn JP, Guthoff RF, Wree A, Neumann AM, Frank M, Glass Ä, Langner S, Stachs O. Morphologic and biometric evaluation of chick embryo eyes in ovo using 7 Tesla MRI. Scientific Reports 2017;1;7(1):2647. (5-year Impact Factor: 4,609)

11) ♦**Stahnke T**, Hadlich S, Wree A, Guthoff RF, Stachs O, Langner S. Magnetic Resonance Microscopy of the Accommodative Apparatus. Klinische Monatsblätter für Augenheilkunde 2016;233(12):1320-1323. (Impact Factor: 0,882)

12) Langner I, **Stahnke T**, Stachs O, Lindner T, Kühn JP, Kim S, Wree A, Langner S. MR microscopy of the human fetal upper extremity - a proof-of-principle study. BMC Developmental Biology 2016;18;16(1):21. (5-year Impact Factor: 2,573)

13) Lindner T, Langner S, Falke K, Walter U, Krüger PC, Pohlmann A, Zimpfer A, **Stahnke T**, Hadlich S, Guthoff R, Erbersdobler A, Niendorf T, Stachs O. Anatomic and pathological characterization of choroidal melanoma using multimodal imaging: what is practical, what is needed? Melanoma Research 2015;25(3):252-258. (Impact Factor: 3,135)

14) ♦Kowtharapu BS*, **Stahnke T***, Wree A, Guthoff RF, Stachs O. Corneal epithelial and neuronal interactions: role in wound healing. Experimental Eye Research 2014;125:53-61. (* Authors contributed equally). (5-Year Impact Factor: 3,307)

15) Hovakimyan M, Falke K, **Stahnke T**, Guthoff R, Witt M, Wree A, Stachs O. Morphological analysis of quiescent and activated keratocytes: a review of ex vivo and in vivo findings. Current Eye Research 2014;39(12):1129-44. (Impact Factor: 2,238)

16) Löbler M, Buß D, Kastner C, Mostertz J, Homuth G, Ernst M, Guthoff R, Wree A, **Stahnke T**, Fuellen G, Voelker U, Schmitz KP. Ocular fibroblast types differ in their mRNA profiles-implications for fibrosis prevention after aqueous shunt implantation. Molecular Vision 2013;12(19):1321-1331. (Impact Factor: 2,219)

17) ♦**Stahnke T**, Löbler M, Kastner C, Stachs O, Wree A, Sternberg K, Schmitz K-P, Guthoff R. Different fibroblast subpopulations of the eye: A therapeutic target to prevent postoperative fibrosis in glaucoma therapy. Experimental Eye Research 2012;100:88-97. (5-Year Impact Factor: 3,307)

18) Goldbaum O, Riedel M, **Stahnke T**, Richter-Landsberg C. The small heat shock protein HSP25 protects astrocytes against stress induced by proteasomal inhibition. Glia 2009;57(14):1566-77. (Impact Factor: 5,846)

19) **Stahnke T**, Stadelmann C, Netzler A, Brück W, Richter-Landsberg C. Differential Up-regulation of Heme Oxygenase-1 (HSP32) in Glial cells after Oxidative Stress and in Demyelinating Disorders. Journal of Molecular Neuroscience 2006;32:25–37. (Impact Factor: 2,454)

20) Mronga T, **Stahnke T**, Goldbaum O, Richter-Landsberg C. Mitochondrial pathway is involved in hydrogen-peroxide-induced apoptotic cell death in oligodendrocytes. Glia 2004;46:446-455. (Impact Factor: 5,846)

21) **Stahnke T**, Richter-Landsberg C. Triethyltin-Induced Stress Responses and Apoptotic Cell Death in Cultured Oligodendrocytes. Glia 2004;46:334-344. (Impact Factor: 5,846)

22) Gorath M, **Stahnke T**, Mronga T, Goldbaum O, Richter-Landsberg C. Developmental changes of tau protein and mRNA in cultured rat brain oligodendrocytes. Glia 2001;36:89-101. (Impact Factor: 5,846)

Sonstige Publikationen (ohne Impact-Factor):

1) **Stahnke T**, Erbersdobler A, Knappe S, Guthoff RF, Kilangalanga N. Management of Congenital Clinical Anophthalmos with Orbital Cyst – A Kinshasa Case Report. Case Reports in Ophthalmological Medicine, Volume 2018, Article ID 5010915, https://doi.org/10.1155/2018/5010915.

2) Brietzke A, Siewert S, Schmidt W, **Stahnke T**, Kreiner C, Grabow N, Guthoff R, Schmitz K-P. Hydrophilic silicone elastomer with excellent cell adhesion capability - A promising material for ophthalmologic micro-implants. Current Directions in Biomedical Engineering 2018; 4(1):571–574. DOI: https://doi.org/10.1515/cdbme-2018-0137.

3) **Stahnke T**, Kilangalanga N, Knappe S, Guthoff RF, Erbersdobler A. Treatment and pathology of an unusual large carcinoma of the conjunctiva. Case Reports in Ophthalmological Medicine, Volume 2018, Article ID 8461737, https://doi.org/10.1155/2018/8461737.

4) Siewert S, Schmidt W, Kaule S, Kohse S, Stiehm M, Kopp F, **Stahnke T**, Guthoff R, Grabow N, Schmitz KP. Development of a Microstent System for minimally invasive Glaucoma Surgery. Current Directions in Biomedical Engineering 2017;3(2): 1-2.

5) ♦**Stahnke T**, Siewert S, Walther E, Schmidt W, Stachs O, Schmitz KP, Guthoff RF. Adopting oculopressure tonometry as a transient in vivo rabbit glaucoma model. Current Directions in Biomedical Engineering 2015;1:127–130.

6) Richter-Landsberg C, Goldbaum O, **Stahnke T**. Gehirnzellen im Stress. Einblicke 2006; 44:4-8.

Eingereichte Manuskripte:

1) Koschmieder A, Stachs O, Kragl B, **Stahnke T**, Henze L, Jünemann AGM, Junghanss C, Guthoff RF, Escobar HM. Non-invasive detection of corneal sub-basal nerve plexus changes in multiple myeloma patients by Confocal Laser Scanning Microscopy. The Ocular Surface, 2019. (5-year Impact Factor: 5,667)

2) Brietzke A, Eickner T, Reske T, Matschegewski C, Guthoff, RF, Grabow N, **Stahnke T**. Actinomycin D for fibrosis management in ophthalmic implant surgery. Current Directions in Biomedical Engineering, 2019.

3) Siewert S, Reske T, Pfensig S, Großmann S, Schmidt W, **Stahnke T**, Guthoff, RF, Grabow N, Schmitz K-P, Stiehm M. Development of an antifibrotic drug-eluting coating for a minimally invasive implantable glaucoma microstent. Current Directions in Biomedical Engineering, 2019.

4) Kilangalanga NJ, **Stahnke T**, Dinkulu S, Makwanga E, Moanda A, Ngweme G, Mukwanseke E, Kundt G, Thiesen F, Hopkins A, Guthoff RF. Bilateral Paediatric Cataract Surgery - Outcomes of 298 children from Kinshasa, the Democratic Republic of the Congo. African Health Sciences, 2019. (Impact Factor: 0,842)

5) Kilangalanga JN, **Stahnke T**, Moanda A, Makwanga E, Hopkins A, Guthoff RF. Role of a Community-Based Programme for Identification and Referral of Paediatric Cataract Patients in Kinshasa, DRC. Middle East Afr J Ophthalmol., 2018. (Impact Factor: 1,08)

6) Essende L, Kilangalanga N, Bambi N, Komi B, Vonor K, Atipo T, **Stahnke T**. Frequency and risk factors of diabetic retinopathy in Kinshasa, D.R. Congo. Pan African Medical Journal, 2018. (Impact Factor: 0,33)

7) **Stahnke T**, Lindner T, Guthoff RF, Stachs O, Wree A, Langner S, Niendorf T, Grabow N, Glass Ä, Polei S. Ultrahigh-field MRI determination of water diffusion rates in ex vivo human lenses of different age. Biosci Rep., 2018. (5-year Impact Factor: 2,903)

Eingereichte Erfindungsmeldungen/Patentschriften:

1) Struckmann S, Füllen G, **Stahnke T**, Jünemann AGM. Josamycin for use in prevention and treatment of fibrosis. 2019.

Appendix (Kopien der Originalarbeiten)

Experimental Eye Research 100 (2012) 88–97

Contents lists available at SciVerse ScienceDirect

Experimental Eye Research

journal homepage: www.elsevier.com/locate/yexer

Different fibroblast subpopulations of the eye: A therapeutic target to prevent postoperative fibrosis in glaucoma therapy

Thomas Stahnke [a,*], Marian Löbler [b], Christian Kastner [b], Oliver Stachs [a], Andreas Wree [c], Katrin Sternberg [b], Klaus-Peter Schmitz [b], Rudolf Guthoff [a]

[a] Department of Ophthalmology, University of Rostock, Doberaner Straße 140, D-18057 Rostock, Germany
[b] Institute of Biomedical Engineering, University of Rostock, Friedrich-Barnewitz-Straße 4, 18119 Rostock, Germany
[c] Institute of Anatomy, University of Rostock, Gertrudenstraße 9, 18057, Rostock, Germany

ARTICLE INFO

Article history:
Received 4 February 2012
Accepted in revised form 23 April 2012
Available online 10 May 2012

Keywords:
glaucoma
microstent
fibrosis
fibroblasts
suprachoroidal space
Tenon's space
orbital fat
paclitaxel
mitomycin C

ABSTRACT

The aim of this study is the characterization of fibroblasts mainly responsible for fibrosis processes associated with trabeculectomy or microstent implantation for glaucoma therapy. Therefore we isolated human primary fibroblasts from choroidea, sclera, Tenon capsule, and orbital fat tissues. These fibroblast subpopulations were analysed *in vitro* for expression of the extracellular matrix components which are responsible for postoperative scarring in glaucoma therapy. For scarring the proteins of the collagen family are predominant and so we focused on the expression of collagen I, collagen III and collagen VI in every fibroblast subpopulation. Also, the extracellular matrix protein fibronectin which crosslinks collagen fibres or other extracellular matrix components and cell surfaces, was analyzed. Collagen I, III and VI were prominent in every fibroblast subpopulation. The highest amounts of collagen III were found in hCF and hOF, whereas the signal in hSF and hTF was negligible. Additionally, there is a link between scarring processes and proliferating potential of fibroblasts, in case of microstent implantation triggered through the infiltration of inflammatory cells. Thus we analyzed fibroblast subpopulations for the presence of TGF-β1 which is one of the most important cytokines involved in proliferation processes. TGF-β1 was prominent in all fibroblast subpopulations with lowest expression in hCF cultures. To prevent postoperative fibroblast proliferation we analyzed *in vitro* the proliferation-inhibitors paclitaxel and mitomycin C which are potential candidates in drug eluting drainage systems on ocular fibroblast subpopulations. These inhibitors arrest fibroblast proliferation and viability, being, however, not very specific and have a cytotoxic potential also on healthy tissues surrounding the microstent outflow area. Significant differences in protein synthesis of fibroblasts subpopulations which could be specific targets for inhibition may help to find out fibroblast specific inhibitors to prevent postoperative scarring and could prevent patients from secondary surgery after microstent implantation.

1. Introduction

Glaucoma is a worldwide occurring eye disease and one of the predominant reasons for blindness. The disease mostly results from an impaired flow of aqueous through the trabecular meshwork which, when constipated with extracellular matrix (ECM) compounds leads to an increase of intraocular pressure (IOP) (Acott and Kelley, 2008). A permanent high IOP leads to progressive and irreversible destruction of optic nerve fibres (Schwartz, 2003) which results in total blindness of the afflicted eye. Most glaucoma patients are successfully treated with medication to reduce IOP. However, sometimes medication fails or patients develop allergic reactions against used medications. In these cases trabeculectomy (Cairns, 1968) and deep sclerectomy (Fedorov et al., 1982; Lim et al., 1998) were used to drain aqueous from the anterior chamber, and cyclo-photocoagulation (Noureddin et al., 2006) to decrease aqueous production to reduce IOP. If microsurgery also fails, caused through postoperative scarring, the implantation of alloplastic systems seems to be a method to decrease IOP to normal levels. These systems based on a drainage system developed and published by Molteno in 1969, who implanted a silicon tube near the anterior chamber angle to drain the liquid episclerally into the Tenon's space. Most of the

* Corresponding author. Tel.: +49 3814948428; fax: +49 3814948402.
E-mail addresses: thomas.stahnke@med.uni-rostock.de (T. Stahnke), marian.loebler@uni-rostock.de (M. Löbler), christian.kastner@uni-rostock.de (C. Kastner), oliver.stachs@med.uni-rostock.de (O. Stachs), andreas.wree@med.uni-rostock.de (A. Wree), katrin.sternberg@uni-rostock.de (K. Sternberg), klaus-peter.schmitz@uni-rostock.de (K.-P. Schmitz), rudolf.guthoff@med.uni-rostock.de (R. Guthoff).

0014-4835/$ – see front matter © 2012 Elsevier Ltd. All rights reserved.
doi:10.1016/j.exer.2012.04.015

subsequent drainage devices also use the subconjunctival space as outflow area for aqueous humour. To prevent ocular hypotony new systems often equipped with valves maintain healthy IOP-levels (Coleman et al., 1995). However, these drainage systems may also cause fibrotic reactions within Tenon's space leading to an obstruction of the system followed by a decrease in liquid outflow and again an IOP increase (Dietlein et al., 2008; Hong et al., 2005). In contrast to trabeculectomy implanted drainage devices have important advantages to prevent postoperative stenosis by fibrotic processes. First, different drainage spaces like suprachoroidale space (SCS) could be used to improve long-term liquid outflow (Allemann et al., 2011; Guthoff et al., 2009; Jordan et al., 2006; Ozdamar et al., 2003; Schmidt et al., 2010). In a new concept, the retroocular orbital fat tissue also could be considered as a potential drainage space.

Additionally, anti-fibrotic drugs can be added to implanted drainage systems similar to the drug eluting stents developed in cardiovascular treatment (Sousa et al., 2003) to inhibit fibroblast proliferation and postoperative scarring. Potent inhibitors of mitotic processes are the well characterized drugs paclitaxel (Choritz et al., 2010; Löbler et al., 2011) and mitomycin C (Mostafaei, 2011) which suppress mitosis by different mechanisms. Moreover, other cytostatics like 5-fluorouracil (Mostafaei, 2011) and Idarubicin (Heilmann et al., 1999) were studied in this context. However, the cytotoxic potential of these drugs is not limited on fibroblasts alone; there is also an influence on implant surrounding healthy tissues which may lead to undesirable side effects (Dunn et al., 1991; Guillemard and Saragovi, 2001; Fujitani et al., 1993). After glaucoma drainage surgery postoperative fibrosis is often accompanied by inflammation. The infiltration and cytokine secretion of inflammatory cells can activate fibroblasts followed by their proliferation (Cunliffe et al., 1995; He et al., 2011). Thus, inhibition of inflammatory processes indirectly controls fibrotic processes. Therefore, the use of inflammation inhibitors seems to be a gentler treatment because the main effect targets immune response and inflammatory cells. On the other hand a decrease of Tenon fibroblast proliferation rate *in vitro* was obvious after tocotrinole treatment (Tappeiner et al., 2010) and triamcinolone acetonide treatment (Löbler et al., 2011). However, most drainage systems in glaucoma therapy are using the Tenon's space as drainage area leading to a lack of information about other ocular fibroblast subpopulations.

The aim of this study was the characterization of fibroblasts mainly responsible for fibrotic processes associated with trabeculectomy or microstent implantation for glaucoma therapy. In order to characterize ECM expression of relevant cell types of the connective tissues around the microstent outflow area primary human ocular fibroblasts were isolated. Fibroblasts were obtained from choroidea (hCF), sclera (hSF), Tenon capsule (hTF) and orbital fat (hOF). These cells were analysed *in vitro* concerning their expression of the ECM components which are responsible for postoperative scarring in glaucoma therapy. Additionally, the cytotoxic potential of the proliferation-inhibitors paclitaxel (PTX) and mitomycin C (MitC) on these fibroblast subpopulations was analyzed *in vitro*.

2. Materials and methods

2.1. Materials

Cell culture media were purchased from PAA (Pasching, Austria). Antibodies against components of ECM were supplied from Abcam (Cambridge, UK): mouse monoclonal anti-collagen I (ab90395) and mouse monoclonal anti-collagen IA2 (Abnova, MAB 6616), mouse monoclonal anti-collagen III (ab6310), mouse monoclonal anti-collagen VI (ab78504) and DPC Biermann GmbH: rabbit polyclonal fibronectin (DP013). Antibodies against cytoskeleton, membrane-proteins and cytokines were from Sigma–Aldrich (Munich, Germany): mouse monoclonal anti-β-tubulin (T5293), mouse monoclonal anti-vimentin (V2258), mouse monoclonal anti-fibroblast surface protein (F4771), mouse monoclonal anti-TGF-β1 (T0438) and mouse monoclonal anti-TGF-β1 (Abcam, ab64715). All antibodies used in this study were raised against human antigen. Secondary HRP-conjugated anti-mouse IgG (NA931) was from Amersham (Buckinghamshire, UK) and HRP-conjugated anti-rabbit IgG (170–6515) from BIO-RAD (Munich, Germany). Enzymes for Tenon tissue digestion were obtained from Sigma–Aldrich (Trypsin, Munich, Germany) and Serva Electrophoresis GmbH (Collagenase NB4, Heidelberg, Germany). TPP® 25 cm^2 and 75 cm^2 culture flasks were provided from Sigma–Aldrich (Munich, Germany), 10 cm dishes and 12 well plates from Nunc (Thermo Fisher scientific, Massachusetts, USA), 12 mm coverslips and 96-well microtiter plates from PAA (Cölbe, Germany). CellQuanti-Blue reagent was supplied from BioAssaySystems (Hayward, CA, USA) and Cell Proliferation ELISA, BrdU (chemiluminescence) from Roche Diagnostics (Mannheim, Germany). The molecular weight standard (Roti®-Mark PRESTAINED, T852.1) for SDS-PAGE was purchased from Carl Roth GmbH & Co. KG (Karlsruhe, Germany).

2.2. Cell culture

This study was approved by the ethics committee of the University of Rostock and followed the guidelines of the Declaration of Helsinki. Primary cultures of human scleral and choroideal fibroblasts were prepared from donor eyeballs (Institute of Anatomy, University of Rostock, Germany). Briefly, the retinas were removed and choroids were separated from scleral tissues. Each tissue was cut into pieces approximately 1 × 1 mm in size, placed in 12 well plastic culture plates in DMEM with 50 U/ml of penicillin, 50 μg/ml streptomycin and 10% FCS, and incubated at 37 °C in a humidified (95%) incubator under 5% CO_2. Growth medium was changed three times a week. When outgrowing primary fibroblasts reached a confluent monolayer, cells were trypsinized in 0.25% trypsin/EDTA solution in phosphate buffered saline (PBS) and subcultured in 25 cm^2 plastic cell culture flasks.

Primary cultures of human fibroblasts from orbital fat were prepared after lateral decompression surgery (Department of Ophthalmology, University of Rostock, Germany). Orbital fat tissues were treated like scleral and choroideal tissues.

Primary cultures of human Tenon fibroblasts were prepared after child strabismus surgery (Department of Ophthalmology, University of Rostock, Germany) after obtaining of participants' informed consent in writing. Briefly, small pieces of non-functional episclera (Tenon tissues) were removed during surgery. Tissue samples were transferred into 1.5 ml caps containing DMEM without FCS, supplemented with trypsin and collagenase NB4, each at a final concentration of 2 mg/ml and incubated at 37 °C. After tissue digestion cells were centrifuged at 1500 rpm for 5 min. The cell pellet was resuspended in DMEM containing 10% FCS and seeded in 12 well plates. After Tenon fibroblasts proliferated to a confluent monolayer, cells were trypsinized and subcultured in 25 cm^2 cell culture flasks.

When fibroblasts were grown to confluence in 25 cm^2 culture flasks they were trypsinized again and seeded in 10 cm culture dishes and in 75 cm^2 cell culture bottles. For immunofluorescence analysis cells were seeded on 12 mm plastic coverslips (PAA, Cölbe, Germany) until 60%–70% confluence was reached. For analyses fibroblasts of third or fourth passage were used.

2.3. Immunoblot analysis

Cellular monolayers of primary human fibroblast subpopulations were washed in PBS once, scraped off in sample buffer

containing 1% SDS and boiled for 10 min. Protein contents in the samples were determined according to Neuhoff et al. (1979). For immunoblotting, total cellular extracts (10–30 μg protein per lane) were separated by SDS-PAGE using 7.5% or 10% polyacrylamide gels for larger and smaller proteins, respectively, and transferred to PVDF membranes (0.2 μm, BIO-RAD, Munich, Germany). The blots were blocked with 5% non fat dry milk powder in TBS for 30 min and incubated with the individual primary antibodies. The following antibodies were used (dilutions are given in brackets): mouse monoclonal anti-collagen I, III, VI (1:500), mouse monoclonal anti-TGF-β1 (1:250), mouse monoclonal anti-vimentin (1:500), mouse monoclonal anti-β-tubulin (1:1000), mouse monoclonal anti-fibroblast surface protein (1:500). After washing, membranes were incubated with secondary HRP-conjugated anti-mouse (1:2500) or anti-rabbit (1:2500) IgG, and visualized by the enhanced chemiluminescence (ECL) procedure as described by the manufacturer (Thermo scientific, Pierce, Rockford, USA).

2.4. Immunofluorescence

For immunocytochemistry cells were allowed to grow on plastic coverslips (12 mm, PAA, Cölbe, Germany). After washing with PBS, cells were fixed with 3% paraformaldehyde buffered with PBS for 10 min. For intracellular staining paraformaldehyde-fixed cells were pretreated with 0.1% Triton X-100 containing 2% FCS (30 min). Thereafter, fixed cells were incubated with the primary antibodies in PBS for 60 min. The antibodies were used at the following dilutions: Rabbit polyclonal anti-fibronectin (1:100), mouse monoclonal anti-vimentin (1:100), mouse monoclonal anti-collagen I, III, VI (1:100), mouse monoclonal anti-TGF-β1 (1:100), mouse monoclonal anti-fibroblast surface protein (1:100). After washing with PBS, cells were incubated with donkey anti-mouse IgG (H + L)-Alexa Fluor 488 (Dianova GmbH, Hamburg, Germany) (1:50) or donkey anti-rabbit IgG (H + L)-Cy3 (Dianova GmbH, Hamburg, Germany) (1:100) for 45 min, washed with PBS and mounted. Control experiments, using the secondary antibodies only, did not show unspecific staining. Nuclei were stained by 4,6-diamidino-2-phenylindole (DAPI) (1 μg/ml) included in the mounting medium (Vectashield, Vector Laboratories LTD., Peterborough, UK). Fluorescent labelling was studied using a Nikon confocal fluorescence microscope equipped with a digital camera (Nikon Eclipse E400 with D-Eclipse C1, Düsseldorf, Germany). All images depicted in this study were from a single plane through fibroblast cell monolayers equipped with a 40× objective using the same settings.

2.5. Cell viability assay

The drugs PTX and MitC were tested for their potential to control fibroblast viability. 2000 cells were seeded into each well of a 96-well microtiter plate and incubated in their respective growth medium for 1 day at 37 °C, 5% CO_2 and 95% relative humidity. Then growth medium was changed to growth medium including drugs in a concentration range from 10^{-12} to 10^{-4} mol/l. After 2 days, cell viability was determined with the CellQuanti-Blue-Assay. Briefly, culture medium was replaced by 200 μl of freshly prepared 10% CellQuanti-Blue reagent (BioAssaySystems, Hayward, CA, USA) in cell culture medium and incubated for another 2 h. Cellular reductase activity was quantified by fluorescence measurements (Fluostar Optima, BMG, Offenburg, Germany). Excitation wavelength was 544 nm, emission wavelength was 590 nm. The data were analyzed with nonlinear four point curve fit (Graph Pad Prism). All measurements were run in quadruplicate.

2.6. BrdU Cell Proliferation assay

The cytostatic drugs PTX and MitC were tested to arrest fibroblast proliferation. 2000 cells were seeded into each well of a 96-well microtiter plate in growth medium and incubated under standard conditions for 1 day. Then growth medium was exchanged with growth medium including MitC or PTX in a concentration range from 10^{-12} to 10^{-5} or 10^{-12} to 10^{-4} mol/l, respectively. After a 32 h incubation period BrdU (100 μM) was added to each well and incubation continued for additional 16 h. BrdU incorporation into DNA was measured according to the supplier's instructions of the Cell Proliferation ELISA, BrdU (chemiluminescence) (Roche Diagnostics, Mannheim, Germany). Cells not subjected to MitC or PTX served as negative control.

The data were analyzed with nonlinear four point curve fit (Graph Pad Prism). All measurements were run in quadruplicate.

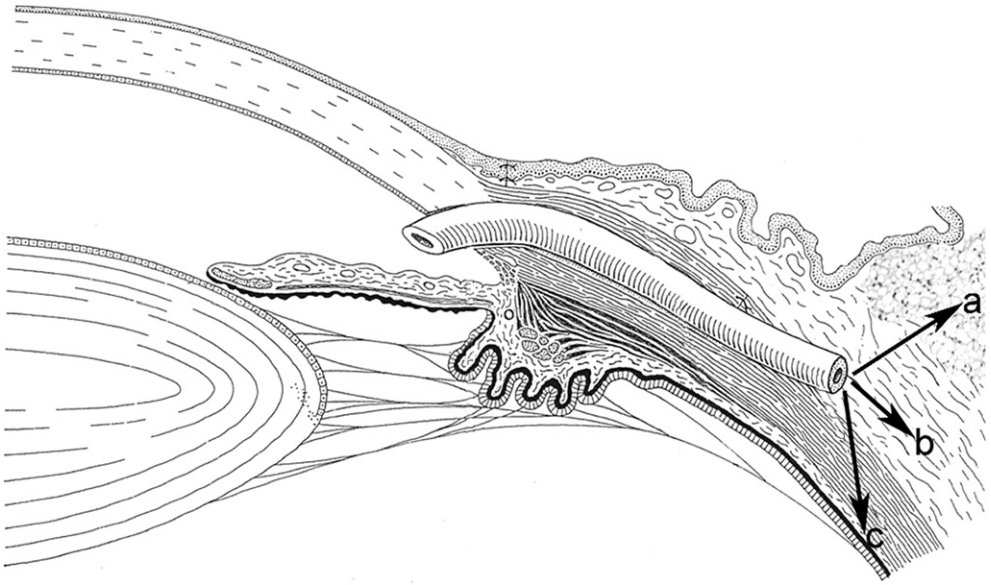

Fig. 1. Schematic representation of possible drainage spaces for implanted microstent systems. a: orbital fat, b: Tenon space, c: suprachoroidal space.

3. Results

In this study human ocular fibroblasts were isolated from ocular tissues which might be in close contact with the outflow area of a microstent system implant (Fig. 1). It is well established that commonly used drainage into Tenon's capsule (Fig. 1b) postoperatively often leads to an intense reaction followed by proliferation of Tenon fibroblasts. Additionally, an increase in production of ECM compounds occurs. These fibrotic processes could result in a total occlusion of the implanted microstent system and make alternative options more interesting. The orbital fat could serve as an alternative site (Fig. 1a) to absorb drained liquid from anterior chamber. Furthermore, the suprachoroidal space (SCS) could be used (Fig. 1c) to prevent postoperative scarring.

To characterize the scarring potential and to retrieve differences in protein expression in distinct ocular tissues primary human fibroblasts (hCF, hSF, hTF and hOF) were cultured *in vitro* (Fig. 2). Morphological examination of fibroblast subpopulations showed little differences concerning size and shape of the cells.

All subpopulations exhibited typical fibroblast morphology with cellular processes. The morphology of fibroblasts was changing towards spindle-shape with increasing time in culture.

To verify that cultivated cells were fibroblasts immunocytochemical fluorescence microscopy was performed using specific antibodies against the protein vimentin (Fig. 3a), fibroblast specific surface protein (FBSP) (Fig. 3b) and fibronectin (Fig. 3a,b). The results were reproducible between cell lines from different donors. In each fibroblast subpopulation high amounts of fibronectin could be detected. It seemed that fibronectin was synthesized and extracellularly organized to fibrillary structures. Additionally, intracellular fibronectin could be detected located in the perinuclear region in every fibroblast subpopulation (Fig. 3a,b). Choroideal fibroblasts, hSF, hTF and hOF subpopulations organized fibronectin in the cytoplasmatic periphery; the protein revealed as fibrillary structures connecting neighbouring cells and built up an ECM network.

The intermediate filament protein vimentin could be detected in each fibroblast subpopulation. Vimentin is the major structural component of the cytoskeleton in cells of mesenchymal origin like fibroblasts (Fig. 3a). The organisation of the intracellular intermediate filaments was homogeneous throughout the cell body and extended into the cell processes to stabilize cellular morphology.

To demonstrate that isolated cells were fibroblasts immunocytochemistry against fibroblast specific surface protein (FBSP) was

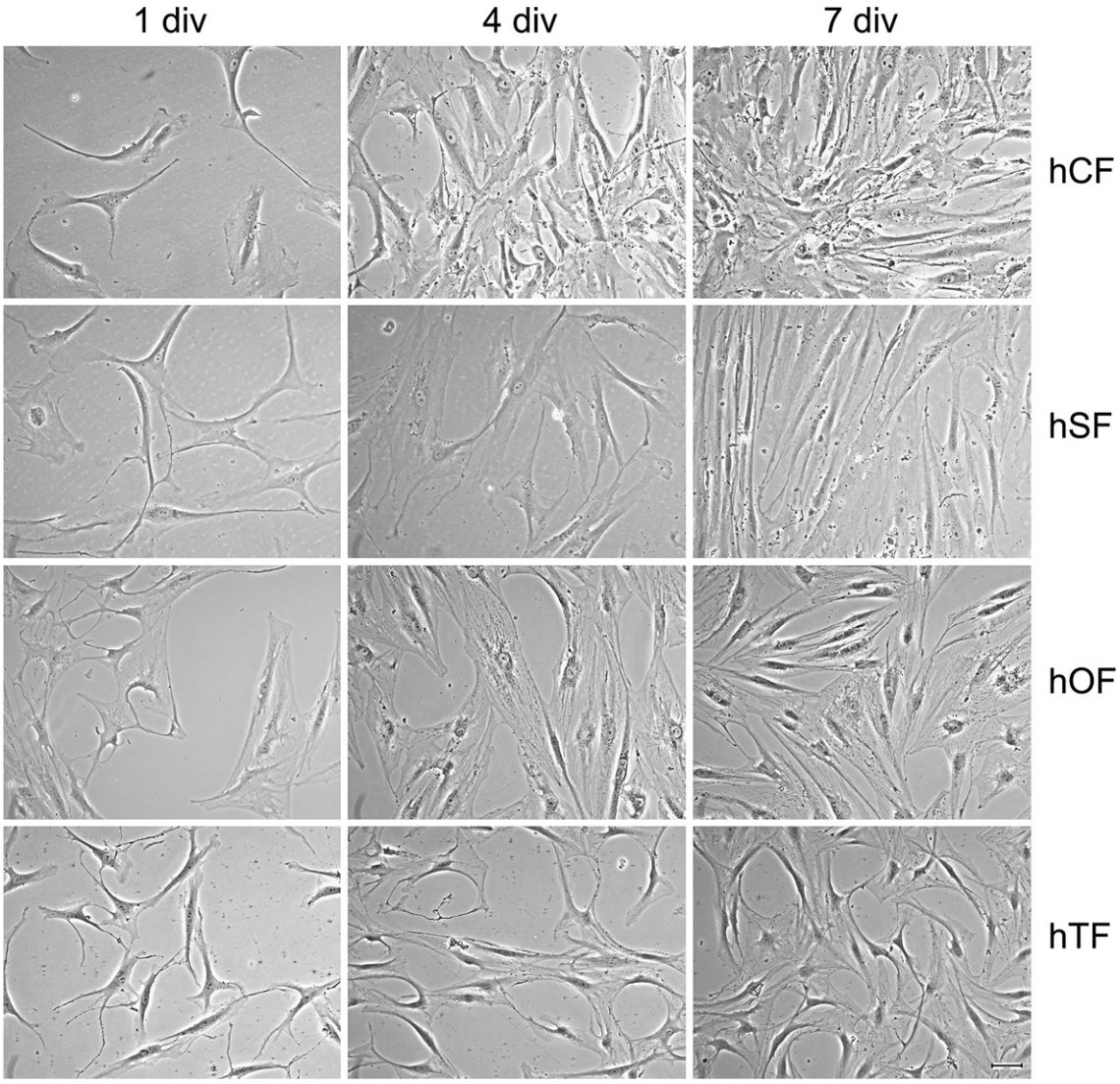

Fig. 2. Human fibroblast subpopulations *in vitro*. Human fibroblast subpopulations (sclera (hSF), choroidea (hCF), Tenon capsule (hTF) and fibroblasts from orbital fat (hOF)) were cultured for 1, 4 and 7 days, respectively. Note that hCF exhibit highest amount of laminar cells. div = days *in vitro*. Bar represents 25 μm.

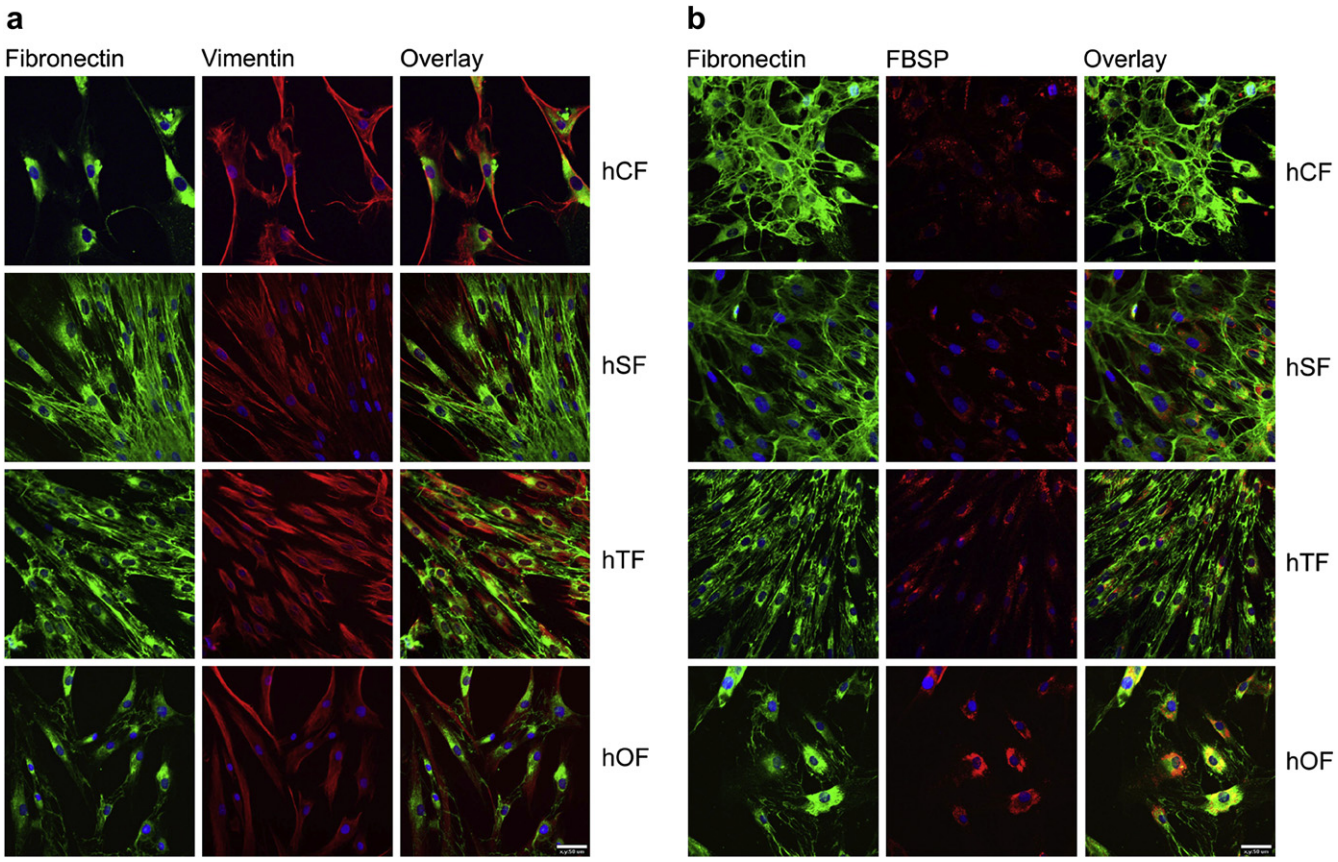

Fig. 3. Immunocytochemical characterisation of human ocular fibroblast subpopulations *in vitro*. After paraformaldehyde fixation human fibroblast subpopulations were incubated with primary antibodies directed to compounds of ECM (fibronectin) and the cytoskeleton (vimentin) (a) and antibodies directed to fibronectin and the membrane located fibroblast specific surface protein (FBSP) (b) as indicated. Note that every fibroblast subpopulation was positive for vimentin showing the mesenchymal origin of every cell type. Also every cell type was positive stained against FBSP indicating that isolated cells were fibroblasts. Nuclei were stained by DAPI included in the mounting medium. Experiments were carried out several times with similar results. Bar represents 50 μm.

performed (Fig. 3b). FBSP was prominent in every cell subpopulation and in every cell, indicating pure fibroblast cultures without contamination of other cell types, e.g. endothelial cells.

The fibrotic potential of fibroblasts is characterized by their capability to synthesize ECM compounds like members of the collagen family which could act as fibrosis marker proteins *in vivo*. The fibrosis marker collagen I was prominent in every fibroblast subpopulation (Fig. 4a). Collagen I was intracellularly localised in the perinuclear region indicating newly synthesized procollagen I before secretion. Extracellular collagen I could not be detected in our cultures as the proteins are not organized as fibrils or fibres extracellularly.

Also the fibrosis marker protein collagen III was found in fibroblast subpopulations (Fig. 4b), however, in differing concentrations. Highest amounts were found in hCF and hOF, whereas the signal in hSF and hTF was negligible. The localisation of identified proteins resembled collagen I and was constricted to the perinuclear region. Similar to the results in collagen I no extracellular collagen III could be detected.

Collagen VI is expressed (Fig. 4c) like the other collagens in the perinuclear region of all fibroblast subpopulations. In hSF, hTF and hOF cultures extracellular collagen VI structures in between neighbouring cells was detected. These collagen VI positive structures seemed to be secreted collagen VI peptides which were extracellularly organized into fibrils and fixed in the ECM and onto cell surfaces as they are colocalized with extracellular fibronectin positive fibril-like structures (Fig. 5).

Fibrosis is not only limited to the synthesis of ECM compounds. Also the proliferation of fibroblasts plays a very important role in fibrotic/scarring processes. The cytokine TGF-β1 is essential for proliferation. TGF-β1 was evident in all fibroblast subpopulations with lowest expression detected in hCF cultures (Fig. 4d). Like collagens TGF-β1 was localized to the perinuclear region. A distinguishing feature of these few cells was the accumulation of many vesicular structures positively stained for TGF-β1 in higher amounts then in neighbouring cells (Fig. 4d).

To compare the amounts of ECM individual proteins were detected by western blot analysis (Fig. 6). As a loading control β-tubulin was analyzed showing no differences in signal intensity among fibroblasts. Also the protein vimentin could be detected in each fibroblast subpopulation in equal amounts. The analyses of the ECM compounds showed differences among the fibroblast cultures, especially in collagen VI. hSF cultures produced much more collagen VI than all other fibroblast cultures. Also in hOF cultures synthesis of collagen VI is higher in comparison to hCF and hTF cultures in which collagen VI could be detected in low amounts. Collagen I expression was prominent in hTF cultures. Collagen III and TGF-β1 signals showed only minor variations between cell types.

As a means for fibrosis prevention the well characterized cytostatic drugs paclitaxel (PTX) and mitomycin C (MitC) were tested on the ocular fibroblast subpopulations using the CellQuanti-Blue-assay to measure cell viability after treatment (Fig. 7). Fibroblast subpopulations were cultured *in vitro* and treated with MitC over

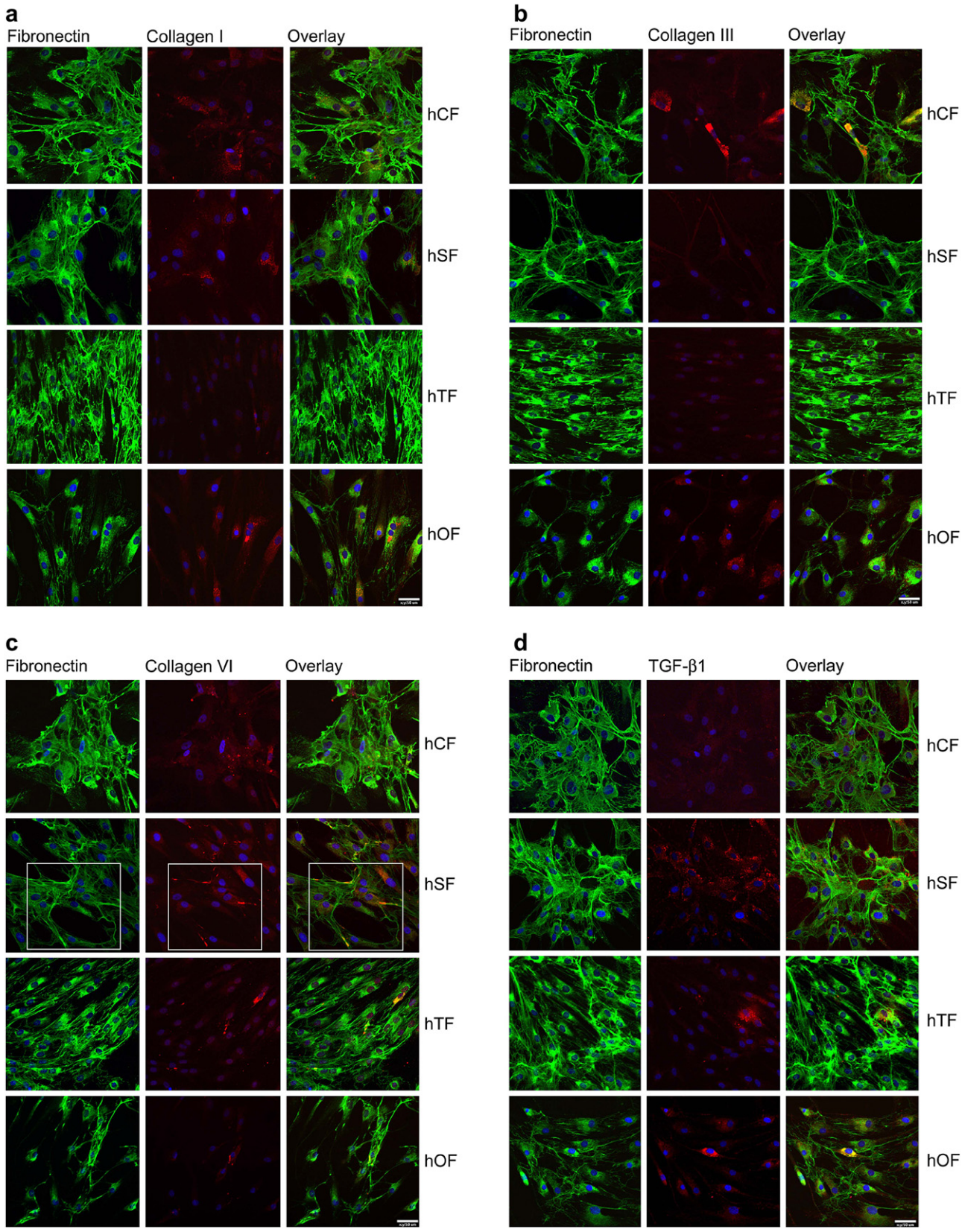

Fig. 4. Demonstration of ECM compounds in human ocular fibroblast subpopulations *in vitro*. After paraformaldehyde fixation cells were incubated with primary antibodies directed to ECM compounds. Fibronectin and collagen I (a), fibronectin and collagen III (b) and fibronectin and collagen VI (c) is demonstrated as indicated. Additionally, fibroblast subpopulations were incubated with primary antibodies directed to fibronectin and the cytokine TGF-β1 (d). Note that the fibroblast subpopulations are positive for intracellular collagen I, III and VI and that hSF, hTF and hOF cultures build out fibillary extracellular structures which are positive for collagen VI. Also intracellular staining of TGF-β1 was seen, in case of hTF and hOF cultures with some occasional cells which express high amounts of protein. Rectangles in (c) are shown in higher magnification separately in Fig. 5 to illustrate extracellulary organization and intracellulary localisation of ECM compounds. Nuclei were stained by DAPI included in the mounting medium. Experiments were carried out several times with similar results. Bar represents 50 μm.

a wide concentration range (Fig. 7a,c). MitC reduced the cell viability and proliferation of every fibroblast subpopulation and, obviously Tenon fibroblasts were less sensitive to MitC. The half maximal inhibitory concentration (IC_{50}) of MitC on Tenon fibroblasts relative viability was 9.93×10^{-6} mol/l while it was lower in fibroblasts from orbital fat ($IC_{50} = 6.71 \times 10^{-6}$ mol/l) and scleral fibroblasts ($IC_{50} = 5.57 \times 10^{-6}$ mol/l), pointing out that these subpopulations were more sensitive to MitC treatment. Fibroblasts from choroidea were most sensitive to MitC with an IC_{50} of 4.82×10^{-6} mol/l. These results were underlined through the measurements of the relative proliferation, where the half maximal inhibitory concentration (IC_{50}) of MitC on Tenon fibroblasts was 5.571×10^{-8} mol/l. In fibroblasts from orbital fat the IC_{50} was 4.212×10^{-8} mol/l and in scleral fibroblasts it was 1.441×10^{-8} mol/l, again, fibroblasts from choroidea were most sensitive to MitC with an IC_{50} of 1.167×10^{-8} mol/l.

Also in PTX treated cell cultures a reduction of cell viability and proliferation could be detected in every fibroblast subpopulation (Fig. 7b,d). In contrast to MitC fibroblasts from orbital fat were less sensitive to PTX in the measurements of the relative viability ($IC_{50} = 6.31 \times 10^{-9}$ mol/l) whereas in Tenon fibroblasts IC_{50} was 1.83×10^{-9} mol/l. The relative proliferation and sensitivity of the fibroblast subpopulations after PTX intoxication was similar to the results measured after MitC treatment. In Tenon fibroblasts the IC_{50} was 1.834×10^{-9} mol/l and in fibroblasts from orbital fat it was 1.771×10^{-9} mol/l. A decrease of cell viability also occurred in scleral fibroblasts ($IC_{50} = 1.72 \times 10^{-9}$ mol/l) and choroideal fibroblasts ($IC_{50} = 7.77 \times 10^{-10}$ mol/l). These findings were also underlined by the results of the relative proliferation measurements. In scleral fibroblasts the IC_{50} was 9.965×10^{-10} mol/l and in most sensitive fibroblasts from choroidea IC_{50} it was 1.576×10^{-10} mol/l. These results resemble the sensitivity of hSF and hCF cultures to MitC.

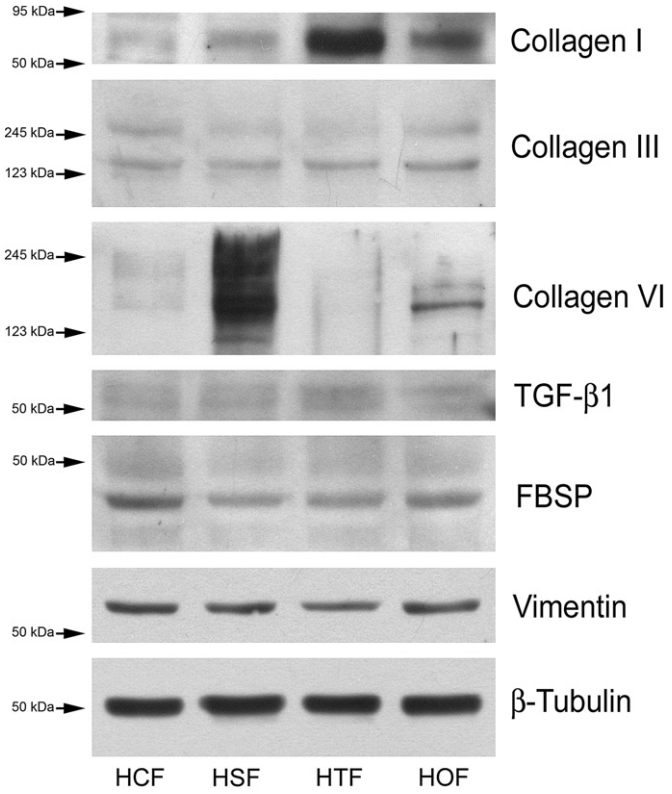

Fig. 6. Immunoblot analysis of human fibroblast subpopulations (7 div). Cell lysates of fibroblast subpopulations were prepared and subjected to immunoblot analysis using antibodies against collagen I, collagen III, collagen VI, TGF-β1, FBSP, vimentin and β-tubulin, as indicated on the right. Note the differing amounts of collagen I, III and VI among fibroblast subpopulations. The results represent the means of three independent experiments.

4. Discussion

Trabeculectomy and the implantation of glaucoma drainage devices are currently used if medication failed in glaucoma therapy to lower IOP. Unfortunately, also these surgical therapy methods are accompanied by short- and long-term complications such as cataract progression, hypotony and fibrotic processes which could lead to complete obstruction of the new implanted drainage device (Gedde et al., 2007; Memarzadeh et al., 2009). In case of microstent implantation most devices drain the aqueous into Tenon's space (Minckler et al., 2008; Molteno, 1969). Therefore an alternative drainage into the suprachoroidal space (SCS) has been proposed to improve long-term liquid outflow (Melamed et al., 2009; Schmidt et al., 2010). Additionally, the retroocular orbital fat could be an alternative drainage space through its lower hydrostatic pressure in contrast to the anterior chamber. Recently, in addition to new outflow areas, drug eluting stent systems known from cardiovascular surgery (Sousa et al., 2003) and loaded with anti-proliferative substances were also discussed in glaucoma therapy to prevent postoperative scarring (Löbler et al., 2011; Schmidt et al., 2010). However, episcleral fibroblasts were well characterized in terms of their fibrotic potential because they surround the commonly used drainage region (Gross, 1999; Mietz et al., 1996). Also scleral fibroblasts have been characterized (McBrien et al., 2009; Jobling

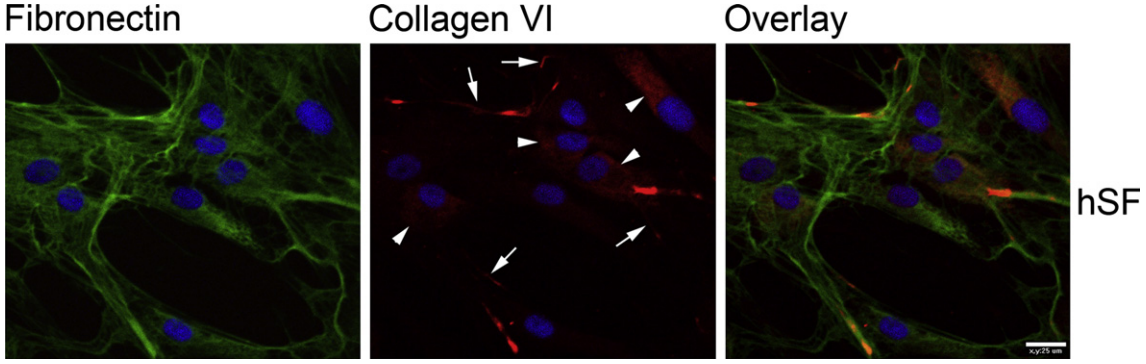

Fig. 5. Exemplary demonstration of intracellular and extracellular localisation of collagen VI in hSF *in vitro*. Detailed enlargements of fibronectin and collagen VI expression in hSF (as demonstrated in Fig. 4). Note that collagen VI can also be found as extracellular fibrillar structures colocalized with fibronectin (arrows) and vesicular intracellular structures (arrowheads). Nuclei were stained by DAPI included in the mounting medium. Bar represents 25 μm.

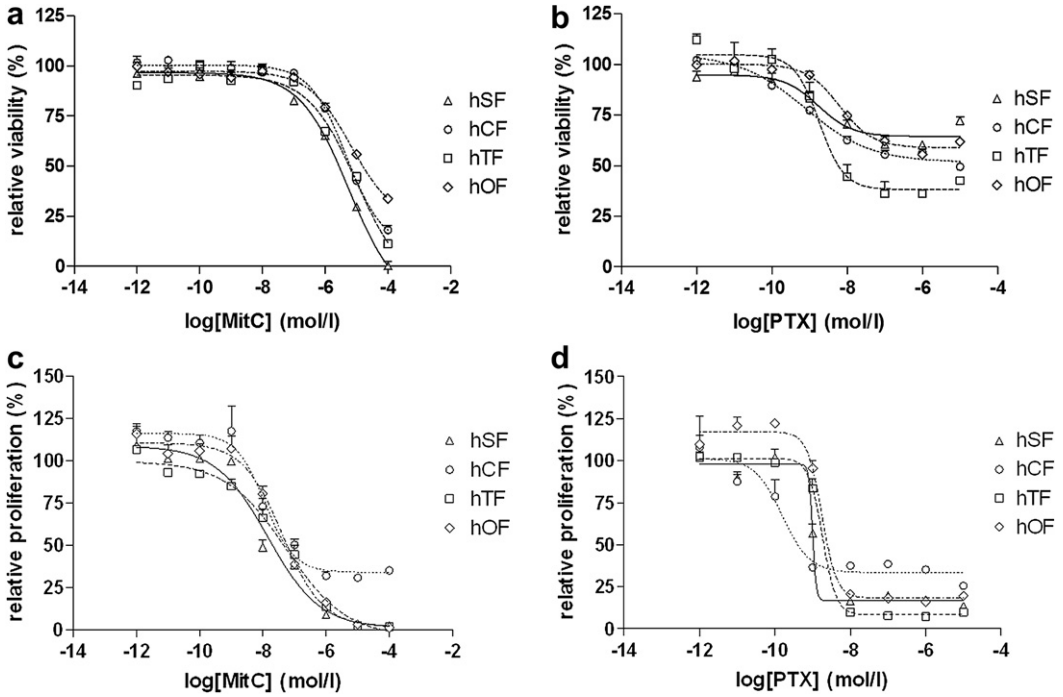

Fig. 7. Relative viability and relative proliferation of human ocular fibroblasts in response to cytostatic drugs *in vitro*. Human fibroblast subpopulations were treated with cytostatic drugs mitomycin C (MitC) (a, c) and paclitaxel (PTX) (b, d) in concentrations as indicated. CellQuanti-Blue-assay was carried out to quantify relative cell viability. Cell Proliferation ELISA, BrdU (chemiluminescence)-assay was carried out to quantify relative proliferation. IC_{50} was defined using nonlinear four point curve fit with the analysing software Graph Pad Prism. In response to MitC choroideal fibroblasts (○) are most sensitive in contrast to scleral fibroblasts (△) and fibroblasts from orbital fat (◇). Fibroblasts from Tenon capsule (□) are slightly less sensitive to MitC treatment (a, c). In PTX treated cell cultures choroideal fibroblasts are most sensitive while hSF and hTF subpopulations show similar results. Fibroblasts from orbital fat are less sensitive to PTX treatment (b). The quantification of relative proliferation (d) differs a little from these findings. Tenon fibroblasts are less sensitive to PTX treatment with nearly similar results to fibroblasts from orbital fat. All measurements were run in quadruplicate.

et al., 2004), while information about choroideal and retroocular fibroblast with regard to their fibrotic potential are rare (Kim et al., 2010; Oh et al., 2007).

Here, we compare all primary human ocular fibroblast subpopulations which theoretically could get in contact with the outflow area of the implanted microstent systems. These subpopulations were analyzed for their synthesis of ECM compounds. Fibrotic processes and postoperative scarring are characterized by an increase of ECM components synthesized mainly by fibroblasts. The most important proteins in these processes are the members of the collagen family. These secreted proteins are extracellularly organized to collagen fibrils which were bundled to collagen fibres (Alberts et al., 1994). An increase in collagen synthesis can lead to a cystic bleb surrounding the draining end of a microstent implant preventing aqueous outflow which results in an increase of IOP (Alvarado et al., 2008; Dietlein et al., 2008; Hong et al., 2005). Our investigations focus on the synthesis of collagen I, collagen III, collagen VI, which are involved in fibrotic processes, and the cell surface-ECM linking protein fibronectin in fibroblast subpopulations. The interesting result that fibroblasts taken from different topographic sites in the orbita differ under equal culture conditions in synthesis rate of collagen I, III and collagen VI point out the heterogeneity and specialisation among these subpopulations. Collagen I is the most abundant member of the collagen family constituting the main component of collagen fibres. It is associated *in vivo* with collagen VI which is arranged like a string of pearls and is functionally a linking protein among cell surface and collagen fibrils and fibres. Additionally collagen III is also a fibril forming member of the collagen family.

We could demonstrate by immunofluorescence analysis that collagen VI in hSF, hTF and hOF subpopulations appears to be organized in fibres whereas it is intracellularly detectable in the hCF subpopulation. The differences in the organisation of collagens in the examined fibroblast subpopulations point to a different expression pattern of additional ECM components. However, further investigations of additional collagens and other proteins of ECM have to be carried out. Furthermore, in this study we cannot detect secreted ECM components which were not organized to stable structures. To evaluate total amounts of secreted ECM compounds the conditioned culture medium has to be analyzed.

The multifunctional cytokine TGF-β1 which is one of the most important cytokines in proliferation processes is also secreted to effect neighbouring cells through its binding to their TGF-β1 receptors. It is one of three highly conserved TGF-β isoforms (TGF-β1, TGF-β2 and TGF-β3) found in mammals which is involved in wound healing through modulating proliferation and ECM regulation in scleral fibroblasts (Jobling et al., 2004). The members of the TGF-β family are also present in Tenon fibroblasts where they are involved in ocular scarring processes (Cordeiro et al., 2000a) and in retroocular fat tissue TGF-β1 is implicated in human primary orbital fibroblast proliferation and hyaluronan synthesis (Guo et al., 2011). In our study only intracellular TGF-β1 was analyzed because of the extracellular solubility of TGF-β1. We could demonstrate that hTF subpopulation contained the highest amounts of TGF-β1 followed by the hOF. The elevated levels of TGF-β1 in hTF in contrast to the other examined fibroblast subpopulations could explain the high proliferation potential of hTF after glaucoma surgery.

These findings make it necessary to protect against excess fibrosis using proliferation-inhibitors, while on the other hand wound healing after eye surgery is imperative. Healing processes follow determined events starting with an eye injury or surgery (Cordeiro et al., 2000b). Wounding triggers the inflammatory phase

where the infiltration of neutrophils and monocytes is followed by lymphocytes. Inflammatory cell infiltration leads to an increase in fibroblast proliferation followed by a remodelling phase where ECM is synthesized to form scar tissue (Cordeiro et al., 2000b). To prevent excess fibrosis after wounding or surgery up to now mostly the well characterized cytostatic drugs MitC and PTX were applied (Choritz et al., 2010; Mostafaei, 2011). The involvement of inflammatory processes in wound healing also makes anti-inflammatory drugs very interesting with respect to scar formation. Here we tested the cytostatic drugs MitC and PTX to their anti-proliferative potential to human fibroblast subpopulations. We could demonstrate that both, MitC and PTX reduce fibroblast viability and proliferation in every subpopulation as expected. The inhibitory effects of these cytostatics are equivalent to examinations of sclera and Tenon fibroblasts (Choritz et al., 2010; Mostafaei, 2011; Seong et al., 2005). Additionally, we also could demonstrate the inhibiting potential of MitC and PTX to choroideal and orbital fibroblasts indicating the effectiveness of a drug eluting microstent implant also in new draining areas.

To summarize, cultured human primary ocular fibroblast subpopulations exhibit different protein expression patterns. Especially the synthesis of ECM components and the proliferation relevant cytokine TGF-β1 was highest in hSF and hTF cultures demonstrating a different potential for fibrotic processes. In addition, ocular fibroblasts could be inhibited by cytostatics.

This *in vitro* model-system provided an opportunity to characterize collagen synthesis and the proliferation potential between different ocular fibroblast subpopulations. Furthermore, fibroblasts of the various subpopulations could be differently inhibited. Further investigations will open up new possibilities for prevention in postoperative scarring processes and fibrosis and could prevent patients from secondary surgery after microstent implantation.

Declaration of interest

The authors report no conflicts of interest. The authors alone are responsible for the content and writing of the paper.

Acknowledgements

The authors thank Mrs. C. Leyh, Mrs. J. Weiß-Müller and Mrs. A. Schümann for skilful technical assistance. We also thank Mr. G. Ritschel for drawing Fig. 1.

The work was financially supported by Bundesministerium für Bildung und Forschung (BMBF) within the REMEDIS project “Höhere Lebensqualität durch neuartige Mikroimplantate” (FKZ: 03IS2081).

References

Acott, T.S., Kelley, M.J., 2008. Extracellular matrix in the trabecular meshwork. Exp. Eye Res. 86, 543–561.

Alberts, B., Bray, D., Lewis, J., Raff, M., Roberts, K., Watson, J.D., 1994. Molecular Biology of the Cell, third ed. Garland science, New York.

Allemann, R., Langner, S., Witt, M., Schmidt, W., Schmitz, K.-P., Hosten, N., Guthoff, R., Stachs, O., 2011. Ultra high-field magnetic resonance imaging of a glaucoma microstent. Curr. Eye Res. 36, 719–726.

Alvarado, J.A., Hollander, D.A., Juster, R.P., Lee, L.C., 2008. Ahmed valve implantation with adjunctive mitomycin C and 5-fluorouracil: long-term outcomes. Am. J. Ophthalmol. 146, 276–284.

Cairns, J.E., 1968. Trabeculectomy. Preliminary report of a new method. Am. J. Ophthalmol. 66, 673–679.

Choritz, L., Grub, J., Wegner, M., Pfeiffer, N., Thieme, H., 2010. Paclitaxel inhibits growth, migration and collagen production of human Tenon's fibroblasts - potential use in drug-eluting glaucoma drainage devices. Graefes Arch. Clin. Exp. Ophthalmol. 248, 197–206.

Coleman, A.L., Hill, R., Wilson, M.R., Choplin, N., Kotas-Neumann, R., Tam, M., Bacharach, J., Panek, W.C., 1995. Initial clinical experience with Ahmed glaucoma valve implant. Am. J. Ophthalmol. 120, 23–31.

Cordeiro, M.F., Bhattacharya, S.S., Schultz, G.S., Khaw, P.T., 2000a. TGF-β1, -β2, and -β3 in vitro: biphasic effects on Tenon's fibroblast contraction, proliferation, and migration. Invest. Ophthalmol. Vis. Sci. 41, 756–763.

Cordeiro, M.F., Chang, L., Lim, K.S., Daniels, J.T., Pleass, R.D., Siriwardena, D., Khaw, P.T., 2000b. Modulating conjunctival wound healing. Eye 14, 536–547.

Cunliffe, I.A., Richardson, P.S., Rees, R.C., Rennie, I.G., 1995. Effect of TNF, IL-1, and IL-6 on the proliferation of human Tenon's capsule fibroblasts in tissue culture. Br. J. Ophthalmol. 79, 590–595.

Dietlein, T.S., Jordan, J., Lueke, C., Krieglstein, G.K., 2008. Modern concepts in antiglaucomatous implant surgery. Graefes Arch. Clin. Exp. Ophthalmol. 246, 1653–1664.

Dunn, J.P., Seamone, C.D., Ostler, H.B., Nickel, B.L., Beallo, A., 1991. Development of scleral ulceration and calcification after pterygium excision and mitomycin therapy [letter]. Am. J. Ophthalmol. 112, 343–344.

Fedorov, S.N., Ioffe, D.I., Ronkina, T.I., 1982. Glaucoma surgery – deep sclerectomy. Vestn. Ophthal. 4, 6–10.

Fujitani, A., Hayasaka, S., Shibuya, Y., Noda, S., 1993. Corneoscleral ulceration and corneal perforation after pterygium excision and topical mitomycin C therapy. Ophthalmologica 207, 162–164.

Gedde, S.J., Herndon, L.W., Brandt, J.D., Budenz, D.L., Feuer, W.J., Schiffman, J.C., 2007. Surgical complications in the tube versus trabeculectomy study during the first year of follow-up. Am. J. Ophthalmol. 143, 23–31.

Gross, R.L., 1999. Collagen type I and III synthesis by Tenon's capsule fibroblasts in culture: individual patient characteristics and response to mitomycin C, 5-fluorouracil, and ascorbic acid. Trans. Am. Ophthalmol. Soc. 97, 513–543.

Guillemard, V., Saragovi, H.U., 2001. Taxane-antibody conjugates afford potent cytotoxicity, enhanced solubility, and tumor target selectivity. Cancer Res. 61, 694–699.

Guo, N., Woeller, C.F., Feldon, S.E., Phipps, R.P., 2011. Peroxisome proliferator-activated receptor γ ligands inhibit transforming growth factor-β-induced, hyaluronan-dependent, T cell adhesion to orbital fibroblasts. J. Biol. Chem. 286, 18856–18867.

Guthoff, R.F., Schmidt, W., Buß, D., Schultze, C., Ruppin, U., Stachs, O., Sternberg, K., Klee, D., Chichkov, B., Schmitz, K.-P., 2009. Development of a glaucoma microstent with drainage into the suprachoroidal space: fluid mechanical model approach. Ophthalmologe 106, 805–812.

He, Y.H., Zhang, H.N., Zhang, G.P., Hou, N., Xiao, O., Huang, Y., Wu, J.H., Luo, M.S., Zhang, G.S., Yi, Q., Chen, M.S., Luo, J.D., 2011. A physiological concentration of glucocorticoid inhibits the pro-inflammatory cytokine-induced proliferation of adult rat cardiac fibroblasts: roles of extracellular signal-regulated kinase 1/2 and nuclear factor-κB. Clin. Exp. Pharmacol. Physiol. 38, 739–746.

Heilmann, C., Schönfeld, P., Schlüter, T., Bohnensack, R., Behrens-Baumann, W., 1999. Effect of the cytostatic agent idarubicin on fibroblasts of the human Tenon's capsule compared with mitomycin C. Br. J. Ophthalmol. 83, 961–966.

Hong, C.H., Arosemena, A., Zurakowski, D., Ayyala, R.S., 2005. Glaucoma drainage devices: a systematic literature review and current controversies. Surv. Ophthalmol. 50, 48–60.

Jobling, A.I., Nguyen, M., Gentle, A., McBrien, N.A., 2004. Isoform-specific changes in scleral transforming growth factor-β expression and the regulation of collagen synthesis during myopia progression. J. Biol. Chem. 279, 18121–18126.

Jordan, J.F., Engels, B.F., Dinslage, S., Dietlein, T.S., Ayertey, H.D., Roters, S., Esser, P., Konen, W., Krieglstein, G.K., 2006. A novel approach to suprachoroidal drainage for the surgical treatment of intractable glaucoma. J. Glaucoma 15, 200–205.

Kim, H., Choi, Y.H., Park, S.J., Lee, S.Y., Kim, S.J., Jou, I., Kook, K.H., 2010. Antifibrotic effect of pirfenidone on orbital fibroblasts of patients with thyroid-associated ophthalmopathy by decreasing TIMP-1 and collagen levels. Invest. Ophthalmol. Vis. Sci. 51, 3061–3066.

Lim, K.S., Allan, B.D., Lloyd, A.W., Muir, A., Khaw, P.T., 1998. Glaucoma drainage devices; past present, and future. Br. J. Ophthalmol. 82, 1083–1089.

Löbler, M., Sternberg, K., Stachs, O., Allemann, R., Grabow, N., Roock, A., Kreiner, C.F., Streufert, D., Neffe, A.T., Hanh, B.D., Lendlein, A., Schmitz, K.P., Guthoff, R., 2011. Polymers and drugs suitable for the development of a drug delivery drainage system in glaucoma surgery. J. Biomed. Mater. Res. B Appl. Biomater. 97, 388–395.

McBrien, N.A., Jobling, A.I., Gentle, A., 2009. Biomechanics of the sclera in myopia: extracellular and cellular factors. Optom. Vis. Sci. 86, E23–E30.

Melamed, S., Ben Simon, G.J., Goldenfeld, M., Simon, G., 2009. Efficacy and safety of gold micro shunt implantation to the supraciliary space in patients with glaucoma: a pilot study. Arch. Ophthalmol. 127, 264–269.

Memarzadeh, F., Varma, R., Lin, L.T., Parikh, J.G., Dustin, L., Alcaraz, A., Eliott, D., 2009. Postoperative use of bevacizumab as an antifibrotic agent in glaucoma filtration surgery in the rabbit. Invest. Ophthalmol. Vis. Sci. 50, 3233–3237.

Mietz, H., Arnold, G., Kirchhof, B., Diestelhorst, M., Krieglstein, G.K., 1996. Histopathology of episcleral fibrosis after trabeculectomy with and without mitomycin C. Graefes Arch. Clin. Exp. Ophthalmol. 234, 364–368.

Minckler, D.S., Francis, B.A., Hodapp, E.A., Jampel, H.D., Lin, S.C., Samples, J.R., Smith, S.D., Singh, K., 2008. Aqueous shunts in glaucoma. A report by the American academy of ophthalmology. Ophthalmology 115, 1089–1098.

Molteno, A., 1969. New implant for drainage in glaucoma. Clinical trial. Br. J. Ophthalmol. 53, 606–615.

Mostafaei, A., 2011. Augmenting trabeculectomy in glaucoma with subconjunctival mitomycin C versus subconjunctival 5-fluorouracil: a randomized clinical trial. Clin. Ophthalmol. 5, 491–494.

Neuhoff, V., Philipp, K., Zimmer, H.G., Mesecke, S., 1979. A simple, versatile, sensitive and volume-independent method for quantitative protein determination which is independent of other external influences. Hoppe-Seyler's Z. Physiol. Chem. 360, 1657–1670.

Noureddin, B.N., Zein, W., Haddad, C., Ma'luf, R., Bashshur, Z., 2006. Diode laser transcleral cyclophotocoagulation for refractory glaucoma: a 1 year follow-up of patients treated using an aggressive protocol. Eye 20, 329–335.

Oh, J., Jung, Y.S., Kim, G.S., Oh, I.K., Rho, B.K., Huh, K., 2007. The effect of short-term exposure of triamcinolone acetonide on fibroblasts and retinal pigment epithelial cells. Acta Ophthalmol. Scand. 85, 786–790.

Ozdamar, A., Aras, C., Karacorlu, M., 2003. Suprachoroidal seton implantation in refractory glaucoma: a novel surgical technique. J. Glaucoma 12, 354–359.

Schmidt, W., Schultze, C., Stachs, O., Allemann, R., Löbler, M., Sternberg, K., Hinze, U., Chichkov, B., Guthoff, R.F., Schmitz, K.-P., 2010. Konzept eines druckgesteuerten Mikrostents für die Glaukomtherapie. Concept of a pressure-controlled microstent for glaucoma therapy. Klin. Monbl. Augenheilkd. 227, 946–952.

Schwartz, M., 2003. Neurodegeneration and neuroprotection in glaucoma: development of a therapeutic neuroprotective vaccine. The Friedenwald lecture. Invest. Ophthalmol. Vis. Sci. 44, 1407–1411.

Seong, G.J., Park, C., Kim, C.Y., Hong, Y.J., So, H.S., Kim, S.D., Park, R., 2005. Mitomycin-C induces the apoptosis of human Tenon's capsule fibroblast by activation of c-Jun N-terminal kinase 1 and caspase-3 protease. Invest. Ophthalmol. Vis. Sci. 46, 3545–3552.

Sousa, J.E., Serruys, P.W., Costa, M.A., 2003. New frontiers in cardiology, drug-eluting stents: part I and II. Circulation 107, 2274–2279. 2283–2289.

Tappeiner, C., Meyenberg, A., Goldblum, D., Mojon, D., Zingg, J., Nesaretnam, K., Kilchenmann, M., Frueh, B.E., 2010. Antifibrotic effects of tocotrienols on human Tenon's fibroblasts. Graefes Arch. Clin. Exp. Ophthalmol. 248, 65–71.

PLOS ONE

RESEARCH ARTICLE

Suppression of TGF-β pathway by pirfenidone decreases extracellular matrix deposition in ocular fibroblasts *in vitro*

Thomas Stahnke[1]*, Bhavani S. Kowtharapu[1], Oliver Stachs[1], Klaus-Peter Schmitz[2], Johannes Wurm[3], Andreas Wree[3], Rudolf Friedrich Guthoff[1], Marina Hovakimyan[2]

1 Department of Ophthalmology, Rostock University Medical Center, Rostock, Germany, **2** Institute for Biomedical Engineering, Rostock University Medical Center, Rostock, Germany, **3** Department of Anatomy, Rostock University Medical Center, Rostock, Germany

* thomas.stahnke@med.uni-rostock.de

OPEN ACCESS

Citation: Stahnke T, Kowtharapu BS, Stachs O, Schmitz K-P, Wurm J, Wree A, et al. (2017) Suppression of TGF-β pathway by pirfenidone decreases extracellular matrix deposition in ocular fibroblasts *in vitro*. PLoS ONE 12(2): e0172592. doi:10.1371/journal.pone.0172592

Editor: Carol Feghali-Bostwick, Medical University of South Carolina, UNITED STATES

Received: July 7, 2016

Accepted: February 7, 2017

Published: February 23, 2017

Data Availability Statement: All relevant data are within the paper; no supplemental material is provided.

Funding: The work was financially supported by Bundesministerium für Bildung und Forschung (BMBF) within the REMEDIS project "Höhere Lebensqualität durch neuartige Mikroimplantate" (FKZ: 03IS2081). The funders had no role in study design, data collection and analysis, decision to publish, or preparation of the manuscript.

Abstract

In glaucoma surgery, fibrotic processes occur, leading to impairment of liquid outflow. Activated fibroblasts are responsible for postoperative scarring. The transforming growth factor-β (TGF-β) pathway plays a key role in fibroblast function, differentiation and proliferation. The aim of this study was the characterization of the fibrotic potential of two subtypes of primary human ocular fibroblasts and the attempt to inhibit fibrotic processes specifically, without impairing cell viability. For fibrosis inhibition we focused on the small molecule pirfenidone, which has been shown to prevent pulmonary fibrosis by the decrease of the expression of TGF-β1, TGF-β2 and TGF-β3 cytokines. For *in vitro* examinations, isolated human primary fibroblasts from Tenon capsule and human intraconal orbital fat tissues were used. These fibroblast subpopulations were analyzed in terms of the expression of matrix components responsible for postoperative scarring. We concentrated on the expression of collagen I, III, VI and fibronectin. Additionally, we analyzed the expression of α-smooth muscle actin, which serves as a marker for fibrosis and indicates transformation of fibroblasts into myofibroblasts. Gene expression was analyzed by rtPCR and synthesized proteins were examined by immunofluorescence and Western blot methods. Proliferation of fibroblasts under different culture conditions was assessed using BrdU assay. TGF-β1 induced a significant increase of cell proliferation in both cell types. Also the expression of some fibrotic markers was elevated. In contrast, pirfenidone decreased cell proliferation and matrix synthesis in both fibroblast subpopulations. Pirfenidone slightly attenuated TGF-β1 induced expression of fibronectin and α-smooth muscle actin in fibroblast cultures, without impairing cell viability. To summarize, manipulation of the TGF-β signaling pathway by pirfenidone represents a specific antifibrotic approach with no toxic side effects in two human orbital fibroblast subtypes. We presume that pirfenidone is a promising candidate for the treatment of fibrosis following glaucoma surgery.

Competing interests: The authors have declared that no competing interests exist.

Introduction

Glaucoma refers to a group of multifactorial optic neuropathies that have in common a progressive degeneration of retinal ganglion cells and their axons, leading to a thinning of the retinal nerve fibers comprising the optic nerve [1]. Worldwide, glaucoma is the leading cause of irreversible blindness, affecting more than 60 million people with 8.4 million people afflicted from bilateral blindness [2]. An epidemiological review has concluded that 1 in 40 adults over 40 years of age suffers from glaucoma, with disease prevalence increasing significantly with age [3,4]. The most prevalent form of glaucoma in Caucasian population is primary open angle glaucoma, characterized by impaired outflow of aqueous humor (AH) through the trabecular meshwork [5].

While the pathogenesis of glaucomatous optic neuropathy still remains an area of research, elevated intraocular pressure (IOP) is believed to be the strongest risk factor [6]. Reducing IOP and its fluctuations is so far the only proven means to slow or halt disease progression [7]. In therapeutic terms, IOP-lowering can be achieved by pharmaceutical treatment and laser application to trabecular meshwork or ciliary body structures, or microsurgical procedures [8]. The goal of these interventions is to adjust corresponding IOP at which disease progression can be halted.

Pharmaceutical treatment with topical eye drops can cause proinflammatory effects, inducing ocular discomfort and burning sensation [9], which may consequently contribute to the poor patient adherence [10]. The laser treatment is not suitable for every glaucoma case and often may need to be repeated or combined with local therapy in the long-term to keep eye pressure stable. Glaucoma filtration surgery is an alternative which is indicated when the glaucomatous optic neuropathy progresses despite medical and laser therapies [11]. Trabeculectomy remains to be the most commonly performed antiglaucomatous surgical procedure and is considered as a gold standard [12–14].

In the recent decade, glaucoma drainage devices (GDDs) have been introduced as an alternative to the glaucoma filtering surgery [15]. Studies have shown that GDD implantation can be at least as effective as trabeculectomy at reducing IOP and the need for further surgery over 5 years [16]. Like filtrating surgery, the GDDs work by creating a new outflow route allowing AH draining from anterior chamber to subconjunctival or suprachoroidal space [17].

Any surgical tissue manipulation is generally accompanied by a wound healing process, which affects the long-term success of these procedures. Particularly, scarring and fibrotic encapsulation at the surgical site can lead to surgical failure. Fibrosis is defined as an excessive tissue growth, characterized by uncontrolled fibroblast proliferation, migration, their transformation into α-smooth muscle actin (α-SMA)-producing myofibroblasts and deposition of extracellular matrix (ECM) components, including various members of collagen superfamily and fibronectin [18]. Therefore, several attempts have been made to suppress the fibroblasts activation in order to inhibit surgical scarring and fibrosis. The most commonly used antimetabolites 5-fluorouracil (5-FU) and mitomycin C (MMC) inhibit cells in a non-selective manner, are cytotoxic and usually accumulate in areas where no inhibitory effect is wanted [19,20]. As a result, antimetabolite treatment is associated with undesired side effects such as corneal endothelial damage or bleb leaking [21]. More recent strategies utilize less cytotoxic molecules which are expected to inhibit fibroblasts through manipulation of different cellular pathways. Promising results have been reported following inhibition of TGF-β (transforming growth factor-β) signal transduction pathway [22].

In the present study, we examined the antifibrotic potential of the small molecule pirfenidone (PFD), which has been used as an oral formulation for systemic treatment of idiopathic pulmonary fibrosis [23]. We hypothesized that PFD inhibits fibroblasts proliferation and

expression of ECM-molecules in TGF-β-induced fibrotic cell cultures of ocular fibroblast subtypes from regions possibly used as drainage outflow areas.

Materials and methods

Materials

Cell culture media (D6429), flasks (TPP 25 cm^2 and 75 cm^2) and pirfenidone ((PFD); P2116) were purchased from Sigma-Aldrich (Taufkirchen, Germany). Cell culture dishes (10 cm) and 12 well plates were from Nunc (Thermo Fisher scientific, Massachusetts, USA), 12 mm coverslips and 96 well microtiter plates from PAA (Cölbe, Germany). Cell Proliferation ELISA, BrdU (chemiluminescence) was supplied from Roche Diagnostics (Mannheim, Germany). SDS-PAGE prestained molecular weight standard (Roti-Mark PRESTAINED, T852.1) was purchased from Carl Roth GmbH & Co. KG (Karlsruhe, Germany). The recombinant human cytokine transforming growth factor β1 ((TGF-β1); 11343160) was purchased from Immunotools (Friesoythe, Germany). All antibodies used in this study were raised against human antigen and are listed in the Table 1.

Cell culture

This study was approved by the ethics committee of the University of Rostock (approval ID: A 2011 11) and followed the guidelines of the Declaration of Helsinki.

Primary cultures of human orbital fibroblasts (hOFs) were prepared from donors' orbital fat tissues (Institute of Anatomy, Rostock University Medical Center, Germany) as described previously [24]. Briefly, after enucleation orbital fat was collected. Each tissue was cut into pieces approximately 1×1 mm in size, placed in 12 well plastic culture plates in DMEM with 50 U/ml of penicillin, 50 μg/ml streptomycin and 10% FCS, and incubated at 37˚C in a humidified (95%) incubator under 5% CO2. Medium was changed three times a week. Upon reaching confluence, cells were trypsinized with 0.25% trypsin/EDTA solution in phosphate buffered saline (PBS) and subcultured in 25 cm^2 plastic cell culture flasks.

Primary cultures of human Tenon fibroblasts (hTFs) were prepared after strabismus and enucleation surgeries (Department of Ophthalmology, Rostock University Medical Center, Germany). A written informed consent was obtained from all participants. Small pieces of non-functional episclera (Tenon tissues) were removed during surgeries. Accordingly, Tenon

Table 1. Antibodies used in this study.

Reagent	Supplier	Cat. number
mouse monoclonal anti-collagen I	Abcam (Cambridge, UK)	ab90395
mouse monoclonal anti-collagen I	Abcam (Cambridge, UK)	ab6308
mouse monoclonal anti-collagen I	Santa Cruz (Dallas, USA)	sc-59772
mouse monoclonal anti-collagen VI	Abcam (Cambridge, UK)	ab78504
mouse monoclonal anti-α-SMA	Abcam (Cambridge, UK)	ab7817
rabbit polyclonal anti-α-SMA	Abcam (Cambridge, UK)	ab5694
rabbit polyclonal fibronectin	DPC Biermann GmbH (Germany)	DP013
mouse monoclonal fibronectin	Sigma-Aldrich (Germany)	F7387
mouse monoclonal anti-β-tubulin	Sigma-Aldrich (Germany)	T5293
secondary HRP-conjugated anti-rabbit IgG	BIO-RAD (Munich, Germany)	170–6515
secondary HRP-conjugated anti-mouse IgG	GE Healthcare (Amersham; Buckinghamshire, UK)	NXA931
secondary Alexa Fluor 488-conjugated donkey anti-mouse IgG (H+L)	Dianova GmbH, (Hamburg, Germany)	715-545-151
secondary Cy3-conjugated donkey anti-rabbit IgG (H+L)	Dianova GmbH, (Hamburg, Germany)	711-165-152

doi:10.1371/journal.pone.0172592.t001

tissues were treated like orbital fat tissues. After Tenon fibroblasts proliferated to a confluent monolayer, cells were trypsinized and subcultured in 25 cm^2 cell culture flasks.

After reaching a confluent layer in 25 cm^2 culture flasks, fibroblasts were trypsinized again and seeded in 10 cm culture dishes and in 75 cm^2 cell culture flasks, respectively. For immunofluorescence analysis cells were seeded on 12 mm plastic coverslips (PAA, Cölbe, Germany) and cultured until 60%–70% confluence was reached. For all analyses fibroblasts of passage three to five were used. The fibroblastic phenotype was confirmed by immunohistochemistry using anti-vimentin antibody to verify the mesenchymal origin of cells, and anti-FBSP (fibroblast surface protein), as a fibroblast marker (data not shown).

For stimulation- and inhibition experiments, human fibroblast subpopulations were starved for 24 h under serum-free conditions, followed by the application of TGF-β1 [10 ng/ml], PFD [10^{-3} mol/l] or the combination of TGF-β1 [10 ng/ml] and PFD [10^{-3} mol/l] for 48 h. The effective concentration of TGF-β1 was determined earlier by the induction of α-SMA expression (data not shown). The concentration of PFD was chosen based on own previous experiments, demonstrating the non-toxicity of PFD at 10^{-3} mol/l.

Untreated fibroblasts serum-starved for 72 h served as a control.

BrdU cell proliferation assay

TGF-β1, PFD and the combination of both were also tested for their impact on fibroblast proliferation. 2000 cells were seeded into each well of a 96-well microtiter plate in growth medium and incubated under standard conditions for one day. After starving for 24 h, cells were incubated with TGF-β1 [10 ng/ml], PFD [10^{-3} mol/l] and the combination of both in culture medium with or without FCS. After a 32 h incubation period BrdU (100 μM) was added to each well and cells were allowed to grow for additional 16 h. The incorporation of BrdU into DNA was measured according to the supplier's instructions of the Cell Proliferation ELISA, BrdU (chemiluminescence) (Roche Diagnostics, Mannheim, Germany). Cells not subjected to TGF-β1 or PFD served as a negative control (NC). All measurements were run in quadruplicate and proliferation values were calculated relative to the NC whose viability was set to 100%.

RNA isolation and reverse transcription

For RNA isolation, cells were harvested into TRIzol (Life Technologies GmbH, Darmstadt, Germany) reagent. Briefly, after the addition of 10% chloroform (Baker, Deventer, Netherlands), cells were vortex mixed and purified RNA was isolated in two centrifugation steps. The aqueous supernatant was adjusted to 35% ethanol and loaded onto an RNeasy column (QIAGEN, Hilden, Germany). After washing the column, residual DNA was digested with DNase I (QIAGEN) treatment followed by three washing steps. Total RNA was eluted with 100 μl of sterile, RNase free water. RNA quality was assessed for size and purity on a 1.5% agarose gel.

For reverse transcription of isolated RNA into cDNA, 1 μg of the extracted total RNA was subjected to reverse transcription using random hexamer primers (First Strand cDNA Synthesis Kit, Fermentas, St. Leon-Rot, Germany). Sequences for PCR primers were generated with the Primer3 software (primer3.ut.ee/). Primers used in this study (Table 2) were purchased from Eurofins MWG-Operon (Ebersberg, Germany), which included alpha smooth muscle actin (a-SMA), fibronectin1, collagen type I alpha 2 (COL1A2), collagen type III alpha 1 (COL3A1), matrix metalloproteinase-2 (MMP2) and thrombospondin (THBS2). Glyceraldehyde-3-phosphate dehydrogenase (GAPDH) and 18S ribosomal RNA (RNA18S5) were used as internal reference.

Table 2. Primer sequences used in this study.

Primer	sequence [5' - 3']
aSMA	GTGTGTGACAATGGCTCTGG
	GCCAGATCTTTTCCATGTCG
Fibronectin1	AATATCTCGGTGCCATTTGC
	CGGGAATCTTCTCTGCTAGC
COL1A2	CTGGACCTCCAGGTGTAAGC
	TGGCTGAGTCTCAAGTCACG
COL3A1	AACACGCAAGGCTGTGAGACT
	GCCAACGTCCACACCAAATT
MMP2	TGATCTTGACCAGAATACCATCGA
	GGCTTGCGAGGGAAGAAGTT
THBS2	CGTGGACAATGACCTTGTTG
	GCCATCGTTGTCATACTCAG

doi:10.1371/journal.pone.0172592.t002

Quantitative PCR

Quantitative PCR reactions were performed by using equal amounts of cDNAs along with the required set of primers and PCR master mix (Thermo Scientific Finnzymes, Schwerte, Germany) containing dNTPs, Taq polymerase and SYBR green. Initially, cDNA was denaturated and Thermus aquaticus DNA polymerase was activated at 98˚C for 10 min. Afterwards, 40 PCR cycles (94˚C 10 s denaturation, 60˚C 20 s annealing, 72˚C 30 s elongation) were run in a Master Cycler realplex (Eppendorf, Hamburg, Germany). Samples without any cDNA were also included in each amplification reaction to serve as negative controls. After the PCR, amplification products were analyzed on 1.5% agarose gels by electrophoresis. All PCR reactions were run in quadruplicate and the data were analyzed by using Graph Pad Prism 5 software. One way ANOVA was performed to determine differences between the groups, and p-values <0.05 were considered statistically significant.

Immunofluorescence

For immunocytochemistry cells were allowed to grow on plastic cover slips (12 mm, PAA, Cölbe, Germany) until they reached an optimal density (subconfluent monolayer). After the incubation times with TGF-β1 and/or PFD the coverslips were washed with PBS and cells were fixed with 3% paraformaldehyde (PFA) for 10 min. After fixation, cells were pretreated with 0.1% Triton X-100 containing 2% FCS (30 min) to permeabilize cell membranes for intracellular protein staining, followed by incubation with the primary antibodies in PBS for 60 min. Antibodies were used at the following dilutions: rabbit polyclonal anti-fibronectin (1:100), mouse monoclonal anti-α-SMA (1:100), mouse monoclonal anti-collagen I and VI (1:100). After incubation cells were washed three times with PBS, followed by an incubation with the secondary antibodies for 45 min. Secondary antibodies were used at the following dilutions: donkey anti-mouse IgG (H+L)-Alexa Fluor 488 (1:50), or donkey anti-rabbit IgG (H+L)-Cy3 (1:100). After incubation with secondary antibodies, cells were washed again three times with PBS and mounted. Control experiments, using the secondary antibodies only, did not show unspecific staining. Nuclei were stained with 4, 6-diamidino-2-phenylindole (DAPI) (1μg/ml) included in the mounting medium (Vectashield, Vector Laboratories LTD., Peterborough, UK). Fluorescent labeling was analyzed using a Nikon confocal fluorescence microscope equipped with a digital camera (Nikon Eclipse E400 with D-Eclipse C1, Düsseldorf,

Germany). All images depicted in this study were from a single plane through fibroblast cell monolayers equipped with a 40x objective using the same settings.

Western blot analysis

For Western blot analysis, primary human fibroblast subpopulations were washed with PBS and scraped off into sample buffer containing 1% SDS. All samples were boiled for 10 minutes. After cooling on ice, protein contents in the samples were determined according to Neuhoff et al. [25]. For separation by SDS-PAGE, total cellular extracts (10–30 μg protein per lane) were loaded in 7.5% or 10% polyacrylamide gels for larger and smaller proteins, respectively. By immunoblotting proteins were transferred to PVDF membranes (0.2 μm, BIO-RAD, Munich, Germany). After blocking the membranes with 5% nonfat dry milk powder in TRIS-buffered saline (TBS) for 30 min, blots were incubated with individual primary antibodies at 4˚C over night. Following antibodies were used (dilutions are given in brackets): mouse monoclonal anti-collagen I and VI (1:500), mouse monoclonal anti-fibronectin (1:1,000), mouse monoclonal anti-β-tubulin (1:1,000) and mouse monoclonal anti-α-SMA (1:500). After three washing steps with TBS including Tween 20, membranes were incubated with secondary HRP-conjugated anti-mouse (1:2,500) or anti-rabbit (1:2,500) IgG. Visualization of bound antibodies was performed by the enhanced chemiluminescence (ECL) procedure as described by the manufacturer (Thermo scientific, Pierce, Rockford, USA).

Optical density of each band was normalized to corresponding β-tubulin band. The blots were quantified using ImageJ software as per guidelines given by Gassmann et al. [26].

Statistical analysis

Statistical analyses were performed using GraphPad Prism 5 data analysis software (GraphPad Software, La Jolla, USA). Significance tests of different culture conditions were conducted using one way ANOVA. Differences were considered as statistically significant for p-values <0.05. Bar charts were generated using means and the standard deviation (SD).

Results

In this study we examined the antifibrotic effect of the orphan drug PFD on different human ocular fibroblast subpopulations, which are involved in postsurgical events of glaucoma treatment. In postoperative wound healing processes these fibroblasts are activated to obturate surgical wounds by migration, proliferation and production of ECM components.

Cell morphology

For our experiments, primary human fibroblasts from Tenon's capsule (hTFs) and from the intraconal orbital fat depot (hOFs) were examined *in vitro* (Fig 1). Fibroblast subpopulations exhibited typical spindle-shaped morphology and no differences concerning size and shape of the cells could be observed between hTFs and hOFs.

Cell proliferation

The stimulation of hTFs with TGF-β1 resulted in an increase of cell proliferation to 640% of NC (Fig 2A).

In contrast, cells incubated with PFD exhibited only 51% of NC's proliferation, though this decrease was statistically significant. When incubated with a combination of TGF-β1 and PFD in serum-free conditions, the hTFs exhibited 641% relative proliferation (Fig 2A).

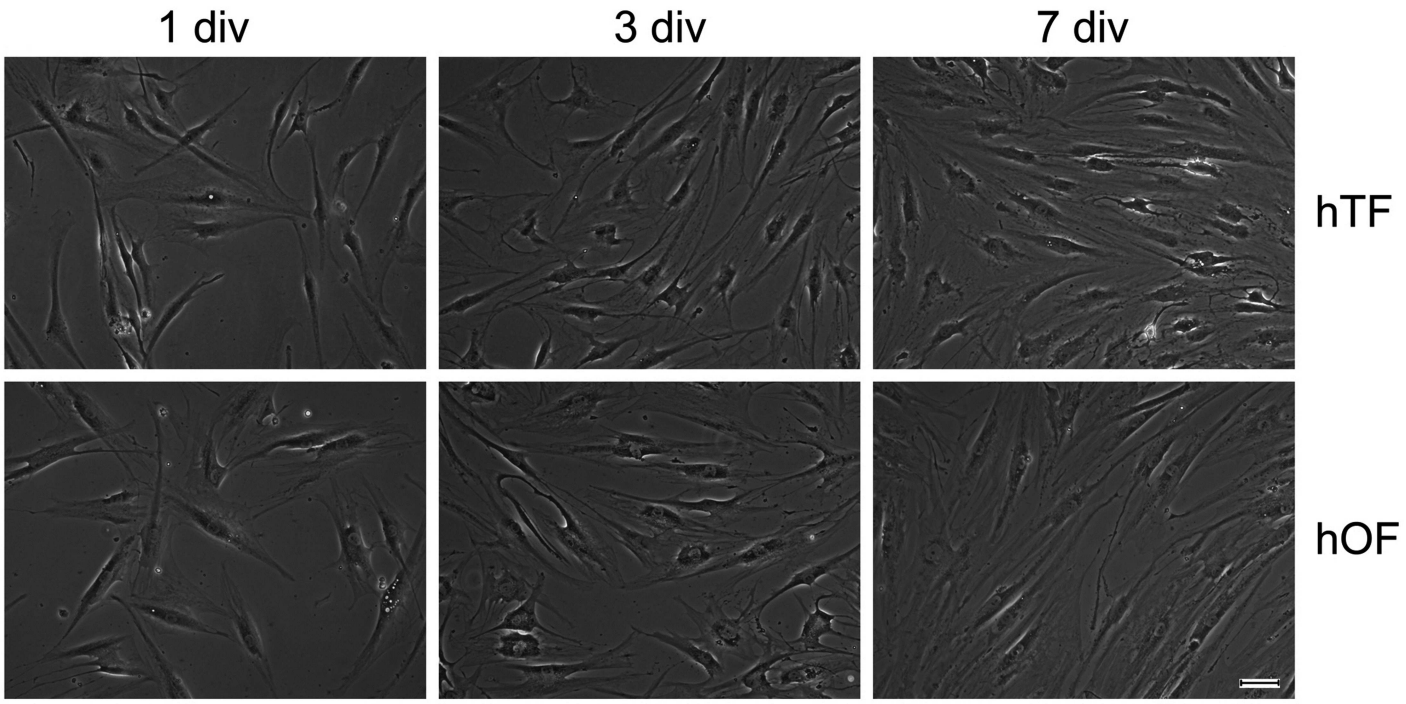

Fig 1. Human fibroblast subpopulations *in vitro*. Primary fibroblast subpopulations from Tenon's capsule (hTFs) and fibroblasts from orbital fat (hOFs) were cultured for 1, 3 and 7 days, respectively. div = days *in vitro*. Bar represents 25 μm.

doi:10.1371/journal.pone.0172592.g001

Under 10% FCS conditions (Fig 2B), the proliferation rate was 174% for hTFs incubated with TGF-β1 alone and 172% for cells incubated with a combination of TGF-β1 and PFD (Fig 2B). PFD alone did not influence the cell proliferation at all (Fig 2B).

In general, similar observations were made for hOFs (Fig 2C and 2D). Alterations of proliferation rate of hOFs under serum free (Fig 2C) and 10% FCS (Fig 2D) conditions demonstrated the same trends as observed for hTFs. Following stimulation of hOFs with TGF-β1 under serum free conditions, the relative proliferation of hOFs increased to 339% of NC. In contrast PFD acted antiproliferative by significantly dropping the proliferation rate to 70% of NC (Fig 2C). The stimulatory effect of TGF-β1 was weakened in hOFs incubated with a combination of TGF-β1 and PFD; these cells exhibited 293% of relative proliferation which was less compared with that of cells with TGF-β1 alone (339%) (Fig 2C). Under 10% FCS conditions, hOFs incubated with TGF-β1 alone or its combination with PFD exhibited comparable proliferation rates (135% and 146% of NC, respectively) (Fig 2D). PFD alone led to a non-significant proliferation decrease by 12% (Fig 2D).

Given the fact that TGF-β1 induced cell stimulation was more pronounced in serum-free cell culture conditions, which was expectable as TGF-β has better access to fibroblast cell surface receptors in serum free media, all further experiments were performed in serum-free cell culture conditions.

Gene expression patterns

In the presence of TGF-β1, a 12-fold increase in the expression of α-SMA mRNA was seen in hTF cultures, whereas there was no difference in α-SMA expression in the presence of PFD alone compared to the control cultures (Fig 3A). In hTFs cultured with a combination of TGF-β1 and PFD, a 9-fold increase could be observed, suggesting that the effect of TGF-β1 can be

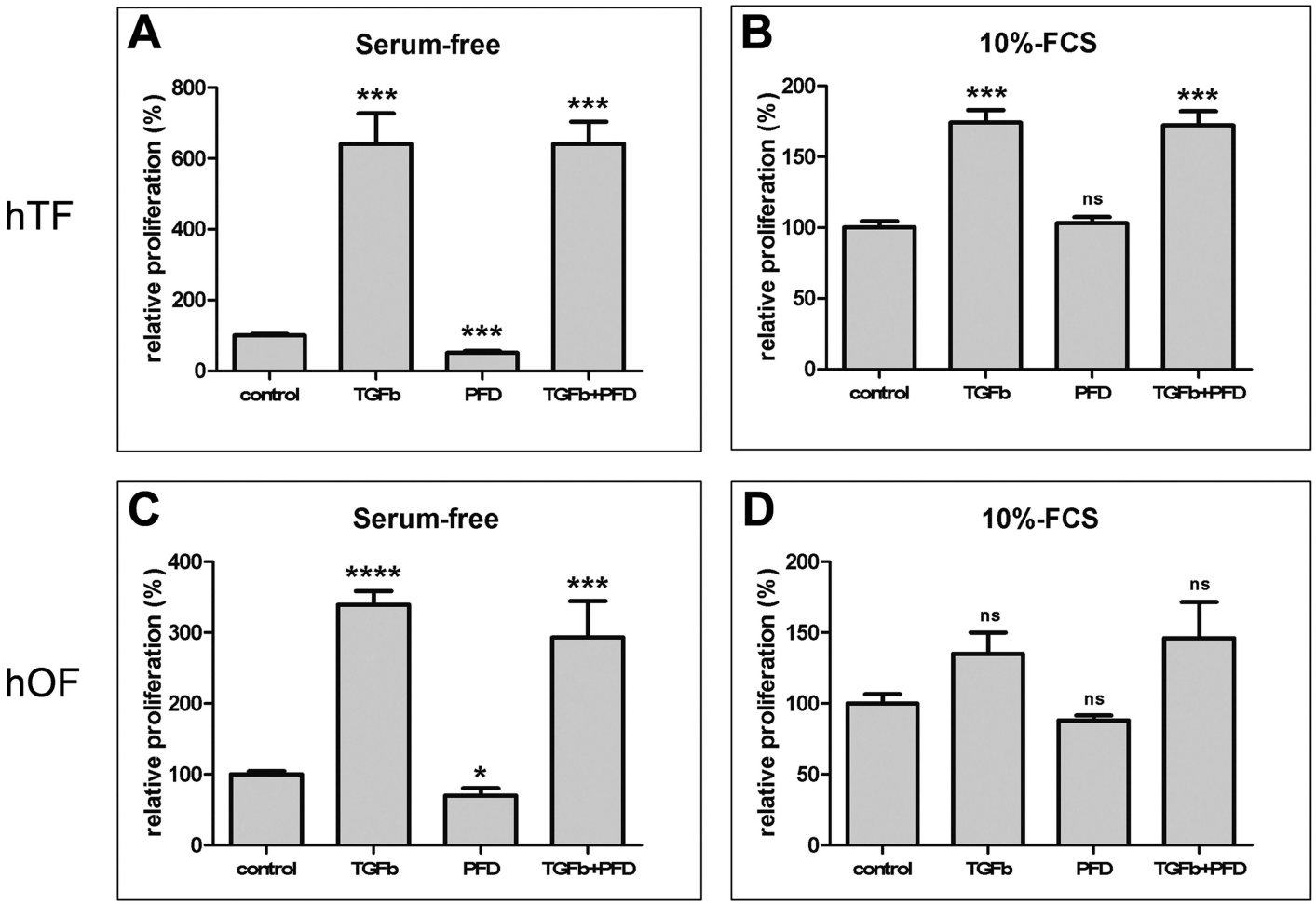

Fig 2. Relative proliferation of hTFs and hOFs in response to TGF-β1 and PFD *in vitro*. Fibroblasts were treated with TGF-β1 [10 ng/ml], PFD [10^{-3} mol/l] or the combination of TGF-β1 [10 ng/ml] and PFD [10^{-3} mol/l] for 48 h under serum-free (A and C) and serum (10% FCS) conditions (B and D) as indicated. NC (proliferation rate of untreated cells) was set to 100%. Data are presented as mean ± SD. The results represent the means of three independent experiments. Level of significances: *p≤0.05; **p≤0.01; ***p≤0.001; ****p≤0.0001.

doi:10.1371/journal.pone.0172592.g002

partly abrogated by the addition of PFD (Fig 3A). However, by comparison of TGF-β1 and combination of TGF-β1 and PFD the difference did not reach statistical significance.

In contrast, fibronectin (Fig 3B) and THBS2 (Fig 3C) mRNA expression was doubled in the presence of TGF-β1 and in the combination of TGF-β1 and PFD. It remained same to the control baseline values in the presence of PFD alone, revealing that PFD has no effect on the expression of these mRNAs (Fig 3B and 3C).

In case of COL1A2 mRNA expression, no change was noticed in the presence of TGF-β1 or its combination with PFD when compared to control values. Instead, a decrease of mRNA expression was observed after treatment with PFD alone (Fig 3D). An almost 3-fold increase in the expression of COL3A2 mRNA was observed in the presence of TGF-β1 or its combination with PFD compared to the control conditions (Fig 3E). However, treatment with PFD alone reduced COL3A2 mRNA expression when compared to the baseline values (Fig 3E). Conversely, we observed an increase in the expression of MMP2 mRNA in the presence of PFD alone, whereas the same gene was slightly downregulated in cells cultured with TGF-β1 or its combination with PFD (Fig 3F).

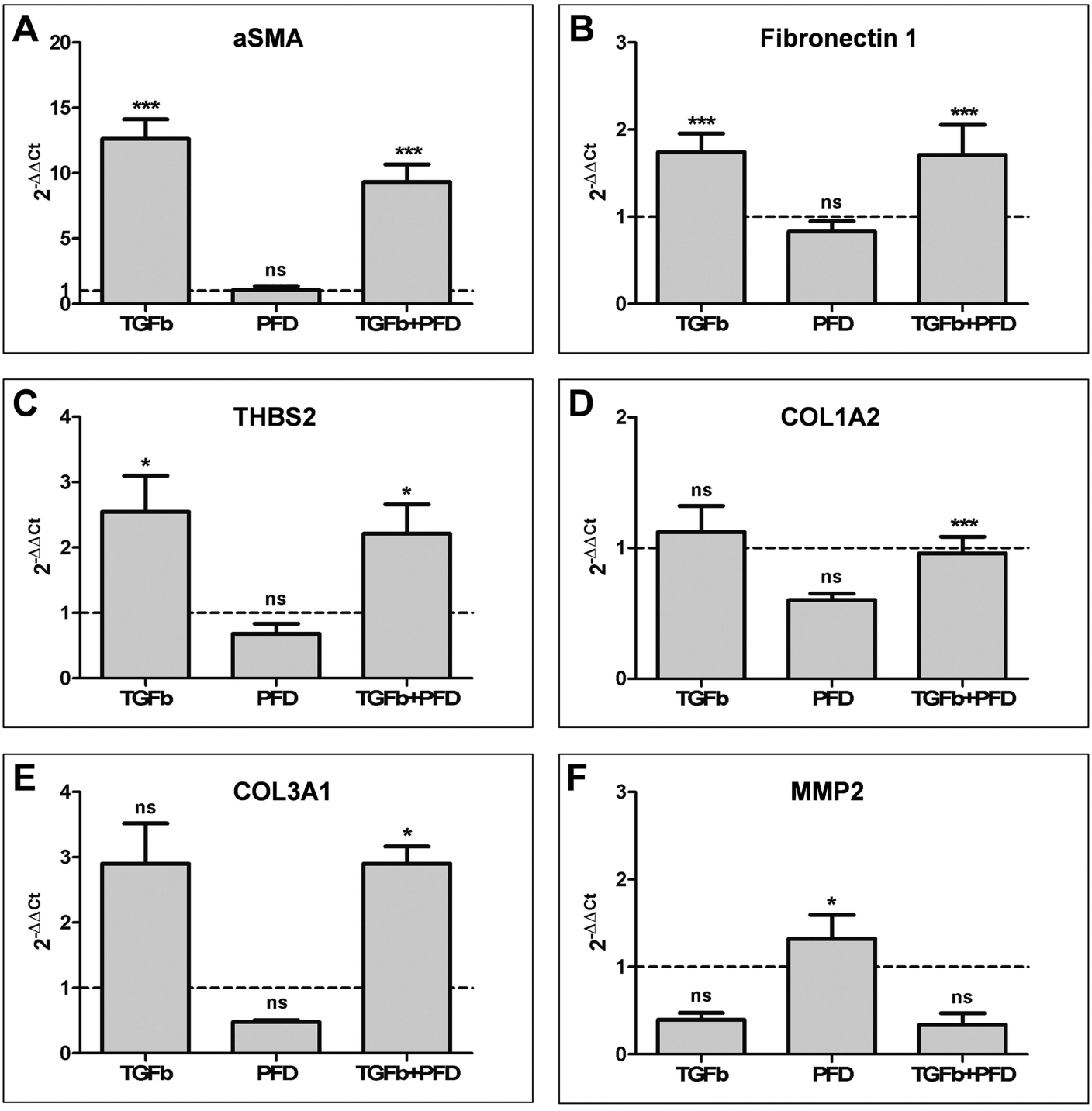

Fig 3. RT-PCR analysis of stimulated (TGF-β1) and suppressed (PFD) primary hTFs. Cultures of hTFs were treated with TGF-β1 [10 ng/ml], PFD [10^{-3} mol/l] or the combination of both, TGF-β1 and PFD for 48 h under serum-free culture conditions. NC (expression level of respective gene in untreated cells, dotted line) was set to 1. Data are presented as mean ± SD. The results represent the means of four independent experiments. Level of significances: *p≤0.05; **p≤0.01; ***p≤0.001. Differences between TGF-β1 and TGF-β1+PFD are statistically not significant.

doi:10.1371/journal.pone.0172592.g003

Notably, when comparing the expression levels of fibronectin (B), THBS2 (C), COL1A2 (D), COL3A1 (E) and MMP2 (F) between cultures treated with TGF-β1 only or TGF-β1 and PFD in combination, no statistically significant difference could be observed.

In hOF cultures, almost similar results in the relative expression profiles of the abovementioned mRNAs were detected. Briefly, a 4-fold increase of α-SMA mRNA expression was observed in the presence of TGF-β1 or its combination with PFD, whereas PFD alone yielded no difference to control cultures (Fig 4A). Approximately, a 2-fold increase of the expression profiles of fibronectin (Fig 4B), THBS2 (Fig 4C), COL1A2 (Fig 4D) COL3A1 (Fig 4E) mRNAs was observed in the presence of TGF-β1 or its combination with PFD when compared to control values. In all these cases, PFD had no effect on the expression profiles of these mRNAs when compared to control hOF cultures. Similar to hTFs, also in hOFs, only a small increase in the MMP2 gene expression was observed in the presence of PFD alone, which was downregulated in the presence of TGF-β1 or TGF-β1 and PFD combination (Fig 4F).

The comparison of gene expression levels between cell cultures treated with TGF-β1 and combination of TGF-β1 and PFD revealed no statistically significant differences (Fig 4A through 4F).

Taken together, these data confirm the role of TGF-β1 as a stimulator and PFD as a suppressor of fibrosis in both fibroblast subpopulations. These effects, however, were more pronounced in hTFs.

Immunohistochemistry

Immunocytochemical analysis revealed TGF-β1 induced activation of primary ocular fibroblasts (hTFs) (Fig 5). In untreated hTF cell cultures or in those incubated with PFD alone, no α-smooth muscle actin (α-SMA) stress fibers were visible (Fig 5). Incubation of cells with cytokine TGF-β1 led to an expression of α-SMA, which could serve as an indicator for fibroblast transformation into fibrotic active myofibroblasts. Additionally, transformation was accompanied by an increase of fibronectin expression. A decrease of α-SMA expression could be observed in cells incubated with combination of TGF-β1 and antifibrotic agent PFD.

A similar response to TGF-β1 stimulation could be detected in hOF cultures (Fig 6). While untreated control cells and cultures with PFD alone showed no expression of α-SMA stress fibers, TGF-β1 stimulation strongly increased α-SMA and fibronectin expression (Fig 6). An obvious decrease of α-SMA expression could be shown in hOF cultures with combined application of TGF-β1 and PFD (Fig 6).

Due to the fact that the transformation into myofibroblasts is associated with an increase in ECM production, we further examined the synthesis of ECM components in primary hTFs and hOFs under different culture conditions.

The immunohistochemical stainings of ECM components (collagen I, collagen III, collagen VI) under given culture conditions revealed an obvious increase in the expression in presence of TGF-β1, and only a subtle reduction in presence of PFD (data not shown).

Western blot analysis

To compare the amounts of different ECM components, total cell lysates were obtained and analyzed by immunoblotting. As a loading control β-tubulin was analyzed, showing no differences in signal intensity and equal amounts of loaded proteins among hTFs and hOFs.

The immunoblot analyses showed an increase in detected amounts of fibronectin, collagen I, and collagen VI in hTF cultures stimulated with TGF-β1 when compared to untreated controls (Fig 7A). When culturing hTFs with PFD alone, no changes in synthesized amounts of respective proteins could be observed. Compared to the TGF-β1 application, the combined

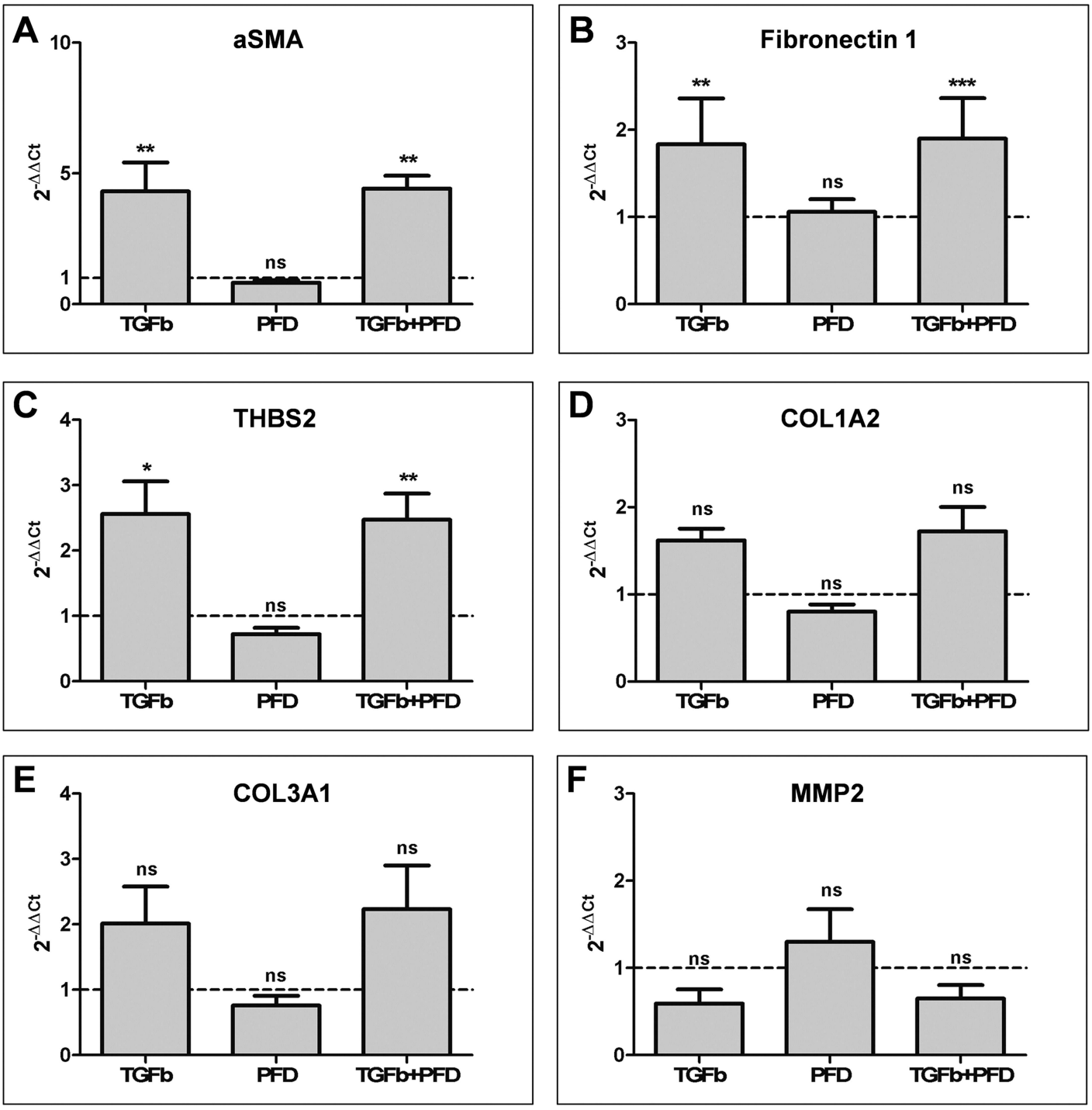

Fig 4. RT-PCR analysis of stimulated (TGF-β1) and suppressed (PFD) primary hOFs. Cultures of hOFs were treated with TGF-β1 [10 ng/ml], PFD [10^{-3} mol/l] or the combination of both, TGF-β1 and PFD for 48 h under serum-free culture conditions. NC (expression level of respective gene in untreated cells, dotted line) was set to 1. Data are presented as mean ± SD. The results represent the means of four independent experiments. Level of significances: *p≤0.05; **p≤0.01; ***p≤0.001. Overall, no statistically significant differences between TGF-β1 and TGF-β1+PFD groups could be observed.

doi:10.1371/journal.pone.0172592.g004

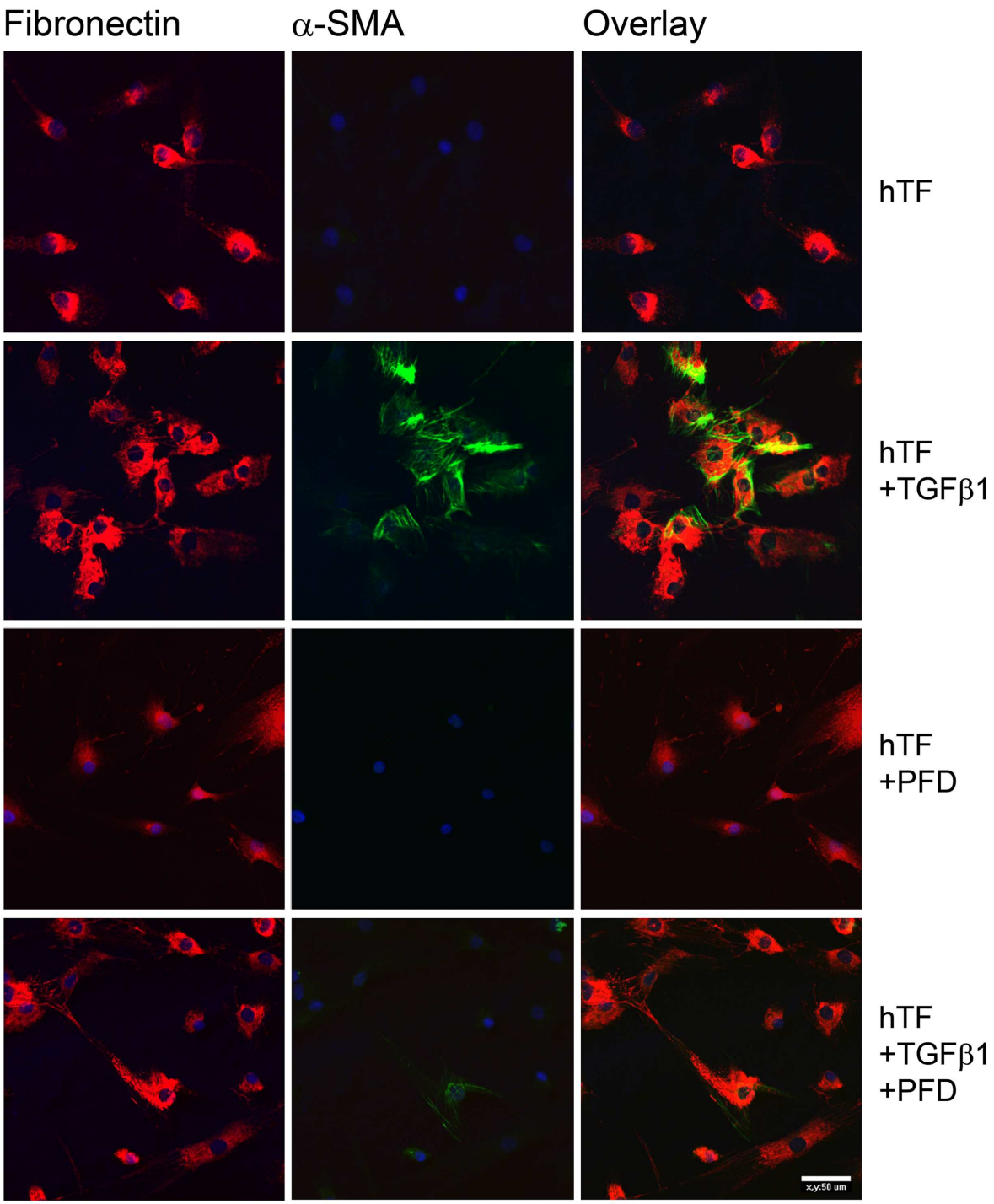

Fig 5. Immunocytochemical characterization of TGF-β1 induced fibronectin and α-SMA expression in primary hTFs *in vitro*. After PFA fixation, cells were incubated with primary antibodies directed against fibronectin and α-SMA. Nuclei were stained by DAPI included in the mounting medium. PFD decreased fibronectin and α-SMA expression. Experiments were carried out four times with similar results. Bar represents 50 μm.

doi:10.1371/journal.pone.0172592.g005

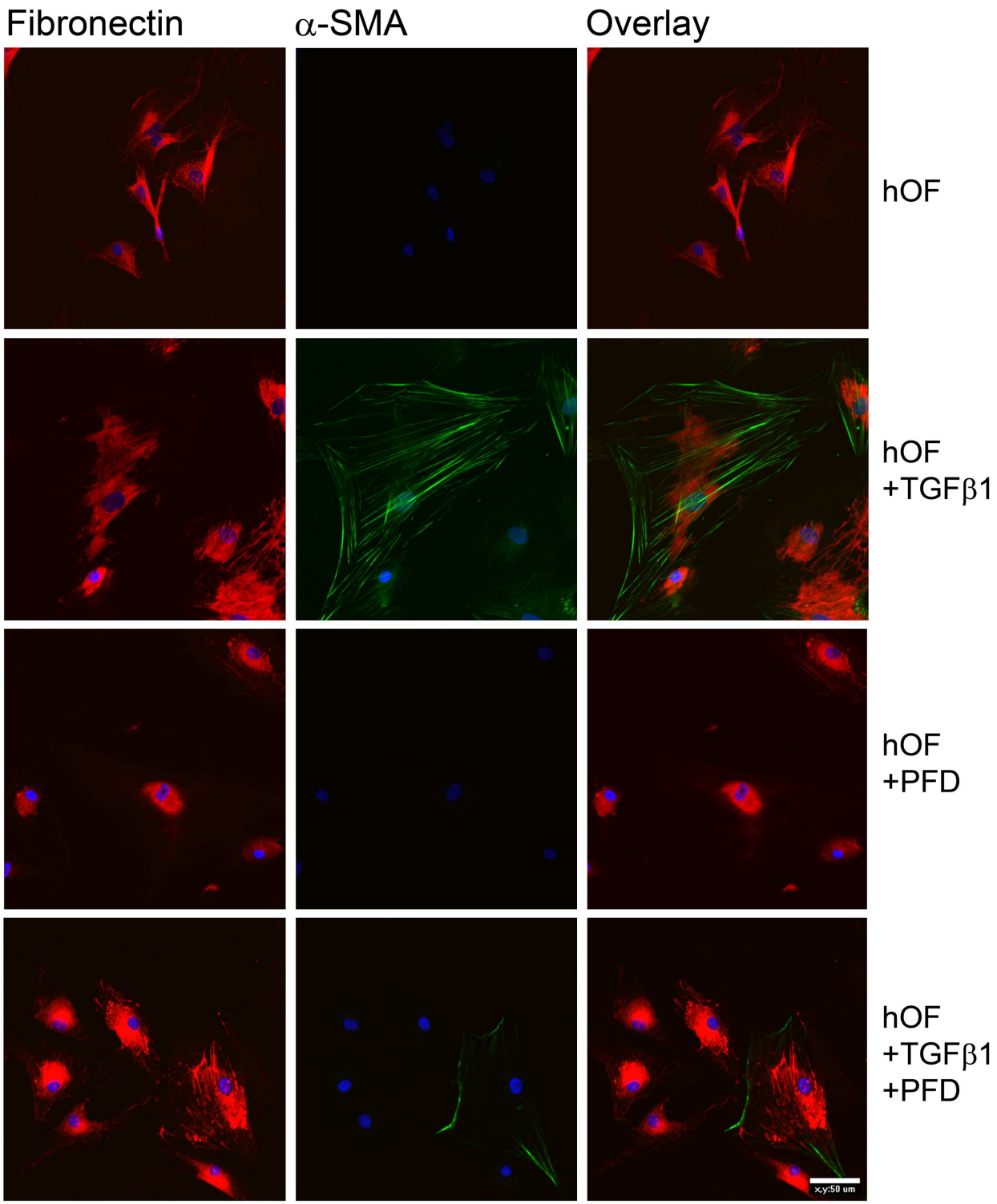

Fig 6. Immunocytochemical characterization of TGF-β1 induced fibronectin and α-SMA expression in primary hOFs *in vitro*. After PFA fixation, cells were incubated with primary antibodies directed against fibronectin and α-SMA. Nuclei were stained by DAPI included in the mounting medium. PFD decreased fibronectin and α-SMA expression. Experiments were carried out four times with similar results. Bar represents 50 μm.

doi:10.1371/journal.pone.0172592.g006

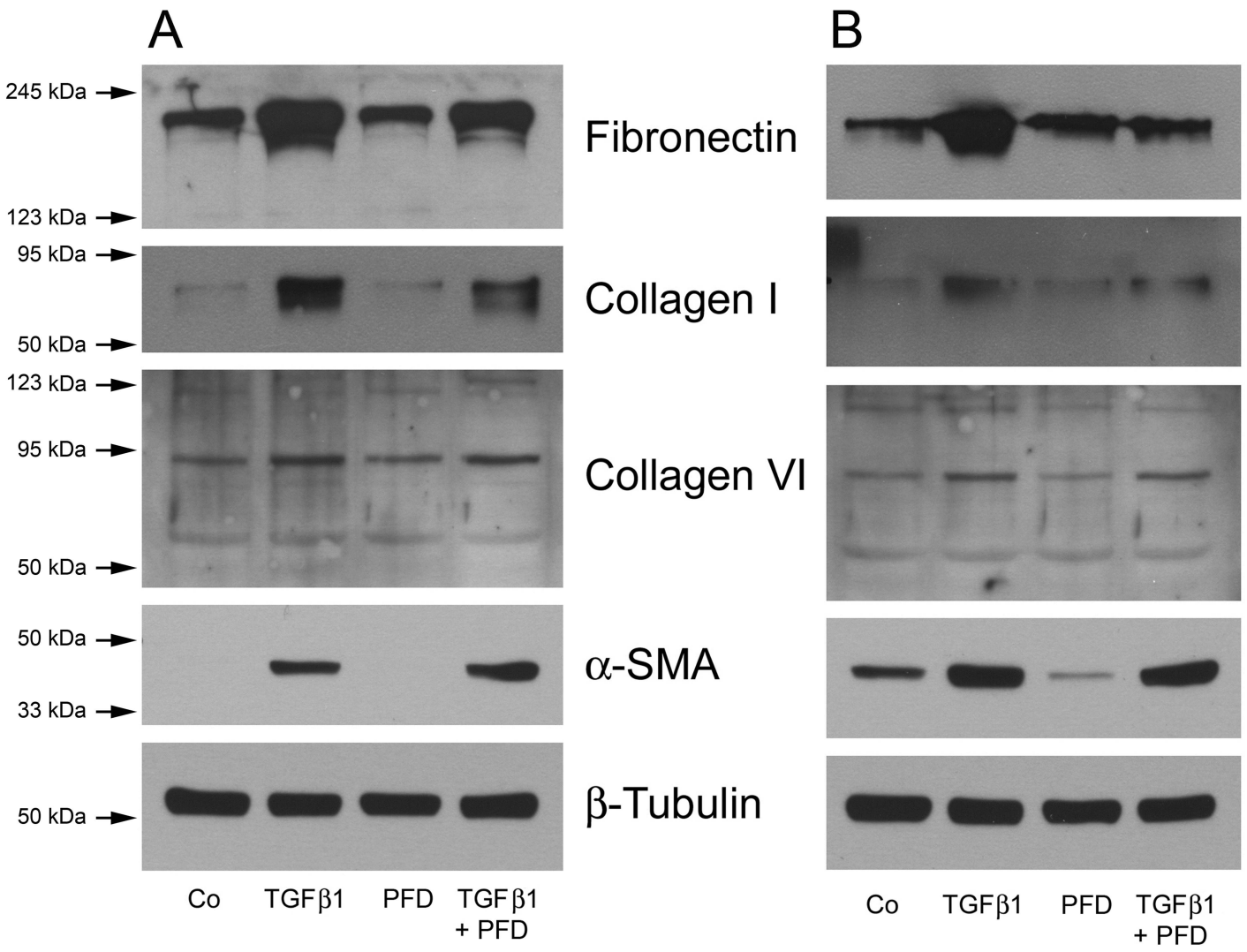

Fig 7. Western blot analysis of hTFs (A) and hOFs (B) under different culture conditions. Cell lysates of fibroblast subpopulations were prepared and subjected to Western blot analyses using antibodies against fibronectin, collagen I, collagen VI, α-SMA and β-tubulin as a loading control, as indicated.

doi:10.1371/journal.pone.0172592.g007

application of TGF-β1 and PFD resulted in a decrease of collagen I and collagen VI expression (Figs 7A and 8A).

These results were also confirmed in hOF cultures (Figs 7B and 8B). Stimulation of hOFs with TGF-β1 increased the expression of fibronectin, collagen I, collagen VI and α-SMA when compared to untreated controls. When culturing hOF cultures with PFD alone, a decrease in the α-SMA expression was detected. Compared to TGF-β1 stimulated hOF cultures, the ones with combined application of TGF-β1 and PFD exhibited a statistically significant decrease of fibronectin and collagen I expression ($p<0.001$), as shown in Fig 8B.

Discussion

Currently, strategies to minimize the incidence of postoperative fibrosis in glaucoma surgeries are focusing on anti-fibrotic agents, which are supposed to suppress fibrotic events in a specific and targeted way without affecting other cell types than fibroblasts.

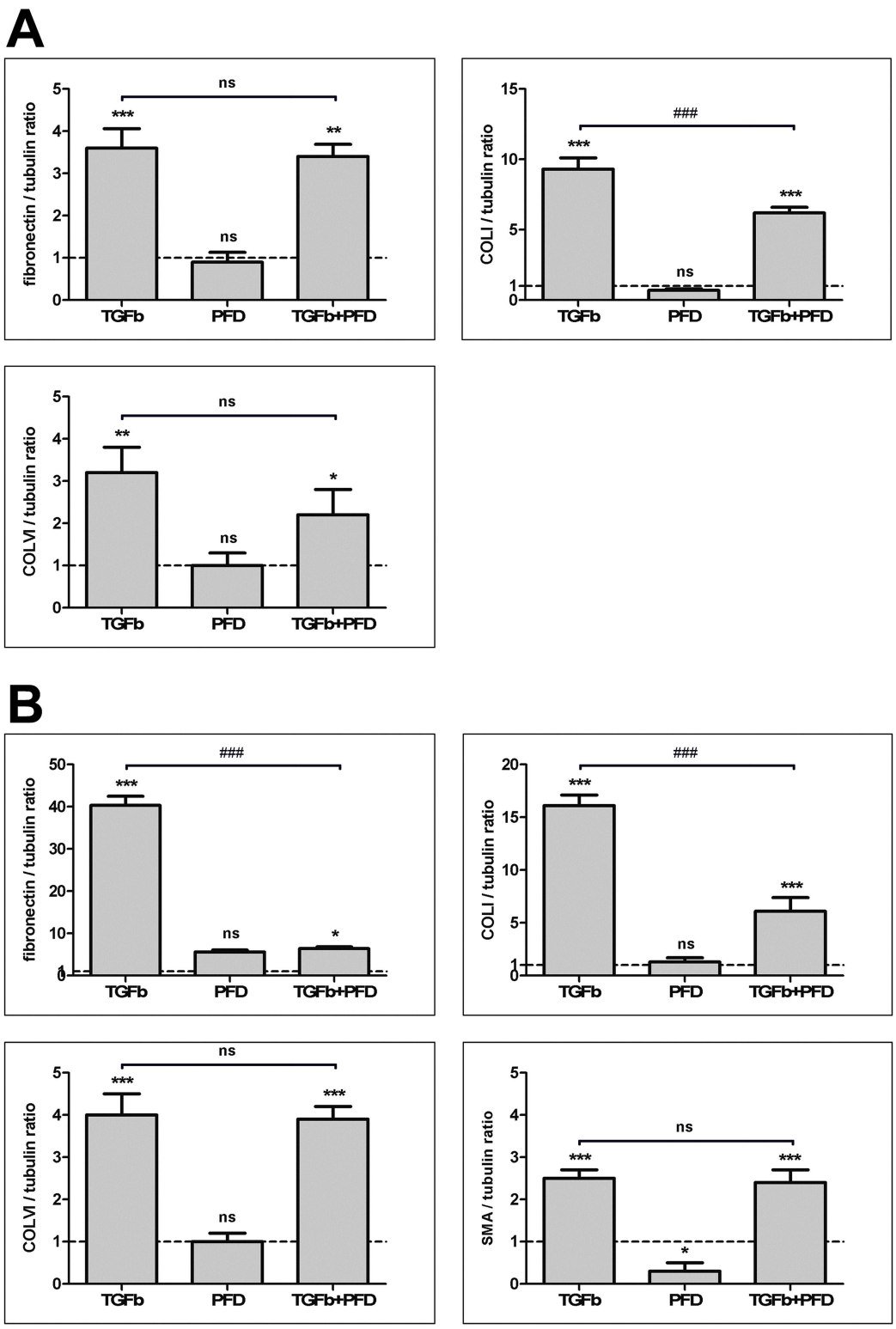

Fig 8. Quantification of Western blot data for hTFs (A) and hOFs (B). Each column represents the mean ± SD from three independent experiments. * indicates significances obtained by comparison of TGF-β1, PFD and TGF-β1+PFD to untreated cultures. # indicates significances obtained by comparison of TGF-β1-treated cultures and cultures with combined treatment TGF-β1+PFD. Level of significances: $*^{(\#)}p \leq 0.05$; $**^{(\#\#)}p \leq 0.01$; $***^{(\#\#\#)}p \leq 0.001$. No quantification could be performed for α-SMA in hTFs because of the absence of the protein in control and PFD-treated samples (Fig 7).

doi:10.1371/journal.pone.0172592.g008

In this context, we designed the present study to explore the effects of the antifibrotic small molecule pirfenidone (PFD), which has been previously shown to inhibit TGF-β induced protein expression and to ameliorate fibrotic processes in lung [27], kidney [28] and liver [29]. The *in vitro* experiments in our study were conducted with two different subtypes of ocular cells, namely Tenon's and intraconal fat fibroblasts (hTFs and hOFs, respectively). As the most important cells, synthesizing ECM in the Tenon's capsule, TFs play a key role in healing and scarring processes after glaucoma surgery at the level of the subconjunctival and episcleral tissue. The orbital fat fibroblasts, on the other hand, are of growing interest with regard to the orbital fat tissue as a possible drainage area of new generation drainage devices.

To possibly mimic the *in vivo* situation, we established fibrotic cell cultures of these ocular fibroblast subpopulations through incubation of primary cells with cytokine TGF-β1, which is considered the "master cytokine" in fibrosis [30]. It promotes fibroblast proliferation, differentiation and their transition into myofibroblasts. We could recently show that TGF-β1 was expressed in primary human ocular fibroblast subpopulations [24]. Binding of TGF-β1 to the TGF-β-receptor 1 and 2 results in a fusion of both receptors and a phosphorylation of TGF-β-receptor 1 through the TGF-β-receptor 2. This phosphorylation is transferred to the intracellular downstream-mediators SMAD2 and 3, proteins, which further transduce the signal from cell surface over cytoplasm into the nucleus, where they act as transcription factors and regulate proliferation and fibrotic genes, e.g. collagen I and fibronectin. Following incubation with TGF-β1, elevated amounts of ECM-components and α-SMA could be demonstrated in both Tenon and orbital fat fibroblasts. Furthermore, the TGF-β1 treatment resulted in up-regulation of THSB2 and downregulation of MMP2.

THSB2 belongs to a small family of secreted glycoproteins which activate the inactive, latent form of TGF-β thus enabling its interaction with cellular receptors [31]. Functionally, THSB2 plays a role in ECM turnover and is involved in physiological wound healing processes [32]. However, in fibrosis, due to the excessive ECM production, THSBs expression is increased [33]. More recently, a study examining fibrosis-related gene expression in excised capsules of failed GDDs, revealed a strong upregulation of THSB1 and THSB2 genes compared to age-matched control Tenon specimens [34].

ECM degradation under normal conditions is mediated by MMPs. One of the most important MMPs is MMP2. Down-regulation of MMP2 alters the balance of synthesis and degradation and lead to a decrease of ECM turnover with negative consequences in fibrotic matrix deposition. A down-regulation of MMP2 following TGF-β stimulation in embryonic rat fibroblasts (REF-52) was shown by Howard and colleagues [35]. Furthermore, MMP2 was clearly down-regulated in murine fibroblastic cells (NIH/3T3) and neonatal primary cardiac fibroblasts, when the cells were exposed to TGF-β [36].

These findings highlight the importance of TGF-β1 in inducing pro-fibrogenic factors (like THSB2) and suppressing proteins responsible for ECM homeostasis (like MMP2). Expectedly, upon TGF-β1 incubation the cells exhibited also an increase in cell proliferation, compared to untreated cultures (6- and 3-fold for hTFs and hOFs, respectively).

In the next step we examined the antiproliferative and antifibrotic effects of PFD, both in control and TGF-β1 treated "fibrotic" cell cultures. The broad antifibrotic spectrum of PFD, including TGF-β1-suppression was demonstrated in numerous *in vitro* and *in vivo* studies [37]. PFD was also shown to inhibit cell proliferation, myofibroblast differentiation, collagen contractility and migratory ability of cardiac fibroblasts [38]. Similar effects were observed in hepatic and renal fibroblasts following PFD treatment [39,40]. Also in human Tenon fibroblast cell cultures PFD inhibited cell proliferation in a concentration- and time-dependent manner by arresting the cells in the G1 phase of the cell cycle [41]. The same study also demonstrated for the first time the antifibrotic effects of PFD on ocular fibroblasts, as shown by reduced cell

motility, collagen contraction and down regulation of TGF-β1 and 2 gene transcription along with decreased expression of respective proteins. In good agreement with existing literature, our results also demonstrate that PFD inhibits cell proliferation and slightly inhibits ECM production and cell differentiation into myofibroblasts in unstimulated cell cultures. We can rule out any possibility, that antiproliferative effects of PFD are mediated by drug toxicity as viability assays showed that PFD is not cytotoxic in the given concentration.

All above mentioned literature findings on PFD have been obtained from *in vitro* experiments using unstimulated cells. So far, there is only one study, which has demonstrated the antifibrotic effects of PFD in a "fibrotic" cell culture of ocular fibroblasts [42]. This culture was induced by exposure to interleukine-1β (IL-1β), while TGF-β and other cytokines failed to stimulate the cells. In contrast, here, we could successfully establish a "fibrotic" culture through exposure of Tenon and orbital fat fibroblasts to TGF-β1.

Surprisingly, in such cultures the antiproliferative and antifibrotic effects of PFD were less pronounced. Cells, simultaneously incubated with TGF-β1 and PFD were almost completely comparable with "fibrotic" ones (incubated with TGF-β1 alone) by mean of cell proliferation and production of ECM-components. The only markers, which were reduced compared to fibrotic cultures were the hallmark of myofibroblasts α-SMA and the ECM component fibronectin.

In clinical terms, the above mentioned results might implicate, that once fibrosis has developed, PFD would not be able to make the scarring processes reversible.

When translating these observations to the *in vivo* situation, one possibility is to apply PFD either postoperatively in form of eye drops after filtration surgery or GDD implantation, or incorporated in GDD for a sustained local drug delivery. In both cases, PFD will be present on the target site before fibrosis occurs, which means that this drug can play a preventive role in the development of fibrotic events. A randomized, controlled masked-observer rabbit study has shown that a postoperative use of PFD was associated with less scarring and improved trabeculectomy bleb survival [43].

In conclusion, we report about the differential expression of several genes and proteins in TGF-β1 stimulated ocular fibroblasts, compared with normal untreated cells. The results of the present study suggest that PFD is able to exert antifibrotic effects on untreated cells, while being less effective in TGF-β1-stimulated "fibrotic" cultures.

Combined with the results of previous *in vitro* studies performed on ocular fibroblasts, we propose that PFD may be a promising candidate for the treatment of fibrosis following glaucoma filtration surgery or GDD implantation.

Acknowledgments

The authors thank Mrs. C. Leyh and Mrs. J. Weiß-Müller for skillful technical assistance. The work was financially supported by Bundesministerium für Bildung und Forschung (BMBF) within the REMEDIS project "Höhere Lebensqualität durch neuartige Mikroimplantate" (FKZ: 03IS2081).

Author Contributions

Conceptualization: TS RFG MH.

Data curation: TS BSK JW MH.

Formal analysis: TS BSK JW MH.

Funding acquisition: KPS AW RFG.

Investigation: TS BSK JW MH.

Methodology: TS BSK JW.

Project administration: TS MH.

Resources: OS KPS AW RFG.

Validation: TS BSK JW MH.

Visualization: TS BSK JW.

Writing – original draft: TS OS AW MH.

Writing – review & editing: TS RFG MH.

References

1. Fechtner RD, Weinreb RN. Mechanisms of optic nerve damage in primary open angle glaucoma. Survey of ophthalmology. 1994; 39 (1): 23–42. PMID: 7974188
2. Quigley HA, Broman AT. The number of people with glaucoma worldwide in 2010 and 2020. The British journal of ophthalmology. 2006; 90 (3): 262–267. doi: 10.1136/bjo.2005.081224 PMID: 16488940
3. Astrom S, Stenlund H, Linden C. Incidence and prevalence of pseudoexfoliations and open-angle glaucoma in northern Sweden: II. Results after 21 years of follow-up. Acta ophthalmologica Scandinavica. 2007; 85 (8): 832–837. doi: 10.1111/j.1600-0420.2007.00980.x PMID: 17986292
4. Quigley HA. Glaucoma. The Lancet 377 2011:(9774): 1367–1377.
5. Pfeiffer N, Lamparter J, Gericke A, Grus FH, Hoffmann EM, Wahl J Neuroprotection of medical IOP-lowering therapy. Cell and tissue research. 2013; 353 (2): 245–251. doi: 10.1007/s00441-013-1671-1 PMID: 23836043
6. Palmberg P. Risk factors for glaucoma progression: Where does intraocular pressure fit in. Archives of ophthalmology (Chicago, Ill.: 1960). 2001; 119 (6): 897–898.
7. Kass MA, Heuer DK, Higginbotham EJ, Johnson CA, Keltner JL, Miller JP et al. The Ocular Hypertension Treatment Study: a randomized trial determines that topical ocular hypotensive medication delays or prevents the onset of primary open-angle glaucoma. Archives of ophthalmology (Chicago, Ill.: 1960). 2002; 120 (6): 701–13; discussion 829–30.
8. Schwartz K, Budenz D. Current management of glaucoma. Current opinion in ophthalmology. 2004; 15 (2): 119–126. PMID: 15021223
9. Baudouin C, Labbe A, Liang H, Pauly A, Brignole-Baudouin F. Preservatives in eyedrops: the good, the bad and the ugly. Progress in retinal and eye research. 2010; 29 (4): 312–334. doi: 10.1016/j.preteyeres.2010.03.001 PMID: 20302969
10. Nordstrom BL, Friedman DS, Mozaffari E, Quigley HA, Walker AM. Persistence and adherence with topical glaucoma therapy. American journal of ophthalmology. 2005; 140 (4): 598–606. doi: 10.1016/j.ajo.2005.04.051 PMID: 16226511
11. Quigley HA. European Glaucoma Prevention Study. Ophthalmology. 2005; 112 (9): 1642–3; author reply 1643–5. doi: 10.1016/j.ophtha.2005.05.024 PMID: 16139678
12. Bettin P, Di Matteo F. Glaucoma: present challenges and future trends. Ophthalmic research. 2013; 50 (4): 197–208. doi: 10.1159/000348736 PMID: 24030362
13. Coleman AL. Advances in glaucoma treatment and management: surgery. Investigative ophthalmology & visual science. 2012; 53 (5): 2491–2494.
14. Olali C, Rotchford AP, King AJ. Outcome of repeat trabeculectomies. Clinical & experimental ophthalmology. 2011; 39 (7): 658–664.
15. Hong CH, Arosemena A, Zurakowski D, Ayyala RS. Glaucoma drainage devices: a systematic literature review and current controversies. Survey of ophthalmology. 2005; 50 (1): 48–60. doi: 10.1016/j.survophthal.2004.10.006 PMID: 15621077
16. Gedde SJ, Schiffman JC, Feuer WJ, Herndon LW, Brandt JD, Budenz DL et al. Treatment outcomes in the Tube Versus Trabeculectomy (TVT) study after five years of follow-up. American journal of ophthalmology. 2012; 153 (5): 789–803.e2. doi: 10.1016/j.ajo.2011.10.026 PMID: 22245458
17. Gedde SJ, Panarelli JF, Banitt, Lee RK. Evidenced-based comparison of aqueous shunts. Current opinion in ophthalmology. 2013; 24 (2): 87–95. doi: 10.1097/ICU.0b013e32835cf0f5 PMID: 23287104

18. Wynn TA. Cellular and molecular mechanisms of fibrosis. The Journal of pathology. 2008; 214 (2): 199–210. doi: 10.1002/path.2277 PMID: 18161745

19. Min J, Lukowski ZL, Levine MA, Meyers CA, Beattie AR, Schultz GS et al. Prevention of ocular scarring post glaucoma filtration surgery using the inflammatory cell and platelet binding modulator saratin in a rabbit model. PloS one. 2012; 7 (4): e35627. doi: 10.1371/journal.pone.0035627 PMID: 22558182

20. Spitzer MS, Sat M, Schramm C, Schnichels S, Schultheiss M, Yoeruek E et al. Biocompatibility and anti-fibrotic effect of UV-cross-linked hyaluronate as a release-system for tranilast after trabeculectomy in a rabbit model–a pilot study. Current eye research. 2012; 37 (6): 463–470. doi: 10.3109/02713683.2012.658593 PMID: 22577763

21. Hollo G. Wound healing and glaucoma surgery: modulating the scarring process with conventional anti-metabolites and new molecules. Developments in ophthalmology. 2012; 50: 79–89. doi: 10.1159/000334790 PMID: 22517175

22. Cordeiro MF, Mead A, Ali RR, Alexander RA, Murray S, Chen C et al. Novel antisense oligonucleotides targeting TGF-beta inhibit in vivo scarring and improve surgical outcome. Gene therapy. 2003; 10 (1): 59–71. doi: 10.1038/sj.gt.3301865 PMID: 12525838

23. Hilberg O, Simonsen U, Du Bois R, Bendstrup E. Pirfenidone: significant treatment effects in idiopathic pulmonary fibrosis. The clinical respiratory journal. 2012; 6 (3): 131–143. doi: 10.1111/j.1752-699X.2012.00302.x PMID: 22697264

24. Stahnke T, Lobler M, Kastner C, Stachs O, Wree A, Sternberg K et al. Different fibroblast subpopulations of the eye: a therapeutic target to prevent postoperative fibrosis in glaucoma therapy. Experimental eye research. 2012; 100: 88–97. doi: 10.1016/j.exer.2012.04.015 PMID: 22579993

25. Neuhoff V, Philipp K, Zimmer HG, Mesecke S. A simple, versatile, sensitive and volume-independent method for quantitative protein determination which is independent of other external influences. Hoppe-Seyler's Zeitschrift fur physiologische Chemie. 1979; 360 (11): 1657–1670. PMID: 92445

26. Gassmann M, Grenacher B, Rohde B, Vogel J. Quantifying Western blots: pitfalls of densitometry. Electrophoresis. 2009; 30 (11): 1845–1855. doi: 10.1002/elps.200800720 PMID: 19517440

27. Tian X-l, Yao W, Guo ZJ, Gu L, Zhu YJ. Low dose pirfenidone suppresses transforming growth factor beta-1 and tissue inhibitor of metalloproteinase-1, and protects rats from lung fibrosis induced by bleomycina. Chinese medical sciences journal = Chung-kuo i hsueh k'o hsueh tsa chih / Chinese Academy of Medical Sciences. 2006; 21 (3): 145–151.

28. Takakuta K, Fujimori A, Chikanishi T, Tanokura A, Iwatsuki Y, Yamamoto M et al. Renoprotective properties of pirfenidone in subtotally nephrectomized rats. European journal of pharmacology. 2010; 629 (1–3): 118–124. doi: 10.1016/j.ejphar.2009.12.011 PMID: 20006961

29. Grizzi F. Pirfenidone: a potential therapeutic option in the treatment of liver fibrosis. Clinical and experimental pharmacology & physiology. 2009; 36 (10): 961–962.

30. Zeisberg M, Kalluri R. Cellular mechanisms of tissue fibrosis. 1. Common and organ-specific mechanisms associated with tissue fibrosis. American journal of physiology. Cell physiology. 2013; 304 (3): C216–25. doi: 10.1152/ajpcell.00328.2012 PMID: 23255577

31. Annes JP, Munger JS, Rifkin DB. Making sense of latent TGFbeta activation. Journal of cell science. 2003; 116 (Pt 2): 217–224. PMID: 12482908

32. Bornstein P. Thrombospondins as matricellular modulators of cell function. The Journal of clinical investigation. 2001; 107 (8): 929–934. doi: 10.1172/JCI12749 PMID: 11306593

33. Pohjolainen V, Mustonen E, Taskinen P, Napankangas J, Leskinen H, Ohukainen P et al. Increased thrombospondin-2 in human fibrosclerotic and stenotic aortic valves. Atherosclerosis. 2012; 220 (1): 66–71. doi: 10.1016/j.atherosclerosis.2011.10.003 PMID: 22035575

34. Mahale A, Othman MW, Al Shahwan S, Al Jadaan I, Owaydha O, Khan Z et al. Altered expression of fibrosis genes in capsules of failed Ahmed glaucoma valve implants. PloS one. 2015; 10 (4): e0122409. doi: 10.1371/journal.pone.0122409 PMID: 25879570

35. Howard EW, Crider BJ, Updike DL, Bullen EC, Parks EE, Haaksma CJ et al. MMP-2 expression by fibroblasts is suppressed by the myofibroblast phenotype. Experimental cell research. 2012; 318 (13): 1542–1553. doi: 10.1016/j.yexcr.2012.03.007 PMID: 22449415

36. Sassoli C, Chellini F, Pini A, Tani A, Nistri S, Nosi D et al. Relaxin prevents cardiac fibroblast-myofibroblast transition via notch-1-mediated inhibition of TGF-beta/Smad3 signaling. PloS one. 2013; 8 (5): e63896. doi: 10.1371/journal.pone.0063896 PMID: 23704950

37. Burghardt I, Tritschler F, Opitz CA, Frank B, Weller M, Wick W. Pirfenidone inhibits TGF-beta expression in malignant glioma cells. Biochemical and biophysical research communications. 2007; 354 (2): 542–547. doi: 10.1016/j.bbrc.2007.01.012 PMID: 17234158

38. Shi Q, Liu X, Bai Y, Cui C, Li J, Li Y et al. In vitro effects of pirfenidone on cardiac fibroblasts: proliferation, myofibroblast differentiation, migration and cytokine secretion. PloS one. 2011; 6 (11): e28134. doi: 10.1371/journal.pone.0028134 PMID: 22132230

39. Di Sario A, Bendia E, Svegliati Baroni G, Ridolfi F, Casini A, Ceni E et al. Effect of pirfenidone on rat hepatic stellate cell proliferation and collagen production. Journal of hepatology. 2002; 37 (5): 584–591. PMID: 12399223

40. Hewitson TD, Kelynack KJ, Tait MG, Martic M, Jones CL, Margolin SB et al. Pirfenidone reduces in vitro rat renal fibroblast activation and mitogenesis. Journal of nephrology. 2001; 14 (6): 453–460. PMID: 11783601

41. Lin X, Yu M, Wu K, Yuan H, Zhong H. Effects of pirfenidone on proliferation, migration, and collagen contraction of human Tenon's fibroblasts in vitro. Investigative ophthalmology & visual science. 2009; 50 (8): 3763–3770.

42. Kim H, Choi YH, Park SJ, Lee SY, Kim SJ, Jou I et al. Antifibrotic effect of Pirfenidone on orbital fibroblasts of patients with thyroid-associated ophthalmopathy by decreasing TIMP-1 and collagen levels. Investigative ophthalmology & visual science. 2010, 51 (6): 3061–3066.

43. Zhong H, Sun G, Lin X, Wu K, Yu M. Evaluation of pirfenidone as a new postoperative antiscarring agent in experimental glaucoma surgery. Investigative ophthalmology & visual science. 2011; 52 (6): 3136–3142.

Bioscience Reports (2018) **38** BSR20180628
https://doi.org/10.1042/BSR20180628

Research Article

Development of a biodegradable antifibrotic local drug delivery system for glaucoma microstents

Thomas Stahnke[1], Stefan Siewert[2], Thomas Reske[2], Wolfram Schmidt[3], Klaus-Peter Schmitz[2,3], Niels Grabow[3], Rudolf F. Guthoff[1] and Andreas Wree[4]

[1]Department of Ophthalmology, Rostock University Medical Center, Doberaner Str. 140, Rostock 18057, Germany; [2]Institute for Implant Technology and Biomaterials e.V., Friedrich-Barnewitz-Straße 4, Rostock 18119, Germany; [3]Institute of Biomedical Engineering, Rostock University Medical Center, Friedrich-Barnewitz-Straße 4, Rostock 18119, Germany; [4]Institute of Anatomy, Rostock University Medical Center, Gertrudenstraße 9, Rostock 18057, Germany

Correspondence: Thomas Stahnke (thomas.stahnke@med.uni-rostock.de)

To prevent implant failure due to fibrosis is a major objective in glaucoma research. The present study investigated the antifibrotic effects of paclitaxel (PTX), caffeic acid phenethyl ester (CAPE), and pirfenidone (PFD) coated microstent test specimens in a rat model. Test specimens based on a biodegradable blend of poly(4-hydroxybutyrate) biopolymer and atactic poly(3-hydroxybutyrate) (at.P(3HB)) were manufactured, equipped with local drug delivery (LDD) coatings, and implanted in the subcutaneous white fat depot. Postoperatively, test specimens were explanted and analyzed for residual drug content. Fat depots including the test specimens were histologically analyzed. *In vitro* drug release studies revealed an initial burst for LDD devices. *In vivo*, slow drug release of PTX was found, whereas it already completed 1 week postoperatively for CAPE and PFD LDD devices. Histological examinations revealed a massive cell infiltration in the periphery of the test specimens. Compact fibrotic capsules around the LDD devices were detectable at 4–36 weeks and least pronounced around PFD-coated specimens. Capsules stained positive for extracellular matrix (ECM) components. The presented model offers possibilities to investigate release kinetics and the antifibrotic potential of drugs *in vivo* as well as the identification of more effective agents for a novel generation of drug-eluting glaucoma microstents.

Introduction

Glaucoma is a leading cause of irreversible blindness worldwide and is mostly characterized by an increased intraocular pressure (IOP), which results from disturbances in the outflow of aqueous humor from the eye. Permanently increased pressure conditions lead to damage of the retinal ganglion cells and degeneration of the optic nerve fibers, resulting in a loss of vision and finally blindness, if untreated [1]. Until now, reduction in IOP is the only available treatment to prevent nervous degeneration [2,3]. Medicinal therapy represents the first-line treatment for IOP lowering [4,5]. In case of insufficient IOP reduction by means of medicinal therapy, surgical interventions have been used to drain aqueous humor from the anterior chamber of the eye into an extraocular compartment. Trabeculectomy and deep sclerectomy [6-8] have been used most commonly. Additionally, cyclophotocoagulation [9,10] provides an alternative therapy to lower IOP by decreasing the aqueous humor production.

As a further approach to conventional surgical interventions, alloplastic devices for the drainage of aqueous humor from the anterior chamber into different outflow areas, particularly into Tenon's capsule, have been used [11]. Clinically used implants in a tube and plate design are the Molteno (Molteno Ophthalmic Ltd., Dunedin, New Zealand), the BAERVELDT (Abbott Medical Optics Inc., Santa Ana, CA, U.S.A.), and the Ahmed (New World Medical Inc., Rancho Cucamonga, CA, U.S.A.) drainage devices. These implants differ in terms of material and design, and the Ahmed implant has a flow-restricting valve mechanism [12]. Other approaches prefer the suprachoroidal space as outflow area to lower IOP [13-15].

Received: 23 April 2018
Revised: 27 June 2018
Accepted: 26 July 2018

Accepted Manuscript Online: 30 July 2018
Version of Record published: 31 August 2018

Bioscience Reports (2018) **38** BSR20180628
https://doi.org/10.1042/BSR20180628

The disadvantages of surgical interventions as well as implantations of drainage devices are the fibrotic and uncontrollable scarring processes, which can lead to a failure of the newly created draining channels or to an implant occlusion [16] and as a consequence to an IOP increase. Thus, the development of an antifibrotic drug-eluting microstent represents a major objective for improving the clinical success rates of glaucoma drainage devices (GDD).

Fibrotic and scarring processes are mainly driven by the proliferation of fibroblasts and exuberant extracellular matrix (ECM) expression. It was shown that fibroblasts from different ocular tissues differ in their mRNA profiles [17] and in their expression of ECM components [18]. The retro-orbital white fat depot (corpus adiposum orbitae) with probably a different fibrotic behavior and low pressure values of 4–14 mmHg [19-21] has been discussed as a possible drainage area. The advantage of the retro-orbital white fat depot for drug-eluting drainage devices is its distance from the very sensitive structures of the eye, like the retina. Cinti [22] demonstrated in his work that in rodents the subcutaneous white fat depots anterior to the hind legs are metabolically much less active compared with the very active brown fat areas, which makes these regions comparable with the corpus adiposum orbitae in humans and thus a suitable model to analyze postoperative reactions.

To address the problem of fibrosis, alloplastic drainage devices can be coated with antifibrotic drugs as it is done with drug-eluting stents in cardiovascular treatment [23,24]. The most commonly used antifibrotic agents are the cytostatics mitomycin C and 5-fluorouracil [25], which inhibit mitotic processes. Additionally, the potent inhibitor of mitosis, paclitaxel (PTX) [26,27], was studied in this context. Some disadvantages of these cytostatics are unspecific influences and toxic effects on all cell types as a result of their mechanisms of action. For side effect minimization, specific drugs/agents have to be identified, which only act on fibrotic relevant fibroblasts and their synthesis of ECM components without impairing cell and tissue viability. In this context, caffeic acid phenethyl ester (CAPE) is one of the most interesting bioactive compounds. CAPE was shown to be an effective agent to prevent fibrotic processes in pulmonary fibrosis by influencing some profibrotic/antifibrotic key mediators including TGF-β1, TNF-α and prostaglandin E2 [28], and the synthesis of collagen I [29]. Also its antioxidant activity and modulatory impact on the immune system has been described [30].

Another specific antifibrotic agent is pirfenidone (PFD), which has been shown to decrease the expression of fibrosis relevant cytokines (TGF-β1–3) [31] and ECM components [32]. PFD has also been used as an oral formulation for systemic treatment of idiopathic pulmonary fibrosis [33]. PFD can also modulate immune responses as demonstrated in an abdominal adhesion rat model [34].

In the present study, a local drug delivery (LDD) coating for a novel biodegradable glaucoma microstent was developed and analyzed *in vitro* and *in vivo* in terms of drug release behavior and tissue response to address the postoperative problem of scarring and fibrosis around the stent in the outflow area. The concept of our implant-based regenerative approach for the drainage of aqueous humor into the retro-orbital intraconal fat tissue is shown in Figure 1A.

As an alternative to conventional permanent, biostable GDDs, the presented biodegradabale microstent serves as temporary pathway for controlled drainage of aqueous humor. Our initial experiments using these biodegradable polymers as GDD provided promising results [35]. An LDD coating in the outflow area was designed to prevent fibrosis in the postoperative period. After microstent degradation, the remnant channel should allow for long-term effective drainage without the complications associated with foreign-body reactions to the biomaterial or mechanical irritation, often observed in cases of permanent GDD.

The aim of the current study was the evaluation of drug release and antifibrotic effects of different LDD coatings, containing the drugs PTX and the more specific agents CAPE and PFD, in a rat model. Therefore, GDD test specimens with different LDD coatings were implanted subcutaneously into the white fat depots in front of the right hind leg of rats. After explantation at different postoperative points in time, tissue samples including the test specimens were analyzed with regard to residual drug-loading and fibrotic responses.

Materials and methods

Manufacturing and characterization of test specimens

Test specimens were composed of tubing and an LDD coating, both manufactured based on biodegradable polymeric materials. A polymer blend from poly(4-hydroxybutyrate) (P(4HB); P4HB biopolymer, Tepha, Inc., Lexington, MA, U.S.A.), and amorphous atactic poly(3-hydroxybutyrate) (at.P(3HB)) in a blend ratio of 50/50% (w/w) was used to prepare the tubing and the coatings. Synthesis of at.P(3HB) was conducted according to Jedlinski et al. [36] and Hubbs et al. [37] by ring-opening polymerization of β-butyrolactone using potassium acetate as a catalyst [38]. Three different LDD coatings were based on a homogeneous mixture of the polymer blend and the drug PTX (Cfm Oskar Tropitzsch e.K., Marktredwitz, Germany), CAPE (Sigma–Aldrich Corp., St. Louis, MO, U.S.A.), or PFD (Sigma–Aldrich

Table 1 Summary of HPLC conditions used for *in vitro* drug release studies

	PTX	CAPE	PFD
Column	Chromolith fast gradient RP-18e 50-2 (Merck KGaA, Darmstadt, Germany)	Eurospher 100 C18, 5 μm, 125 × 4 mm ID (Knauer GmbH, Berlin, Germany)	Eurospher 100 C18, 5 μm, 125 × 4 mm ID (Knauer GmbH, Berlin, Germany)
Mobile phase	Acetonitrile/phosphate buffer solution (0.005 M, pH 3.5) (50/50% v/v)	Methanol/water (65/35% v/v)	Acetonitrile/water (27/73%) v/v with 0.2% acetic acid
Flow rate	0.3 ml.min^{-1}	1.0 ml.min^{-1}	1.0 ml.min^{-1}
Column temperature	23°C	30°C	45°C
Detection wavelength (UV)	230 nm	323 nm	310 nm
Injected sample volume	20 μl	20 μl	20 μl
Retention time	3.0 min	4.5 min	6.0 min
Measurement range	0.1–20 μg.ml^{-1}	0.1–20 μg.ml^{-1}	0.1– 20 μg.ml^{-1}

Corp., St. Louis, MO, U.S.A.) in a mixing ratio of 85/15% (w/w), respectively. In a control group, tubing without LDD coating was used.

Tubing with a wall thickness of 75 μm was manufactured in a semiautomatic process using a dip-coating robot (KSV NIMA Dip Coater, Biolin Scientific Holding AB, Stockholm, Sweden). Stainless steel mandrels (diameter: 300 μm, length: 60 mm) were dipped repeatedly into the polymer solution prepared from 1150 mg chloroform (Sigma–Aldrich Corp., St. Louis, MO, U.S.A.) and 100 mg of the polymer blend P(4HB)/at.P(3HB) 50/50% (w/w). A withdrawal speed of 300 mm.min^{-1} was used. After each repetition, the mandrels were dried for 20 min at ambient temperature and rotated at 180°. Tubing diameter was measured in 0.5 mm increments along the longitudinal axis using a biaxial laser scanner (ODAC 32 XY, Zumbach Electronic AG, Orpund, Switzerland) after the mandrels were removed.

The LDD coatings of the tubular test specimens (length: 10 mm) were applied with an airbrush process using a polymer solution prepared from 28.5 g chloroform (Sigma–Aldrich Corp., St. Louis, MO, U.S.A.) and 100 mg of the polymer blend/drug mixture. A mass of 126 μg, corresponding to a drug loading of 1.4 μg.mm^{-2}, was the desired nominal coating weight. Measurement of the coating mass was conducted using an ultramicrobalance (XP6U, Mettler-Toledo International, Inc., Greifensee, Switzerland).

After preparation, the test specimens were dried for 7 days in vacuum at ambient temperature. Test specimens from the control, the PTX and the CAPE groups were sterilized by means of ethylene oxide as described previously [35]. For PFD-coated test specimens, cooled β sterilization at −15°C in a nitrogen atmosphere was applied, using a radiation dose of 25 kGy in 4 min. Prior to β sterilization, test specimens were cooled at −40°C for 24 h.

Morphological analysis of the manufactured test specimens was performed using SEM (Quanta 250 FEG, FEI, Hillsboro, OR, U.S.A.) in environmental mode (ESEM) at a vacuum pressure of 0.5 mbar and an accelerating voltage of 5 kV.

Drug release *in vitro*

Analysis of temporal drug release from the test specimens was performed *in vitro* in 2 ml of 0.9% saline solution at 37°C. To protect CAPE from oxidation, 0.2% of ascorbic acid (Sigma–Aldrich Corporation, St. Louis, MO, U.S.A.) was added to the saline solution.

During *in vitro* drug release studies, the test specimens were incubated on a rotating platform-shaking device (Unimax 1010, Heidolph Instruments GmbH & Co. KG, Schwabach, Germany) at 100 rpm. After a defined time of incubation Δt_i, the saline solution was collected and drug content $m_i\ (\Delta t_i)$ was analyzed by means of HPLC (KNAUER Wissenschaftliche Geräte GmbH, Berlin, Germany). Prior to HPLC analysis, the saline extracts were diluted 1:1 (v/v) with methanol. Cumulative released drug mass m_j after j cycles was calculated by summation of individual values.

After drug release stagnated, the residual drug in the test specimen was extracted by methanol and analyzed using HPLC. Individual test specimens additionally were taken after extraction and completely dissolved in chloroform again and analyzed using HPLC to find residual drug amounts. A summary of HPLC conditions used for analysis of the different drugs PTX, CAPE, and PFD is shown in Table 1.

Drug release *in vivo*

For the analysis of temporal drug release *in vivo*, test specimens explanted at different postoperative points in time t_i were analyzed for residual drug loading $m_{res}\ (t_i)$ by means of HPLC. Prior to HPLC, the drugs were extracted from

Bioscience Reports (2018) **38** BSR20180628
https://doi.org/10.1042/BSR20180628

test specimens by methanol. Released drug mass $m_i\ (t_i)$ at the time t_i was calculated by subtracting $m_{res}\ (t_i)$ from the initial drug loading m_{init}.

Ethical consent

All animal studies were approved by the local authorities (Landesamt für Landwirtschaft, Lebensmittelsicherheit und Fischerei Mecklenburg-Vorpommern (LALLF-MV)) and conducted in accordance with the German Animal Welfare Act (Approval ID: 7221.3-1.1-085/12).

Animals

Adult male Wistar rats (strain Crl:WI BR, Charles River Wiga GmbH, Sulzfeld, Germany) aged approximately 3 months were used and individually housed in standard cages at 22 ± 2°C under a 12-h light/dark cycle in a specific pathogen-free housing, with free access to tap water and a standard diet.

Surgical intervention

Rats weighing 280–300 g were anesthetized by intraperitoneal injection of ketamine (Bela-pharm GmbH, Vechta, Germany; 50 mg/kg body weight) and xylazine (Rompun, Bayer AG, Leverkusen, Germany; 4 mg/kg body weight). The implantation area was shaved and disinfected with Betaisodona (Mundipharma GmbH, Limburg, Germany). Cutis was carefully opened with a scalpel and by a minimally invasive surgical intervention, the test specimens were implanted into the subcutaneous white fat depots in front of the right hind leg using a PICO-ID-Chip-Injector (AgnTho's, Lidingö, Schweden) (Figure 1B). This region was selected for the implantation because these white fat depots are metabolically less active compared with the active brown fat areas [22]. Therefore, the subcutaneous white fat of rats is comparable with the retrobulbar orbital white fat depot (corpus adiposum orbitae) in humans. At defined postoperative points in time (1, 2, 4, 12, and 36 weeks) animals were killed with an overdose of ketamine and xylazine. Test specimens were explanted from six animals per group: four for HPLC analysis of residual drug content. The remaining two specimens were explanted after the rats were perfused with 3.7% paraformaldehyde (PFA) dissolved in PBS (pH 7.4) prior to histological analysis. Fat depots were explanted, postfixed in 3.7% PFA for 24 h, and embedded in paraffin for histological investigation.

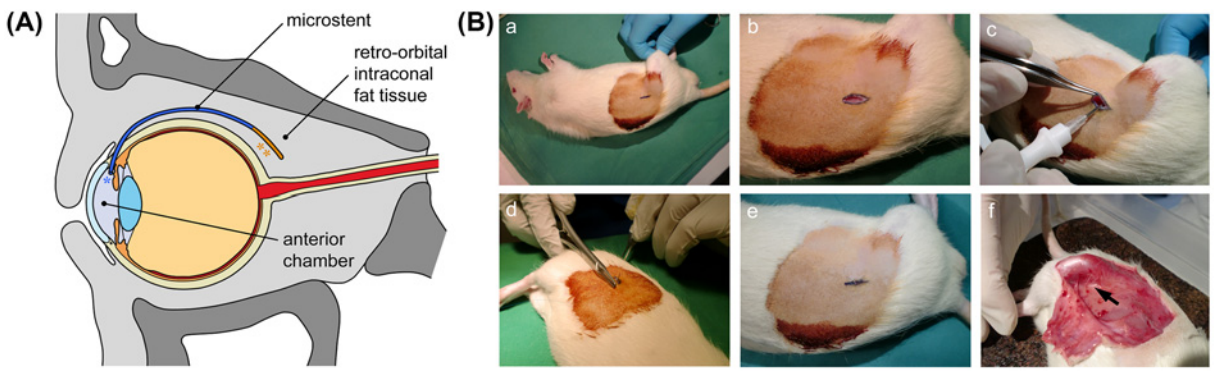

Figure 1. Illustration of the microstent concept and photo documentation of the minimally invasive surgical intervention

(**A**) Schematic drawing of a microstent for the drainage of aqueous humor from the anterior chamber of the eye into the retro-orbital intraconal fatty tissue; microstent with micro-mechanical valve for the prevention of hypotony (*) located in the anterior chamber and LDD coating (**) for the prevention of fibrosis located in the outflow area. (**B**) Implantation of test specimen into the subcutaneous white fat depot of rats and explantation procedure. (a) Shaved and disinfected implantation area with mark for incision. (b) Carefully opened cutis. (c) Test specimen injection into white fat depot using a PICO-ID-Chip-Injector. (d) Wound closure by suture. (e) With two stitches closed cutis. (f) Explantation of test specimen. Arrow marks the implant.

Histology

Histological sections of 5 μm thicknesses were AZAN stained using a standard protocol [39]. Briefly, rehydrated sections were stained in filtered and preheated (56°C) 0.1% aqueous azocarmine G solution (Merck Millipore, Darmstadt, Germany) and transferred into 0.1% aniline in 96% ethanol (Merck Millipore) until cytoplasm, connective tissue, and nuclei were well defined. After staining with 0.25% Aniline Blue, 1% Orange G (Sigma–Aldrich, Taufkirchen,

Table 2 Antibodies used in the present study

Reagent	Supplier	Catalog number
Mouse monoclonal anti-collagen I	Abcam (Cambridge, U.K.)	ab6308
Mouse monoclonal anti-collagen VI	Abcam (Cambridge, U.K.)	ab78504
Rabbit polyclonal fibronectin	DPC Biermann GmbH (Germany)	DP013
Mouse monoclonal fibronectin	Sigma–Aldrich (Germany)	F7387
Rabbit polyclonal CD11b	Abcam (Cambridge, U.K.)	Ab52478
Biotinylated anti-ms IgG (H+L)	Vector/Biozol (Eching, Germany)	VEC-BA-2000-CE
Biotinylated anti-ms IgM	Vector/Biozol (Eching, Germany)	VEC-BA-2020
Biotinylated anti-rb IgG (H+L)	Vector/Biozol (Eching, Germany)	VEC-BA-1000-CE

Table 3 Average wall thickness and drug mass of manufactured test specimens: mean ± S.D. (each *n*=35)

Group	Tubing	LDD coating	
	Wall thickness [μm]	Drug	Drug mass [μg]
1	74.5 ± 9.0	-	-
2	70.9 ± 5.3	PTX	20.3 ± 1.4
3	65.8 ± 5.8	CAPE	19.5 ± 0.8
4	68.8 ± 5.1	PFD	19.8 ± 0.9

Germany; Merck) sections were dehydrated with absolute alcohol and xylene and mounted with Entellan (Merck Millipore).

As a second histological observation, sections were stained with Hematoxylin–Eosin (H&E) [39]. Shortly, after dewaxing in xylene and hydration in a decreasing alcoholic row, sections were stained with Hematoxylin (Merck Millipore), followed by alcoholic dehydration and 1% Eosin G (Merck Millipore) staining. Differentiation occurs in 90% alcohol followed by clearing in xylene and finally mounting in Entellan (Merck Millipore).

For detailed investigation of the fibrotic and inflammatory responses, immunohistochemistry using the avidin–biotin complex immunoperoxidase method (Vector Laboratories, Burlingame, CA, U.S.A.) was carried out as described before [40]. Briefly, paraffin slides were dewaxed, rehydrated, and non-specific protein binding was blocked with 10% BSA in TBS including 100 mM lysine and 1% Triton X-100 at room temperature for 60 min. After washing, sections were incubated with the primary antibodies overnight at 4°C. Following another wash cycle, sections were incubated with either biotinylated rabbit anti-goat IgG or with biotinylated horse anti-mouse IgG for 2 h at room temperature before color development with diaminobenzidine. For control sections, the primary antibody was omitted. After mounting with Entellan (Merck Millipore) sections were analyzed using a BX51 microscope (Olympus, Hamburg, Germany) and Stereoinvestigator 8.0 software.

The following primary and secondary antibodies were used for IHC staining (Table 2).

The datasets generated and analyzed during the current study are available from the corresponding author on reasonable request.

Results

Manufacturing and characterization of test specimens

Average wall thickness and drug mass of the manufactured test specimens are summarized in Table 3. Representative scanning electron microscope (SEM) images of the test specimens are shown in Figure 2A. Scanning electron micrographs showed smooth surfaces for all groups at low magnification (150×). Microporous surfaces of group 2 (PTX LDD coating) and group 3 (CAPE LDD coating) were visible at high magnification (400×).

Drug release *in vitro*

Drug release studies revealed a burst release followed by a more retarded release phase for all LDD devices. Overall drug recovery from *in vitro* studies of PTX, CAPE, and PFD LDD devices was 70.0 ± 6.5, 75.9 ± 0.9, and 81.4 ± 5.4%, respectively (n=4). After dissolution of extracted microstents in chloroform, no residual drug was found. Slow *in vitro* drug release within a time frame of 5–6 weeks was found for PTX and CAPE LDD devices.On the contrary, PFD LDD devices showed fast *in vitro* drug release within 10 h (Figure 2B).

Bioscience Reports (2018) **38** BSR20180628
https://doi.org/10.1042/BSR20180628

Drug release *in vivo*

In vivo, slow drug release of PTX from LDD devices was found within a time frame of 12 weeks. For CAPE and PFD LDD devices, drug release was already completely finished at the first extraction date, 1 week postoperatively. The comparison of drug release *in vitro* and *in vivo* is shown in Figure 2C.

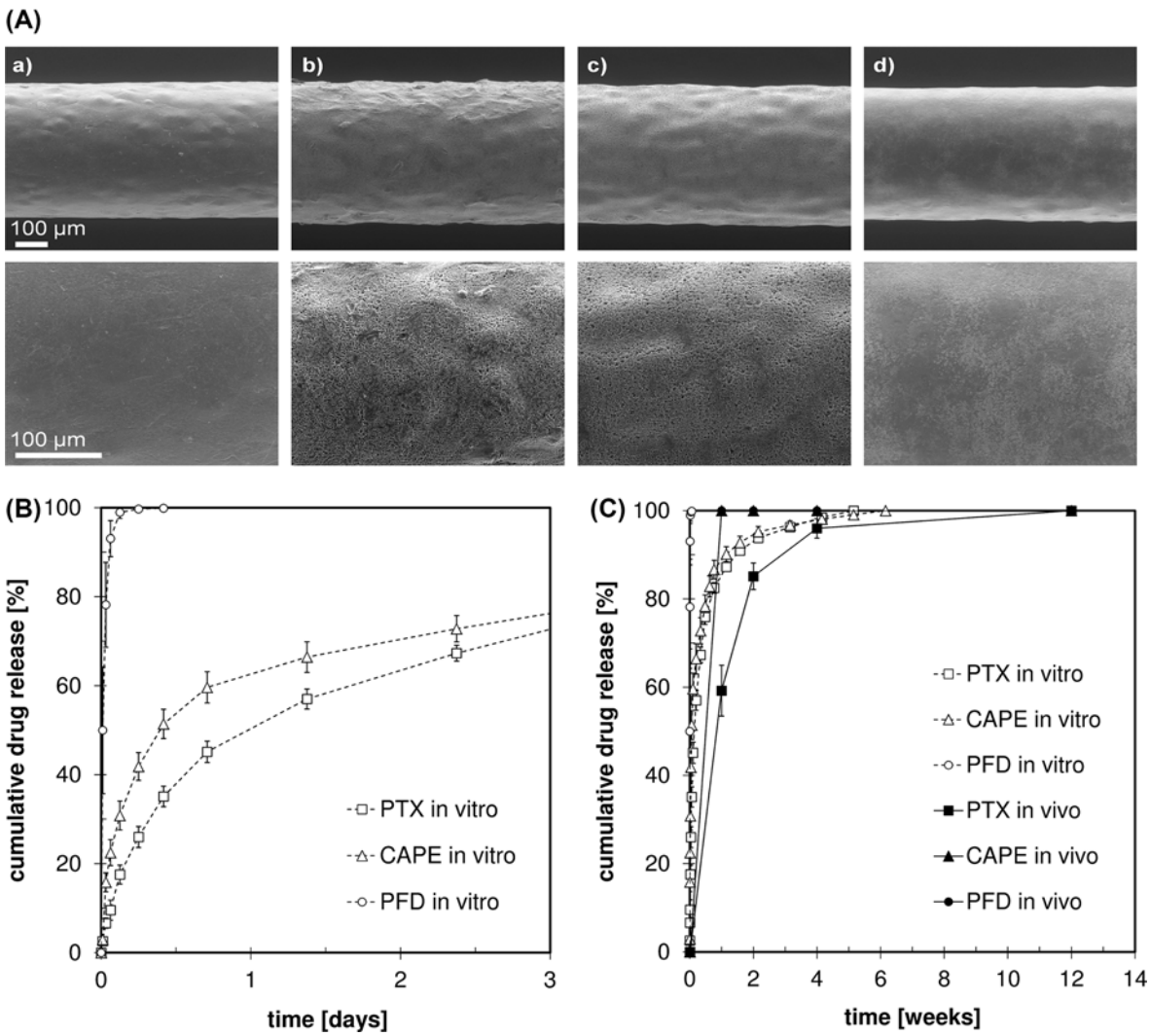

Figure 2. Manufactured test specimens and quantitation of drug release *in vitro* and *in vivo*

(**A**) Representative scanning electron micrographs of test specimens from (a) group 1 (no LDD coating), (b) group 2 (PTX LDD coating), (c) group 3 (CAPE LDD coating), and (d) group 4 (PFD LDD coating) at 150× and 400× magnification, respectively. (**B**) Cumulative drug release from different LDD devices *in vitro* in an initial time frame of the release studies (each n=4, normalized to recovered drug mass). (**C**) Drug release from different LDD devices *in vitro* and *in vivo* within 12 weeks (each n=4).

Histology

Histological examination of explanted fat depots including the test specimen implants revealed a massive cell infiltration around uncoated control, and coated CAPE and PFD test specimens 1–2 weeks after the implantation (Figure 3A,B). In contrast, around the PTX-coated test specimen a breakdown/damage of connective and fat tissues was detectable at these time points. Total 1 month after implantation, compact capsules around the control implants could be observed, which were also present in CAPE and PFD test specimens but not as compact as in controls. The fibrotic capsules increased in thickness up to 6 months in these groups. At this time point, some degradation of the biodegradable stent material was observed, which still formed a functional tube and was explantable for drug recovery examinations.

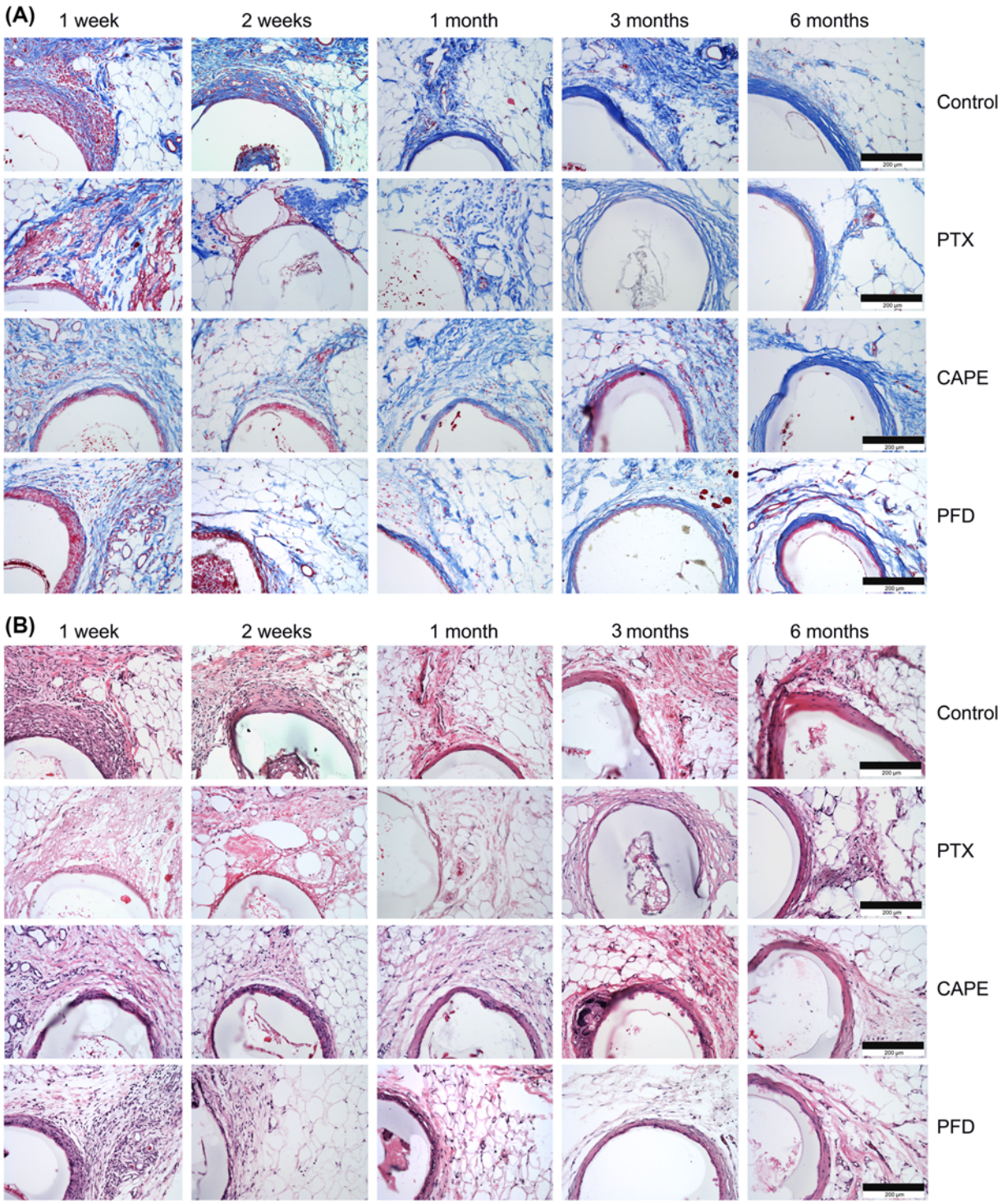

Figure 3. Histology of the subcutaneous white fat depots including the test specimens

(**A**) Cross-sections of the rat white fat depots were stained for connective tissue using AZAN staining. A connective tissue-rich fibrotic capsule is obvious after 6 months in the periphery of uncoated control implants, as well as in the PTX-, CAPE-, and PFD–coated specimens. (**B**) Cross-sections were H&E stained. Comparable with (A), strongest implant encapsulation is obvious after 6 months. Bars represent 200 μm.

Bioscience Reports (2018) **38** BSR20180628
https://doi.org/10.1042/BSR20180628

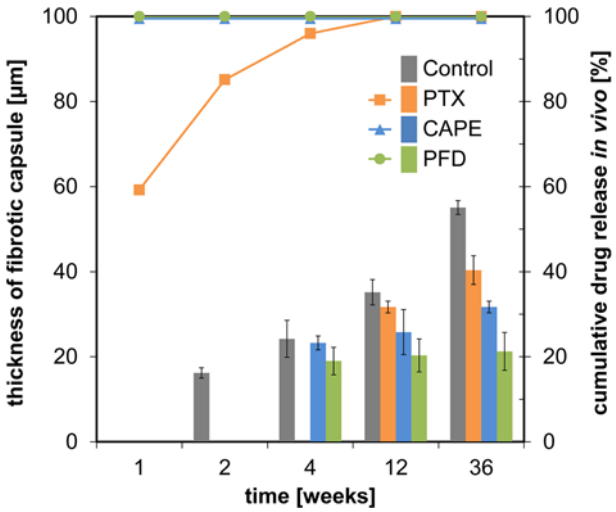

Figure 4. Evaluation of the fibrotic tissue response in comparison with drug release data *in vivo*

Histological sections (Figure 3A) were used to measure the thickness of fibrotic capsules (left *y*-axis) surrounding uncoated and drug-coated test specimens. Results are depicted as colored bars (n=3; mean ± S.D.). Drug release data of coated test specimens (right *y*-axis), as determined with HPLC, are depicted as curves in corresponding colors (n=4, mean). After 1 week no residual drug could be quantitated for CAPE- and PFD-coated test specimens. Fibrotic tissue reactions for these two coatings were visible after 4 weeks, whereas PTX-coated test specimens showed fibrotic capsules after 12 weeks. In uncoated samples, fibrotic capsules were observed starting 2 weeks after implantation. Mean ± S.D. (each n=3).

Total 3 months after implantation, a fibrotic capsule had formed around the PTX test specimens as well. The fibrotic connective tissue was loosely packed and not as compact as in uncoated controls and CAPE- and PFD-coated specimens (Figure 3A,B). However, after 6 months, a compact fibrotic capsule could also be observed around the PTX-coated specimens. A comparison of capsular thicknesses in all groups revealed the thickest fibrotic capsules in the control test specimen group (Figure 4). The fibrotic capsule surrounding the PFD-coated specimens were least pronounced with only a minimal increase in thickness throughout the observation period (Figure 4).

Immunohistochemical examination of the fat depots including the test specimen implants showed positive signals against members of the ECM in the surrounding tissues and the compact fibrotic capsules. The capsules stained positive for collagen I (Figure 5A) and collagen VI (Figure 5B). Additionally, the compact fibrotic capsules stained positively for the ECM component fibronectin (Figure 6A). The strongest reactivity against ECM components could be detected in uncoated test specimens (control) in comparison with the other groups. It is slightly less pronounced in drug-coated test specimen (CAPE), and more obvious in PTX and PFD test specimens. Weakest reactivity against ECM members was detected in PFD-coated test specimens, confirming the results of the standard histological examinations, where thinnest fibrotic capsules were observed in the PFD test specimen group.

Examinations of the immune response following test specimen implantation were carried out using an antibody directed against the antigen CD11b, which is expressed by monocytes, macrophages, and dendritic cells. Positive inflammatory cells could be detected in the periphery of the test specimen in uncoated control and CAPE- and PFD-coated implants after 1 week (Figure 6B). Inflammatory cells could be identified in these groups at time points up to 6 months. In contrast, around PTX-coated implants inflammatory cells could be detected only 2 weeks postsurgery.

Discussion

Prevention of scarring and fibrotic processes represents one of the most prominent challenges in fistulating glaucoma surgery. To overcome fibrosis, which leads to the failure of surgically created draining routes or occlusion of draining implants [41,35], modulating the postoperative fibrotic response with antifibrotic drugs has been a strategy in the recent past. In this context the cytostatics mitomycin C and 5-fluorouracil [25], which inhibit mitotic processes, have been used as antifibrotic agents. Especially, the use of mitomycin C has improved the success rate in fistulating glaucoma surgery, but its associated failure rate of up to 45% 5 years postoperatively is high [42,26] and its use is often coupled with side effects leading to sight-threatening complications like bleb leakage or blebitis, hypotony, choroidal detachment, and corneal impairment [43-45]. The inhibitor PTX, which inhibits mitosis by irreversible

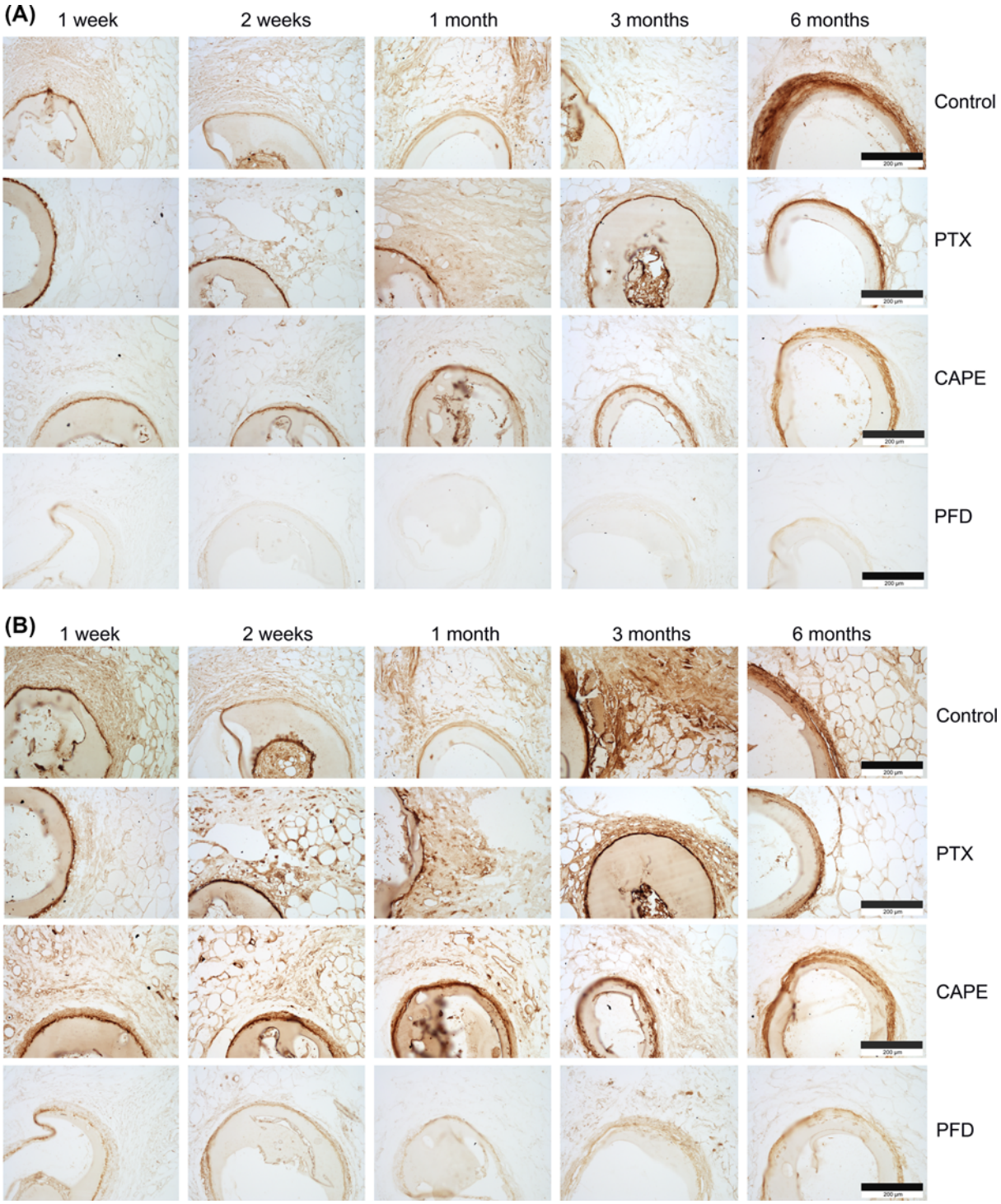

Figure 5. Immunohistochemical evaluation of the fibrotic tissue response to test specimens

(**A**) The cross-sections of the rat fat depots including the test specimens were stained for collagen I. The connective tissue-rich fibrotic capsule is positively stained for collagen I with lowest expression in the PFD group. (**B**) Immunohistochemical examinations of cross-sections stained for collagen VI revealed high reactivity of the connective tissue-rich fibrotic capsules, which ensheath the implants with lowest reactivity in the PFD group. Bars represent 200 μm.

Bioscience Reports (2018) **38** BSR20180628
https://doi.org/10.1042/BSR20180628

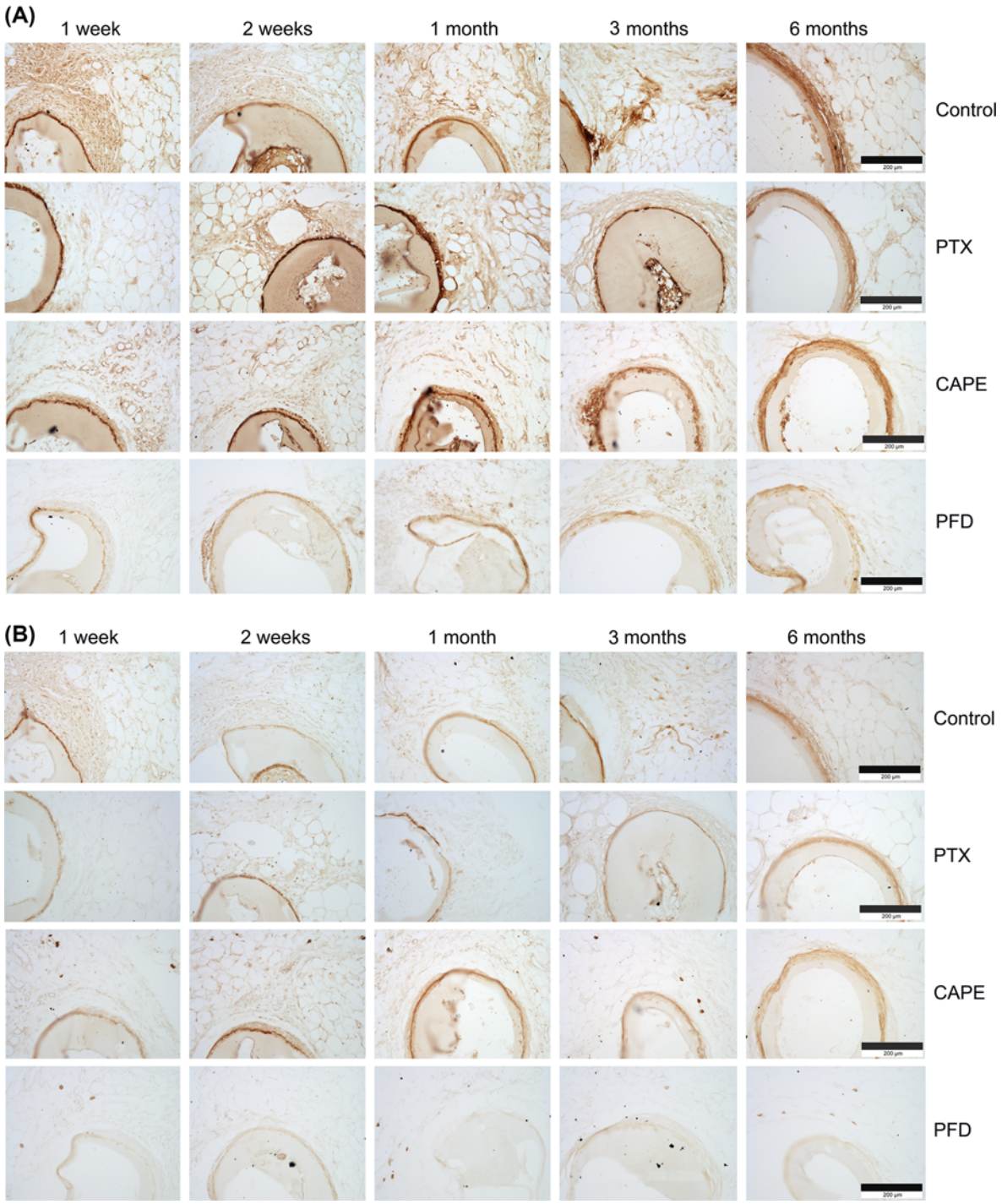

Figure 6:. Immunohistochemistry of the subcutaneous white fat depots including the test specimen implants

(**A**) Immunohistochemical reactivity against fibronectin could be detected after 6 months around the uncoated control and the drug-coated implants with weakest signal in the PFD group. (**B**) The cross-sections of the rat fat depots including the test specimens were stained for CD11b. Expression could be detected around the uncoated control and the drug-coated implants. Bars represent 200 μm.

binding to the microtubule cytoskeleton, also seems to be a promising drug to inhibit postoperative fibrosis [26,27]. However, consistent with its mechanism of action, PTX affects every cell as an unspecific drug. In the last years, the possibility to incorporate antifibrotic drugs into GDDs and use them as drug-delivery systems has been investigated to prevent scarring or fibrotic encapsulation of the implant [25,46]. This approach seems to deliver the opportunity for a slow-release mechanism of antifibrotic drugs in low concentrations over a long period of time directly at the targetted tissue site. In a recent example, it was shown that long-term mitomycin C release could be measured up to 3 months postoperatively but was associated with retinal impairment in rabbit models *in vivo* [25,46]. Hydrogels and non-degradable polymers as well as biodegradable polymers have been used as antifibrotic drug delivery systems in animal studies [25,47,48].

Here, we investigated the fibrotic response to the implantation of test specimens made of a blend of two biodegradable hydroxybutyric acid-based polymers (P(4HB)/at.P(3HB)) 50/50% (w/w) into the white fat depots of rats. This polymer blend is characterized by low cytotoxicity and good *in vivo* biocompatibility [27]. The test specimens were uncoated (controls) or coated with the unspecific cytostatic drug PTX and the more specific antifibrotic drugs CAPE and PFD.

The manufactured test specimens yielded reproducible quality in terms of morphology, initial drug loading and drug recovery after processing. Nevertheless, for PTX and CAPE groups a more porous surface morphology was found when compared with the PFD group. This is probably due to different crystallinities of the used drugs. Irrespective of the drug used, an initial loading and recovery of 20 μg and 76% was found, respectively.

Within the present study, we could show distinct differences in drug release behavior between the *in vitro* and *in vivo* conditions, and the different drugs PTX, CAPE, and PFD. Due to the relatively slow degradation of the used semicrystalline P(4HB) within up to 52 weeks, we assume that drug release primary is diffusion controlled [49]. Nevertheless, our own yet unpublished *in vitro* degradation studies with different P(4HB)/at.P(3HB) blends suggests, that degradation accelerates with increasing content of amorphous at.P(3HB) and therefore, might play a minor role in the current case.

Due to poor solubility of PTX and CAPE in aqueous solutions, *in vitro* drug release profiles are relatively slow compared with PFD. The solubility of PFD in aqueous solutions is approximately five orders of magnitude higher (20.000 $mg.l^{-1}$), compared with PTX (0.3 $mg.l^{-1}$), exemplary [50,51]. Therefore, *in vitro* drug release of PFD is considerably faster (Figure 2B).

In vivo another effect predominates the drug release kinetics. Here, PTX release is decelerated compared with CAPE and PFD and compared with the *in vitro* data of PTX release (Figure 2C). The molecular weight of PTX (853.9 g mol^{-1}) is greater by factors 3–4.6 than CAPE (284.1 g mol^{-1}) and PFD (185.2 g mol^{-1}) and appears to be the dominating parameter, decelerating diffusion controlled drug release of PTX *in vivo* (Sigma–Aldrich Corp. 2017). PTX release *in vivo* may be also decelerated due to its lower lipid solubility and saturation effects and therefore, delayed drug diffusion inside the rat fat tissue. Differences in *in vitro* and *in vivo* release behavior possibly may be influenced through different drug crystallinity. Kind of solvent and drying conditions like time and temperature within the drug-coating process are significant for the drug crystallinity. This may be an explanation for the different morphologies shown in Figure 2A.

Fibrotic encapsulation following GDD implantation is a known process and one of the most important reasons for implant failure [52,53]. In contrast, no fibrotic response was observed in rabbits after 38 weeks *in vivo* following implantation of biologically derived hydroxybutyric acid based polymers in our previous studies [27,35]. Here, for uncoated implants based on polymer blend of the biologically derived P(4HB) and the synthetic at.P(3HB) 50/50% (w/w), we could detect a massive cell infiltration 1 week after implantation in the periphery of the implant. These cells seem to ensheath the implants and start to synthesize ECM components leading to the formation of a fibrotic capsule and total implant-encapsulation 2–4 weeks after implantation. These fibrotic capsules increased in thickness up to 6 months. One difference between the abovementioned studies to our examinations is the implantation into white fat depots in rats, which could have an influence to the wound-healing process and the fibrotic response to implants. It has been reported that mature adipocytes repopulate skin wounds, adipocyte precursor cells proliferate, and that adipocytes as a key player of the intercellular communication are necessary for fibroblast recruitment and function in mice [54]. Additionally, wound-healing processes are different between rabbits and rats as shown by Kim et al. [55]. Both circumstances may explain observed prominent fibrosis in white fat depots in rats in comparison with Tenon's – and suprachoroidal space in rabbit models. These findings support the suitability of the rat model for fibrotic investigations due to fibrotic implant encapsulation at similar intervals in humans.

The formation of a fibrotic capsule around the implant could be delayed by the antifibrotic drug PTX in our examinations. In early postoperative stages (1–2 weeks), a disturbance in the organization of connective and fat tissues

Bioscience Reports (2018) **38** BSR20180628
https://doi.org/10.1042/BSR20180628

and lesions peripherally to the PTX-coated test specimens were obvious. The appearance of lesions and skin ulcers has been described after intradermal injections of PTX in a mouse model [56], and degenerative and necrotic changes in the form of cytoplasmic vacuolization, fatty change, and apoptosis has been observed in a mammary tumor model in rats [57]. However, encapsulation comparable with the other groups and ill-defined fat tissue with abundant adipocytes could be detected after 6 months in our study.

Test specimens coated with CAPE showed only negligible antifibrotic effects. CAPE has been described with a broad spectrum of biological activities, including anti-inflammatory, antifibrotic, antioxidant, and immune-modulatory properties [58]. Mia and Bank [59] demonstrated an antifibrotic effect of CAPE in human dermal and lung fibroblasts, where an inhibition of fibroblast transformation into myofibroblasts and a suppression of collagen and fibronectin expression were shown. In other studies, the antifibrotic effects of CAPE led to reduced collagen and fibronectin deposition in mice and rats *in vivo* [28,60,61].

The same applies for PFD, where *in vitro* studies demonstrated inhibition of cell proliferation, myofibroblast differentiation, collagen contractility, cytokine suppression, decreased collagen and fibronectin expression, and migratory ability of cardiac, renal, lung, hepatic, and ocular fibroblasts [31,32,62-66]. An antifibrotic effect *in vivo* has also been described in a trabeculectomy model in rabbits, where postoperative application of PFD was associated with less scarring and improved bleb survival [67] and following GDI implantation in a rabbit model [68]. In our examination, neither PFD nor CAPE completely prevented fibrosis and implant encapsulation in the white fat depot in rats, but an attenuation of fibrosis was observed in the PFD group, characterized by a reduction in fibrotic capsule thickness (Figure 4), compaction, and immunohistochemical reactivity against examined ECM components.

Based on the presented data, the influence of the surface morphology of the test specimens on fibrotic encapsulation behavior could not be clearly distinguished. However, it is obvious that the use of an antifibrotic drug (i.e. PFD) retards and reduces fibrotic encapsulation compared with the control group with the same surface morphology as the PFD group but with no drug incorporated (Figure 4). It can be speculated that fibrotic encapsulation in the PTX and CAPE groups would also be further retarded and reduced, for a more similar surface morphology to the PFD group.

In wound-healing processes, directly after blood clotting and vasoconstriction, the infiltration of leukocytes and an immune response is initiated [69]. Most immune competent cells are characterized by the expression of the surface antigen CD11b, a member of the integrin family, which is expressed on the surface of leukocytes including monocytes, neutrophils, natural killer cells, granulocytes, and macrophages [70]. In our examinations, we observed an infiltration of immune competent cells in the periphery of uncoated control test specimens as well as around CAPE- and PFD-coated implants after 1 week, which also could be detected up to 6 months in moderate amounts. Other studies revealed an absence of inflammation following suprachoroidal shunt implantation after 15 weeks [71]. We suggest that an ongoing attraction of immune competent cells is triggered by the biodegradation process of the polymer blend and cytokine secretion from activated myofibroblasts [72] also after the acute phase in wound healing. However, in the periphery of PTX-coated implants inflammatory cells were only detectable 2 weeks postsurgically. This finding is comparable with a study of the body reaction in glaucoma drainage implant surgery, in which a peak of inflammation was observed 2 weeks postoperatively [73].

To summarize our findings, postoperative fibrotic and immune responses can be attenuated by glaucoma implants coated with antifibrotic drugs. The management of controlled drug release by avoiding a burst release to guarantee a long-term medication can increase the pharmaceutical effects of antifibrotic drugs with low risk of side effects to sensitive ocular structures. As a further developmental step, the combination of different antifibrotic pharmaceuticals is also conceivable to potentially increase effectiveness. Further investigations will help to develop GDDs with drug delivery characteristics to create a permanent drainage path to lower IOP and prevent glaucoma progression.

Conclusion

Implantation of drug-coated test specimens into the subcutaneous white fat depot in rats opens up new possibilities to investigate the release kinetics of antifibrotic agents *in vivo*, which can be compared with the retrobulbar fat depot in humans. The antifibrotic potential as well as drug-induced side effects were analyzed by histological examinations. PTX delayed the formation of a fibrotic capsule until 12 weeks after implantation. However, the PTX coating caused side effects and could not maintain its antifibrotic activity over the entire observation period of 6 months. The agents CAPE and PFD delayed the formation of a fibrotic capsule around the implants by 2 weeks in comparison with the control group. The PFD coating was overall most effective with regard to capsule thickness and growth of the capsule throughout the observation period.

In conclusion, these investigations help to identify new antifibrotic agents,which can be used as medicinal drug coatings for microstents in the treatment of glaucoma draining aqueous humor into the intra-orbital fat depot or

tenon space. Our examinations allow the analysis of side effects and the quantitation of drug-specific antifibrotic potential.

Acknowledgements

We thank Mrs. J.Weiß-Müller, Mrs. S. Lehmann, and Mrs. F. Winzer for their skillful technical assistance and Mr. David P. Martin (Tepha, Inc., Lexington, MA, U.S.A.) for helpful comments and suggestions.

Competing interests

The authors declare that there are no competing interests associated with the manuscript.

Funding

This work was supported by the Bundesministerium für Bildung und Forschung (BMBF) within the REMEDIS project 'Höhere Lebensqualität durch neuartige Mikroimplantate' [grant number FKZ: 03IS2081].

Author contribution

T.S. and S.S. wrote the manuscript and prepared all figures. S.S. manufactured and coated the test specimens. N.G. conducted SEM investigations. T.R. and W.S. conducted *ex vivo* and *in vivo* drug release studies. A.W. and T.S. performed the implantation and explantation surgeries and T.S. conducted histological examinations. R.F.G., A.W., T.S., and S.S. analyzed the data. R.F.G. and K.-P.S. conceived the study concept and procured funding for the project. All authors reviewed the manuscript and approved the final version.

Abbreviations

at.P(3HB), atactic poly(3-hydroxybutyrate); AZAN, azocarmine G- aniline blue - orange G staining; CAPE, caffeic acid phenethyl ester; ECM, extracellular matrix; GDD, glaucoma drainage device; GDI, glaucoma drainage implant; IHC, immunohistochemistry; IOP, intraocular pressure; LDD, local drug delivery; PFA, paraformaldehyde; PFD, pirfenidone; PTX, paclitaxel; P(4HB), poly(4-hydroxybutyrate); SEM, scanning electron microscope; TGF, transforming growth factor; TNF, tumor necrosis factor.

References

1 Weinreb, R.N., Aung, T. and Medeiros, F.A. (2014) The pathophysiology and treatment of glaucoma: a review. *JAMA* **311**, 1901–1911, https://doi.org/10.1001/jama.2014.3192
2 Kass, M.A. et al. (2002) The ocular hypertension treatment study: a randomized trial determines that topical ocular hypotensive medication delays or prevents the onset of primary open-angle glaucoma. *Arch. Ophthalmol.* **120**, 701–713, https://doi.org/10.1001/archopht.120.6.701
3 Sambhara, D. and Aref, A.A. (2014) Glaucoma management: relative value and place in therapy of available drug treatments. *Ther. Adv. Chronic Dis.* **5**, 30–43, https://doi.org/10.1177/2040622313511286
4 Remo, S.J. and Wang-Pui, S. (2004) Comparison of latanoprost with fixed combination dorzolamide and timolol in adult patients with elevated intraocular pressure: an eight week, randomized, open-label, parallel-group, multicenter study in Latin America. *Clin. Ther.* **26**, 755–756, https://doi.org/10.1016/S0149-2918(04)90075-6
5 Moisseiev, E., Kurtz, S., Lazar, M. and Shemesh, G. (2013) Intraocular pressure reduction using a fixed combination of timolol maleate 0.5% and brimonidine tartrate 0.2% administered three times daily. *Clin. Ophthalmol.* **7**, 1269–1273, https://doi.org/10.2147/OPTH.S47760
6 Cairns, J.E. (1968) Trabeculectomy. Preliminary report of a new method. *Am. J. Ophthalmol.* **66**, 673–679, https://doi.org/10.1016/0002-9394(68)91288-9
7 Fedorov, S.N., Ioffe, D.I. and Ronkina, T.I. (1982) Glaucoma surgery – deep sclerectomy. *Vestn. Ophthal.* **4**, 6–10
8 Lim, K.S., Allan, B.D., Lloyd, A.W., Muir, A. and Khaw, P.T. (1998) Glaucoma drainage devices; past present, and future. *Br. J. Ophthalmol.* **82**, 1083–1089, https://doi.org/10.1136/bjo.82.9.1083
9 Noureddin, B.N., Zein, W., Haddad, C., Ma'luf, R. and Bashshur, Z. (2006) Diode laser transcleral cyclophotocoagulation for refractory glaucoma: a 1 year follow-up of patients treated using an aggressive protocol. *Eye* **20**, 329–335, https://doi.org/10.1038/sj.eye.6701875
10 Kaplowitz, K., Kuei, A., Klenofsky, B., Abazari, A. and Honkanen, R. (2015) The use of endoscopic cyclophotocoagulation for moderate to advanced glaucoma. *Acta Ophthalmol.* **93**, 395–401, https://doi.org/10.1111/aos.12529
11 Molteno, A. (1969) New implant for drainage in glaucoma. Clinical trial. *Br. J. Ophthalmol.* **53**, 606–615, https://doi.org/10.1136/bjo.53.9.606
12 Prata, Jr, J.A., Minckler, D.S., Mermoud, A. and Baerveldt, G. (1996) Effects of mitomycin-C on the function of Baerveldt glaucoma drainage implants in rabbits. *Glaucoma* **5**, 29–38, https://doi.org/10.1097/00061198-199602000-00006
13 Allemann, R. et al. (2011) Ultra high-field magnetic resonance imaging of a glaucoma microstent. *Curr. Eye Res.* **36**, 719–726, https://doi.org/10.3109/02713683.2011.587936
14 Guthoff, R.F. et al. (2009) Development of a glaucoma microstent with drainage into the suprachoroidal space: fluid mechanical model approach. *Ophthalmology* **106**, 805–812, https://doi.org/10.1007/s00347-009-1929-x
15 Schmidt, W. et al. (2010) Konzept eines druckgesteuerten Mikrostents für die Glaukomtherapie. Concept of a pressure-controlled microstent for glaucoma therapy. *Klin. Monbl. Augenheilkd.* **227**, 946–952, https://doi.org/10.1055/s-0029-1245928

16 Dietlein, T.S., Jordan, J., Lueke, C. and Krieglstein, G.K. (2008) Modern concepts in antiglaucomatous implant surgery. *Graef. Arch. Clin. Exp. Ophthalmol.* **246**, 1653–1664, https://doi.org/10.1007/s00417-008-0899-z
17 Löbler, M. et al. (2013) Ocular fibroblast types differ in their mRNA profiles-implications for fibrosis prevention after aqueous shunt implantation. *Mol. Vis.* **19**, 1321–1331
18 Stahnke, T. et al. (2012) Different fibroblast subpopulations of the eye: a therapeutic target to prevent postoperative fibrosis in glaucoma therapy. *Exp. Eye Res.* **100**, 88–97, https://doi.org/10.1016/j.exer.2012.04.015
19 Møller, P.M. (1955) Chapter VII: Orbital pressure in normal subjects (with statistical calculation of the results) . *Acta Ophthalmol.* 53–56, https://doi.org/10.1111/j.1755-3768.1955.tb00096.x
20 Otto, A.J., Koornneef, L., Mourits, M.P. and van Leeuwen, L.D. (1996) Retrobulbar pressures measured during surgical decompression of the orbit. *Br. J. Ophthalmol.* **80**, 1042–1045, https://doi.org/10.1136/bjo.80.12.1042
21 Xie, X. et al. (2013) Noninvasive intracranial pressure estimation by orbital subarachnoid space measurement: the Beijing Intracranial and Intraocular Pressure (iCOP) study. *Crit. Care* **17**, R162, https://doi.org/10.1186/cc12841
22 Cinti, S. (2005) The adipose organ. *Prostaglandins Leukoc. Essent. Fatty Acids* **73**, 9–15, https://doi.org/10.1016/j.plefa.2005.04.010
23 Bielen, R., Bennett, J., Ferdinande, B. and Dubois, C. (2014) Drug-eluting versus bare metal stents after rotational atherectomy: clinical outcome in a single centre. *Acta Cardiol.* **69**, 611–617, https://doi.org/10.1080/AC.69.6.1000003
24 Windecker, S. et al. (2015) Comparison of a novel biodegradable polymer sirolimus-eluting stent with a durable polymer everolimus-eluting stent: results of the randomized BIOFLOW-II Trial. *Circ. Cardiovasc. Interv.* **8**, e001441, https://doi.org/10.1161/CIRCINTERVENTIONS.114.001441
25 Mostafaei, A. (2011) Augmenting trabeculectomy in glaucoma with subconjunctival mitomycin C versus subconjunctival 5-fluorouracil: a randomized clinical trial. *Clin. Ophthalmol.* **5**, 491–494, https://doi.org/10.2147/OPTH.S17328
26 Choritz, L., Grub, J., Wegner, M., Pfeiffer, N. and Thieme, H. (2010) Paclitaxel inhibits growth, migration and collagen production of human Tenon's fibroblasts - potential use in drug-eluting glaucoma drainage devices. *Graef. Arch. Clin. Exp. Ophthalmol.* **248**, 197–206, https://doi.org/10.1007/s00417-009-1221-4
27 Löbler, M. et al. (2011) Polymers and drugs suitable for the development of a drug delivery drainage system in glaucoma surgery. *J. Biomed. Mater. Res. B Appl. Biomater.* **97**, 388–395, https://doi.org/10.1002/jbm.b.31826
28 Larki-Harchegani, A. (2013) Evaluation of the effects of caffeic acid phenethyl ester on prostaglandin E2 and two key cytokines involved in bleomycin-induced pulmonary fibrosis. *Iran J. Basic Med. Sci.* **16**, 850–857
29 Larki, A. et al. (2013) Regulatory effect of caffeic acid phenethyl ester on type I collagen and interferon-gamma in bleomycin-induced pulmonary fibrosis in rat. *Res. Pharm. Sci.* **8**, 243–252
30 Taylan, M. et al. (2016) The protective effects of caffeic acid phenethyl ester on acetylsalicylic acid-induced lung injury in rats. *J. Invest. Surg.* **16**, 1–7
31 Lin, X., Yu, M., Wu, K., Yuan, H. and Zhong, H. (2009) Effects of pirfenidone on proliferation, migration, and collagen contraction of human tenon's fibroblasts *in vitro*. *Invest. Ophthalmol. Vis. Sci.* **50**, 3763–3770, https://doi.org/10.1167/iovs.08-2815
32 Stahnke, T. et al. (2017) Suppression of TGF-β pathway by pirfenidone decreases extracellular matrix deposition in ocular fibroblasts *in vitro*. *PLoS ONE* **12**, e0172592, https://doi.org/10.1371/journal.pone.0172592
33 Hilberg, O., Simonsen, U., du Bois, R. and Bendstrup, E. (2012) Pirfenidone: significant treatment effects in idiopathic pulmonary fibrosis. *Clin. Respir. J.* **6**, 131–143, https://doi.org/10.1111/j.1752-699X.2012.00302.x
34 Hasdemir, P.S. et al. (2016) Effect of pirfenidone on vascular proliferation, inflammation and fibrosis in an abdominal adhesion rat model. *J. Invest. Surg.* **15**, 1–7
35 Hovakimyan, M. et al. (2015) Development of an experimental drug-eluting suprachoroidal microstent as glaucoma drainage device. *Transl. Vis. Sci. Technol.* **4**, https://doi.org/10.1167/tvst.4.3.14
36 Jedlinski, Z., Kowalczuk, M., Glowkowski, W., Grobelny, J. and Szwarc, M. (1991) Novel polymerization of β-butyrolactone initiated by potassium naphthalenide in the presence of a crown ether or a cryptand. *Macromolecules* **24**, 349–352, https://doi.org/10.1021/ma00002a002
37 Hubbs, J. et al. (1997) Biodegradable poly(3-hydroxyalkanoate) compositions and blends. U.S. Pat. 5,625,029A
38 Freier, T. et al. (2002) *In vitro* and *in vivo* degradation studies for development of a biodegradable patch based on poly(3-hydroxybutyrate). *Biomaterials* **23**, 2649–2657, https://doi.org/10.1016/S0142-9612(01)00405-7
39 Mulisch, M. and Welsch, U. (2010) *Romeis - Mikroskopische Technik*, 18 edn., (Mulisch, M. and Welsch, U., eds), Springer, Berlin, ISBN-10: 3827416760
40 Stahnke, T., Stadelmann, C., Netzler, A., Brück, W. and Richter-Landsberg, C. (2007) Differential upregulation of heme oxygenase-1 (HSP32) in glial cells after oxidative stress and in demyelinating disorders. *J. Mol. Neurosci.* **32**, 25–37, https://doi.org/10.1007/s12031-007-0005-8
41 Thieme, H. (2012) Current status of epibulbar antiglaucoma drainage devices in glaucoma surgery. *Dtsch. Arztebl. Int.* **109**, 659–664
42 Giampani, Jr, J., Borges-Giampani, A.S., Carani, J.C., Oltrogge, E.W. and Susanna, Jr, R. (2008) Efficacy and safety of trabeculectomy with mitomycin C for childhood glaucoma: a study of results with long-term follow-up. *Clinics (Sao Paulo)* **63**, 421–426, https://doi.org/10.1590/S1807-59322008000400002
43 Masoumpour, M.B., Nowroozzadeh, M.H. and Razeghinejad, M.R. (2016) Current and future techniques in wound healing modulation after glaucoma filtering surgeries. *Open Ophthalmol. J.* **10**, 68–85, https://doi.org/10.2174/1874364101610010068
44 Mearza, A.A. and Aslanides, I.M. (2007) Uses and complications of mitomycin C in ophthalmology. *Expert. Opin. Drug Saf.* **6**, 27–32, https://doi.org/10.1517/14740338.6.1.27
45 van Bergen, T., van de Velde, S., Vandewalle, E., Moons, L. and Stalmans, I. (2014) Improving patient outcomes following glaucoma surgery: state of the art and future perspectives. *Clin. Ophthalmol.* **8**, 857–867, https://doi.org/10.2147/OPTH.S48745
46 Sahiner, N. et al. (2009) Creation of a drug-coated glaucoma drainage device using polymer technology: *in vitro* and *in vivo* studies. *Arch. Ophthalmol.* **127**, 448–453, https://doi.org/10.1001/archophthalmol.2009.19

47 Blake, D.A. et al. (2006) Inhibition of cell proliferation by mitomycin C incorporated into P(HEMA) hydrogels. *J. Glaucoma* **15**, 291–298, https://doi.org/10.1097/01.ijg.0000212236.96039.9c
48 Polak, M.B. et al. (2008) Controlled delivery of 5-chlorouracil using poly(orthoesters) in filtering surgery for glaucoma. *Invest. Ophthalmol. Vis. Sci.* **49**, 2993–3003, https://doi.org/10.1167/iovs.07-0919
49 Martin, D.P. and Williams, S.F. (2003) Medical applications of poly-4-hydroxybutyrate: a strong flexible ab-sorbable biomaterial. *Biochem. Eng. J.* **16**, 97–105, https://doi.org/10.1016/S1369-703X(03)00040-8
50 Konno, T., Watanabe, J. and Ishihara, K. (2003) Enhanced solubility of paclitaxel using water-soluble and biocompatible 2-methacryloyloxyethyl phosphorylcholine polymers. *J. Biomed. Mater. Res. A* **65**, 209–214, https://doi.org/10.1002/jbm.a.10481
51 Macías-Barragán, J., Sandoval-Rodríguez, A., Navarro-Partida, J. and Armendáriz-Borunda, J. (2010) The multifaceted role of pirfenidone and its novel targets. *Fibrogen. Tissue Rep.* **3**, 16
52 Mahale, A. et al. (2015) Altered expression of fibrosis genes in capsules of failed Ahmed glaucoma valve implants. *PLoS ONE* **10**, e0122409, https://doi.org/10.1371/journal.pone.0122409
53 Quaranta, L. et al. (2016) Needle revision with 5-fluorouracil for the treatment of ahmed glaucoma valve filtering blebs: 5-fluoruracil needling revision can be a useful and safe tool in the management of failing ahmed glaucoma valve filtering blebs. *J. Glaucoma* **25**, e367–e371, https://doi.org/10.1097/IJG.0000000000000366
54 Schmidt, B.A. and Horsley, V. (2013) Intradermal adipocytes mediate fibroblast recruitment during skin wound healing. *Development* **140**, 1517–1527, https://doi.org/10.1242/dev.087593
55 Kim, D.J., Mustoe, T. and Clark, R.A. (2015) Cutaneous wound healing in aging small mammals: a systematic review. *Wound Repair Regen.* **23**, 318–339, https://doi.org/10.1111/wrr.12290
56 Dorr, R.T., Snead, K. and Liddil, J.D. (1996) Skin ulceration potential of paclitaxel in a mouse skin model *in vivo*. *Cancer* **78**, 152–156, https://doi.org/10.1002/(SICI)1097-0142(19960701)78:1%3c152::AID-CNCR21%3e3.0.CO;2-Y
57 Al-Ghananeem, A.M. et al. (2009) Intratumoral delivery of paclitaxel in solid tumor from biodegradable hyaluronan nanoparticle formulations. *AAPS Pharm. Sci. Tech.* **10**, 410–417, https://doi.org/10.1208/s12249-009-9222-5
58 Murtaza, G. et al. (2014) Caffeic acid phenethyl ester and therapeutic potentials. *Biomed. Res. Int.* 145342, https://doi.org/10.1155/2014/145342
59 Mia, M.M. and Bank, R.A. (2016) The pro-fibrotic properties of transforming growth factor on human fibroblasts are counteracted by caffeic acid by inhibiting myofibroblast formation and collagen synthesis. *Cell Tissue Res.* **363**, 775–789, https://doi.org/10.1007/s00441-015-2285-6
60 Zhao, W.X. et al. (2014) Caffeic acid phenethyl ester attenuates pro-inflammatory and fibrogenic phenotypes of LPS-stimulated hepatic stellate cells through the inhibition of NF-B signaling. *Int. J. Mol. Med.* **33**, 687–694, https://doi.org/10.3892/ijmm.2013.1613
61 Chuang, S.T., Kuo, Y.H. and Su, J. (2015) KS370G, a caffeamide derivative, attenuates unilateral obstruction-induced renal fibrosis by the reduction of inflammation and oxidative stress in mice. *Eur. J. Pharmacol.* **750**, 1–7, https://doi.org/10.1016/j.ejphar.2015.01.020
62 Burghardt, I. et al. (2007) Pirfenidone inhibits TGF-beta expression in malignant glioma cells. *Biochem. Biophys. Res. Commun.* **354**, 542–547, https://doi.org/10.1016/j.bbrc.2007.01.012
63 Shi, Q. et al. (2011) *In vitro* effects of pirfenidone on cardiac fibroblasts: proliferation, myofibroblast differentiation, migration and cytokine secretion. *PLoS ONE* **6**, e28134, https://doi.org/10.1371/journal.pone.0028134
64 Di Sario, A. et al. (2002) Effect of pirfenidone on rat hepatic stellate cell proliferation and collagen production. *J. Hepatol.* **37**, 584–591, https://doi.org/10.1016/S0168-8278(02)00245-3
65 Hewitson, T.D. et al. (2001) Pirfenidone reduces in vitro rat renal fibroblast activation and mitogenesis. *J. Nephrol.* **14**, 453–460
66 Kim, H. et al. (2010) Antifibrotic effect of pirfenidone on orbital fibroblasts of patients with thyroid-associated ophthalmopathy by decreasing TIMP-1 and collagen levels. *Invest. Ophthalmol. Vis. Sci.* **51**, 3061–3066, https://doi.org/10.1167/iovs.09-4257
67 Zhong, H., Sun, G., Lin, X., Wu, K. and Yu, M. (2011) Evaluation of pirfenidone as a new postoperative antiscarring agent in experimental glaucoma surgery. *Invest. Ophthalmol. Vis. Sci.* **52**, 3136–3142, https://doi.org/10.1167/iovs.10-6240
68 Jung, K.I. and Park, C.K. (2016) Pirfenidone inhibits fibrosis in foreign body reaction after glaucoma drainage device implantation. *Drug Des. Dev. Ther.* **10**, 1477–1488
69 Engelhardt, E. et al. (1998) Chemokines IL-8, GROalpha, MCP-1, IP-10, and Mig are sequentially and differentially expressed during phase-specific infiltration of leukocyte subsets in human wound healing. *Am. J. Pathol.* **153**, 1849–1860, https://doi.org/10.1016/S0002-9440(10)65699-4
70 Schmid, M., Wege, A.K. and Ritter, U. (2012) Characteristics of "Tip-DCs and MDSCs" and their potential role in leishmaniasis. *Front. Microbiol.* **3**, 74
71 Oatts, J.T. et al. (2013) *In vitro* and *in vivo* comparison of two suprachoroidal shunts. *Invest. Ophthalmol. Vis. Sci.* **54**, 5416–5423, https://doi.org/10.1167/iovs.13-11853
72 Rogler, G. et al. (2001) Differential activation of cytokine secretion in primary human colonic fibroblast/myofibroblast cultures. *Scand. J. Gastroenterol.* **36**, 389–398, https://doi.org/10.1080/003655201300051216
73 Jung, K.I., Lee, S.B., Kim, J.H. and Park, C.K. (2013) Foreign body reaction in glaucoma drainage implant surgery. *Invest. Ophthalmol. Vis. Sci.* **54**, 3957–3964, https://doi.org/10.1167/iovs.12-11310

T. Stahnke*, S. Siewert, E. Walther, W. Schmidt, O. Stachs, K.-P. Schmitz, and R. F. Guthoff

Adopting oculopressure tonometry as a transient *in vivo* rabbit glaucoma model

Abstract: Glaucoma represents a group of eye disorders partly related to raised intraocular pressure (IOP) leading to progressive optic nerve damage resulting in impaired vision and possibly blindness. To assess the suitability of new IOP lowering therapeutic strategies, such as the implantation of glaucoma drainage devices, appropriate animal models have to be used. Currently, a number of rodent glaucoma models are available [1], however, especially for surgical interventions rodent eyes are too small. Rabbits are much more suitable with respect to dimension. Unfortunately, rabbit glaucoma model systems described in literature are difficult to reproduce or fail totally, associated with a high level of discomfort and pain for treated animals. Therefore, development of an *in vivo* rabbit glaucoma model is one of the most important goals in glaucoma research. Here, we describe the adaptation of the oculopressure tonometry, an existing method to quantify the outflow of aqueous humor in humans, to generate a transient glaucoma model in rabbits. The existing suction-cup oculopressor (SCOP) is extended with newly designed suction-cups, which are adjusted to the anatomy of the rabbit eye. The modification of the oculopressure tonometry method facilitates an increase in IOP over a time frame of 9 minutes by vacuum induced deformation of the rabbit eye. This method can be used to test functionality of fistulating glaucoma surgeries or implanted drainage devices in a long term follow-up without any side effects and suffering of the animals.

Keywords: Glaucoma; Oculopressure tonometry (OPT); Rabbit glaucoma model; Intraocular pressure (IOP)

DOI: 10.1515/CDBME-2015-0033

1 Introduction

The second leading cause of blindness and the leading cause of irreversible blindness worldwide is glaucoma. Despite many efforts made in the research of glaucoma formation and therapeutic options glaucoma prevalence is still increasing to date. Approximately 80 million people will be affected by glaucoma in 2020 [2].

For admission of new therapy strategies it is essential to conduct experiments in rabbit model of glaucoma. It is therefore important to have methods at ones disposal to sufficiently increase IOP for the simulation of glaucoma. Different rabbit models for glaucoma induction have been published. Allemann and colleagues chose four of them with respect to ethical, surgical and logistic factors to reproduce in a large scale investigation. Unfortunately, none of these models was reproducible in a satisfactory way [3].

When looking for another approach to increase IOP in a rabbit glaucoma model the oculopressure tonometry (OPT) of Ulrich and Ulrich came to mind [4]. This method is based on creating an elevated IOP in the eye to determine aqueous humor outflow rate and has been used in general ophthalmology since 1987.

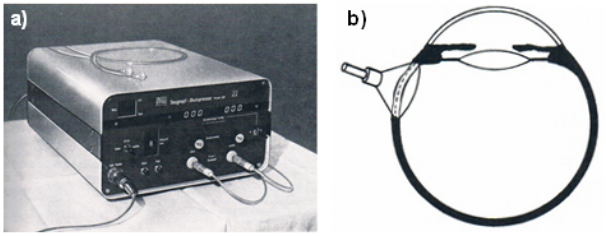

Figure 1: a) suction-cup oculopressor (SCOP); b) contact point close to limbus [3].

The intention of this study is to adapt this diagnostic tool to the rabbit eye and to establish an alternative to conventional models of glaucoma induction without any surgical interventions of animals involved.

***Corresponding Author: T. Stahnke:** Institute for Biomedical Engineering, Rostock University Medical Center, Rostock, Germany, E-mail: thomas.stahnke@uni-rostock.de; Phone: +49-38154945547; Fax: +49-38154945502

S. Siewert, W. Schmidt, K.-P. Schmitz, R. F. Guthoff: Institute for Biomedical Engineering, Rostock University Medical Center, Rostock, Germany

E. Walther, O. Stachs: Department of Ophthalmology, Rostock University Medical Center, Rostock, Germany

2 Methods

2.1 Estimation of suction-cup diameter for rabbits

For the adaptation of OPT to the rabbit eye New Zealand White rabbits were used (Charles River, Sulzfeld, Germany). As a fundamental requirement for adapting OPT to rabbit eyes, the suction-cup diameter had to be adjusted to the average size of rabbit eyeballs. The diameter $d_{s,r}$ for the suction-cups to be used was designed based on the diameter of suction-cups used for humans ($d_{s,h}$ = 13 mm) and the human or rabbit eyeball diameter ($d_{e,h}$ = 22.50 mm and $d_{e,r}$ = 18.25 mm, respectively). The ratio $d_{s,r}/d_{e,r}$ was calculated for suction-cup diameters of $d_{s,r}$ = 10, 11, 12 and 13 mm and compared to the corresponding ratio $d_{s,h}/d_{e,h}$ for human use.

2.2 Design and manufacturing of suction-cups

Suction-cups for rabbit eyes were designed according to original components using Creo Elements/Pro 5.0 (PTC Inc., Needham, USA) (Fig. 2).

Manufacturing of suction-cups was based on Polyoxymethylene (POM, SUSTARIN C, ThyssenKrupp Plastics GmbH, Essen, Germany) machined by a metalworking lathe (EMCO*MAT*-14D, EMCO Maier Ges.m.b.H, Hallein, Austria). Manufactured suction-cups were finally cleaned for 10 minutes in an ultrasonic bath (SONOREX RK 103 H, BANDELIN electronic GmbH & Co. KG, Berlin, Germany).

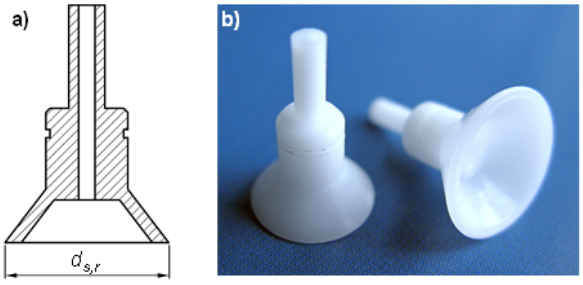

Figure 2: a) Design of suction-cups for rabbit eyes: variable diameter $d_{s,r}$; b) Manufactured suction-cups with a diameter of $d_{s,r}$ = 10 mm (left) and 12 mm (right).

2.3 Application of OPT to rabbits

Application of OPT was tested for rabbits under deep anesthesia. The animals were sedated with a subcutaneously injection of 35 mg kg^{1} Ketamin 10% (Bela-pharm GmbH & Co. KG, Vechta, Germany), 5 mg kg^{1} Rompun®2% (Bayer HealthCare AG, Leverkusen, Germany). Additionally, local anaesthesia using Proparakain-POS®0,5% drops was administered to the eyes (URSAPHARM Arzneimittel GmbH, Saarbrücken, Germany). During OPT rabbits were retained in a regular sitting position.

SCOP (Fa. B. Boucke, Medizin-Elektronik, Tübingen, Germany) is used to increase IOP about 40 mmHg during a maximum examination period of 9 minutes. The SCOP-device, which is licensed for application in human medicine, consists of a vacuum pump that is connected to the eyeball by a flexible tube. The suction-cup at the end of the tube is positioned on the conjunctiva-covered sclera in the temporal canthus near the corneal limbus. Applying a vacuum to the cone-shaped SC results in an eyeball deformation and subsequently in an IOP increase.

During OPT the IOP was measured using a rebound tonometer (TAO1, Icare Finland Oy, Vantaa, Finland). This procedure is also used for IOP measurements in human ophtalmological daily routine. Tonometric IOP recordings p_{ic} with the TAO1 device were corrected according to Löbler *et al.* considering differences in thickness and viscoelastic properties between rabbit and human corneas. Corrected IOP for rabbits p_{corr} is calculated according to formula 1 [5].

$$p_{corr} = 1,4244 \cdot p_{ic} + 4,2421 \quad (1)$$

Prior to anesthesia initial IOP was measured. To record pressure decay during OPT, the IOP is measured every minute (Fig. 3). Finally, IOP was recorded one minute after termination of OPT.

In order to prevent desiccation during OPT, physiologic salt solution was applied to the eyes every two minutes. Upon completion of a series of measurements a moisturizing gel (Vidisic®; Bausch & Lomb/Dr. Mann Pharma, Berlin, Germany) was applied to the eyes.

3 Results

For adaptation of OPT to the rabbit eye three demagnified suction-cups were manufactured. Table 1 illustrates that suction-cups with a diameter of $d_{s,r}$ = 11 mm yield the best match with regard to the suction-cup/eyeball diameter ratio used in human measurements.

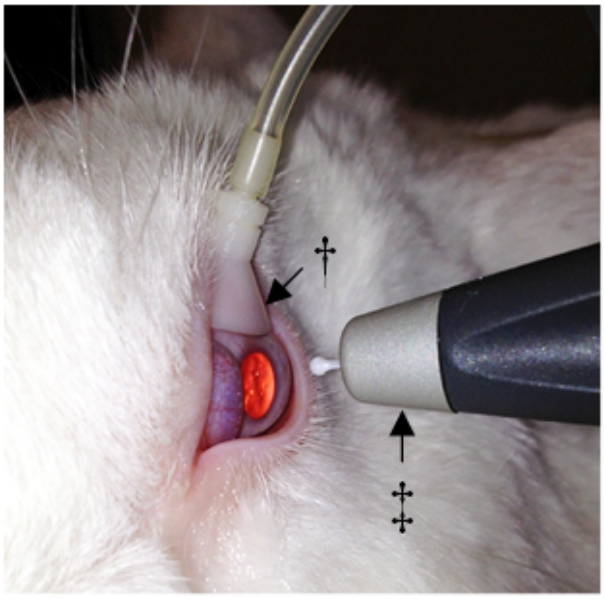

Figure 3: IOP measurement with the Icare rebound tonometer TAO1 during OPT; Suction-cup (†) and tonometer (‡).

Table 1: Calculated diameter ratio of suction-cup and eyeball for humans and rabbits.

Diameter of suction-cup $d_{s,h}$ or $d_{s,r}$	Diameter ratio $d_{s,h}/d_{e,h}$ for human eyeball ($d_{e,h}$ = 22.50 mm)	Diameter ratio $d_{s,r}/d_{e,r}$ for rabbit eyeball ($d_{e,r}$ = 18.25 mm)
$d_{s,h}$ = 13 mm	0.58	
$d_{s,r}$ =12 mm		0.66
$d_{s,r}$ =11 mm		0.60
$d_{s,r}$ =10 mm		0.55

During OPT the measured IOP values obtained by suction-cups with a diameter of $d_{s,r}$ = 10 mm (SC10) generally were below IOP values obtained by suction-cups with a diameter of $d_{s,r}$ = 11 mm and 12 mm (SC11 and SC12) (Fig. 4). As a maximum IOP 34 mmHg was measured after one minute for SC10. Maximum IOP for SC11 and SC12 was 51 mmHg and 47 mmHg after one minute, respectively. IOP decrease was similar for all tested suction-cup sizes during the first five minutes of OPT. In the second half of OPT the pressure decay varied depending on the suction-cup diameter. While IOP decrease decelerated during measurements with SC10 and SC11, IOP decreased more rapidly using SC12. After 9 minutes IOP was still at 37 mmHg for SC11, whereas it had decreased to 23 mmHg with SC12. IOP measurements during OPT confirmed the suction-cup with $d_{s,r}$ = 11 mm (SC11), which is closest to the ratio of cup diameter to eyeball diameter applied in human diagnostics, is most suitable for rabbit OPT.

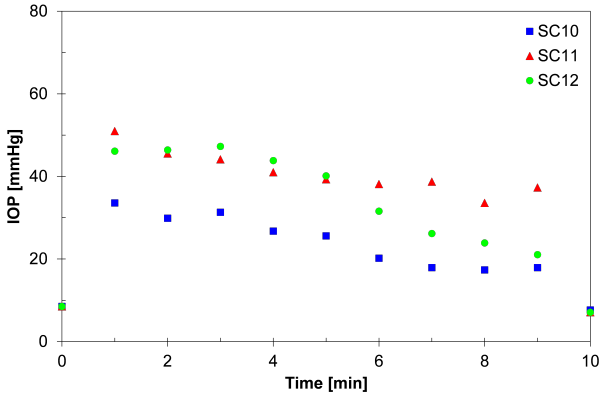

Figure 4: Pressure decay shown for OPT with suction-cups of three diameters ($d_{s,r}$ = 10 mm (SC10), 11 mm (SC11) and 12 mm (SC12)). OPT was performed on the left eye (n = 1).

In a second experiment series, IOP increase on both rabbit eyes was evaluate by OPT using SC11 (Fig. 5). OPT was performed on the right (OD) and left (OS) eye at various points in time (n = 9).

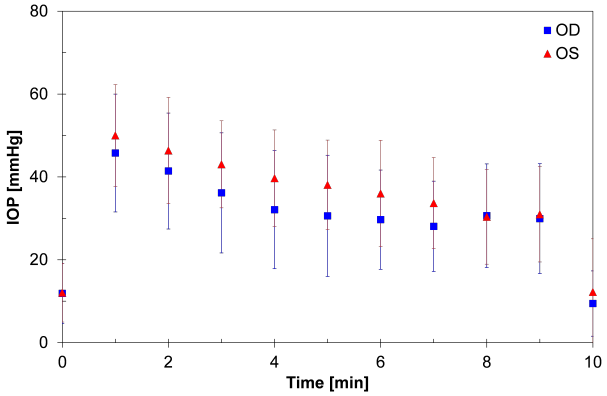

Figure 5: Pressure decay for the right (OD) and left (OS) eye using a suction-cup with a diameter of $d_{s,r}$ = 11 mm (SC11). OPT was performed repeatedly (n = 9).

IOP for OD and OS was 45.8±14.2 mmHg and 50.0±12.3 mmHg (n = 9) after one minute, respectively. After nine minutes IOP decreased to 29.9±13.3 mmHg and 31.0±11.5 mmHg (n = 9) for OD and OS, respectively.

4 Discussion

In the presented study OPT was adapted to rabbit eyes in an effort to create a transient rabbit glaucoma model. Suction-cups with different diameters where tested for their suitability in rabbit OPT.

Using SC10 it was not possible to increase IOP in a satisfactory way. This is due to the fact that the ratio between SC10 to the rabbit eyeball diameter is too small. The effect on the eye was not efficient.

In contrast with SC12 it was possible to reach an appropriate IOP elevation but it had shortcomings when compared to SC11. On the one hand the diameter ratio of SC12 to the rabbit eye is larger than the corresponding human ratio (Table 1). On the other hand the pressure decay with SC12 was faster than that of smaller suction-cups. Additionally, the dimensions of SC12 led to an unsatisfactory handling. Positioning of suction-cup reached either the conjunctival fornix or threatened to slide on the cornea, which could also explain the steeper decrease of IOP values.

Measurements with SC11 accomplished highest IOP values compared with the other suction-cup diameters. During the first minutes of OPT almost a linear pressure decay was detected, which slowed down at the end of OPT. This phenomenon could be explained with the decline in pressure difference between eyeball and drained aqueous humor. High IOP values cause a high outflow rate, which results in lower IOP values. Ongoing constant production of aqueous humor compensates the increasing amount of drained liquid under lower IOP conditions, which results in a slower decrease of IOP. The results from OPT measurements confirmed the theoretical estimation of the ideal suction-cup diameter. A suction-cup with $d_{s,r}$ = 11 mm is most suitable for rabbit OPT.

In conclusion, adopting OPT to the rabbit eye successfully elevated IOP to defined pressure values over a short period of time with SCOP. Elevation of IOP with SC11 was reproducible on right and left eyes. It was possible to establish a non-invasive, transient rabbit glaucoma model. This model system allows verification of new glaucoma therapy interventions, like implanted drainage devices with minimal stress of the examined animals. It might also be of help to measure outflow facilities after application of new potentially IOP lowering medications.

Acknowledgement: This project was partially funded by the Federal Ministry of Education and Research (BMBF) within the research project REMEDIS "Höhere Lebensqualität durch neuartige Mikroimplantate".

Author's Statement

Conflict of interest: Authors state no conflict of interest. Material and Methods: Informed consent: Informed consent has been obtained from all individuals included in this study. Ethical approval: The research related to human use has been complied with all the relevant national regulations, institutional policies and in accordance the tenets of the Helsinki Declaration, and has been approved by the authors' institutional review board or equivalent committee.

References

[1] Bouhenni RA, Dunmire J, Sewell A, Edward DP. Animal Models of Glaucoma. *J Biomed Biotechnol* 2012; 2012:692609

[2] Quigley HA and Broman AT. The number of people with glaucoma worldwide in 2010. *Br J Ophthalmol* 2006;90:262–267

[3] Allemann R, Stachs O, Falke K, Schmidt W, Siewert S, Sternberg K, Chichkov B, Wree A, Schmitz KP, Guthoff RF. Neue Konzepte für druckgesteuerte Glaukomimplantate. *Ophthalmologe.* 2013;110(8):733-9

[4] Ulrich WD, Ulrich C, Neunhöffer E, Fuhrmann P. Oculopression Tonometry (OPT): A New Tonographic Procedure in Glaucoma Diagnosis. *Klin Monatsbl Augenheilkd* 1987; 190(2): 109-113

[5] Löbler M, Rehmer A, Guthoff R, Martin H, Sternberg K and Oliver Stachs. Suitability and calibration of a rebound tonometer to measure IOP in rabbit and pig eyes. *Vet Ophthalmol* 2011;14, 1, 66–68

Bioscience Reports (2019) **39** BSR20181894
https://doi.org/10.1042/BSR20181894

Research Article

Comparison of cytokine/chemokine levels in aqueous humor of primary open-angle glaucoma patients with positive or negative outcome following trabeculectomy

Beata Gajda-Derylo[1,*], Thomas Stahnke[2,*], Stephan Struckmann[3], Gregor Warsow[3], Kerstin Birke[4], Marco T. Birke[4], Bettina Hohberger[5], Robert Rejdak[1], Georg Fuellen[3] and Anselm G. Jünemann[2]

[1]Department of General Ophthalmology, Medical University in Lublin, Lublin, Poland; [2]Department of Ophthalmology, Rostock University Medical Center, Rostock, Germany; [3]Institute for Biostatistics and Informatics in Medicine and Ageing Research, Rostock University Medical Center, Rostock, Germany; [4]Department of Ophthalmology, Tufts University Boston, MA, U.S.A.; [5]Department of Ophthalmology, Friedrich-Alexander University Erlangen-Nuremberg, Erlangen, Germany

Correspondence: Beata Gajda-Derylo (beata.gajdaa@gmail.com) or Georg Fuellen (fuellen@uni-rostock.de) or Anselm G. Jünemann (Anselm.Juenemann@med.uni-rostock.de)

We aimed to identify differences in cytokine/chemokine levels in the aqueous humor (AH) of primary open-angle glaucoma (POAG) patients who suffered from scarring, compared with POAG patients with no scarring after trabeculectomy surgery. Identification of differently expressed cytokines and chemokines may help to understand scarring and fibrotic processes following trabeculectomy, and to make predictions for the outcome of fistulating surgery in the future. Furthermore, the identification of cell signaling pathways involved in fibrosis offers the opportunity for a more specific antifibrotic therapy with reduced side effects, and an improvement in long-term surgical outcome.

Eight samples of AH were collected during trabeculectomy surgery and commercially available cytokine/chemokine arrays were used. Specific, differently expressed proteins (cytokines/chemokines) in AH samples from patients with positive and negative surgery outcomes were detected. These proteins were classified based on their known profibrotic, inflammatory, adhesive, and apoptotic properties. Transforming growth factor β (TGF-β) and vascular endothelial growth factor (VEGF) were among the most important profibrotic cytokines that we detected. Differences in the fold change of protein expression were highly significant between patients after successful and failed trabeculectomy surgery, and these were processed and visualized using *ExprEssence* software.

This pilot study revealed differences in concentrations of cytokines/chemokines in AH between the two examined groups of patients. Our findings suggest that a positive outcome from trabeculectomy is strongly related to an inhibition of the fibrosis process.

[*] These authors contributed equally to this work.

Received: 18 October 2018
Revised: 07 March 2019
Accepted: 01 April 2019

Accepted Manuscript Online: 09 April 2019
Version of Record published: 02 May 2019

Introduction

Glaucoma is the second leading cause of irreversible blindness worldwide [1]. It is a neurodegenerative disease accompanied by the degeneration of retinal ganglion cells (RGCs) and their axons. Patients with glaucoma present with loss of central vision and of the visual field [2]. The most common type of glaucoma is primary open-angle glaucoma (POAG), which can occur with elevated or normal intraocular pressure (IOP). Inequality in production of aqueous humor (AH) and its drainage through the trabecular meshwork leads to increased IOP levels [3,4]. Increased IOP levels are discussed as the main risk factor for glaucoma progression [5].

Bioscience Reports (2019) **39** BSR20181894
https://doi.org/10.1042/BSR20181894

Treatment of glaucoma patients usually starts with eye drops reducing AH production or increasing AH drainage. Surgical procedures are performed among those patients whose topical treatment is insufficient, who develop allergic reactions, or are not in the condition to applicate eye drops. Trabeculectomy is known from the 1960s and is still one of most preferable glaucoma filtration surgeries [6]. Its purpose is to create an outflow channel for AH that connects the anterior chamber (AC) with the sub-Tenon's space [6]. After trabeculectomy, wound healing processes often lead to fibrosis and scar formation at the site of the new drainage which disrupts AH outflow [6,7]. The prolonged presence of myofibroblasts producing α-smooth muscle actin (α-SMA) plays a key role in scar formation that leads to unwanted wound closure [8]. This process is stimulated by growth factors and inflammation [9]. Extracellular matrix (ECM) proteins like fibronectin and collagens are also produced by activated myofibroblasts [10].

Matrix metalloproteinases (MMPs) are proteolytic enzymes whose function is to reduce the number of ECM proteins during ECM remodeling. They are dysregulated in many diseases with excessive scar formation. Down-regulation of MMPs leads to disruption between synthesis and degradation of ECM components [7].

Many experiments demonstrated increased levels of different proteins in the AH of patients with POAG [11–13]. The most important growth factors/cytokines among them, which play an indispensable role in fibrotic processes, are transforming growth factor β (TGF-β), vascular endothelial growth factor (VEGF) and tumor necrosis factor-α (TNF-α). Additionally, members of the interleukin family take a central role in fibrosis. Interleukins with levels distinctly elevated in POAG patients are IL-6 and IL-8 [14,15].

ExprEssence, which we employ as the main post-processing and visualization tool for our protein expression data, has previously been used on gene expression (transcriptomics) data from kidney [16], pluripotency [17], and breast cancer [18], among others. The software can naturally be applied to protein expression data as well. The characteristic feature of *ExprEssence* is its focus on known protein interactions as a guide to select specifically informative changes of gene or protein expression. A frequently used and freely available source of gene–protein and protein–protein interaction data in the form of a network is the STRING database [19].

The aim of this pilot study was to compare proteins from the AH of positive (no fibrosis) versus negative (fibrosis) early outcomes of POAG patients who were surgically treated by trabeculectomy. A differential analysis of protein expression was performed based on a STRING network using *ExprEssence*, to identify protein interactions and signaling pathways involved in fibrosis. The differences in expression levels, mapped on to a network of protein interactions, specifically for growth factors/cytokines, sheds some light on to fibrotic mechanisms following trabeculectomy, and these may partially explain its failure in some patients but not others.

Materials and methods

Ethics statement

The Institutional Review Board of the University of Erlangen-Nürnberg approved this case–control study. The purpose and methods in the present study were explained in detail to patients before participating. Written and informed consent was obtained from the patients. The present study was carried out in accordance with the tenets of the Declaration of Helsinki.

Patients and design

All participants presented to the Department of Ophthalmology at the University of Erlangen-Nuremberg for trabeculectomy. Criteria for POAG were an open anterior chamber angle, glaucomatous changes of the optic nerve head, and an elevated IOP (>21 mmHg). Indications for trabeculectomy were an IOP under maximal medication exceeding the target pressure or progression of glaucomatous damage. Patients with local side effects of antiglaucomatous medications as indication for trabeculectomy were not included. Only eyes without previous ocular surgery were included. All eyes were phakic. One week before surgery, the local antiglaucomatous medications were taken off and local steroids without preservative were given five times a day. The IOP was controlled by systemic carbonic anhydrase inhibitors in all patients.

Criteria for early failure of trabeculectomy was the need for bleb needle revision two times within the first 3 months after trabeculectomy and an IOP > 21 mmHg without medications, 3 months after trabeculectomy. Criteria for early success of trabeculectomy was IOP < 13 and > 8 mmHg without medications, 3 months after trabeculectomy.

Trabeculectomy was performed by one surgeon (A.G.J.) under topical gel anesthesia. The eye was fixed using corneal traction suture. The following surgical steps were performed: (i) limbal opening of the conjunctiva from 11 to 1 o'clock, (ii) opening and hydrodissection of the tenon, (iii) application of mitomycin C (0.03% for 3 min) using a butterfly-shaped sponge and subsequent wash-out, (iv) creation of a rectangular scleral flap 4 by 4 mm, (v)

Table 1 Clinical characteristics of patients

	Age	Gender	Trab outcome	Type of med	Number of med*	Stage of OA	MD	IOP
1	62	F	+	timolol, brimonidine	2	2	1.1	14
2	46	F	+	timolol	1	4	11.4	15
3	58	F	+	timolol	1	3	2	35
4	44	F	+	acetazolamide, latanoprost, brinzolamide	3	3	4.7	24
5	59	M	+	acetazolamide, brimonidine, timolol, brinzolamide	4	1	3.4	28
6	74	F	-		0	3	−0.3	26
7	54	F	-	tImolol, acetazolamide, tafluprost,	3	3	−0.4	17
8	55	M	-	latanoprost, timolol	2	1/2	1.7	11

Abbreviations: med, antiglaucomatous medication; Trab, trabeculectomy.
* = Number of medications before they were taken off 1 week before surgery, stage of OA: glaucomatous optic nerve atrophy according to the stages given by Jonas et al. [20], MD, mean deviation in standard automated perimetry (Octopus 500).

preplacement of two 10/0 nylon sutures at the posterior edges of the scleral flap, (vi) paracentesis at 2 o'clock position, (vii) rectangular corneoscleral excision 2 by 1 mm including Schlemm's canal and trabecular meshwork, (viii) basal iridectomy, (ix) closure of the flap sutures after refilling the anterior chamber using balanced salt solution, (ix) readapting the tenon at the limbus using two 10/0 nylon sutures, (xi) readapting the conjunctiva at the limbus using two 10/0 nylon sutures and (xii) removal of the corneal traction suture.

Patients with positive and negative outcomes were matched by age, duration of glaucoma, preoperative IOP, stage of the glaucoma and number of local antiglaucomatous medications. Two patients with positive outcome (nr 2 and 3) and one patient with negative one (nr 6) received local preservative-free steroids preoperatively for 1 week. An *a priori* power analysis based on preliminary data showed that a sample size of 3–5 per group should be sufficient for detecting significant differences in protein levels in the AH.

Thus, out of the patients undergoing trabeculectomy between June 2009 and July 2009 and for whom samples of AH were available, a total of eight POAG patients met the inclusion criteria and could be admitted into the study. Three of them matched the inclusion criteria for early failure by fibrosis; 1 male, 2 female, mean age: 61 $\pm$ 11, and 5 of them matched the inclusion criteria for early success with no fibrosis; 4 females, 1 male, mean age: 53.8 $\pm$ 8.2. All participants were of Caucasian race, with an average age of 59 ($\pm$ 9.44–74) years. Patient characteristics are given in Table 1. There was no statistical difference in age, number of preoperative medications, duration of glaucoma, MD and preoperative IOP between the two groups of patients.

Laboratory analysis

AH samples were obtained intra-operatively by A.G.J. prior to the opening of the conjunctiva. A total of 100–150 µl of AH was withdrawn through an *ab externo* limbal paracentesis site using a 27-gauge needle on a tuberculin syringe, with special care to avoid blood contamination. The samples were immediately frozen in liquid nitrogen and stored in a deep freezer at −80°C until biochemical analysis. A total of 274 different proteins in total were analyzed in each sample by Cytokine Antibody arrays (RayBio Cytokine Antibody Array C Series 4000; RayBiotech, Inc, Norcross GA 30092, U.S.A.). Antibody arrays were used according to the manufacturer's protocol. Briefly, after an initial blocking step, 50 µl of each aqueous sample was incubated on each membrane overnight at 4°C. Antibodies provided by the company were used to detect the protein levels. Signals were visualized by exposure to light-sensitive films (Hyperfilm ECL; GE Healthcare, Munich, Germany), which were digitized and densitometrically quantitated with the Multi Gauge V3.1 software (Fujifilm, Düsseldorf, Germany), giving rise to 274 protein expression measurements per sample. Supplementary Data S1 (in Excel format) includes the data of the five Cytokine Antibody arrays covering the 274 proteins (excl. positive, negative and blank controls), with two measurements per patient, that is, ten measurements for the five patients without fibrosis, and six measurements for the three patients with fibrosis.

Bioscience Reports (2019) **39** BSR20181894
https://doi.org/10.1042/BSR20181894

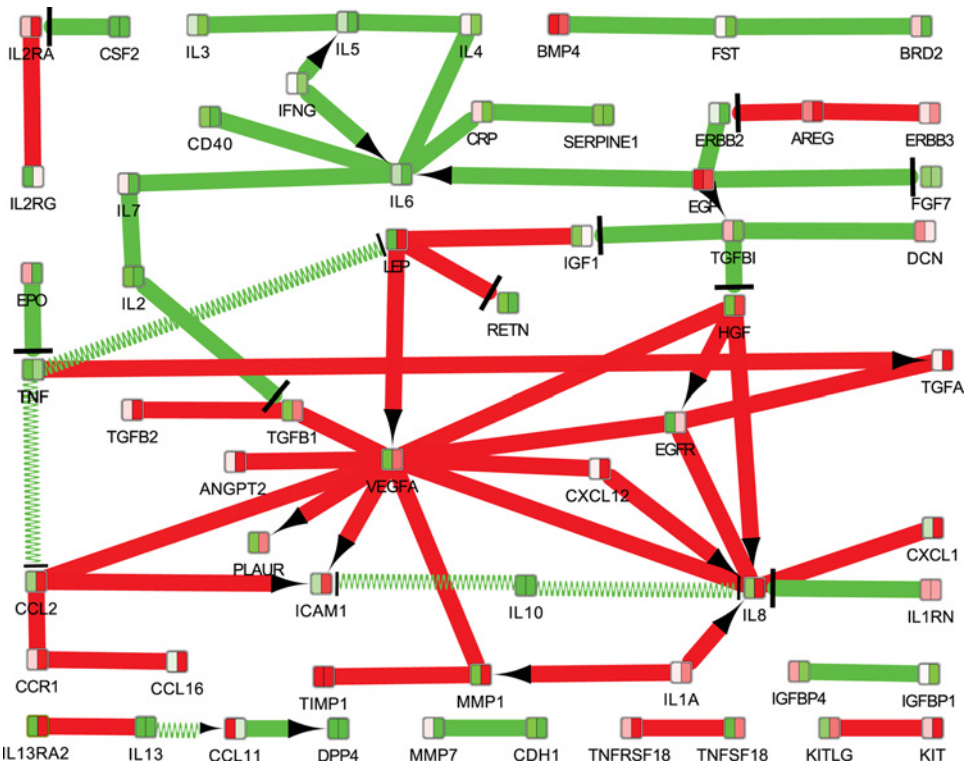

Figure 1. Fibrotic mechanisms following trabeculectomy, visualized based on mapping the protein expression data on to a STRING network

Edges with LinkScores close to zero were removed, keeping only 10% of the edges with the largest and 10% of the edges with the smallest LinkScores. The LinkScore is represented by color (green = small, red = large) and by the thickness of the links. Inhibition links are drawn with a T-bar, activation links with an arrow. Interaction links without known direction are shown without T-bar or arrow. The colors in the nodes represent the protein expression measurements for the two conditions (left = healthy, right = fibrotic).

Statistical analysis

Statistical differences between AH protein levels in patients with and without fibrosis were assessed using the two-way Anova test and Bonferroni correction for multiple comparisons. Statistical analyses were performed using GraphPad Prism Software (GraphPad, Inc. CA, U.S.A.). The significance level was established at $P \leq 0.05$. Data are presented as mean $\pm$ standard deviation (S.D.).

ExprEssence analysis

ExprEssence was applied in version 1.2 within Cytoscape 2.6.0 on a human network downloaded from string-db.org in version 9.1. The experimental score threshold was set to 0.8, the other scores (database and textmining) were set to 0.9, yielding a network comprising 27042 interactions (18685 after removal of redundant interactions stemming from different sources) between 6577 proteins in total. The 274 protein expression measurements were then mapped on to the network using the protein names as common identifiers, yielding a network comprising 358 interactions between 199 proteins. The *ExprEssence* LinkScore (see next paragraph) was mapped on to the links (the interactions between the proteins) and is shown by width of the link as well as a red-green color gradient.

Setting the LinkScore-threshold of the quantile-based sliders to 10 and 90%, we condensed the starting network provided by STRING to 70 interactions between 64 proteins. The condensed network was then analyzed manually.

ExprEssence calculates a score for each undirected interaction and for each activating interaction as the sum of the logarithmic fold changes of the protein expression values. For inhibiting interactions, the score is the difference of the logarithmic fold changes. The network is then condensed by removing all interactions that fail to score above or below a given threshold (in a quantile-based fashion), see Figure 1.

Supplementary Data S2 (in Cytoscape format) includes the data of the Cytokine Antibody arrays covering the 274 proteins, mapped on to the String network and condensed by *ExprEssence*, in the view 'condensed Network 1 (positive − negative)', which was used to generate the figure.

Results

The cytokine antibody arrays identified 274 proteins in the AH samples. A comparison between patients with failed and successful trabeculectomy surgeries revealed different protein expression measurements in AH. One hundred and three of the identified proteins were significantly up-regulated in the failure group compared with the successful group, while 27 proteins were significantly down-regulated. Our study focused on the most important cytokines for fibrosis processes and the ones with the largest fold changes (Figure 2). In the following, the classification of proteins into functional groups was based on expert knowledge.

Proteins with profibrotic properties

Failure of trabeculectomy is usually correlated with scar formation and fibrosis. We found many proteins up-regulated in AH from patients after failed trabeculectomy that are known to be involved in fibrosis. Among them, we found epidermal growth factor receptor (EGFR) with five times higher expression and VEGF (four times higher expression), compared with the group where surgical outcome was successful. TGF-β2 expression showed a 2.71 fold increase in comparison with the successful surgery outcome group, while bone morphogenic protein (BMP) 7, another member of the TGF family, showed 3.21 fold increase. Amid other up-regulated proteins we found nerve growth factor receptor (NGF-R) (5.16 fold increase) and hepatocyte growth factor (HGF) (4.56 fold increase). On the other hand, human EGFR 2 (HER2, also known as ErbB2) (8.3 fold decrease), erythropoietin (8.28 fold decrease), thyroglobulin (4.57 fold decrease), neural cell adhesion molecule 1 (NCAM1) (3.45 fold decrease), growth hormone (3.0 fold decrease) and basal cell adhesion molecule (BCAM) (2.68 fold decrease) were notably down-regulated compared with patients with successful surgery outcome.

Proteins with inflammatory properties

The results indicate that almost 50% of up-regulated proteins from AH of the failed surgery group were linked to stimulation of inflammatory processes. Wound healing after glaucoma surgery is strongly supported by inflammation. We observed 12-times higher expression of B-cell maturation antigen (BCMA) and 10-times higher expression of granulocyte colony-stimulating factor (GCSF). IL-11, IL-13, IL-8, IL-1 and monocyte chemotactic protein (MCP) were also among the up-regulated cytokines, with expression up to eight-times higher compared with the successful surgery group. Overall, 49 proteins were up-regulated. In turn, six proteins (IL-22, IL-31, cluster of differentiation (CD) 40 (CD40), IL-28A, IL-29, osteopontin) which are involved in inflammatory processes were down-regulated in the failed surgery group, in comparison with the successful group.

Proteins with adhesion properties

Our analysis showed up-regulation of certain adhesion molecules in AH from patients after failed trabeculectomy. Many of these are proteins that are responsible for the adhesion of inflammatory cells. L-selectin was six fold higher in the failed surgery group compared with the successful surgery group. Intercellular adhesion molecules 1, 2 and 3 (ICAM1, ICAM2, ICAM3), CD166 antigen, carcinoembryonic antigen-related cell adhesion molecule 1 (CEACAM1), stromal cell-derived factor 1 (SDF1), C–X–C motif chemokine 5 (CXCL5) and phosphatidylinositol-glycan biosynthesis class F protein were also markedly up-regulated with fold changes up to 4.95. Down-regulated adhesion molecules were β-IG-H3 (3.08 fold decrease) and neuronal cell adhesion molecule (NrCAM) (2.10 fold decrease).

Proteins with apoptotic properties

Additionally, several proteins involved in apoptotic processes were significantly up-regulated in the AH of the failed surgery group compared with the successful group. The average fold change of these proapoptotic proteins was 2. Identified proteins were TRAIL receptor 4 (TRAILR4), FAS receptor (FasR), human soluble tumor necrosis factor receptor I (sTNF-RI), fas ligand (FasL), osteoprotegrin (OPG) and tumor necrosis factor receptor superfamily member 18 (TNFRSF18).

We also discovered that in AH of patients with failed trabeculectomy, MMP-1, MMP-3 and MMP-13 were significantly up-regulated, whereas MMP-2, MMP-7, MMP-8 and MMPs-10 were down-regulated.

Finally, all proteins detected in AH from patients were analyzed using *ExprEssence* based on a STRING network. The condensed network of Figure 1 reflects many previously known mechanisms of fibrosis, including interactions

Bioscience Reports (2019) **39** BSR20181894
https://doi.org/10.1042/BSR20181894

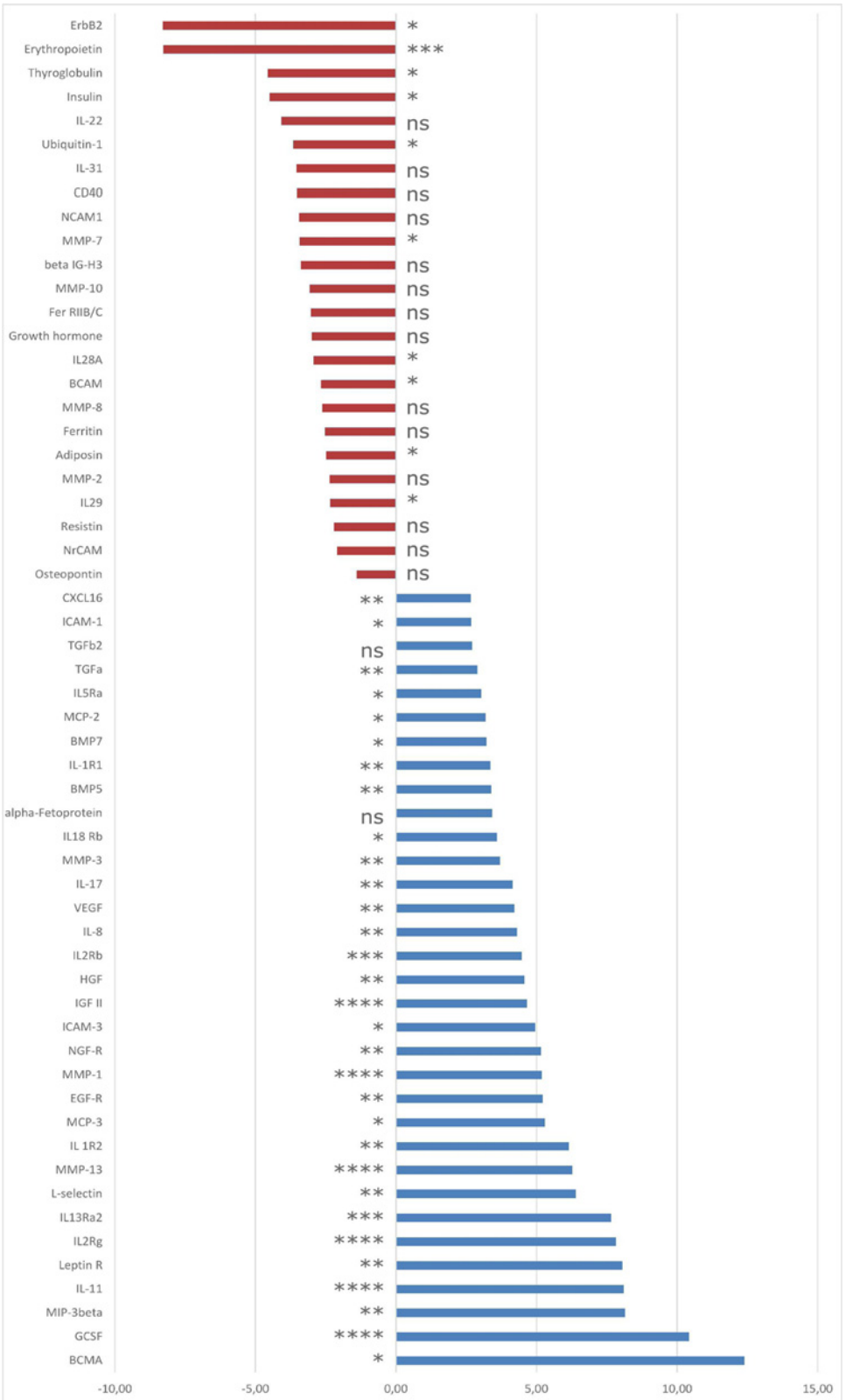

Figure 2. Fibrotic mechanisms following trabeculectomy, differentially expressed genes/proteins

Selection of gene names of the proteins with significantly diminished (red) or increased (blue) expression in the AH of POAG patients after failed trabeculectomy compared with patients with successful surgery outcome. Data are presented as mean ± S.D. Levels of significance: *$P \leq 0.05$; **$P \leq 0.01$; ***$P \leq 0.001$; ****$P \leq 0.0001$; ns, not significant.

between cytokines. One of the most important mechanisms are the interactions of VEGF (which plays a key role in the condensed network) with many pro-fibrotic cytokines and growth factors, based on a consistent up-regulation together with TGF-β1, MMP-1, IL-8, EGFR, HGF, leptin and chemokine ligand 2. Another protein that was highlighted as being up-regulated in cases of failed trabeculectomy is IL-8, which interacts with VEGF and EGFR and is strongly up-regulated by CXCL1, HGF and IL-1a.

Discussion

The present study aimed to identify cytokine/chemokine profiles of the AH of POAG patients, correlated with the early fibrosis processes after trabeculectomy. The early failure of trabeculectomy as defined by two needlings within the first 3 months and IOP > 21 mmHg with medications versus the early success as defined by an IOP within the range of the episcleral venous pressure (that is, IOP < 13 and > 8 mmHg) without medications is expected to give the most pronounced differences in the cytokine/chemokine profiles and may help to identify some of the key players of fibrosis. The present study was not designed to identify differences in the cytokine/chemokine profiles between glaucoma patients and healthy people.

Our results suggest that there are notable differences in the expression of many proteins in the AH of patients after early failed versus early successful trabeculectomy. In our findings we observed a large number of up-regulated and down-regulated proteins correlated with fibrotic processes, which were already suggested in the literature to play a key role in trabeculectomy outcome.

One of the proteins that was strongly up-regulated in our study was VEGF (4.21 fold). This cytokine had many interactions with other proteins identified by *ExprEssence* analysis (Figure 1). Besides its known role in neovascularization, many publications demonstrated a significant involvement of VEGF in fibrotic processes in a variety of organs [21,22], stimulating the growth of vascular endothelial cells and possibly taking part in wound healing after trabeculectomy [23,24]. VEGF was also reported to be elevated in AH of POAG and neovascular glaucoma patients [7]. Another report showed that VEGF plays a key role in activating TGF-β1 expression, especially the Smad/Snail pathway after glaucoma surgery, noting that it was significantly elevated after trabeculectomy [25].

We also found a strong up-regulation of VEGF and TGF-β in the failed surgery group in comparison with the successful surgery group. *ExprEssence* identified their strong interaction, confirming the findings of Park et al. [25], where TGF-β was already described as a fibrosis-stimulation cytokine. TGF-β promotes fibroblasts contraction, proliferation and migration [26]. It is a mediator of matrix proteins [27,28], fibronectin [29], collagens [30] and proteoglycan secretion processes [31]. It down-regulates proteolytic enzymes that are responsible for the degradation of matrix proteins and the turnover of the ECM [30,32]. Isoforms of TGF-β activate cell surface TGF-β serine/threonine kinase receptors which are connected to signal transduction networks, such as mitogen-activated protein kinase (MAPK)/extracellular signal-regulated kinase (ERK), p38Mapk, C-Jun-N-terminal kinase (JNK) and Smads [7]. As mentioned above, the Smad pathway was already described to be deeply involved in stimulating fibrosis induced by TGF-β. Cordeiro et al. [33] demonstrated that anti-TGF-β2 antibodies suppressed scar formation after filtering surgery in rabbits and glaucoma patients, resulting in longer bleb survival compared with untreated controls. Another study reported that a more desirable bleb development in POAG patients was among those with normal TGF-β2 levels in AH compared with those with higher ones [34].

As mentioned before, almost half of the proteins that we found to be up-regulated after failed trabeculectomy were connected to immune/inflammation processes. Both increased cytokine expression and tissue injury after surgical management lead to activation of fibroblasts, neutrophils and macrophages. Inflammatory cells infiltrate the wound directly after surgery and start to secrete pro-inflammatory cytokines, leading to inflammation and fibrosis [7]. One of the latest publications compared AH from glaucoma and cataract patients, demonstrating an up-regulation of cytokines correlated to innate immune processes among glaucoma patients compared with control groups. The authors observed an up-regulation of many proteins in AH from glaucoma patients, which were mostly related to innate immunity, for example higher values of CD14 and CD163, which are monocyte/macrophage markers [35]. In accordance, we also observed changes in values of CD14 (2.01 higher expression) in the failed surgery group compared with the successful surgery group.

Many of the cytokines with increased expression measurements in our study (IL-1α, IL-1β, IL-6, TNF-α, FasL) were already described as being elevated in glaucoma patients [36]. Additionally, IL-1 and IL-6 were also described to be up-regulated in fibrotic processes in other organs [37,38]. In accordance with already published data, Il-22 (which was described to have antifibrotic properties [7]) was strongly down-regulated in our group of patients with failed surgery outcome. This cytokine is an IL-10 family member, which was also shown to have an anti-inflammatory effect [39,40].

Bioscience Reports (2019) **39** BSR20181894
https://doi.org/10.1042/BSR20181894

MCP-1 levels in AH of glaucoma patients were already described as a very relevant prognostic factor for trabeculectomy outcome [41]. In our protein examination we found that MCP family cytokines (MCP-2 and 3) were highly up-regulated in patients with failed trabeculectomy outcome, underlining this result. These cytokines can activate macrophage infiltration into local tissue [42] as well as leukocytes, which leads to excessive inflammatory and fibrotic responses [41]. It was already found that elevated MCP-1 levels in tears [43] and in AH [41] among patients with glaucoma are correlated with a higher tendency to postoperative scarring in an early phase after surgery, including trabeculectomy. MCP-1 was also shown to be a pro-fibrotic agent in other organs [44–46]. Additionally, an involvement of MCP-2 [47] and MCP-3 [48] in glaucoma and its treatment were described.

MMPs are one of the most characteristic proteases that are responsible for ECM degradation. Apart from wound healing processes they are also involved in embryogenesis, bone growth and angiogenesis [49]. It was already suggested they can play a role in excessive scarring processes. Observations using a rabbit model and the MMP inhibitor, GM6001, showed a reduction in scarring after filtering glaucoma surgery [50]. We observed a significant down-regulation of some MMPs. One of the most important is MMP-2, which is responsible for degradation of collagen (IV–VI, X) elastin and fibronectin [49]. This protease was 2.37-times down-regulated in patients after failed trabeculectomy, suggesting it plays a key role in ECM levels during excessive wound healing processes.

Based on the literature, the groups of proteins discussed above play a significant role in the fibrotic processes after trabeculectomy surgery. In our study we found a number of strongly up-regulated cytokines, already described in the literature as pro-fibrotic. Moreover, activated inflammatory cells infiltrate the post-surgery wound and secrete pro-inflammatory cytokines which also lead to fibrosis. We observed up-regulation of certain apoptotic markers in the group of patients after failed trabeculectomy, indicating that programmed cell death occurs in this case. It is known that myofibroblasts undergo apoptosis at the end of the healing process [51]. This process is strongly influenced by the cytokine TGF-β which inhibits programmed cell death in myofibroblasts [52] and on the other hand induces the transformation of fibroblasts into myofibroblasts. Our observations indicate a misbalance between these processes which leads to a continuous activation of fibroblasts by increased levels of TGF-β and therefore an uninterrupted but extenuated process of apoptosis in myofibroblasts, which finally results in fibrosis. Additionally, glaucoma and increased IOP can lead to neuronal cell death due to oxidative stress [53,54]. Peroxireduxin 2 and 6, and superoxide dismutase, are proteins responsible for antioxidant protection, which were already described as down-regulated among glaucoma patients. The same authors also observed down-regulation of proteins connected to neuronal physiology [35]. Apoptotic cell death in RGCs was already described in an experimental glaucoma model in monkeys [55] and in humans suffering from glaucoma [56]. Increasing IOP levels after failed trabeculectomy can lead to the progression of apoptosis in RGCs and to an accumulation of apoptotic markers. Taking into consideration that the vitreous is more fluidic with age due to a decrease in the elasticity of the hyaluronic acid and that a posterior vitreous detachment (PVD) is more prominent in elderly people (who form the majority of glaucoma patients), it is conceivable that the apoptotic factors found in our study could have their origin also in RGCs. Furthermore, an increase in the prevalence of PVD was demonstrated in glaucoma patients in comparison with healthy subjects [57] which facilitates diffusion of apoptotic factors to the AH. On the other hand, most of the cytokines and factors identified in our study are correlated to fibrosis, inflammation, wound healing and ECM modulation. Therefore, we assume that the apoptotic factors also have their origin in the apoptosis of myofibroblasts. To finally clear this phenomenon further investigations are necessary.

There are some limitations of the study: first, results were based on one experimental approach (antibody arrays); second, the sample size of eight patients is quite small; and third, the study had a retrospective design. This might limit the conclusions of the study.

Conclusion

This pilot study indicated alterations in the expression of various proteins in AH of early successful and failed trabeculectomy surgeries. We demonstrated that many of the differences in expression of affected proteins are linked to fibrotic processes. These findings suggest that a negative outcome of trabeculectomy is strongly related to the stimulation of fibrotic processes. These results could be used to identify substances such as inhibitors which may be able to limit early fibrotic mechanisms in specific ways and thus to avoid surgical interventions like bleb needling in the early postoperative period. Further studies on cytokine/chemokine profiles of AH after trabeculectomy are needed to identify further fibrotic mechanisms, to validate the findings, and to subsequently improve early as well as late trabeculectomy outcomes.

Acknowledgments

We thank Elke Meier and Carolin Neumann for technical assistance, Matthias Zenkel for fruitful discussions during the present study, and Emily Wheeler and Richard Holland for language editing.

Funding

This work was supported in part by the 'Verein für Wundheilung e.V.'; the analysis of the data was supported by the German Federal Ministry of Education and Research [grant number VIP, FKZ 03V0396]; and in part by the European Union's Horizon 2020 Research And Innovation Programme [grant number 633589 (to G.F.)].

Author Contribution

B.G.-D. and T.S. wrote the manuscript. S.S. and G.W. prepared Figure 1 and B.G.-D. prepared Figure 2. K.B., M.T.B. and B.H. conducted laboratory studies. A.G.J. obtained AH samples. B.G.-D., T.S., S.S., A.G.J. and G.F. analyzed the data. S.S., G.W. and G.F. conducted the ExprEssence analyses. A.G.J., R.R. and G.F. conceived the study concept and procured funding for the project. All authors reviewed the manuscript and approved the final version.

Competing Interests

The authors declare that there are no competing interests associated with the manuscript.

Abbreviations

AH, aqueous humor; ANOVA, Analysis of Variance; CD , cluster of differentiation; ECM, extracellular matrix; EGFR, epidermal growth factor receptor; FAS, Tumor Necrosis Factor Receptor Superfamily Member 6; FasL, fas ligand; HGF, hepatocyte growth factor; IL, Interleukin; IOP, intraocular pressure; MCP, monocyte chemotactic protein; POAG, primary open-angle glaucoma; PVD, posterior vitreous detachment; RGC, retinal ganglion cell; STRING, search tool for recurring instances of neighboring genes; TGF-β, transforming growth factor β; TNF-α, tumor necrosis factor-α; TRAIL, Tumor Necrosis Factor Related Apoptosis Inducing Ligand; VEGF, vascular endothelial growth factor.

References

1 Tham, Y.C., Li, X., Wong, T.Y., Quigley, H.A., Aung, T. and Cheng, C.Y. (2014) Global prevalence of glaucoma and projections of glaucoma burden through 2040: a systematic review and meta-analysis. *Ophthalmology* **121**, 2081–2090, https://doi.org/10.1016/j.ophtha.2014.05.013
2 Weinreb, R.N., Aung, T. and Medeiros, F.A. (2014) The pathophysiology and treatment of glaucoma: a review. *JAMA* **311**, 1901–1911, https://doi.org/10.1001/jama.2014.3192
3 Quigley, H.A. (2011) Glaucoma. *Lancet* **377**, 1367–1377, https://doi.org/10.1016/S0140-6736(10)61423-7
4 Schwartz, M. (2003) Neurodegeneration and neuroprotection in glaucoma: development of a therapeutic neuroprotective vaccine: the Friedenwald lecture. *Invest. Ophthalmol. Vis. Sci.* **44**, 1407–1411, https://doi.org/10.1167/iovs.02-0594
5 Coleman, A.L. and Miglior, S. (2008) Risk factors for glaucoma onset and progression. *Surv. Ophthalmol.* **53**, S3–S10, https://doi.org/10.1016/j.survophthal.2008.08.006
6 Khaw, P.T., Chiang, M., Shah, P., Sii, F., Lockwood, A. and Khalili, A. (2012) Enhanced trabeculectomy: the Moorfields Safer Surgery System. *Dev. Ophthalmol.* **50**, 1–28, https://doi.org/10.1159/000334776
7 Yamanaka, O., Kitano-Izutani, A., Tomoyose, K. and Reinach, P.S. (2015) Pathobiology of wound healing after glaucoma filtration surgery. *BMC Ophthalmol.* **15**, 157, https://doi.org/10.1186/s12886-015-0134-8
8 Gabbiani, G. (2003) The myofibroblast in wound healing and fibrocontractive diseases. *J. Pathol.* **200**, 500–503, https://doi.org/10.1002/path.1427
9 Wynn, T.A. and Ramalingam, T.R. (2012) Mechanisms of fibrosis: therapeutic translation for fibrotic disease. *Nat. Med.* **18**, 1028–1040, https://doi.org/10.1038/nm.2807
10 Schlunck, G., Meyer-ter-Vehn, T., Klink, T. and Grehn, F. (2016) Conjunctival fibrosis following filtering glaucoma surgery. *Exp. Eye Res.* **142**, 76–82, https://doi.org/10.1016/j.exer.2015.03.021
11 Tripathi, R.C., Li, J., Chan, W.F. and Tripathi, B.J. (1994) Aqueous humor in glaucomatous eyes contains an increased level of TGF-beta 2. *Exp. Eye Res.* **59**, 723–727, https://doi.org/10.1006/exer.1994.1158
12 Hu, D.N., Ritch, R., Liebmann, J., Liu, Y., Cheng, B. and Hu, M.S. (2002) Vascular endothelial growth factor is increased in aqueous humor of glaucomatous eyes. *J. Glaucoma* **11**, 406–410, https://doi.org/10.1097/00061198-200210000-00006
13 Sawada, H., Fukuchi, T., Tanaka, T. and Abe, H. (2010) Tumor necrosis factor-alpha concentrations in the aqueous humor of patients with glaucoma. *Invest. Ophthalmol. Vis. Sci.* **51**, 903–906, https://doi.org/10.1167/iovs.09-4247
14 Kuchtey, J., Rezaei, K.A., Jaru-Ampornpan, P., Sternberg, Jr, P. and Kuchtey, R.W. (2010) Multiplex cytokine analysis reveals elevated concentration of interleukin-8 in glaucomatous aqueous humor. *Invest. Ophthalmol. Vis. Sci.* **51**, 6441–6447, https://doi.org/10.1167/iovs.10-5216
15 Chen, K.H., Wu, C.C., Roy, S., Lee, S.M. and Liu, J.H. (1999) Increased interleukin-6 in aqueous humor of neovascular glaucoma. *Invest. Ophthalmol. Vis. Sci.* **40**, 2627–2632
16 Warsow, G., Endlich, N., Schordan, E., Schordan, S., Chilukoti, R.K., Homuth, G. et al. (2013) PodNet, a protein-protein interaction network of the podocyte. *Kidney Int.* **84**, 104–115, https://doi.org/10.1038/ki.2013.64

17 Som, A., Harder, C., Greber, B., Siatkowski, M., Paudel, Y., Warsow, G. et al. (2010) The PluriNetWork: an electronic representation of the network underlying pluripotency in mouse, and its applications. *PLoS ONE* **5**, e15165, https://doi.org/10.1371/journal.pone.0015165
18 Warsow, G., Struckmann, S., Kerkhoff, C., Reimer, T., Engel, N. and Fuellen, G. (2013) Differential network analysis applied to preoperative breast cancer chemotherapy response. *PLoS ONE* **8**, e81784, https://doi.org/10.1371/journal.pone.0081784
19 Franceschini, A., Szklarczyk, D., Frankild, S., Kuhn, M., Simonovic, M., Roth, A. et al. (2013) STRING v9.1: protein-protein interaction networks, with increased coverage and integration. *Nucleic Acids Res.* **41**, D808–D815, https://doi.org/10.1093/nar/gks1094
20 Jonas, J.B., Gusek, G.C. and Naumann, G.O. (1988) Optic disc morphometry in chronic primary open-angle glaucoma. I. Morphometric intrapapillary characteristics. *Graef. Arch. Clin. Exp. Ophthalmol.* **226**, 522–530, https://doi.org/10.1007/BF02169199
21 Boutet, A., De Frutos, C.A., Maxwell, P.H., Mayol, M.J., Romero, J. and Nieto, M.A. (2006) Snail activation disrupts tissue homeostasis and induces fibrosis in the adult kidney. *EMBO J.* **25**, 5603–5613, https://doi.org/10.1038/sj.emboj.7601421
22 Li, Z.D., Bork, J.P., Krueger, B., Patsenker, E., Schulze-Krebs, A., Hahn, E.G. et al. (2005) VEGF induces proliferation, migration, and TGF-beta1 expression in mouse glomerular endothelial cells via mitogen-activated protein kinase and phosphatidylinositol 3-kinase. *Biochem. Biophys. Res. Commun.* **334**, 1049–1060, https://doi.org/10.1016/j.bbrc.2005.07.005
23 Van Bergen, T., Vandewalle, E., Van de Veire, S., Dewerchin, M., Stassen, J.M., Moons, L. et al. (2011) The role of different VEGF isoforms in scar formation after glaucoma filtration surgery. *Exp. Eye Res.* **93**, 689–699, https://doi.org/10.1016/j.exer.2011.08.016
24 Li, Z., Van Bergen, T., Van de Veire, S., Van de Vel, I., Moreau, H., Dewerchin, M. et al. (2009) Inhibition of vascular endothelial growth factor reduces scar formation after glaucoma filtration surgery. *Invest. Ophthalmol. Vis. Sci.* **50**, 5217–5225, https://doi.org/10.1167/iovs.08-2662
25 Park, H.Y., Kim, J.H. and Park, C.K (2013) VEGF induces TGF-beta1 expression and myofibroblast transformation after glaucoma surgery. *Am. J. Pathol.* **182**, 2147–2154, https://doi.org/10.1016/j.ajpath.2013.02.009
26 Cordeiro, M.F., Bhattacharya, S.S., Schultz, G.S. and Khaw, P.T. (2000) TGF-beta1, -beta2, and -beta3 in vitro: biphasic effects on Tenon's fibroblast contraction, proliferation, and migration. *Invest. Ophthalmol. Vis. Sci.* **41**, 756–763
27 Heckmann, M., Aumailley, M., Chu, M.L., Timpl, R. and Krieg, T. (1992) Effect of transforming growth factor-beta on collagen type VI expression in human dermal fibroblasts. *FEBS Lett.* **310**, 79–82, https://doi.org/10.1016/0014-5793(92)81151-B
28 Madri, J.A., Pratt, B.M. and Tucker, A.M. (1988) Phenotypic modulation of endothelial cells by transforming growth factor-beta depends upon the composition and organization of the extracellular matrix. *J. Cell Biol.* **106**, 1375–1384, https://doi.org/10.1083/jcb.106.4.1375
29 Ignotz, R.A. and Massague, J. (1986) Transforming growth factor-beta stimulates the expression of fibronectin and collagen and their incorporation into the extracellular matrix. *J. Biol. Chem.* **261**, 4337–4345
30 Stahnke, T., Kowtharapu, B.S., Stachs, O., Schmitz, K.P., Wurm, J., Wree, A. et al. (2017) Suppression of TGF-beta pathway by pirfenidone decreases extracellular matrix deposition in ocular fibroblasts in vitro. *PLoS ONE* **12**, e0172592, https://doi.org/10.1371/journal.pone.0172592
31 Morales, T.I. and Roberts, A.B. (1988) Transforming growth factor beta regulates the metabolism of proteoglycans in bovine cartilage organ cultures. *J. Biol. Chem.* **263**, 12828–12831
32 Agarwal, P., Daher, A.M. and Agarwal, R. (2015) Aqueous humor TGF-beta2 levels in patients with open-angle glaucoma: a meta-analysis. *Mol. Vis.* **21**, 612–620
33 Cordeiro, M.F., Gay, J.A. and Khaw, P.T (1999) Human anti-transforming growth factor-beta2 antibody: a new glaucoma anti-scarring agent. *Invest. Ophthalmol. Vis. Sci.* **40**, 2225–2234
34 Picht, G., Welge-Luessen, U., Grehn, F. and Lutjen-Drecoll, E. (2001) Transforming growth factor beta 2 levels in the aqueous humor in different types of glaucoma and the relation to filtering bleb development. *Graef. Arch. Clin. Exp. Ophthalmol.* **239**, 199–207, https://doi.org/10.1007/s004170000252
35 Kaeslin, M.A., Killer, H.E., Fuhrer, C.A., Zeleny, N., Huber, A.R. and Neutzner, A. (2016) Changes to the aqueous humor proteome during glaucoma. *PLoS ONE* **11**, e0165314, https://doi.org/10.1371/journal.pone.0165314
36 Borkenstein, A., Faschinger, C., Maier, R., Weger, M., Theisl, A., Demel, U. et al. (2013) Measurement of tumor necrosis factor-alpha, interleukin-6, Fas ligand, interleukin-1alpha, and interleukin-1beta in the aqueous humor of patients with open angle glaucoma using multiplex bead analysis. *Mol. Vis.* **19**, 2306–2311
37 Smolen, J.S., Beaulieu, A., Rubbert-Roth, A., Ramos-Remus, C., Rovensky, J., Alecock, E. et al. (2008) Effect of interleukin-6 receptor inhibition with tocilizumab in patients with rheumatoid arthritis (OPTION study): a double-blind, placebo-controlled, randomised trial. *Lancet* **371**, 987–997, https://doi.org/10.1016/S0140-6736(08)60453-5
38 Piguet, P.F., Vesin, C., Grau, G.E. and Thompson, R.C. (1993) Interleukin 1 receptor antagonist (IL-1ra) prevents or cures pulmonary fibrosis elicited in mice by bleomycin or silica. *Cytokine* **5**, 57–61, https://doi.org/10.1016/1043-4666(93)90024-Y
39 Kong, X., Feng, D., Wang, H., Hong, F., Bertola, A., Wang, F.S. et al. (2012) Interleukin-22 induces hepatic stellate cell senescence and restricts liver fibrosis in mice. *Hepatology* **56**, 1150–1159, https://doi.org/10.1002/hep.25744
40 Zhang, L.J., Zheng, W.D., Chen, Y.X., Huang, Y.H., Chen, Z.X., Zhang, S.J. et al. (2007) Antifibrotic effects of interleukin-10 on experimental hepatic fibrosis. *Hepatogastroenterology* **54**, 2092–2098
41 Inoue, T., Kawaji, T. and Tanihara, H. (2014) Monocyte chemotactic protein-1 level in the aqueous humour as a prognostic factor for the outcome of trabeculectomy. *Clin. Exp. Ophthalmol.* **42**, 334–341, https://doi.org/10.1111/ceo.12204
42 Leibovich, S.J. and Ross, R. (1975) The role of the macrophage in wound repair. A study with hydrocortisone and antimacrophage serum. *Am. J. Pathol.* **78**, 71–100
43 Chong, R.S., Jiang, Y.Z., Boey, P.Y., Yu, S.J., Htoon, H.M., Aung, T. et al. (2010) Tear cytokine profile in medicated glaucoma patients: effect of monocyte chemoattractant protein 1 on early posttrabeculectomy outcome. *Ophthalmology* **117**, 2353–2358, https://doi.org/10.1016/j.ophtha.2010.03.064
44 Taniguchi, H., Kojima, R., Sade, H., Furuya, M., Inomata, N. and Ito, M. (2007) Involvement of MCP-1 in tubulointerstitial fibrosis through massive proteinuria in anti-GBM nephritis induced in WKY rats. *J. Clin. Immunol.* **27**, 409–429, https://doi.org/10.1007/s10875-007-9085-z

45 Ferreira, A.M., Takagawa, S., Fresco, R., Zhu, X., Varga, J. and DiPietro, L.A. (2006) Diminished induction of skin fibrosis in mice with MCP-1 deficiency. *J. Invest. Dermatol.* **126**, 1900–1908, https://doi.org/10.1038/sj.jid.5700302
46 Lloyd, C.M., Dorf, M.E., Proudfoot, A., Salant, D.J. and Gutierrez-Ramos, J.C. (1997) Role of MCP-1 and RANTES in inflammation and progression to fibrosis during murine crescentic nephritis. *J. Leukoc. Biol.* **62**, 676–680, https://doi.org/10.1002/jlb.62.5.676
47 Garweg, J.G., Zandi, S., Pfister, I.B., Skowronska, M. and Gerhardt, C. (2017) Comparison of cytokine profiles in the aqueous humor of eyes with pseudoexfoliation syndrome and glaucoma. *PLoS ONE* **12**, e0182571, https://doi.org/10.1371/journal.pone.0182571
48 Wang, Y., Chen, S., Liu, Y., Huang, W., Li, X. and Zhang, X. (2018) Inflammatory cytokine profiles in eyes with primary angle-closure glaucoma. *Biosci. Rep.* **38**, 1–9, https://doi.org/10.1042/BSR20181411
49 Jablonska-Trypuc, A., Matejczyk, M. and Rosochacki, S. (2016) Matrix metalloproteinases (MMPs), the main extracellular matrix (ECM) enzymes in collagen degradation, as a target for anticancer drugs. *J. Enzyme Inhib. Med. Chem.* **31**, 177–183, https://doi.org/10.3109/14756366.2016.1161620
50 Wong, T.T., Mead, A.L. and Khaw, P.T (2003) Matrix metalloproteinase inhibition modulates postoperative scarring after experimental glaucoma filtration surgery. *Invest. Ophthalmol. Vis. Sci.* **44**, 1097–1103, https://doi.org/10.1167/iovs.02-0366
51 Hinz, B., Phan, S.H., Thannickal, V.J., Galli, A., Bochaton-Piallat, M.L. and Gabbiani, G. (2007) The myofibroblast: one function, multiple origins. *Am. J. Pathol.* **170**, 1807–1816, https://doi.org/10.2353/ajpath.2007.070112
52 Zhang, H.Y. and Phan, S.H. (1999) Inhibition of myofibroblast apoptosis by transforming growth factor beta(1). *Am. J. Respir. Cell Mol. Biol.* **21**, 658–665, https://doi.org/10.1165/ajrcmb.21.6.3720
53 Osborne, N.N. and del Olmo-Aguado, S. (2013) Maintenance of retinal ganglion cell mitochondrial functions as a neuroprotective strategy in glaucoma. *Curr. Opin. Pharmacol.* **13**, 16–22, https://doi.org/10.1016/j.coph.2012.09.002
54 Tezel, G., Yang, X. and Cai, J. (2005) Proteomic identification of oxidatively modified retinal proteins in a chronic pressure-induced rat model of glaucoma. *Invest. Ophthalmol. Vis. Sci.* **46**, 3177–3187, https://doi.org/10.1167/iovs.05-0208
55 Quigley, H.A., Nickells, R.W., Kerrigan, L.A., Pease, M.E., Thibault, D.J. and Zack, D.J. (1995) Retinal ganglion cell death in experimental glaucoma and after axotomy occurs by apoptosis. *Invest. Ophthalmol. Vis. Sci.* **36**, 774–786
56 Kerrigan, L.A., Zack, D.J., Quigley, H.A., Smith, S.D. and Pease, M.E. (1997) TUNEL-positive ganglion cells in human primary open-angle glaucoma. *Arch. Ophthalmol.* **115**, 1031–1035, https://doi.org/10.1001/archopht.1997.01100160201010
57 Schwab, C., Glatz, W., Schmidt, B., Lindner, E., Oettl, K., Riedl, R. et al. (2017) Prevalence of posterior vitreous detachment in glaucoma patients and controls. *Acta Ophthalmol. Scand.* **95**, 276–280, https://doi.org/10.1111/aos.13339

Experimental Eye Research 125 (2014) 53–61

Contents lists available at ScienceDirect

Experimental Eye Research

journal homepage: www.elsevier.com/locate/yexer

Corneal epithelial and neuronal interactions: Role in wound healing

Bhavani S. Kowtharapu [a, *, 1], Thomas Stahnke [a, 1], Andreas Wree [b], Rudolf F. Guthoff [a], Oliver Stachs [a]

[a] Department of Opthalmology, University of Rostock, Doberaner Strasse 140, 18057 Rostock, Germany
[b] Institute of Anatomy, University of Rostock, Gertrudenstrasse 9, 18057 Rostock, Germany

ARTICLE INFO

Article history:
Received 11 December 2013
Accepted in revised form 7 May 2014
Available online 28 May 2014

Keywords:
corneal epithelial cells
trigeminal neurons
substance P
bone morphogenetic protein 7
wound healing
epithelial-to-mesenchymal transition

ABSTRACT

Impaired corneal innervation and sensitivity are the main causes of corneal neurotrophic keratopathy which simultaneously also leads to poor epithelial wound healing. Restoration of the diminished communication between the corneal epithelium and trigeminal nerve is indispensable for the proper functioning of the epithelium. The present study aims to investigate corneal epithelial and trigeminal neuron interactions to shed light on corneal wound healing during neurotrophic keratopathy. Mouse trigeminal neurons and corneal epithelial cells were cultured according to standard methods. To study the effect of corneal epithelial cells on trigeminal neurons as well as the effect of trigeminal neurons on corneal epithelial cells during wound healing, conditioned media from the cultures of pure trigeminal neurons (CNM) and corneal epithelial cells (CEM) were collected freshly and applied on the other cell type. Neurite outgrowth assay and RT-PCR analysis using primers specific for substance P (SP), Map1a, Map1b were performed on trigeminal neurons in the presence of CEM. We observed an increase in the neurite outgrowth in the presence of CEM and also in co-culture with corneal epithelial cells. Increase in the expression of SP mRNA and a decrease in the expression of Map1b mRNA was observed in the presence of CEM. We also observed the presence of epithelial-to-mesenchymal transition (EMT)-like phenomenon during wound healing using a scratch assay in primary corneal epithelial cultures. This system was further employed to study the effect of CNM on corneal epithelial cells in the context of wound healing to find the effect of trigeminal neurons on epithelial cells. RT-PCR analysis of Pax6 expression in corneal epithelial cell cultures with scratch served as a positive control. Further, we also show the expression of bone morphogenetic protein 7 (BMP7) mRNA in corneal epithelial cells which is decreased gradually along with Pax6 mRNA when cultured together in the presence of CNM. The expression and down regulation of BMP7 in the presence of CNM was further confirmed at the protein level by western blotting. From this study it seems that the epithelial and neuronal interactions in the cornea may contribute to the corneal innervation as well as recovery of corneal epithelial cells during injury. Appraising the differences in the expression of various signalling molecules during EMT of epithelial cells in the presence of SP and BMP7 gives an insight into the detailed dissection of the involved signalling pathways to develop future therapeutics.

1. Introduction

The cornea, the outermost layer of the eye, is a transparent, clear, convex avascular structure that is one of the most highly innervated tissues in the body. Its outer epithelial layer is the region where nerve endings are localized. The ophthalmic branch of the trigeminal ganglion (TG) sensory nerve fibres entering the corneal stroma through the limbal area is responsible for the innervation of the corneal epithelium (de Leeuw and Chan, 1989). Before penetrating Bowman's layer in the cornea, the trigeminal sensory nerve fibres lose their myelin sheath and densely innervate the apical wing cell level of the epithelium (Müller et al., 2003). These corneal nerves include peptidergic, sympathetic and parasympathetic nerve fibres and, by secreting neurotransmitters such as calcitonin gene-related peptide, neuropeptide Y, catecholamines, and

* Corresponding author. Tel.: +49 3814948545; fax: +49 3814948502.
E-mail addresses: kbhavanis@gmail.com, kowthara@med.uni-rostock.de (B.S. Kowtharapu), thomas.stahnke@med.uni-rostock.de (T. Stahnke), andreas.wree@med.uni-rostock.de (A. Wree), rudolf.guthoff@med.unirostock.de (R.F. Guthoff), oliver.stachs@med.uni-rostock.de (O. Stachs).
[1] Equal contribution.

http://dx.doi.org/10.1016/j.exer.2014.05.006
0014-4835/

acetylcholine (Shimizu, 1982; Tervo et al., 1982), they modulate the proliferation and differentiation of the epithelium and also play an important role in corneal epithelial wound healing.

Diminished TG nerve function causes epithelial alterations and adversely affects the wound healing process (Beuerman and Schimmelpfennig, 1980). Through the release of neurotrophic factors, TG sensory nerves influence signal transduction cascades involved in epithelial wound healing and homeostasis (Garcia-Hirschfeld et al., 1994; Kim et al., 2009). Altered corneal epithelial barrier function and delayed wound healing have been observed following disruption of TG (Gallar et al., 1990; Goins, 2005), leading to decreased vision, which can be treated by administration of substance P (SP) and insulin-like growth factor-1 (Nagano et al., 2003). These findings highlight the influence of sensory nerves on corneal epithelial functional restoration and suggest that the trophic effects of sensory nerves on corneal epithelium are mediated partly by the neuropeptides secreted from the nerve terminals (Gallar et al., 1990).

Impairment of trigeminal nerve function and insufficient supply of neural factors are the principal causes of corneal neurotrophic keratopathy, a condition that may consequently also lead to dry eye because of the disruption of neural input to the cornea (Nishida and Yanai, 2009). Clinical application of autologous serum eye drops as well as other neurotransmitters and peptides (Matsumoto et al., 2004) promotes corneal reinnervation and accelerates wound healing (Freire et al., 2012; Müller et al., 2003; Rao et al., 2010). Similarly, secreted neurotrophic factors from cultured corneal epithelial cells can stimulate the outgrowth of neurites from TG neurons and prolong their survival (Chan and Haschke, 1981, 1982). Development of a tissue culture model of the innervated ocular surface for studying functional relationships of various cornea–-trigeminal interactions (Forbes et al., 1987) has further helped to show the trophic effect of TG neurons on corneal epithelial cells (Baker et al., 1993; Garcia-Hirschfeld et al., 1994). These reports demonstrate that, during treatment for corneal epithelial disorders, it is necessary to maintain the cooperative interplay between the corneal epithelial and neural cell microenvironments: the resultant activation of neural cells in turn provides sufficient neural signals to support the corneal epithelial cells, and vice versa (Nishida and Yanai, 2009).

In the process of corneal wound healing, transforming growth factor-β and upregulation of Slug (Aomatsu et al., 2011, 2012; Chandler et al., 2007) are known to induce epithelial-to-mesenchymal transition (EMT)-like cellular morphology, migration and cadherin switching in corneal epithelial cells. Since the cornea is highly innervated with nerve endings, studies explaining the role of neuronal involvement in the induction of EMT help to increase our understanding of epithelial–neuronal interactions during wound healing.

The aim of the present study was to analyse epithelial–neuronal interactions and their involvement in controlling EMT during wound healing using murine corneal epithelial and TG neuron primary cell cultures. To assess the influence of TG neurons on epithelial cells and vice versa, we collected the conditioned media from corneal epithelial and TG neuron cultures, applied them to the other cell type and studied the expression of different molecules in the presence of conditioned medium.

2. Materials and methods

2.1. Materials

Serum-free culture media for the culture of mouse primary neurons (NeuroCult SM1 and SM2 Neuronal Culture Kit) was purchased from Stemcell Technologies (Grenoble, France). Keratinocyte-serum free medium (KSFM) for mouse corneal epithelial cell culture was purchased from Life Technologies (Darmstadt, Germany). Neurite outgrowth staining kit was obtained from Molecular Probes (Darmstadt, Germany). Antibodies used in this study were: anti-BMP7 (ab56023, Abcam, Cambridge, UK), anti-Substance P (250865, Abbiotec, Köln, Germany), anti-E-cadherin (24E10, Cell Signaling, Frankfurt, Germany), anti-cytokeratin 12 (Sc-17101, Santacruz, Heidelburg, Germany), monoclonal anti-β-tubulin (T5293, Sigma–Aldrich, Munich, Germany), monoclonal anti-vimentin (V6630, Sigma–Aldrich), anti-β-III-tubulin (ab18207, Abcam), monoclonal anti-NeuN (MAB377, Chemicon, Darmstadt, Germany), anti-ZO-1 (MAB1520, Chemicon), anti-GAPDH (Sc-25778, Santacruz). HRP-conjugated secondary anti-rabbit IgG (170–6515) was from Bio-Rad (Munich, Germany). Papain and Dispase enzymes for the digestion of mouse trigeminal ganglion were obtained from Sigma–Aldrich (Munich, Germany) and Collagenase NB4 from Serva Electrophoresis GmbH (Heidelberg, Germany). Tissue culture 10 cm dishes and 6-well, 12-well plates were obtained from Nunc (Thermo Fisher scientific, Massachusetts, USA). Coverslips and glass slides were from Marienfeld (Bonn, Germany) and 96-well microtiter plates were from PAA (Cölbe, Germany). ECL prime detection western blotting reagent was purchased from Amersham and other western blotting reagents were from Bio-Rad (Munich, Germany). FastLane Cell cDNA kit was from Qiagen and HotMaster mix and other molecular biology reagents were purchased from 5 Prime GmbH, Germany. Primers required for RT-PCR were synthesized from Metabion GmbH (Martinsried, Germany). All other biochemical reagents and growth factors used in this study were purchased from Sigma–Aldrich.

2.2. Ethics statement

All animals used in this study were treated in accordance with the guidelines of the Institutional Animal Ethics Committee of the University of Rostock.

2.3. Cell culture

TG sensory neurons from BALB/c mice (Charles River, Germany), aged between 45 and 60 days, were cultured according to the protocol described by Malin et al. (2007). Briefly, mouse skull caps were removed after death and brain was lifted to expose the TGs (two from each mouse) at the base of the skull cavity. By cutting at the anterior and posterior ends, the TG were removed carefully, washed in calcium and magnesium-free Hanks' balanced salt solution (HBSS). Later, collected TGs were diced into small pieces, and incubated in papain (Sigma–Aldrich) 20 U/mL for 20 min at 37 °C. After triturating and further incubation in 0.3% Dispase-II (Sigma–Aldrich) and 0.4% collagenase (Serva) for another 20 min at 37 °C, centrifugation through 30% and 60% Percoll (PAA) density gradients was performed to remove cell debris from the neuron cell bodies. After isolation procedure, dissociated TG neurons were seeded at a plating density of approximately 3000 neurons/well in serum-free neuronal basal medium supplemented with SM1 (Stemcell Technologies) and 1% penicillin/streptomycin on poly-L-lysine (PAA) and laminin I (Trevigen) coated culture dishes and cultured under humidified conditions (37 °C, 95% humidity, 5% CO_2) with regular replacement of medium every second day. For the collection of conditioned neuron medium (CNM), neuronal basal medium without any supplements was added to the PBS washed TG neuron cultures and the medium was collected after 24 h.

For primary culture, mouse corneas were isolated and cultured by explant method of Hazlett et al. (1996) as this method was

shown to express major corneal epithelial markers similar to fresh corneal epithelia. Central corneal buttons were cut from the mouse eye under a stereo microscope, washed in HBSS and transferred to cell culture dishes epithelial side up for 5 min to allow for attachment of the explant before addition of complete culture medium (15 ml KSFM, 19 ml DMEM:F12, 5 ml fetal bovine serum (12.5% v/v), 125 μM β-mercaptoethanol, 25 mM HEPES supplemented with 100 ng/ml cholera toxin and antibiotics). The cultures were incubated at 37 °C, 95% humidity, 5% CO_2 with regular medium changes every second day. After 7 days the explant was removed and the cultured cells were used for experiments. For the collection of conditioned epithelial medium (CEM), KSFM without any supplements was added to the PBS washed confluent epithelial cultures and the respective medium was collected after 24 h.

During co-culture of corneal epithelial cells and TG neurons, the corneal explant was removed after 7 days in culture and seeded with dissociated TG neurons resuspended in neuronal basal medium supplemented with SM2.

2.4. Reverse transcription-polymerase chain reaction (RT-PCR)

First-strand cDNAs were generated directly from cultured corneal epithelial cells or TG neurons to represent accurate *in situ* cellular gene expression profile using FastLane Cell cDNA kit (Qiagen) according to the manufacturer instructions. Equal amount of cDNA was amplified by PCR to study the expression profile of mRNAs using specific primers for SP, microtubule-associated protein 1a (Map1a), microtubule-associated protein 1b (Map1b), Pax6, bone morphogenetic protein 7 (BMP7), E-cadherin and β-actin (Table 1). Intron/exon spanning primers were designed from the respective GenBank sequences using VectorNTI software (Invitrogen) based on minimal hairpin, duplex formation and guanine cytosine composition. Samples were denatured for 5 min at 94 °C followed by 30 PCR cycles of denaturation for 30 s at 94 °C, annealing 30 s at 55 °C and extension for 30 s at 72 °C. The final elongation was performed at 72 °C for 5 min. The quality of cDNA was confirmed in each PCR reaction using primers specific for β-actin which was also served as a positive control for RT-PCR method. Samples without any cDNA were also included in each amplification reaction to serve as negative controls. PCR products were analysed on 1.5% agarose gels by electrophoresis.

2.5. Quantification of neurite outgrowth

Neurite outgrowth of TG neurons in the presence of CEM was measured by using neurite outgrowth staining kit (Molecular Probes) following manufacturer's instructions. Briefly, neuronal basal medium and freshly collected CEM was mixed in 1:1 ratio and added to the 2 days old TG neuron cultures. After 24 h, cell viability and the neurite outgrowth were measured (relative fluorescence units, RFU) simultaneously using a fluorescence plate reader (Wallac 1420 Multilabel Counter, Perkin Elmer) by adding a cell-permeable viability indicator dye which emits green fluorescence in live cells (excitation/emission: 485/535 nm), whereas neurite outgrowth was measured by bright orange–red fluorescence coming from the staining of outer cell membrane surface (excitation/emission: 530/590 nm). All measurements were taken in quadruplicate.

2.6. Immunofluorescence

Cells grown on glass coverslips were fixed with 3% paraformaldehyde for 10 min after washing with PBS and then permeabilized with PBS containing 0.1% Triton X-100 (Sigma–Aldrich) and 2% FCS for 30 min. Fixed and permeabilized cells were then incubated with primary antibodies for intracellular staining. All primary antibodies in this study were used at the 1:100 dilutions in PBS and incubated for 60 min at room temperature. The cells were then washed with PBS before adding secondary donkey anti-mouse IgG (H + L)-Alexa Fluor 488 (diluted 1:50) or donkey anti-rabbit IgG (H + L)-Cy3 (diluted 1:100) and incubated at room temperature for 45 min, washed with PBS and mounted in mounting medium (Vector Labs) containing 4,6-diamidino-2-phenylindole (DAPI). Cells stained with only secondary antibodies were served as a control and did not show any specific staining. Cells were observed under Nikon confocal fluorescence microscope equipped with digital camera (Nikon Eclipse E400 with D-Eclipse C1) and all images were taken from a single plane through the cell monolayers with 40× or 10× objectives using the same settings.

Quantification of the intensity of SP immunofluorescence in TG neurons was performed using ImageJ software and the corrected total cell fluorescence (CTCF) for each condition was calculated in arbitrary units (arb. unit) using the following formula according to Gavet and Pines (2010).

$$\text{CTCF} = \text{whole cell fluorescence signal density} - (\text{area of measured cell X mean fluorescence of background signal})$$

Table 1
PCR primers used in this study.

Target	Primer	Primer sequence (5′–3′)	Amplicon size (bp)	GenBank accession
Substance P	fwd	TAAATTATTGGTCCGACTGGTCCG	291	NM_009311
	rev	AGTTCTGCATCGCGCTTCTTTC		
Map1a	fwd	AGGATCCACAGCCTTGGGGTC	240	NM_032393
	rev	ATCAGAGTCACCTGAAGGTTCTCCC		
Map1b	fwd	GAGCTGGGGATCCGATCGTG	361	NM_008634
	rev	GGTGGGTGGTGCTTAGGAGCTC		
actin	fwd	GCTGTCCCTGTATGCCTCTGGTC	463	NM_007393
	rev	GAGGTCTTTACGGATGTCAACGTCAC		
Pax6	fwd	GCTTGGTGGTGTCTTTGTCAACG	341	NM_001244198
	rev	CCCTCGGATAATAATCTGTCTCGGA		
BMP7	fwd	TCACAGCCACCAGCAACCACTG	451	NM_007557
	rev	ATGGCGTGGTTGGTGGCG		
E-cadherin	fwd	GCTTGGATTTTGAGGCCAAGCA	284	NM_009864
	rev	AATCTCCAGCCAGTTGGCAGTGTC		

Five different individual measurements from different images were taken for each condition to calculate the mean CTCF.

2.7. Immunoblotting

Corneal epithelial monolayers were washed in PBS and lysed in RIPA buffer (Sigma–Aldrich) containing protease and phosphatase inhibitors (Roche). Equal amount of total cell lysates (30 μg protein per lane) were loaded into the wells and separated by SDS-PAGE using 10% polyacrylamide gels and transferred onto PVDF membranes (Bio-Rad). Membranes were blocked with 5% non-fat dry milk powder in TBS for 30 min and incubated with anti-BMP7 (diluted 1:500) and anti-GAPDH (diluted 1:500) primary antibodies overnight at 4 °C. After washing, membranes were incubated with secondary HRP-conjugated anti rabbit IgG (diluted 1:2500) for 1 h at room temperature and developed using ECL detection system (Amersham).

2.8. Statistical analyses

Statistical analyses were performed using SPSS software. Analysis of variance (ANOVA) was performed to determine differences among fluorescence intensities between the groups. *P*-values were determined by one-way ANOVA and the values <0.05 were considered statistically significant.

3. Results

3.1. TG neurons in culture

After seeding the dissociated TG neurons in culture dishes, gradual development of profuse axonal arborizations from the cultured TG neurons was observed until 3 days as shown in Fig. 1A–D. Neuron specific anti-β-III tubulin and anti-NeuN antibodies as well as glial cell- specific GFAP antibody were used to confirm the presence of neurons in TG culture (Fig. 1E–J).

3.2. Neuron–epithelial interactions and effect of CEM on TG neurons in culture

To study the effect of epithelial cells on neurons, we cultured neurons in freshly collected CEM and measured cell viability and neurite outgrowth after 24 h. Control cultures received fresh KSFM during this period of time. We have observed an increase in the neurite outgrowth of TG neurons in the presence of CEM without any significant difference in cell viability when compared to control cultures treated with only neuronal basal medium (Fig. 2A–B). This phenomenon was also observed in neuron–epithelial co-cultures, with significant increase in neurite outgrowth and neurons contacting the epithelial cells with their elongated neurites were observed within 24 h of seeding (Fig. 2C–D). These observations

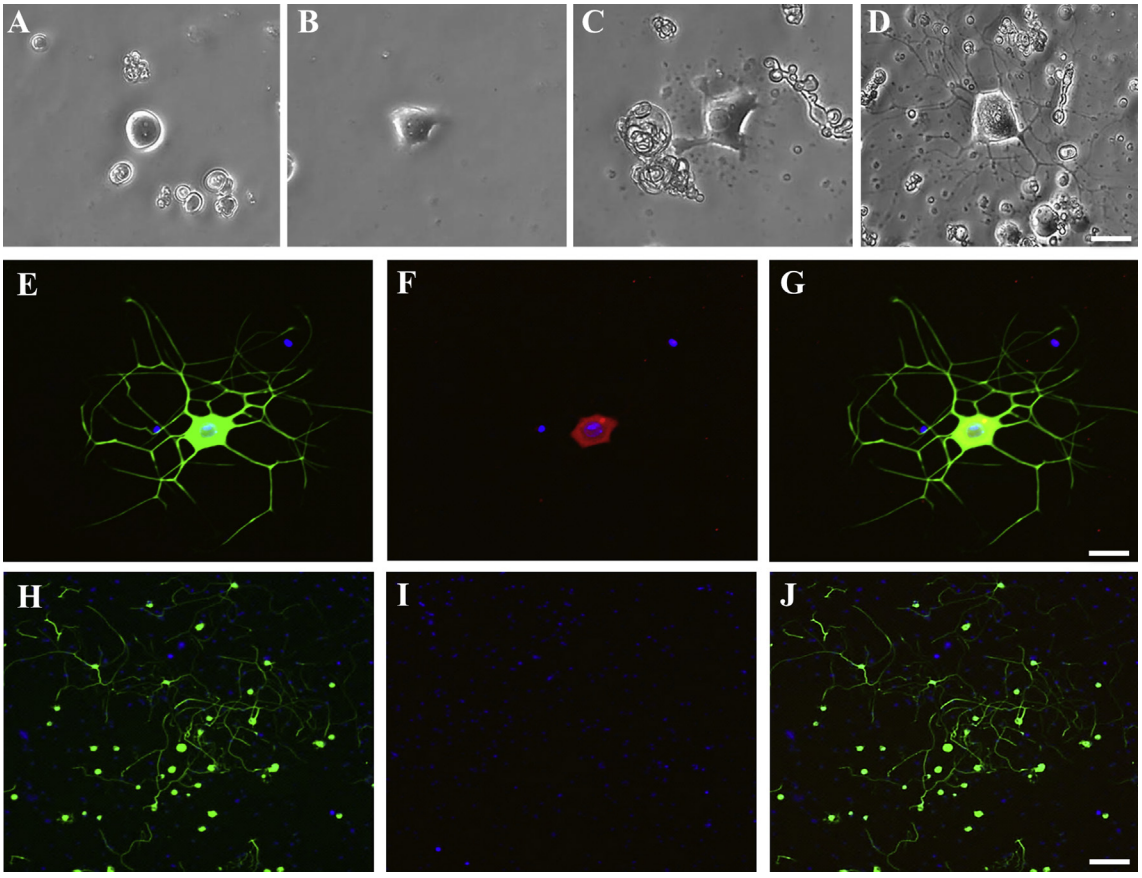

Fig. 1. Mouse trigeminal (TG) neurons in culture. Light microscopic images of TG neurons (A) immediately after seeding on poly-L-lysine and laminin coated culture dishes; (B, C) after 24 and 48 h of plating, neurite outgrowth was visible from the neurons; (D) by 3 days after plating, neurons fully develop an extensive network of dendrites in culture. Scale Bar: 25 μm. Fluorescence microscopic images of TG neurons (E) stained with neuron specific anti-β-III tubulin (green) and (F) anti-NeuN antibodies (red), respectively. Nuclei stained with DAPI (blue); (G) overlay of the images E, F. Scale bar: 25 μm. Cytoskeletal and cytoplasmic localization of fluorescence signal in TG neurons stained with anti-β-III tubulin and anti-Neu-N antibodies were evident. Fluorescence microscopic images of TG neurons (H) stained with neuron specific anti-β-III tubulin (green) and (I) glial cell specific anti-GFAP (red) antibodies, respectively. Absence of GFAP staining (red) confirms the presence of only neurons without any glial cells in culture. Nuclei stained with DAPI (blue); (J) overlay of the images H, I. Scale bar: 100 μm. (For interpretation of the references to colour in this figure legend, the reader is referred to the web version of this article.)

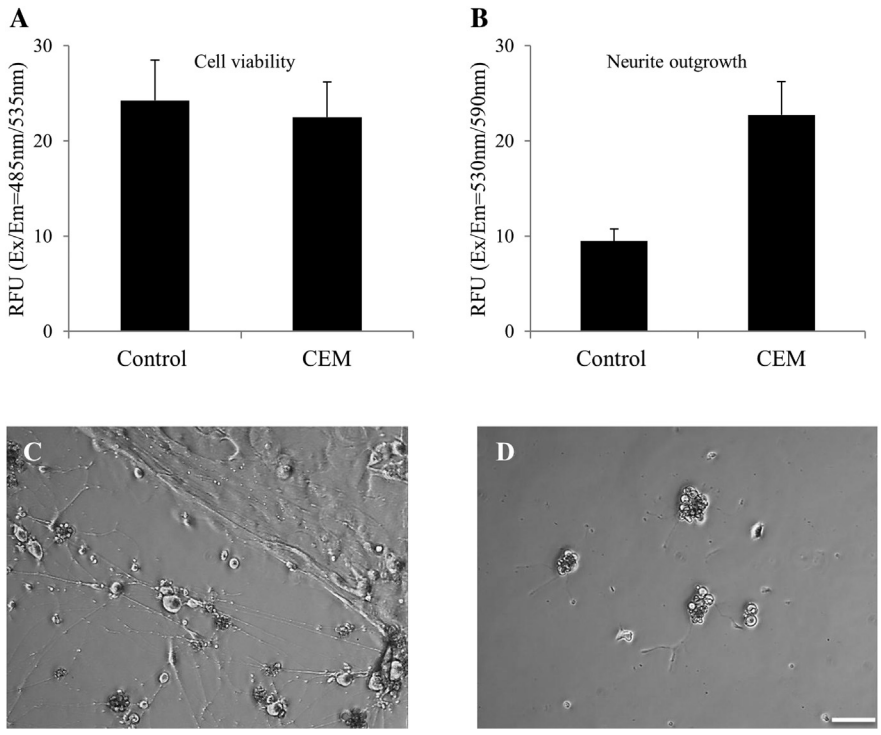

Fig. 2. Trigeminal neuron and corneal epithelial cell interactions in culture. Extensive neurite outgrowth from neurons was observed when cultured together with epithelial cells. This is also confirmed further by culturing neurons in the presence of conditioned medium from the corneal epithelial cells (CEM). Cell viability (A) in the presence of CEM was measured in relative fluorescence units (RFU) at Ex/Em = 485/535 nm whereas the neurite outgrowth from neurons (B) was measured at Ex/Em = 530/590 nm by using a fluorescent plate reader at 37 °C. Each experiment was repeated three times and all measurements were performed in quadruplicate. Light microscopic images of TG neurons (C) seeded and co-cultured in the presence of epithelial cells, and (D) in the absence of epithelial cells, respectively. Scale bar: 25 μm.

confirm the ongoing interactions between corneal epithelial cells and TG neurons. To study the differences related to this phenomena, we performed RT-PCR analysis of SP, Map1a and Map1b mRNAs in TG neurons after the addition of CEM. We observed an increase in the expression of SP mRNA and a substantial decrease in Map1b mRNA expression levels without any significant difference in the expression of Map1a mRNA under these conditions. The appearance of two sharp bands on the gel using SP specific primers denotes the differential processing of the gene preprotachykinin I (PPT-I), which encodes SP and neurokinin A (Nelson and Bost, 2005) by posttranslational processing of precursor PPT-I (Fig. 3A). Immunocytochemistry was later performed using an anti-SP antibody on the TG neuron cultures. Confirming our RT-PCR data, an increase in the intensity of SP fluorescence signal was observed ($P < 0.05$, one-way ANOVA) along with elongated neurite outgrowth in the presence of CEM as well as in neuron-epithelial co-cultures (Fig. 3B–C).

3.3. Corneal epithelial cells and EMT

During the culture of corneal epithelial cells from mouse cornea, cells with cobblestone morphology were seen growing out of the corneal explants in 3–4 days. The confluent corneal epithelial cells were stained with anti-cytokeratin12 antibody to confirm their epithelial origin. Expression of E-cadherin, a marker for epithelial cells, and the formation of functional epithelial tight junctions in culture were also confirmed by staining with anti-E-cadherin and anti-ZO-1 antibodies (Fig. 4). To observe the presence of EMT in mouse corneal epithelial cells *in vitro*, a scratch assay was performed on confluent epithelial cultures and these cells were stained with anti-vimentin antibody, a specific marker for the cells undergoing EMT. Two days later, the scratch was renewed by cells migrating from the scratch edge and the occurrence of vimentin-positive cells in the wound area confirms the appearance of EMT in corneal epithelial cell cultures during wound healing (Fig. 5).

3.4. Effect of CNM on corneal epithelial cells during wound healing

Since it was possible to detect the appearance of EMT in culture with the scratch assay, we used the same experimental system to detect the effect of CNM on corneal epithelial cells in order to study the influence of neurons on epithelial cells in the context of wound healing. After the scratch was made on confluent epithelial culture, cells were washed and cultured in the presence of freshly collected CNM for 2 days. Cultures with scratch and without scratch and treated with neuronal basal medium were served as control. RT-PCR analysis of Pax6, E-cadherin and BMP7 mRNAs were performed on cDNAs prepared from the above mentioned culture conditions. We observed a substantial decrease in the expression of Pax6 and BMP7 mRNAs after the addition of CNM to the epithelial cultures, whereas no difference in E-cadherin mRNA expression was noted under all culture conditions and β-actin mRNA expression served as an internal control. Appearance of two successive bands (299 + 341 bp) using Pax6 primers corresponds to the two isoforms that are expressed together in the eye (Kiselev et al., 2012). The decrease in the expression of BMP7 mRNA after the addition of CNM to the epithelial cells was further confirmed at the protein level – using lysates collected under similar experimental conditions – by western blotting using an anti-BMP7 antibody (Fig. 6).

4. Discussion

Establishing reliable and reproducible culture conditions is an essential step towards studying the role of corneal epithelial and neuronal interactions. In order to confirm the accuracy of our TG neuron and corneal epithelial culture conditions, we first studied

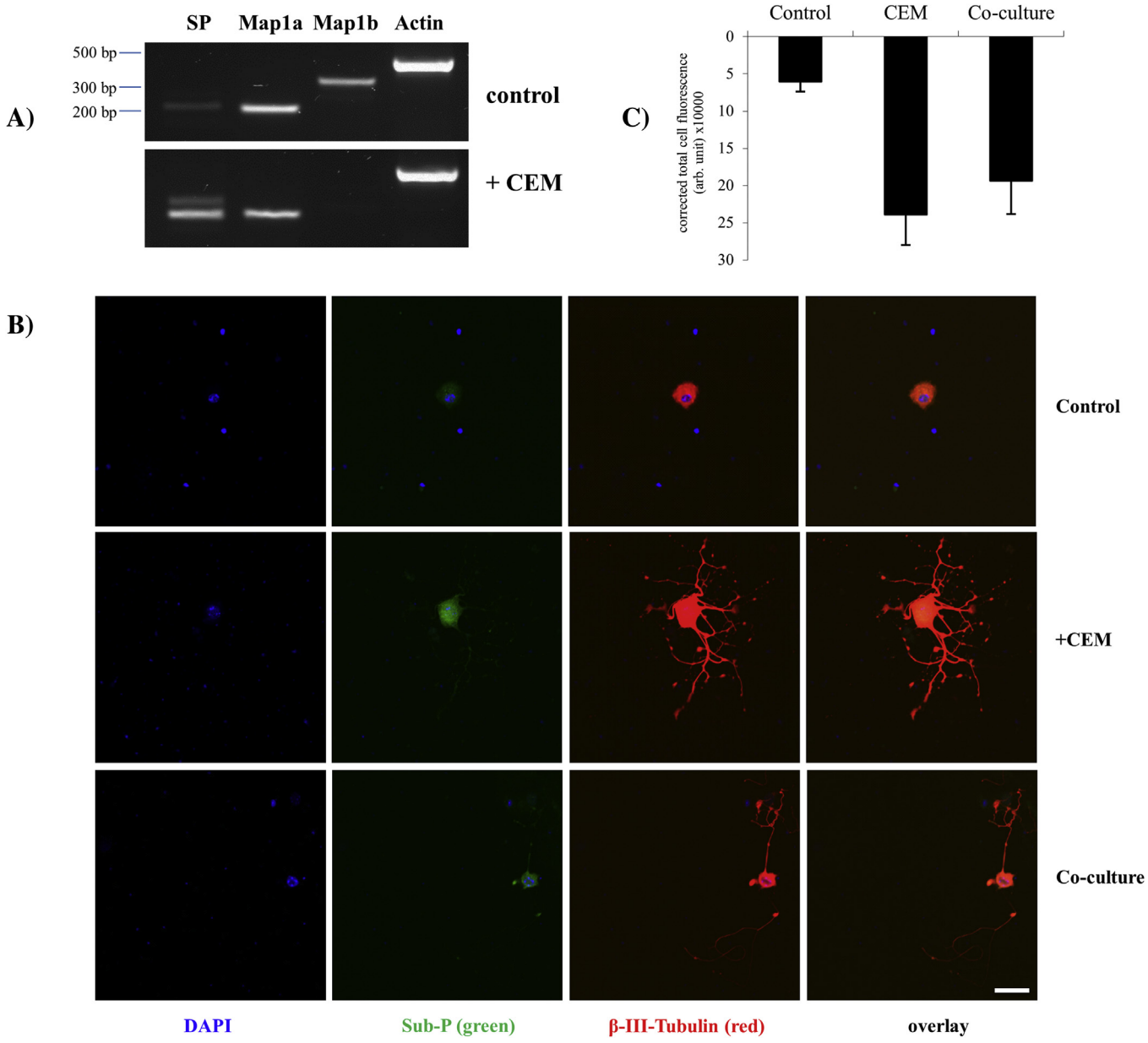

Fig. 3. Effect of corneal epithelial cells on TG neurons. (A) RT-PCR analysis of the expression of substance P (SP), Map1a, Map1b mRNA in TG neurons cultured in the presence of conditioned epithelial medium (CEM) from corneal epithelial cells. An increase in the expression of SP mRNA and a decrease in the expression of Map1b mRNA were observed in TG neurons cultured with CEM. No difference in the expression of Map1a mRNA was observed. A fragment specific for β-actin was amplified as a control for the RT-PCR method. After RT-PCR, samples were separated using 1.5% agarose gels in electrophoresis and the UV illuminated DNA was visualized by staining with ethidium bromide. (B) Immunofluorescence detection of the expression of SP in TG neurons after staining with anti-SP antibody. TG neurons cultured in control medium, with CEM or along with corneal epithelial cells were used in this experiment. An increase in SP fluorescence signal (green) along with an increase in the neurite outgrowth as shown by anti-β-III tubulin staining (red) in TG neurons cultured with CEM and also in epithelial co-cultures further confirms the previously shown RT-PCR and epithelial–neuronal co-culture results. Nuclei were counter stained with DAPI (blue). Scale bar: 25 μm. An overlay of the merged images of DAPI, SP and tubulin staining was also presented. (C) Fluorescence signal intensity was calculated using ImageJ software and plotted as corrected total cell fluorescence (CTCF) in arbitrary units (arb. unit) for each experimental condition to further confirm the differences observed in B. Statistical significance was determined by one-way ANOVA ($p < 0.05$). (For interpretation of the references to colour in this figure legend, the reader is referred to the web version of this article.)

the effect of epithelial cells on the neurite outgrowth of TG neurons as a functional parameter in culture. It had previously been shown that the presence of corneal epithelial cells alone can induce neurite outgrowth from dissociated TG neurons, suggesting the role of a neuronotrophic factor from epithelial cells (Chan and Haschke, 1982). In agreement with this report, in our system also, when co-cultured together or in the presence of CEM, we observed a substantial increase in the neurite outgrowth of TG neurons without any difference in cell viability. Having confirmed the interactions of TG neurons with corneal epithelial cells, the functional differences in TG neurons at the mRNA level were studied in the presence of CEM. Since cooperative interplay between the corneal epithelial and neural cell microenvironments is a known prerequisite for activating neural cells to provide sufficient neural signals to support the corneal epithelial cells and vice versa (Nishida and Yanai, 2009), the observed increase in the expression of SP mRNA and decrease in the expression of Map1b mRNA in the presence of CEM confirms ongoing communication between these

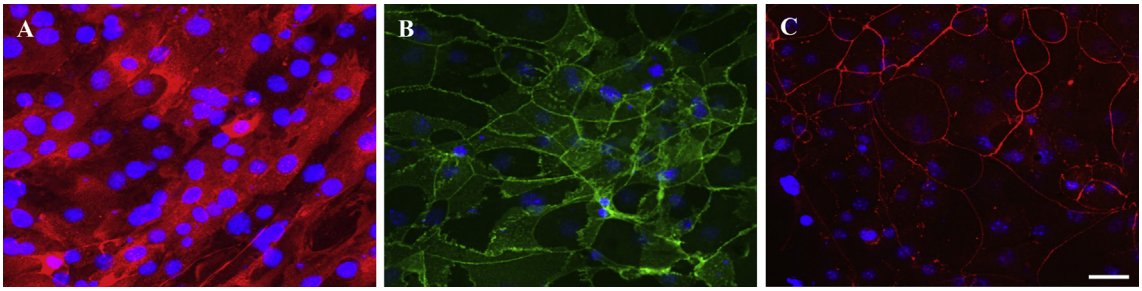

Fig. 4. Mouse corneal epithelial cells in culture. Corneal epithelial cells were cultured by corneal explant method and the presence of epithelial cells was confirmed by immunofluorescence detection of corneal epithelial cell marker (A) cytokeratin12 (red). The presence of E-cadherin in epithelial cell adhesion and the formation of specialized epithelial tight junctions in the cultured corneal epithelial cells were further confirmed by staining with (B) anti-E-cadherin (green) and (C) anti-ZO-1 antibodies (red), respectively. Nuclei were counterstained with DAPI (blue). Scale bar: 25 μm. (For interpretation of the references to colour in this figure legend, the reader is referred to the web version of this article.)

two cell types. SP functions as an injury-inducible messenger (Hong et al., 2009) and is involved in corneal epithelial wound healing (Nakamura et al., 2003; Yamada et al., 2004), in cell growth (Reid et al., 1993; Villablanca et al., 1994) as well as in inducing the expression of E-cadherin (Araki-Sasaki et al., 2000). Given its participation in the events related to wound healing it is possible that an increase in the expression of SP mRNA, in the presence of CEM, may also contribute to the recovery of corneal epithelial cells during injury. Map1b is associated with growing axons in neurons (Fischer and Romano-Clarke, 1991) and plays an important role in

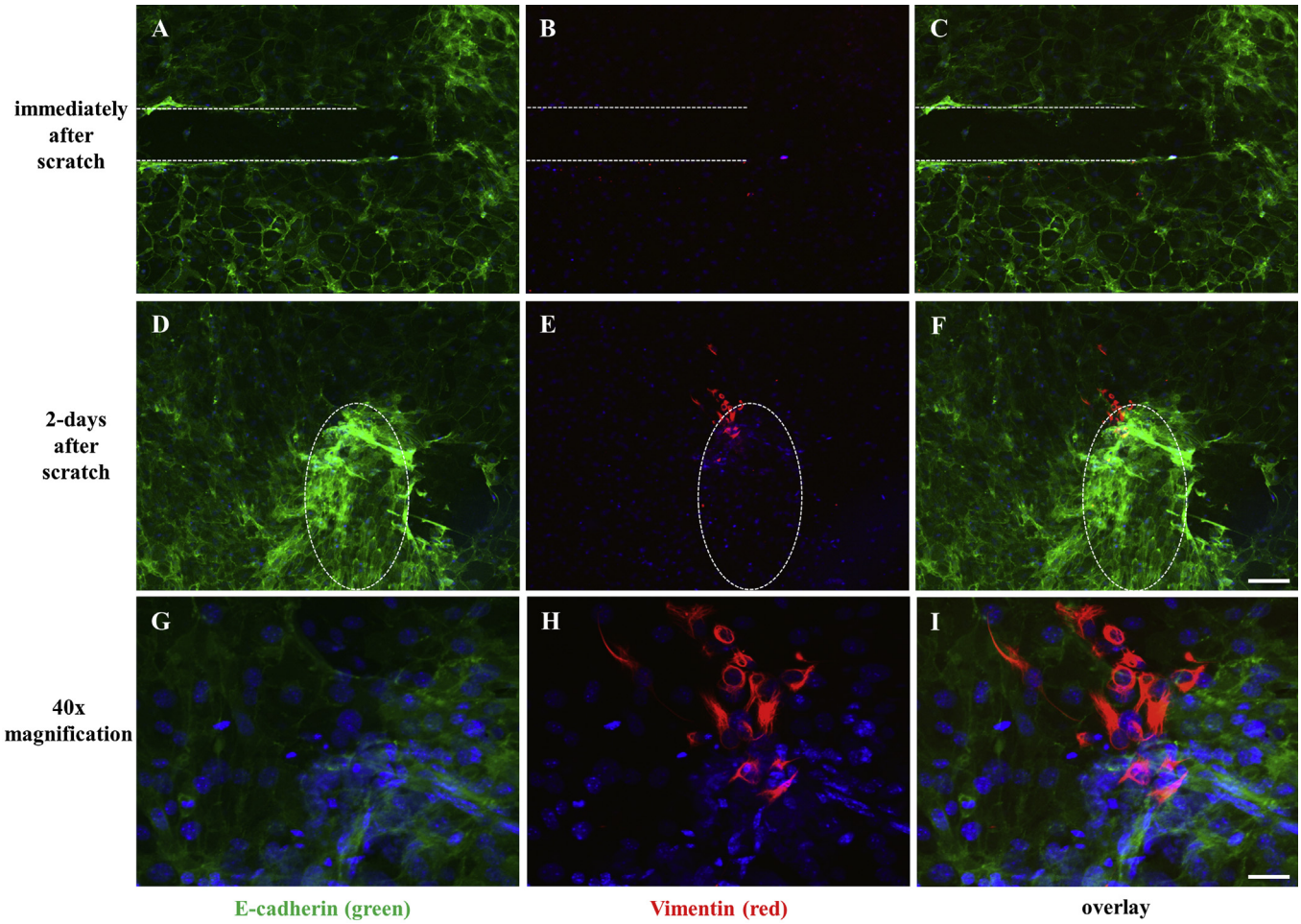

Fig. 5. Epithelial-to-mesenchymal transition (EMT) in cultured corneal epithelial cells. To study the presence of EMT in corneal epithelial cells a scratch was made on confluent epithelial cultures and the cells were fixed immediately, 2-days after scratch and immune stained for the detection of vimentin, a marker for the cells undergoing an EMT. Immediately after scratch, cells were stained with (A) anti-E-cadherin antibody (green) to show their epithelial origin and with (B) anti-vimentin antibody (red) to show their mesenchymal origin whereas (C) represents the merge of the images A, B and the white dotted lines depict the scratch area. Appearance of (D) anti-E-cadherin (green) and (E) anti-vimentin (red) positive cells in the scratch area, 2-days after scratch, confirms the transformation of epithelial cells into mesenchymal cells (EMT) in culture. The dotted circle denotes the scratch area and (F) represents the merge of the images E, F, respectively. Scale bar: 25 μm. Frames D, H and I represent the 40× magnification of the pictures D, E and F, respectively in the area of vimentin (red) positive cells. Nuclei were counterstained with DAPI (blue). Scale bar: 10 μm. (For interpretation of the references to colour in this figure legend, the reader is referred to the web version of this article.)

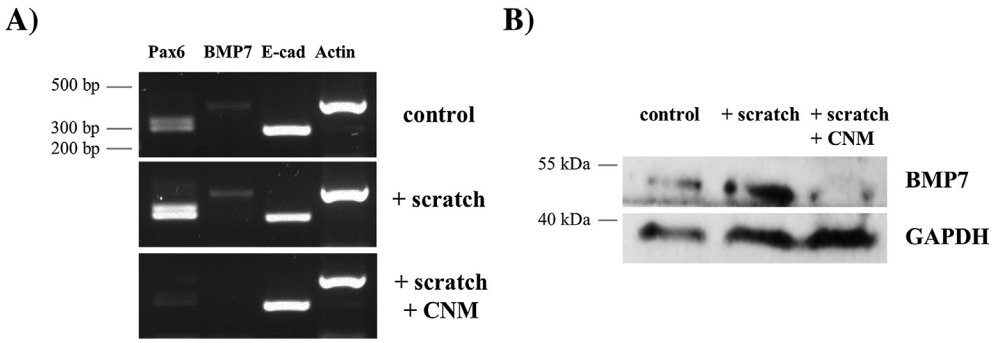

Fig. 6. Effect of TG neurons on corneal epithelial cells. (A) RT-PCR analysis of the expression of Pax6, bone morphogenetic protein 7 (BMP7) and E-cadherin (E-cad) in mouse corneal epithelial cells cultured with conditioned neuron medium (CNM) from TG neurons. Confluent corneal epithelial cell cultures without (control) and with scratch were used in this experiment. Cultures with scratch were maintained either in control media or in CNM for 2 days before the cDNA was prepared. An increase in the expression of Pax6 mRNA was observed immediately after the scratch which was gradually decreased after the addition of CNM. Expression of BMP7 mRNA, which was observed in control cultures, was decreased in the presence of CNM. No difference in the expression of E-cadherin mRNA was observed and a fragment specific for β-actin was amplified as a control for the RT-PCR method. Amplified samples were separated using 1.5% agarose gels in electrophoresis and the UV illuminated DNA was visualized by staining with ethidium bromide. (B) Western blotting analysis of the expression of BMP7 (49 kDa) protein in mouse corneal epithelial cells. Cell lysates of corneal epithelial cells from the above experiment were prepared and subjected to immunoblot analysis using antibody against BMP7. Amounts of the GAPDH protein levels which were detected with an anti-GAPDH antibody served as a loading control. Gradual decrease in the BMP7 protein levels in corneal epithelial cells was observed after the addition of CNM.

neuronal differentiation *in vitro* (Gordon-Weeks and Fischer, 2000). In our experiments, the observed decrease in the expression of Map1b mRNA in the presence of CEM correlates with its decreased expression in cultured mature hippocampal neurons (Fischer and Romano-Clarke, 1991) and is also consistent with the relative decline of Maplb levels observed during development (Safaei and Fischer, 1989). In Map1b null mice, deletion of *Map1b* induces axonal branching without any loss in nerve regeneration capacity and cultured dissociated neurons from this mouse line exhibit higher terminal and collateral branching (Bouquet et al., 2004). Since the extension of axon branches is a mechanism of target innervation (Kuo et al., 2009), the observed decrease in the expression of Map1b in TG neurons after the addition of CEM may have a role in generating nerve terminal branching to innervate the cornea. From these observations it may be postulated that ongoing interactions between epithelial cells and neuron endings in the cornea may contribute to its innervation and nerve regeneration after injury.

To date, evidence for the presence of EMT in corneal epithelial cells during wound repair has been reported either *in vivo* or in immortalized cells (Aomatsu et al., 2011, 2012; Chandler et al., 2007). The present study demonstrates the existence of EMT in primary corneal epithelial cells in culture, thus providing an opportunity to study the involvement of EMT in corneal wound healing in the context of epithelial–neuronal interactions. Since it is known that corneal epithelial cells show an increase in the amount of Pax6 at the migrating front of the epithelium after injury (Sivak et al., 2004), the detected sharp increase in the expression of Pax6 mRNA immediately after scratch supports our experimental system. Even though the expression of BMP7 has been reported to be absent in mouse cornea during alkali burn (Saika et al., 2005), we detected its expression in corneal epithelial cells along with a significant decrease in wounded epithelial cells in the presence of CNM. BMP7 is known to be involved in the induction of mesenchymal-to-epithelial transition (Na et al., 2009), alongside its role in sustaining the epithelial phenotype (Wang et al., 2001) and wound healing (Saika et al., 2005). In view of this, it may be postulated that in corneal epithelial cells BMP7 helps to maintain the epithelial characteristics and its decrease in the presence of CNM may accelerate the loss of epithelial phenotype, which in turn leads to the early onset of EMT during the initial phase of corneal epithelial wound healing. Further studies are underway to elucidate the functional role of BMP7 in mouse corneal EMT.

Our data provide direct evidence of ongoing communication between corneal epithelial cells and TG neurons, as reflected in the alterations in neurons and corneal epithelial cells respectively in the presence of the other cell type. The role of TG neurons on corneal epithelial cells appears to be more than merely sensory. At the onset of injury, study of differences in the expression of various signalling molecules during EMT of epithelial cells in the presence of SP and BMP7 yields insights into the detailed dissection of the signalling pathways involved in epithelial–neuronal interactions and corneal wound healing and offers fresh perspectives for the development of future therapeutic targets.

Declaration of interest

The authors declare no conflicts of interest. The authors alone are responsible for the content and writing of the paper.

Author's contributions

BSK designed the study, performed the cell cultures, biochemical studies and their analysis and drafted the manuscript; TS participated in the design of the study and carried out the biochemical studies and their analysis; AW, RG and OS participated in the design and coordination of the study. All authors read and approved the final manuscript.

Acknowledgements

The authors thank C. Leyh for her technical skill and expertise and M. Lietz for timely supply of experimental mice throughout the project. We also thank Prof. Dr. S. Baltrusch for supporting our molecular biology experiments, M. Reichard for stimulating scientific discussions, and D. Beattie for editorial assistance in preparing the manuscript for publication. This work was financially supported by the FORUN programme of the University of Rostock Medical Faculty (889011) (grant to BS Kowtharapu) and by the Federal Ministry of Education and Research within the REMEDIS project "Higher quality of life through novel micro-implants" (FKZ: 03IS2081).

References

Aomatsu, K., Arao, T., Sugioka, K., Matsumoto, K., Tamura, D., Kudo, K., Kaneda, H., Tanaka, K., Fujita, Y., Shimomura, Y., Nishio, K., 2011 Apr 14. TGF-β induces sustained upregulation of SNAI1 and SNAI2 through Smad and non-Smad pathways in a human corneal epithelial cell line. Invest. Ophthalmol. Vis. Sci. 52 (5), 2437–2443.

Aomatsu, K., Arao, T., Abe, K., Kodama, A., Sugioka, K., Matsumoto, K., Kudo, K., Kimura, H., Fujita, Y., Hayashi, H., Nagai, T., Shimomura, Y., Nishio, K., 2012 Feb 16. Slug is upregulated during wound healing and regulates cellular phenotypes in corneal epithelial cells. Invest. Ophthalmol. Vis. Sci. 53 (2), 751–756.

Araki-Sasaki, K., Aizawa, S., Hiramoto, M., Nakamura, M., Iwase, O., Nakata, K., Sasaki, Y., Mano, T., Handa, H., Tano, Y., 2000 Feb. Substance P-induced cadherin expression and its signal transduction in a cloned human corneal epithelial cell line. J. Cell. Physiol. 182 (2), 189–195.

Baker, K.S., Anderson, S.C., Romanowski, E.G., Thoft, R.A., SundarRaj, N., 1993 Jan. Trigeminal ganglion neurons affect corneal epithelial phenotype. Influence on type VII collagen expression in vitro. Invest. Ophthalmol. Vis. Sci. 34 (1), 137–144.

Beuerman, R.W., Schimmelpfennig, B., 1980 Jul. Sensory denervation of the rabbit cornea affects epithelial properties. Exp. Neurol. 69 (1), 196–201.

Bouquet, C., Soares, S., von Boxberg, Y., Ravaille-Veron, M., Propst, F., Nothias, F., 2004 Aug 11. Microtubule-associated protein 1B controls directionality of growth cone migration and axonal branching in regeneration of adult dorsal root ganglia neurons. J. Neurosci. 24 (32), 7204–7213.

Chan, K.Y., Haschke, R.H., 1982 Aug. Isolation and culture of corneal cells and their interactions with dissociated trigeminal neurons. Exp. Eye Res. 35 (2), 137–156.

Chan, K.Y., Haschke, R.H., 1981 Oct. Action of a trophic factor(s) from rabbit corneal epithelial culture on dissociated trigeminal neurons. J. Neurosci. 1 (10), 1155–1162.

Chandler, H.L., Colitz, C.M., Lu, P., Saville, W.J., Kusewitt, D.F., 2007 Mar. The role of the slug transcription factor in cell migration during corneal re-epithelialization in the dog. Exp. Eye Res. 84 (3), 400–411.

de Leeuw, A.M., Chan, K.Y., 1989 Sep. Corneal nerve regeneration. Correlation between morphology and restoration of sensitivity. Invest. Ophthalmol. Vis. Sci. 30 (9), 1980–1990.

Fischer, I., Romano-Clarke, G., 1991 Feb. Association of microtubule-associated protein (MAP1B) with growing axons in cultured hippocampal neurons. Mol. Cell. Neurosci. 2 (1), 39–51.

Forbes, D.J., Pozos, R.S., Nelson, J.D., 1987 Mar. Co-culture of rat trigeminal ganglion neurons and corneal epithelium. Curr. Eye Res. 6 (3), 507–514.

Freire, V., Andollo, N., Etxebarria, J., Durán, J.A., Morales, M.C., 2012 Aug 15. In vitro effects of three blood derivatives on human corneal epithelial cells. Invest. Ophthalmol. Vis. Sci. 53 (9), 5571–5578.

Gallar, J., Pozo, M.A., Rebollo, I., Belmonte, C., 1990 Oct. Effects of capsaicin on corneal wound healing. Invest. Ophthalmol. Vis. Sci. 31 (10), 1968–1974.

Garcia-Hirschfeld, J., Lopez-Briones, L.G., Belmonte, C., 1994 Nov. Neurotrophic influences on corneal epithelial cells. Exp. Eye Res. 59 (5), 597–605.

Gavet, O., Pines, J., 2010 Apr 20. Progressive activation of CyclinB1-Cdk1 coordinates entry to mitosis. Dev. Cell. 18 (4), 533–543.

Goins, K.M., 2005 Apr. New insights into the diagnosis and treatment of neurotrophic keratopathy. Ocul. Surf. 3 (2), 96–110.

Gordon-Weeks, P.R., Fischer, I., 2000 Jan 15. MAP1B expression and microtubule stability in growing and regenerating axons. Microsc. Res. Tech. 48 (2), 63–74.

Hazlett, L., Masinick, S., Mezger, B., Barrett, R., Kurpakus, M., Garrett, M., 1996. Ultrastructural, immunohistological and biochemical characterization of cultured mouse corneal epithelial cells. Ophthalmic Res. 28 (1), 50–56.

Hong, H.S., Lee, J., Lee, E., Kwon, Y.S., Lee, E., Ahn, W., Jiang, M.H., Kim, J.C., Son, Y., 2009 Apr. A new role of substance P as an injury-inducible messenger for mobilization of CD29(+) stromal-like cells. Nat. Med. 15 (4), 425–435.

Kim, S.Y., Choi, J.S., Joo, C.K., 2009 Feb. Effects of nicergoline on corneal epithelial wound healing in rat eyes. Invest. Ophthalmol. Vis. Sci. 50 (2), 621–625.

Kiselev, Y., Eriksen, T.E., Forsdahl, S., Nguyen, L.H., Mikkola, I., 2012. 3T3 cell lines stably expressing Pax6 or Pax6(5a) – a new tool used for identification of common and isoform specific target genes. PLoS One 7 (2), e31915.

Kuo, T.Y., Hong, C.J., Hsueh, Y.P., 2009 Nov. Bcl11A/CTIP1 regulates expression of DCC and MAP1b in control of axon branching and dendrite outgrowth. Mol. Cell. Neurosci. 42 (3), 195–207.

Malin, S.A., Davis, B.M., Molliver, D.C., 2007. Production of dissociated sensory neuron cultures and considerations for their use in studying neuronal function and plasticity. Nat. Protoc. 2 (1), 152–160.

Matsumoto, Y., Dogru, M., Goto, E., Ohashi, Y., Kojima, T., Ishida, R., Tsubota, K., 2004 Jun. Autologous serum application in the treatment of neurotrophic keratopathy. Ophthalmology 111 (6), 1115–1120.

Müller, L.J., Marfurt, C.F., Kruse, F., Tervo, T.M., 2003 May. Corneal nerves: structure, contents and function. Exp. Eye Res. 76 (5), 521–542. Review. Erratum in: Exp Eye Res. 2003 Aug; 77(2):253.

Na, Y.R., Seok, S.H., Kim, D.J., Han, J.H., Kim, T.H., Jung, H., Lee, B.H., Park, J.H., 2009 Nov. Bone morphogenetic protein 7 induces mesenchymal-to-epithelial transition in melanoma cells, leading to inhibition of metastasis. Cancer Sci. 100 (11), 2218–2225.

Nagano, T., Nakamura, M., Nakata, K., Yamaguchi, T., Takase, K., Okahara, A., Ikuse, T., Nishida, T., 2003 Sep. Effects of substance P and IGF-1 in corneal epithelial barrier function and wound healing in a rat model of neurotrophic keratopathy. Invest. Ophthalmol. Vis. Sci. 44 (9), 3810–3815.

Nakamura, M., Kawahara, M., Nakata, K., Nishida, T., 2003 Jul. Restoration of corneal epithelial barrier function and wound healing by substance P and IGF-1 in rats with capsaicin-induced neurotrophic keratopathy. Invest. Ophthalmol. Vis. Sci. 44 (7), 2937–2940.

Nelson, D.A., Bost, K.L., 2005 Oct. Quantification of hemokinin-1 peptide production and secretion from mouse B cells. Cell. Immunol. 237 (2), 115–122.

Nishida, T., Yanai, R., 2009 Jul. Advances in treatment for neurotrophic keratopathy. Curr. Opin. Ophthalmol. 20 (4), 276–281.

Rao, K., Leveque, C., Pflugfelder, S.C., 2010 May. Corneal nerve regeneration in neurotrophic keratopathy following autologous plasma therapy. Br. J. Ophthalmol. 94 (5), 584–591.

Reid, T.W., Murphy, C.J., Iwahashi, C.K., Foster, B.A., Mannis, M.J., 1993 Aug. Stimulation of epithelial cell growth by the neuropeptide substance P. J. Cell. Biochem. 52 (4), 476–485.

Safaei, R., Fischer, I., 1989 Jun. Cloning of a cDNA encoding MAP1B in rat brain: regulation of mRNA levels during development. J. Neurochem. 52 (6), 1871–1879.

Saika, S., Ikeda, K., Yamanaka, O., Flanders, K.C., Nakajima, Y., Miyamoto, T., Ohnishi, Y., Kao, W.W., Muragaki, Y., Ooshima, A., 2005 Apr. Therapeutic effects of adenoviral gene transfer of bone morphogenic protein-7 on a corneal alkali injury model in mice. Lab. Invest. 85 (4), 474–486.

Shimizu, Y., 1982. Localization of neuropeptides in the cornea and uvea of the rat: an immunohistochemical study. Cell. Mol. Biol. 28 (1), 103–110.

Sivak, J.M., West-Mays, J.A., Yee, A., Williams, T., Fini, M.E., 2004 Jan. Transcription factors Pax6 and AP-2alpha interact to coordinate corneal epithelial repair by controlling expression of matrix metalloproteinase gelatinase B. Mol. Cell. Biol. 24 (1), 245–257.

Tervo, K., Tervo, T., Eränkö, L., Vannas, A., Cuello, A.C., Eränkö, O., 1982 Nov. Substance P-immunoreactive nerves in the human cornea and iris. Invest. Ophthalmol. Vis. Sci. 23 (5), 671–674.

Villablanca, A.C., Murphy, C.J., Reid, T.W., 1994 Dec. Growth-promoting effects of substance P on endothelial cells in vitro. Synergism with calcitonin gene-related peptide, insulin, and plasma factors. Circ. Res. 75 (6), 1113–1120.

Wang, S.N., Lapage, J., Hirschberg, R., 2001 Nov. Loss of tubular bone morphogenetic protein-7 in diabetic nephropathy. J. Am. Soc. Nephrol. 12 (11), 2392–2399.

Yamada, N., Yanai, R., Nakamura, M., Inui, M., Nishida, T., 2004 Apr. Role of the C domain of IGFs in synergistic promotion, with a substance P-derived peptide, of rabbit corneal epithelial wound healing. Invest. Ophthalmol. Vis. Sci. 45 (4), 1125–1131.

Magnetresonanzmikroskopie des Akkommodationsapparats

DOI 10.1055/s-0042-118599
Klin Monatsbl Augenheilkd 2016; 233: 1320–1323

ISSN 0023-2165

Magnetresonanzmikroskopie des Akkommodationsapparats

Magnetic Resonance Microscopy of the Accommodative Apparatus

Autoren T. Stahnke[1], S. Hadlich[2], A. Wree[3], R. F. Guthoff[1], O. Stachs[1], S. Langner[2]

Institute
[1] Universitätsaugenklinik, Universitätsmedizin Rostock
[2] Institut für Diagnostische Radiologie und Neuroradiologie, Universitätsmedizin Greifswald
[3] Institut für Anatomie, Universitätsmedizin Rostock

Schlüsselwörter
- Magnetresonanztomografie
- Akkommodation
- Linse
- Ziliarkörper
- Iris

Key words
- magnetic resonance tomography
- accommodation
- lens
- ciliary body
- iris

eingereicht 15. 9. 2016
akzeptiert 4. 10. 2016

Bibliografie
DOI http://dx.doi.org/10.1055/s-0042-118599
Klin Monatsbl Augenheilkd 2016; 233: 1320–1323 © Georg Thieme Verlag KG Stuttgart · New York · ISSN 0023-2165

Korrespondenzadresse
Dr. rer. nat. Thomas Stahnke
Universitätsaugenklinik
Universitätsmedizin Rostock
Doberaner Straße 140
18057 Rostock
Tel.: + 49/(0)3 81/4 94 85 75
Fax: + 49/(0)3 81/4 94 85 49
thomas.stahnke@med.uni-rostock.de

Zusammenfassung

Die Ultrahochfeld-Magnetresonanzmikroskopie (MRM) erlaubt die Akquisition von Magnetresonanzbildern (MR-Bildern) mit einer Auflösung im Submillimeterbereich. Damit ermöglicht sie eine weitestgehend artefaktfreie, untersucherunabhängige Darstellung der Strukturen und der Konfiguration des humanen Auges, die üblicherweise durch herkömmliche Visualisierungstechniken nicht erreicht werden kann. Der vorliegende Artikel korreliert die MRM des anterioren Augenabschnitts und des Akkommodationsapparats bei 9,4 Tesla mit der konventionellen Histologie.

Abstract

Magnetic resonance microscopy (MRM) at ultrahigh magnetic fields allows acquisition of high resolution MR images in the micrometre range. The use of ultra-high magnetic fields opens the possibility of user-independent and artefact-free detailed characterisation of the anatomical tissue of the human eye, which is not achievable with classical imaging techniques. This article correlates MRM of the anterior eye segment and the accommodative apparatus at 9.4 Tesla with conventional histology.

Einleitung

Das Verständnis der Akkommodation des Auges stellt eine der großen Herausforderungen innerhalb der Augenheilkunde dar. Entscheidend hierfür ist u. a. die anatomisch korrekte Darstellung der am Akkommodationsprozess beteiligten Strukturen, wie Linse, Ziliarkörper und Ziliarmuskel. Hierfür stehen eine Vielzahl etablierter ophthalmologischer Untersuchungstechniken zur Verfügung, welche diese Strukturen sowohl ex vivo als auch in vivo darstellen können. Die durch Gullstrand 1911 entwickelte Spaltlampenmikroskopie ermöglichte bereits eine Begutachtung beinahe aller lichtoptisch zugänglichen Abschnitte des Auges mit lichtmikroskopischer Auflösung [1]. Mit dem Einzug modernerer Lichtquellen, insbesondere des Lasers, wurden weitere diagnostische Verfahren, wie die Scheimpflug-Fotografie [2], die Scanning-Laser-Ophthalmoskopie (SLO) und die optische Kohärenztomografie (OCT) [3] sowie die konfokale Laser-Scanning-Mikroskopie (CLSM) [4] entwickelt. Darüber hinaus ist auch die Ultraschallbiomikroskopie (UBM) ein in der klinischen Routine verwendetes Verfahren zur Beurteilung dieser Strukturen [5].

Bei allen hervorragenden Möglichkeiten der genannten Methoden besitzen sie jedoch alle entscheidende Nachteile bei der Visualisierung und Charakterisierung des Akkommodationsapparats. Dies liegt zum einen an der methodenspezifisch bedingten geringen Eindringtiefe, aber auch an der Tatsache, dass das Irispigmentepithel sowohl sichtbares Licht als auch Laserlicht absorbiert, wodurch eine Beurteilung der äquatorialen Linse und des Ziliarkörpers verhindert wird. Aufgrund der Reflexionsgeometrien kann die Äquatorialregion der Linse auch in der UBM nicht ausreichend beurteilt werden [6].

Daher beruhen die Kenntnisse über die Anatomie des Akkommodationsapparats i. d. R. auf pathologisch-anatomischen Studien [7]. Neben dem Nachteil der nur ex vivo durchzuführenden Untersuchung kommt es bei der histologischen Aufarbeitung durch die Konservierungs- und Schnitttechniken zu Schrumpfungsartefakten, welche die Beurteilung erschweren können.

Als Alternative zu den klassischen ophthalmologischen Untersuchungstechniken bietet sich die Magnetresonanztomografie (MRT) an. Die MRT zeichnen ein exzellenter Weichteilkontrast sowie die Fähigkeit zur multiplanaren Darstellung aus.

Die in der klinischen Routine etablierten Feldstärken von 1,5 bzw. 3 Tesla (T) ermöglichen i. d. R. jedoch keine ausreichende Ortsauflösung. Die MR-Bildgebung im Ultrahochfeld mit Feldstärken > 7 T adressiert dieses Problem und erlaubt eine örtliche Auflösung im Submillimeterbereich. Dieses Verfahren wird als Magnetresonanzmikroskopie (MRM) bezeichnet [8–10]. Neben der Erhöhung der Feldstärke kann auch eine Optimierung der Spulentechnologie zu einer Erhöhung des Signal-zu-Rausch-Verhaltens (SNR) und damit zu einer Verbesserung der Auflösung führen [11].
Die vorliegende Arbeit zeigt die Möglichkeiten der MRM bei 9,4 T zur Charakterisierung des anterioren Augenabschnitts und vergleicht diese mit der konventionellen Histologie. Der Fokus der Untersuchung liegt dabei auf der Charakterisierung von Strukturen und Geweben des Akkommodationsapparats.

Untersuchungstechnik

Die in diesem Artikel vorgestellte MR-Mikroskopie erfolgte an einem 9,4-T-Ultrahochfeld-MRT (BioSpec 94/30 USR, Bruker BioScan GmbH, Ettlingen, Deutschland) unter Verwendung einer gekühlten 4-Kanal-Empfangsspule (MRI CryoProbe, Bruker BioScan GmbH, Ettlingen, Deutschland) und einem Untersuchungsfeld (field of view, FOV) von 20 mm. Aufgrund der besseren Abgrenzbarkeit der Strukturen des Auges gegenüber dem stark wasserhaltigen Glaskörper sowie der flüssigkeitsgefüllten vorderen und hinteren Augenkammer wurden für die MR-Mikroskopie T2-gewichtete 3-D-Sequenzen akquiriert, in denen wasserhaltige Strukturen hyperintens (= hell) erscheinen. Die Bildmatrix der akquirierten Aufnahmen betrug 1536 × 1536 Pixel mit einer daraus resultierenden räumlichen Auflösung von 13 × 13 µm in der Untersuchungsebene bei einer Schichtdicke von 300 µm. Weitere Bildparameter waren: TE 13,3 ms, TR 100 ms, Flip Angle 12°. Die Untersuchungszeit betrug 1:21 h pro Untersuchungsebene, welche jeweils in 8 Schichten abgebildet wurde. Der Schichtabstand betrug dabei 300 µm. Die hier präsentierten Untersuchungen erfolgten an einem enukleierten humanen Spenderauge (65 Jahre) ohne okulare Vorerkrankungen 24–36 Stunden nach Enukleation.
Für die histologischen Untersuchungen wurde ein enukleiertes humanes Spenderauge (67 Jahre) für 48 h in Formalin fixiert, mit Paraffin durchtränkt und im Anschluss in einem Paraffinblock eingebettet. Nach Aushärten des Blocks wurden mit einem Mikrotom 5 µm dünne Schnitte erstellt und mit Hämatoxylin-Eosin (HE) gefärbt. Die HE-Färbung stellt die klassische Standardfärbung der Histologie dar. Das natürlich vorkommende Hämatoxylin färbt in Form des basischen Hämalauns alle Strukturen blau, die sauer bzw. basophil sind, z. B. DNA, Zellkerne, Ribosomen und das raue endoplasmatische Retikulum. Der synthetische Farbstoff Eosin färbt hingegen alle Strukturen rot, die basisch bzw. azidophil sind. Dazu gehören vor allem die Proteine des Zytoplasmas, Mitochondrien, das glatte endoplasmatische Retikulum und Kollagen.
Die gefärbten Dünnschnitte wurden anschließend mit Entellan® eingedeckelt und lichtmikroskopisch mit einem Olympus BX-51 (Hamburg, Deutschland) mikroskopiert.

Resultate und Diskussion

Abb. 1 a zeigt eine T2-gewichtete Darstellung des gesamten Vorderabschnitts des Auges. Das korneale Gewebe zeigt bereits Degenerations- und Suszeptibilitätsartefakte und wurde bei der folgenden Diskussion nicht berücksichtigt. Die mit Kammerwasser gefüllte vordere und hintere Augenkammer erscheinen homogen hyperintens und grenzen sich sehr gut gegen die Gewebe des anterioren Augenabschnitts, wie Kornea, Iris, Ziliarkörper und Sklera ab. Weiterhin erscheint die Linse aufgrund des geringeren Wassergehalts hypointens (= dunkel), wodurch sich auch der posteriore Linsenpol deutlich vom Glaskörper abgrenzen lässt. Die Konturen der Linse und der anderen Gewebe des anterioren Augenabschnitts werden mittels der MRM verzerrungs- und artefaktfrei dargestellt.
Das Stroma der Iris erscheint im Vergleich zu den mit Kammerwasser gefüllten Strukturen gering hypointens (**Abb. 1 b**). Das Irispigmentepithel imponiert aufgrund der paramagnetischen Eigenschaften des Pigments als eine lineare hypointense Struktur an der dorsalen Begrenzung der Iris. Angrenzend an die Pupille lässt sich der M. sphincter pupillae abgrenzen. Der Muskel erscheint im Vergleich zum Stroma ebenfalls gering hypointens.
Analog zur Iris imponiert auch das Pigmentepithel des Ziliarkörpers hypointens (**Abb. 1 c**). Mittels MRM ist es möglich, die verschiedenen Abschnitte des Pigmentepithels im Bereich des Ziliarkörpers (Processus ciliares), der Einfaltungen (Plicae circulares) und der Pars plana, welche dem Glaskörper anliegt, zu differenzieren. Wie der M. sphincter pupillae imponiert auch der M. ciliaris als hypointense Struktur gegenüber dem Stroma des Ziliarkörpers, wobei sich die zirkulären und radiären Faseranteile MR-morphologisch nicht differenzieren lassen. Ebenso gelingt mit konventionellen MR-Techniken eine Darstellung der Zonulafasern nicht, welche die Linsenkapsel mit dem Ziliarmuskel verbinden.
Auch innerhalb der Linse lässt sich in der T2-gewichteten Detaildarstellung eine Ultrastruktur differenzieren (**Abb. 1 d**). Dabei erscheint die anteriore Linsenkapsel als hypointense lineare Struktur. Das direkt unterhalb der anterioren Linsenkapsel gelegene einschichtige Linsenepithel sowie Bereiche des hieran angrenzenden Linsenkortexes erscheinen im Vergleich zur Linsenkapsel hyperintens, wohingegen die an den Kortex anschließende Kernregion der Linse wieder hypointens imponiert und einen Hinweis auf einen geringeren Wassergehalt liefert. Eine Auflösung der Ultrastruktur der Linse bis auf zelluläre Ebene ist nicht möglich.
Die konventionelle histologische Aufarbeitung ermöglicht eine um ein Vielfaches höhere örtliche Auflösung, wodurch sich die Strukturen des anterioren Augenabschnitts bis auf zelluläre Ebene darstellen lassen (**Abb. 1 e**). Eine Beurteilung der vorderen und hinteren Augenkammer sowie des Glaskörpers ist jedoch methodenspezifisch nur eingeschränkt möglich, weil das Kammerwasser und die wässrigen Anteile des Glaskörpers bei der histologischen Aufarbeitung ausgewaschen werden.
Analog zur Darstellung in der MRM imponiert das Pigmentepithel der Iris auch in der HE-Färbung als homogen dunkle lineare Struktur (**Abb. 1 f**). Die Schwarzfärbung beruht auf dem in den Epithelzellen eingelagerten Melanin, dessen paramagnetische Eigenschaften auch für die Signalminderung in den MRT-Aufnahmen verantwortlich sind. Es besteht eine sehr gute Korrelation zwischen MRM und konventioneller Histologie für den M. sphincter pupillae. Aufgrund der besseren örtlichen Auflösung lassen sich in der konventionellen Histologie auch die einzelnen Muskelzellen abgrenzen. Das in der HE-Färbung sichtbare Myoepithel (M. dilatator pupillae) lässt sich in der MRM nur angedeutet abgrenzen.
Auch für den Ziliarkörper und sein Pigmentepithel besteht eine sehr gute Korrelation zwischen MRM und Histologie (**Abb. 1 g**).

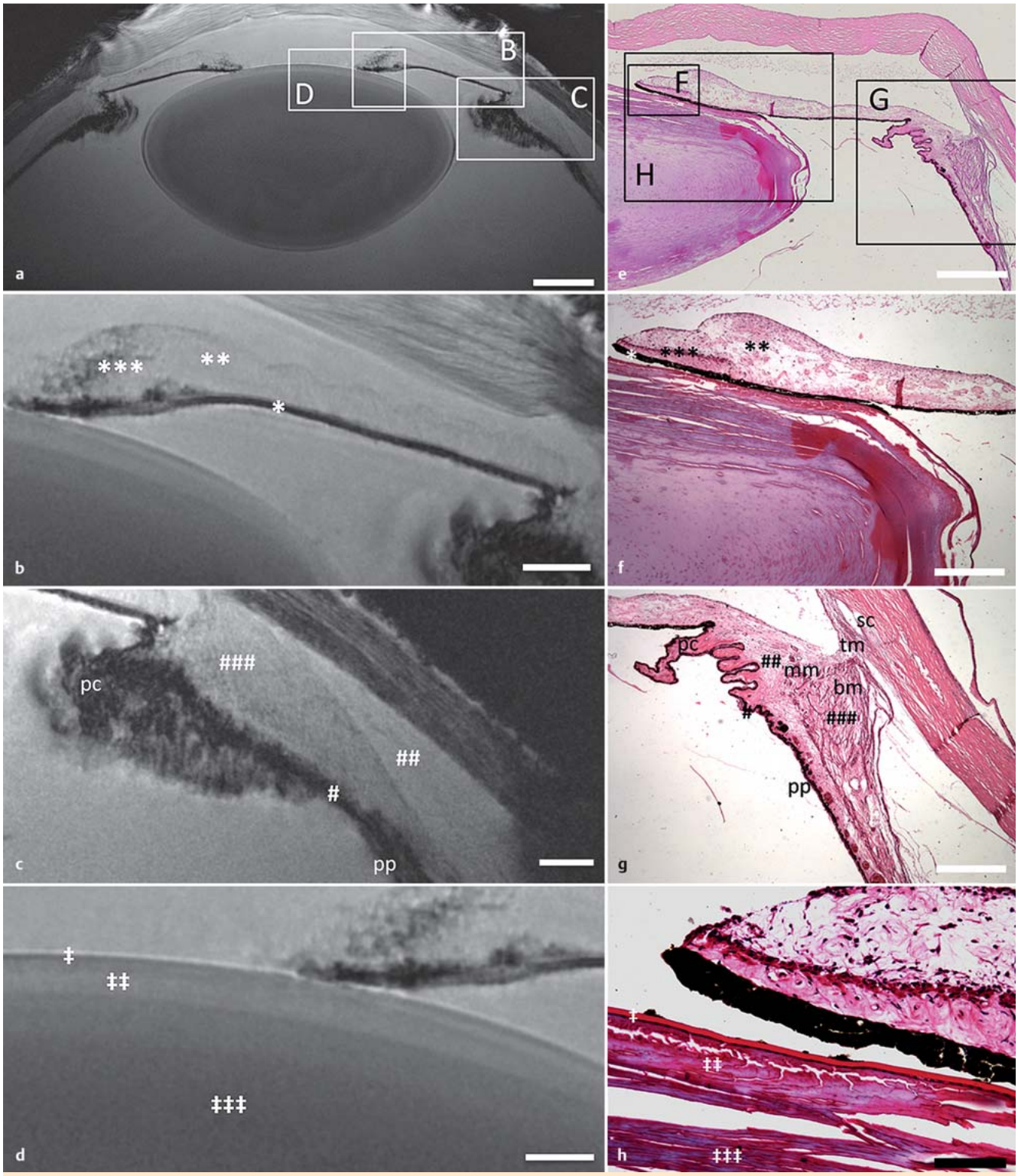

Abb. 1 T2-gewichtete MR-Mikroskopie des anterioren Abschnitts eines humanen Auges im Vergleich mit konventioneller Histologie (HE-Färbung). Axiale T2-gewichtete 3-D-Aufnahmen mit einer örtlichen Auflösung von 13 × 13 µm (**a**–**d**). **a** Übersichtsdarstellung des humanen anterioren Augenabschnitts und des Akkommodationsapparats. Die weißen Markierungen (**B**–**D**) geben die jeweiligen Ausschnitte der Detaildarstellungen wieder. Messbalken: 1500 µm. **b** Detaildarstellung der Iris. * = Irispigmentepithel; ** = Stroma der Iris; *** = M. sphincter pupillae. Messbalken: 500 µm. **c** Detaildarstellung des Ziliarkörpers. # = Pigmentepithel des Ziliarkörpers; ## = Stroma des Ziliarkörpers; ### = M. ciliaris; pc = Plicae circulares; pp = Pars plana. Messbalken: 500 µm. **d** Detaildarstellung der Linse. ‡ = Linsenkapsel; ‡‡ = Linsenepithel und Linsenkortex; ‡‡‡ = adulter Nukleus der Linse. Messbalken: 150 µm. **e** Übersichtsdarstellung des humanen anterioren Augenabschnitts und des Akkommodationsapparats in der HE-Färbung. Die schwarzen Markierungen (**F**–**H**) geben die jeweiligen Ausschnitte der Detaildarstellungen wieder. Messbalken: 1000 µm. **f** Detaildarstellung der Iris. * = Irispigmentepithel; ** = Stroma der Iris; *** = M. sphincter pupillae. Messbalken: 500 µm. **g** Detaildarstellung des Ziliarkörpers. # = Pigmentepithel des Ziliarkörpers; ## = Stroma des Ziliarkörpers; ### = M. ciliaris; pc = Plicae circulares; pp = Pars plana; mm = Müller-Muskel; bm = Brücke-Muskel; sc = Schlemm-Kanal; tm = Trabekelmaschenwerk. Messbalken: 500 µm. **h** Detaildarstellung der Linse. ‡ = Linsenkapsel; ‡‡ = Linsenepithel und Linsenkortex; ‡‡‡ = adulter Nukleus der Linse. Messbalken: 100 µm.

Aufgrund der besseren Auflösung der Histologie lässt sich jedoch die Struktur der Plicae circulares besser beurteilen. Darüber hinaus erlaubt die konventionelle Histologie eine Differenzierung der beiden Bestandteile des M. ciliaris in die meridionalen Fasern des Brücke-Muskels und die zirkulär angeordneten Fasern des Müller-Muskels. Im Bereich des Kammerwinkels können zudem das Trabekelmaschenwerk und der Schlemm-Kanal identifiziert werden. Im Gegensatz zur MRM hat sich in der konventionellen histologischen Aufarbeitung jedoch der gesamte Ziliarkörper von der Sklera abgelöst und ist nur noch über den Skleralsporn mit der Kornea im Bereich des Kammerwinkels verbunden.

Insbesondere die Linse ist aufgrund ihrer Ultrastruktur sehr anfällig gegenüber Schrumpfungs- und Schnittartefakten, was zu einer Auffaserung der einzelnen Linsenfasern führt. Wie in der MRM lassen sich auch in der HE-Färbung verschiedene Schichten der Linse im Bereich des anterioren Linsenabschnitts erkennen (**Abb. 1 h**). Direkt angrenzend an die in der HE-Färbung stark rot gefärbte Linsenkapsel kann das einschichtige Linsenepithel, gekennzeichnet durch die dunkelblauen Zellkerne der Linsenepithelzellen, identifiziert werden. Unterhalb des Linsenepithels liegt der hellrosa gefärbte Bereich des zellkernlosen Linsenkortexes, an den der adulte Linsenkern angrenzt. Auch hier zeigt sich eine gute Korrelation zwischen MRM und Histologie.

Limitationen

Derzeit ist die Verfügbarkeit von Ultrahochfeld-MR-Systemen mit einer Feldstärke > 7 T für die humane Bildgebung in vivo noch sehr limitiert, weshalb die MRM des humanen Auges überwiegend ex vivo möglich und ophthalmologisch-experimentellen Fragestellungen vorbehalten ist. Im Verhältnis zu den klassischen ophthalmologischen Untersuchungstechniken ist die Untersuchungszeit der MRM deutlich länger, wodurch sich das Risiko für Bewegungsartefakte und konsekutiver Reduktion der Bildqualität erhöht. Durch die Verwendung geeigneter Untersuchungs- [12] bzw. Sequenztechniken [13–14] können diese Limitationen minimiert werden. Bewegungsartefakte sind bei Ex-vivo-MRM methodenbedingt weitestgehend auszuschließen, es können jedoch Artefakte durch Verlagerungen wässriger Anteile oder Gewebedegeneration bei langen MR-Sequenzen auftreten. Im Vergleich zur konventionellen Histologie ist die Auflösung der MRM derzeit noch geringer, weshalb eine Darstellung auf zellulärer Ebene gegenwärtig nicht möglich ist. Jedoch erlaubt die MRM neben rein anatomischen Darstellungen auch die Durchführung funktioneller Untersuchungstechniken [14], die eine Quantifizierung von Gewebeeigenschaften ermöglicht.

Gegenüber der konventionellen Histologie unterliegt die MRM nicht den Limitationen von konservierungsbedingten Schrumpfungs- und Schnittartefakten, wodurch eine exakte Biometrie anatomischer Strukturen möglich wird. Methodenbedingt wird die konventionelle Histologie standardmäßig an Ex-vivo-Präparaten durchgeführt.

Fazit

Die MRM im Ultrahochfeld kann als eine komplementäre Methode zur konventionellen Histologie betrachtet werden, welche offensichtliche Nachteile der Histologie des Auges kompensieren kann. Die bei Magnetfeldern von 9,4 T und unter Verwendung von modernen Scanner- und Spulentechnologien erreichbare Ortsauflösung in Verbindung mit einem entsprechenden Kontrast und SNR eröffnet völlig neuartige Möglichkeiten für anatomische Studien des Akkommodationsapparats und kann weitestgehend ohne Präparation am ungeöffneten Bulbus durchgeführt werden. Lichtundurchlässige Strukturen innerhalb des Auges haben keinen limitierenden Einfluss auf die MRM. Gegenwärtig ist die MRM allerdings noch nicht in der Lage, Strukturen bis auf zelluläre Ebene aufzulösen, der technologische Fortschritt wird diese Grenzen zukünftig sicherlich überwinden. Die MRM wird jedoch die Histologie bzw. Immunhistochemie nicht ersetzen können, da hier gewebe- und zellspezifische Färbungen einmalige Möglichkeiten bieten.

Danksagung

Diese Arbeit wurde ermöglicht durch das Bundesministerium für Bildung und Forschung (BMBF) innerhalb von RESPONSE „Partnerschaft für Innovation in der Implantattechnologie“. Weiterhin danken wir der Bruker BioScan GmbH (Ettlingen, Deutschland) und Dr. Tim Wokrina für die Unterstützung.

Interessenkonflikt

Nein.

Literatur

1 *Timoney PJ, Breathnach CS.* Allvar Gullstrand and the slit lamp 1911. Ir J Med Sci 2013; 182: 301–305
2 *Fink W.* Refractive correction method for digital charge-coupled device-recorded Scheimpflug photographs by means of ray tracing. J Biomed Opt 2005; 10: 024003
3 *Linnola RJ, Findl O, Hermann B et al.* Intraocular lens-capsular bag imaging with ultrahigh-resolution optical coherence tomography pseudophakic human autopsy eyes. J Cataract Refract Surg 2005; 31: 818–823
4 *Hovakimyan M, Falke K, Stahnke T et al.* Morphological analysis of quiescent and activated keratocytes: a review of ex vivo and in vivo findings. Curr Eye Res 2014; 39: 1129–1144
5 *Stachs O, Martin H, Behrend D et al.* Three-dimensional ultrasound biomicroscopy, environmental and conventional scanning electron microscopy investigations of the human zonula ciliaris for numerical modelling of accommodation. Graefes Arch Clin Exp Ophthalmol 2006; 244: 836–844
6 *Stachs O, Martin H, Kirchhoff A et al.* Monitoring accommodative ciliary muscle function using three-dimensional ultrasound. Graefes Arch Clin Exp Ophthalmol 2002; 240: 906–912
7 *Apple DJ, Mamalis N, Olson RJ et al.* Intraocular Lenses. Evolution, Designs, Complications, and Pathology. Baltimore, MD, USA: Williams & Wilkins; 1989: 172
8 *Langner S, Martin H, Terwee T et al.* 7.1 T MRI to assess the anterior segment of the eye. Invest Ophthalmol Vis Sci 2010; 51: 6575–6581
9 *Langner S, Krueger PC, Stachs O et al.* [MR microscopy of the human eye]. Klin Monatsbl Augenheilkd 2011; 228: 1073–1078
10 *Lindner T, Langner S, Graessl A et al.* High spatial resolution in vivo magnetic resonance imaging of the human eye, orbit, nervus opticus and optic nerve sheath at 7.0 Tesla. Exp Eye Res 2014; 125: 89–94
11 *Webb AG, Van de Moortele PF.* The technological future of 7 T MRI hardware. NMR Biomed 2016; 29: 1305–1315
12 *Lindner T, Langner S, Falke K et al.* Anatomic and pathological characterization of choroidal melanoma using multimodal imaging: what is practical, what is needed? Melanoma Res 2015; 25: 252–258
13 *Lindner T, Langner S, Paul K et al.* [Diffusion weighted magnetic resonance imaging and its application in ophthalmology]. Klin Monatsbl Augenheilkd 2015; 232: 1386–1391
14 *Paul K, Graessl A, Rieger J et al.* Diffusion-sensitized ophthalmic magnetic resonance imaging free of geometric distortion at 3.0 and 7.0 T: a feasibility study in healthy subjects and patients with intraocular masses. Invest Radiol 2015; 50: 309–321